INVESTIGATION OF THE ROLE OF PODOCALYXIN IN CANCER PROGRESSION AND ITS POTENTIAL AS A CANCER THERAPEUTIC

by

Diana Canals Hernaez

B.Sc., Universidad Autónoma de Madrid, 2015

A THESIS SUBMITTED IN PARTIAL FULFILLMENT OF

THE REQUIREMENTS FOR THE DEGREE OF

DOCTOR OF PHILOSOPHY

in

THE FACULTY OF GRADUATE AND POSTDOCTORAL STUDIES

(Medical Genetics)

THE UNIVERSITY OF BRITISH COLUMBIA

(Vancouver)

April 2021

© Diana Canals Hernaez, 2021

The following individuals certify that they have read, and recommend to the Faculty of Graduate and Postdoctoral Studies for acceptance, the dissertation entitled:

Investigation of the role of podocalyxin in cancer progression and its potential as a cancer therapeutic

submitted by Diana Canals Hernaez in partial fulfillment of the requirements for

the degree of Doctor of Philosophy

in Medical Genetics

Examining Committee:

Kelly M McNagny, Medical Genetics, UBC
Supervisor

Brad Nelson, Medical Genetics, UBC
Supervisory Committee Member

Fabio Rossi, Medical Genetics
Supervisory Committee Member

Karla Williams, Pharmaceutical Sciences, UBC
University Examiner

Xiaoyan Jiang, Medical Genetics, UBC
University Examiner

Additional Supervisory Committee Members:

Kevin Bennewith
Supervisory Committee Member

Abstract

The advent of targeted therapies has vastly improved cancer diagnostics and treatments over the last three decades, however, cancer still remains the second leading cause of death worldwide. Importantly, the majority of cancer-related deaths are the result of metastatic disease. This highlights the need to identify biomarkers of tumors at high risk of metastasizing, and to generate targeted therapies against them. Previous studies have demonstrated a strong association between high expression of podocalyxin and decreased patient survival, however, little is known about the role of podocalyxin in promoting cancer progression or its potential as a therapeutic target.

Here we perform an in-depth characterization of PODO83, an anti-podocalyxin antibody that we previously demonstrated delays primary tumor growth in murine tumor models. We show that despite its ability to delay primary tumor growth, its primary effect is actually the prevention of metastasis to the lung. We identified the binding epitope of PODO83 on the extracellular juxtamembrane domain of podocalyxin and showed that the antibody recognizes the core podocalyxin protein in both tumors and healthy tissue. Further, using urothelial, breast and ovarian carcinomas tissue microarrays, we present PODO83 as a promising diagnostic tool.

Podocalyxin is normally readily expressed in the vascular endothelia and kidney podocytes, representing a source of concern surrounding the use of podocalyxin-based therapies. Here, we identified a novel tumor-restricted glycoepitope on podocalyxin and generated and characterized an antibody (PODO447) to target it. We found that while unconjugated PODO447 does not exert any inhibitory or toxic effect on tumor cells, when used as the targeting arm in a Vedotin

antibody-drug conjugate (ADC), the PODO447-ADC specifically targets cancerous cells and increases the survival in pre-clinical models.

The work presented in this thesis contributes directly to scientific understanding of the role of podocalyxin in tumor growth and metastasis. Further, we provide pre-clinical evidence supporting the furthered development of the novel podocalyxin antibodies PODO83, and PODO447 as diagnostic and targeted immunotherapies, respectively, to be used in the fight against cancer and to improve patient outcome.

Lay Summary

Despite great improvements in the diagnosis and treatment of cancer over the last 30 years, cancer remains one of the leading causes of death worldwide. Cancer deaths are predicted to climb due to a growing and ageing population, highlighting the need to better understand the biology of cancer and how it becomes more aggressive. This knowledge is also crucial for the development of new diagnostic tools and treatments. The work in this dissertation provides an in-depth characterization of a promising cancer diagnostic tool based on the presence of a biomarker (podocalyxin) on the surface of tumor cells. In addition, we identify a new protein modification that is only expressed in cancer cells. Moreover, we show that by targeting this modification with an antibody-based therapy we can eliminate tumors and increase survival in pre-clinical models. This work presents exciting advancements in the understanding and treatment of cancer.

Preface

All work presented in this dissertation was performed at the Biomedical Research Centre at the University of British Columbia, Point Grey Campus.

Chapter 2: I designed and conducted the majority of the experiments, data analysis and results interpretation. Pamela Dean generated the SKOV3 *PODXL*-KO cells. The project was initiated by previous student K Snyder in collaboration with MR Hughes and KM McNagny, who continued to provide technical and theoretical guidance.

Parts of Chapter 3 are modified from a published manuscript: Snyder KA, Hughes MR, Hedberg B, Brandon J, **Canals Hernaez D**, Bergqvist P, Cruz F, Po K, Graves ML, Turvey ME, Nielsen JS, Wilkins JA, McColl SR, Babcook JS, Roskelley CD, McNagny KM. Podocalyxin enhances breast tumor growth and metastasis and is a target for monoclonal antibody therapy. *Breast Cancer Res.* 2015; doi: 10.1186/s13058-015-0562-7. My contributions to the results presented in this chapter include experimental design, data collection, analysis and interpretation with the help of MR Hughes and KM McNagny. I generated all the figure panels presented in this Chapter. The Centre for Drug Research and Development generated the PODO83 antibody and performed its initial characterization, and generated the CHO cells expressing CD34 and Podxl orthologs that I then tested. Copyright permissions were granted by the publisher for academic use.

Chapter 4 is modified from a published manuscript: **Canals Hernaez D**, Hughes MR, Dean P, Bergqvist P, Samudio I, Blixt O, Wiedemeyer K, Li Y, Bond C, Cruz E, Köbel M, Gilks CB, Roskelley C, McNagny KM. *J Immunother Cancer.* 2020; doi:10.1136/jitc-2020-001128. I designed and performed most experiments, analyzed and interpreted data, and was the primary author of this manuscript. MR Hughes assisted with experimental design and manuscript writing. P Dean created the SKOV3 and MIAPACA *PODXL*-KO cell lines, initiated the enzymatic treatment experiments, and assisted in flow cytometry assays. PODO83 and PODO447 antibodies were generated at the Centre for Drug Research and Development (P Bergqvist, I Samudio, C Bond and E Cruz). O Blixt performed the glycan array experiments and analysis. M Köbel and K Wiedemeyer assisted with the ovarian carcinoma TMA immunohistochemical scoring, Y Li repeated the glycobiology flow cytometry assays, and B Gilks contributed the ovarian TMAs. CD Roskelley and KM McNagny were key contributors to the experimental concept and design. Copyright permissions were granted by the publisher for academic use.

Chapter 5 is modified from a manuscript in preparation: **Canals Hernaez D**, Hughes MR, Dean P, Li Y, Blixt O, Bergqvist P, Samudio I, Roskelley C, McNagny KM. PODO447 use as an antibody-drug conjugate for cancer therapy. The Center for Drug Research and Development generated PODO447 and OVA ADCs, and performed unconjugated PODO447 MIAPACA, THP-1, HUVEC, Jurkat and A172 *in vitro* cytotoxic assays, as well as the THP-1 and Jurkat PODO447-ADC *in vitro* cytotoxic assays. The National Research Council Canada generated the PODO447 and palivizumab control ADCs. P Dean initiated SKOV3 and MIAPACA ADC *in vitro* cytotoxicity experiments. Y Li assisted with *in vitro* internalization assays and tumor

monitoring. My contributions include experimental design, data collection, analysis and manuscript preparation.

All research involving animals was conducted following the protocols approved by UBC Animal Care Committee (A11-035, A16-007)

Table of Contents

List of Tables

List of Figures

List of Abbreviations

Ab	antibody
ADC	antibody-drug conjugate
cntrl	control
CTx	chemotherapy treatment
EOC	epithelial ovarian carcinoma
FcRn	neonatal Fc receptor
GalNAc	N-acetylgalactosamine
GBM	glioblastoma
i.p.	intraperitoneally
i.v.	intravenously
kDa	kilodalton
mAbs	monoclonal antibodies
Podxl	podocalyxin
pt	pre-treatment
RT	room temperature
s.c.	subcutaneously
SLAM	selected lymphocyte antibody method
V_H	heavy chain variable region
V_L	light chain variable region

Acknowledgements

The research in this thesis would not have been possible without the support and guidance of my supervisor Dr. Kelly McNagny. He provided me with the opportunity to shadow his lab many moons ago, which started a journey of scientific and personal growth that led up to today. I would also like to thank the members of my supervisory committee, Dr. Brad Nelson, Dr. Fabio Rossi and Dr. Kevin Bennewith, for their support and guidance. Additionally, thanks to Dr. Cal Roskelley for sharing his expertise and guidance in all things podocalyxin.

I would also like to thank all members of my lab, past and present. A special thanks to Dr. Michael Hughes for his constant support, advice, encouragement, puns (which you are not short on!) and friendship. Thank you for being an incredible scientific mentor and for having my back.

I'd like to highlight the incredible contributions to my personal and scientific development by Dr. Alissa Cait, Dr. Christine Eisner and Jessie Cait. Thank you for all your support throughout these years, for always giving me advice, helping me practice my presentations (imagine…), and for being my on-call counsellors, editors and comedians.

To the members of the BRC, thank you for creating a welcoming and collaborative environment. A special thanks to Rupi Dhesi and to Ingrid Bartha for their constant willingness to help.

To my cheerleaders and friends: Alicia, Alissa, Christine, Elena, Jessie and Marcela. Thank you for keeping me sane! I truly couldn't have done it without your support, laughter and love.

To Darren for his endless support, pragmatism, calming ability and nickname creator. Thank you for believing in me and for always knowing how to make me laugh.

And finally, to my family, who has been by my side through every step of the journey, no matter how far apart we are. Thank you for encouraging me to pursue my passions, for your constant support, advice and love. Os quiero!

Dedication

For my family and friends

Chapter 1: Introduction

1.1 Overview of cancer

Cancer is not a single disease, but rather a collection of related diseases characterized by uncontrollable cell growth and dissemination of tumor cells throughout the body (1). While in a normal state (tissue homeostasis) there is a tightly regulated balance between cell proliferation and death (apoptosis), cancer arises when normal cells progressively acquire a series of genetic changes that ultimately allow them to "escape" such regulations and transform into malignant cells (2). There are nine alterations that have been deemed essential for malignant growth and, collectively, these alterations are known as "the hallmarks of cancer" (3). Briefly, the hallmarks of cancer are as follows:

Sustainment of proliferative signaling

Normal tissues carefully regulate the production and secretion of growth factors to ensure a homeostasis of cell numbers and maintenance of tissue architecture and function. In contrast, cancer cells acquire independence from tissue proliferative signals in a number of ways: tumor cells may produce growth factors themselves or stimulate neighboring cells to produce them; they can elevate the levels of receptor proteins and become hyper-responsive to otherwise-limiting amounts of growth factor ligands; or they might constitutively activate signaling pathways downstream from these receptors in the absence of a stimulating ligand (4,5).

Insensitivity to growth suppressor signals

Normal tissues maintain their homeostasis by tightly regulating cell growth and that includes the release of anti-proliferative signals. Cancer cells may circumvent programs that negatively regulate cell proliferation, most of which depend on tumor suppressor genes to limit cell proliferation (6-8). A classic tumor suppressor example is the retinoblastoma-associated (RB) protein which, if lost, causes tumor growth in the eye in early childhood (9-11).

Resistance of cell death

Cell programmed death by apoptosis is a natural barrier to the development of cancer. Yet recent studies have revealed that advanced tumors have attenuated apoptosis, suggesting that cancer cells evolve to become resistant to programmed cell death (12,13). One common strategy to avoid cell death is the loss of tumor suppressor TP53, which is found in a wide variety of tumors (14).

Enablement of replicative immortality

Normal cells often undergo a limited number of successive replication cycles before entering a state of senescence followed by cell death. In contrast, cancer cells acquire the ability to replicate endlessly, in most cases, due to the up-regulation of the telomerase enzyme that lengthens telomeres to avoid triggering cell senescence or apoptosis (3).

Induction of angiogenesis

Formation and maintenance of blood vessels is key for the supply of oxygen and nutrients. Thus, tumors shift the balance of angiogenesis and promote the formation of new blood vessels to

satisfy their high nutrient demand. One mechanism cancer cells use to promote tumor vascularization is by upregulating expression of vascular endothelial growth factor (VEGF), a well-known inducer of angiogenesis (1).

Active invasion and metastasis

Cancer cells can spread from the primary tumor mass to other sites of the body in a process called metastasis. Thus, for a cell to become malignant it must gain the ability to metastasize - a sequential, multi-step process including invasion of the stroma, survival in circulation, extravasation and growth of a secondary tumor. This succession of biologic processes is often termed the metastatic cascade (see section 1.1.2) (15).

Reprogramming of energy metabolism

Chronic uncontrolled cell growth of cancer cells is the result of dysregulated cell proliferation and metabolism processes. To meet the demands of their high proliferative rate, tumor cells often display aberrant energy metabolism. For example, cancer cells can reprogram their energy production balance to glycolysis, in part, by up-regulating the expression of glucose transporters such as GLUT1 (16-18).

Evasion of immune system destruction

The immune system is responsible for surveying and destroying arising cancer cells. Thus, to avoid eradication, cancer cells have developed strategies to both avoid detection and limit the extent of killing by the immune system. One of these strategies may be the recruitment of immunosuppressive cells, such as myeloid-derived suppressor (MDSCs) cells (19).

1.1.1 Classification of cancers based on cellular origin

Cancers can be classified by either their histological type, the tissue in which the cancer originated, or the location in the body where the tumor first developed. Here we provide a brief overview of the major cancer groups based on histological type as dictated by the International Classification of Diseases for Oncology (20).

Carcinoma

Carcinomas are malignant neoplasms derived from epithelial tissue. They are the most common type of cancer, accounting for 80-90% off all cancer cases. Carcinomas can be further subdivided into two major subgroups: adenocarcinomas and squamous cell carcinomas. Adenocarcinomas are a type of carcinoma that originates in a tissue with a glandular origin or with glandular characteristics (i.e. pancreatic adenocarcinoma). Glandular epithelia secrete products into blood or ducts. In contrast, squamous cell carcinomas originate in the squamous epithelium (a surface epithelium) (20).

Sarcoma

Sarcomas are cancers of mesenchymal origin that arise from connective and supportive tissue such as bones, tendons, cartilage or muscle. The most common types are soft tissue and bone sarcomas, with osteosarcoma being the most common type of sarcoma arising from the bone (20).

Myeloma, Leukemia and Lymphoma

Blood cancers is a broad term used to described multiple cancers that originate from blood cells and can spread throughout the body via the bloodstream or the lymphatic system. The three most common types of blood cancers are leukemia, lymphoma and myeloma, which are classified based on the cell type and tissue of origin. Leukemias originate from white blood cells in the bone marrow and are often classified based on the growth rate (acute vs. chronic) and the cellular origin (lymphoid vs. myeloid) (21,22). In contrast, transformed lymphocytes that give rise to solid tumors in the lymphatic system are termed lymphomas, which are classified based on the presence (Hodgkin lymphomas) or absence (Non-Hodgkin lymphomas) of Reed-Sternberg cells (23). Lastly, myelomas originate from cancerous plasma cells (antibody-secreting B cells), and can be classified based on where they originated and the extent of their spreading. Multiple myeloma is the most common type, accounting for 90% of all myeloma cases (24).

1.1.2 Metastatic disease

Despite the significant advancements in diagnoses, patient care and adjuvant therapies, 90% of all cancer deaths occur because of metastatic disease (25). Metastasis occurs when cancer cells disseminate from the primary tumor and subsequently colonize one or more distant organs. Whereas distinct primary tumors can often be treated surgically, surgical intervention is usually not feasible or provides only temporary relief in metastatic disease. Thus, systemic treatments are required to eradicate cancer cells in disseminated disease. One barrier to treating metastatic disease is the biological heterogeneity between the cells of the primary tumor and the different metastatic locations. These challenges, together with the specific organ microenvironment, can

lead to various degrees of therapeutic efficacy (15). Thus, understanding of metastatic disease at a cellular and molecular level is critical for the development of better treatments.

Cancer metastasis occurs in a multistep process known as the invasion-metastatic cascade where cancer cells follow a series of long, interrelated steps (**Figure 1.1**). First, cellular transformation and growth occurs resulting in a tumor mass that requires high influx of nutrients and oxygen, thus needing extensive vascularization (26). From this primary lesion, a few tumor cells will leave to invade the local stroma and subsequently enter local blood or lymphatic vessels. Once in circulation, tumor cells (as single cells or aggregates) must survive until they become trapped in the capillary beds of distant organs where they extravasate into the parenchyma. Lastly, once at the distant organ, they proliferate and form micrometastases. For micrometastasis to continue growing (macrometastases), they must develop a vascular network and evade immune destruction. Cells within the macrometastatic lesion may also leave and repeat the metastatic cascade to form a tertiary tumor (15).

Metastasis is a complex mechanism that remains poorly understood. Each of the invasion-metastasis cascade steps can be limiting since failure at any step can put a halt to the entire process. The success of the process depends on both the intrinsic properties of tumor cells as well as the host's response (15). Fortunately, the process of metastasis is highly inefficient, with only a few cells (0.01%) believed to be able to give rise to a metastatic tumor, whereas most circulating tumor cells are eliminated (27). Unfortunately, the "attempts" to metastasize are relentless and may eventually be successful.

Traditionally, it was believed that establishment of metastasis occurred at a late stage in tumor progression in a process called “linear model of metastasis”. In this model, tumor cells disseminate only when the primary tumor has reached a certain size, by which point the cell populations within it have gained advantageous genetic mutations and are progressively selected (28,29). The process by which subpopulations of tumor cells acquire genetic mutations that confer them with a competitive advantage to metastasize is called “clonal evolution theory”. The idea that tumor size correlates with tumor dissemination is supported by the observation that surgical resection lowers the risk of metastasis for tumors smaller than 2 cm in diameter (30-32). In contrast, there is a “parallel model of metastasis” whereby tumor cells can disseminate early in tumor progression, independently from the primary tumor size (30,33). Though the debate continues, current data support a clonal origin for metastases whereby the metastatic process favors the survival of a few subpopulations that preexist within the parental tumor (27).

It is not possible to predict an individual’s risk of developing metastases; indeed, in most patients, metastasis has already occurred at the time of diagnosis (34). Therefore, it is imperative that we focus our efforts on the discovery of biomarkers for early detection of tumors likely to metastasize. Further, the characterization of these potential biomarkers might reveal a functional role in promoting tumor progression and the metastatic cascade, thus highlighting potential therapeutic targets (35).

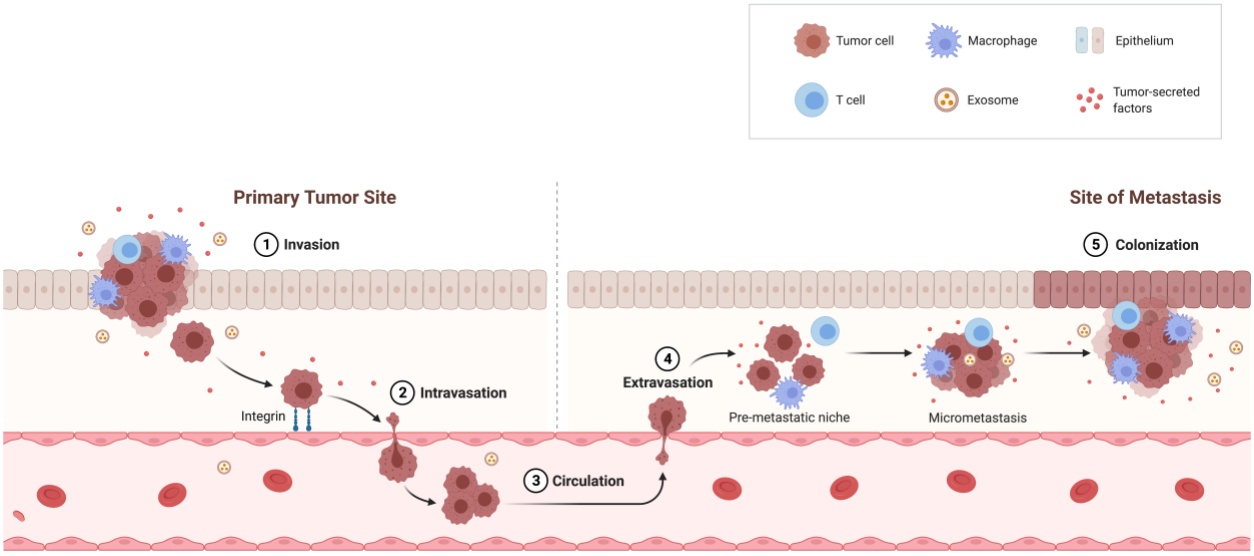

Figure 1.1 Overview of the invasion-metastasis cascade.

Metastasis is the result of a complex, multistep cell-biological process known as the invasion-metastasis cascade. During metastatic progression, tumor cells exit the primary tumor site to invade the local stroma and subsequently enter local blood or lymphatic vessels. Once in circulation, tumor cells must survive until they arrest at a distant organ site and extravasate into the parenchyma. Lastly, metastatic cells adapt to survive in the new foreign microenvironment, and proliferate to form micrometastasis and subsequent macrometastasis (colonization). Adapted from "Overview of Metastatic Cascade", by BioRender.com (2020). Retrieved from https://app.biorender.com/biorender-templates

1.1.3 Common processes promoting cancer progression

Previously, we have reviewed the complexity of cancer dissemination (**sections 1.1 and 1.1.2**). Here, we discuss two common processes known to promote tumor dissemination in carcinomas.

1.1.3.1 Epithelial to Mesenchymal Transition (EMT)

One important process in carcinoma tumor dissemination is a program termed epithelial-to-mesenchymal transition (EMT), which is normally employed during embryogenesis and adult tissue regeneration but is hijacked by tumor cells during cancer development. The EMT program confers carcinoma cells with multiple malignant traits associated with the loss of epithelial properties and acquirement of mesenchymal features, which include increased motility and invasiveness and the ability to degrade components of the extracellular matrix (ECM) (36,37). Indeed, EMT has roles in invasion and intravasation into blood vessels (38), extravasation (39) and post-extravasation, proliferation, and formation of macrometastasis (metastatic colonization) (40,41).

Although, as previously discussed (**section 1.1.2**), some models of tumorigeneses propose that metastasis is established at a late stage in tumor progression, recent studies have shown that acquisition of EMT-related features can occur early in the process, as they have been shown to be present in cells of preneoplastic lesions (42). Moreover, though the EMT program is portrayed as being of binary nature, where cancer cells reside either in a mesenchymal or an epithelial state, reality might be more complex. EMT programs that activate within cancer cells usually confer them with certain mesenchymal traits while allowing them to retain some epithelial features and thus, carcinoma cells can display a mixed mesenchymal/epithelial phenotype (43).

Though important for the invasion and dissemination of most carcinomas, some EMT fundamentals remain unclear, such as the extent to which they are activated in the various stages of cancer progression or the roles of intra- and extracellular signaling pathways sustaining already-activated EMT programs (43). Better understanding of the EMT programs in the context of cancer progression will likely help the development of new therapeutic strategies.

1.1.3.2 Altered glycosylation

Glycosylation is a type of post-translation modification that increases the functional diversity of the proteome. Defects in glycosylation in humans can lead to disease, therefore highlighting the functional importance of the glycome (44). Moreover, altered glycosylation of cell surface and secreted glycoproteins is a quasi-universal modification in cancer (45)

Glycosylation is the enzymatic process linking a saccharide to other saccharides, proteins or lipids (46,47). Glycoproteins are formed by the covalent attachment of a glycan to a protein backbone via nitrogen- (N-glycans) or oxygen- (O-glycans) linkages. A common type of protein O-glycosylation, called mucin-type O-glycosylation, consists of an initial attachment of an N-acetylgalactosamine (GalNAc) to a serine or threonine in the core polypeptide, which can then be further extended to generate diverse structures (48). Further, glycan diversity is achieved by differences in monosaccharide composition (i.e. galactose or mannose), linkage between monosaccharides (i.e. between carbons 1 and 3 or 1 and 4), anomeric state (α or β), and branching structures and substitutions (i.e. sulfation) (49).

Two mechanisms have been proposed to explain the observed unique glycosylation patterns in tumor cells: the incomplete synthesis and neo-synthesis processes (50). The incomplete synthesis process is thought to occur at early stages of cancer development because of impairment of appropriate glycosylation in epithelial cells, which leads to truncated glycan structures such as the sialyl Tn (STn) expression in breast and gastrointestinal cancers (51). In contrast, the neo-synthesis process occurs at later stages of cancer progression as a result of the induction of certain cancer-associated genes involved in glycosylation, which leads to *de novo* expression of antigens such as sialyl Lewis x (SLe^X) (52,53).

Glycans alter protein structure, conformation, and stability, thus modulating protein functionality. Moreover, glycans have been shown to be involved in numerous biological processes that facilitate cancer progression, such as inflammation and immune surveillance (49), cellular metabolism (54,55), cell-cell adhesion (56-58), cell-matrix interaction (56), and inter- and intracellular signalling (59-62). As such, a better understanding of the biologic functionality of glycans in cancer will likely contribute to deciphering the molecular mechanisms promoting cancer progression.

Moreover, glycans can provide a source of new cancer biomarkers. Indeed, some of the most commonly used biomarkers for cancer diagnosis and monitoring of disease progression are glycoproteins (45,63). Examples of these include the prostate-specific antigen (PSA) for prostate cancer (64), the aberrantly glycosylated MUC1 glycoprotein in breast cancer (65) or the carcinoma antigen 125 (CA125, also known as MUC16) in ovarian carcinoma (66). Though these serological biomarkers are known to have altered glycosylation in cancer, due to their low

specificity, they have limited screening and diagnostic potential (49). Thus, there is an urgent need for new biomarkers with higher specificity for early detection and diagnosis of cancer. Additionally, since glycans play an important role in cancer progression, these new cancer biomarkers might also provide unique tumor-specific targets for the development of antibody-based drugs that are either directly cytotoxic or block the glycoprotein-mediated function without affecting normal cells.

1.1.4 Overview of cancer therapy

Cancer treatment is a collection of procedures aimed at removing, destroying, controlling or modifying primary or metastatic tumor cells. The purpose of cancer treatment depends on the extent of the malignant disease, and can include the complete eradication of tumors, prevention of spreading or recurrence, or symptom relief (if all other avenues have failed) (1,67). Here we briefly review some of the most common therapeutic approaches to treat malignant disease.

1.1.4.1 Traditional therapy

Surgery

Curative surgery most commonly attempts to completely remove or reduce localized tumors so that follow-up radiotherapy or chemotherapy treatments can be more effective. Additionally, there are several other types of surgery, including preventative surgery, where the surgeon removes tissue that does not yet contain a malignant growth but that has a high probability of becoming cancerous in the future; diagnostic surgery (also known as biopsy) which is performed to remove a sample from a suspected tumor to obtain a definitive diagnosis; and palliative

surgery, performed to alleviate symptoms or prolong a patient's life when the disease is not responsive to curative treatments (68).

Radiotherapy

Radiotherapy uses X- and gamma-rays as well as other sources of radiation to kill cancer cells by damaging their DNA to trigger cell death pathways. However, radiation energy does not distinguish between normal and cancerous cells and thus can cause undesired cellular toxicity. For that reason, radiation targeting areas and doses are carefully planned to minimize exposure of healthy tissue. Radiation is often used as an adjuvant therapy, usually in combination with surgery or chemotherapy (69).

Chemotherapy

In contrast to surgery or radiotherapy, chemotherapy is a systemic treatment that uses chemical agents to control or eradicate the growth of cancer cells. There are different classes of chemotherapeutic agents based on their chemical structure and mode of action. Chemotherapy agents can act by cross-linking DNA strands (alkylating agents such as cyclophosphamide; or platinum compounds like cisplatin), preventing DNA synthesis by inhibiting topoisomerase II (anti-tumor antibiotics like doxorubicin; or plant alkaloids like etoposide), purine or pyrimidine analogues that are antagonists to DNA synthesis (anti-metabolites such as gemcitabine), binding to microtubular proteins and causing mitotic arrest (taxanes such as docetaxel), or interfering with the topoisomerase I functionality (camptothecins such as irinotecan) (1).

Chemotherapy drugs target DNA synthesis and mitosis in order to destroy cancer cells; however, since these processes are not exclusive to cancer cells but are rather intrinsic to all proliferative cells, chemotherapy cannot distinguish between normal and cancer cells and treatment is often burdened with undesired side effects – particularly in tissues with rapidly growing cells such as cells from the hair follicles or the gastrointestinal tract (70).

1.1.4.2 Targeted therapies

For decades, the hallmark for disseminated cancer treatment has been cytotoxic chemotherapy. However, as discussed earlier, chemotherapy treatment (CTx) is associated with undesired toxicity due to non-specific targeting of rapidly dividing cells. As a result, patients experience a variety of side-effects, including alopecia, gastrointestinal symptoms, and myelosuppression (71). For this reason (and the limited efficacy of CTx), in the last decade, targeted therapies have gained momentum and are now a component of treatment for many cancer types, including breast, pancreatic, lung or colorectal cancers.

In contrast to chemotherapy, targeted therapy blocks tumor proliferation by specifically targeting molecules required for cancer development and growth (71). Though some of these targets may be present in normal tissue, they are often overexpressed, mutated or otherwise unique in malignant tissue (71). There are two major classes of targeted therapies: monoclonal antibodies and small inhibitory molecules. For this introduction, we will focus on the monoclonal antibody class.

1.1.4.2.1 Monoclonal antibodies

Monoclonal antibodies (mAbs) are large (150 kDa), circulating proteins that bind to extracellular antigens expressed on the surface of cells. In the context of treatment for solid tumors such as breast or colorectal cancer, mAbs often target extracellular components supporting tumor progression. Example targets include epidermal growth factor receptors (EGFR/HER1 and EGFR2/HER2) and vascular endothelial growth factor (VEGF) (71). Monoclonal antibodies can exert their anti-tumor effect by causing immune-mediated cell killing (including complement-mediated cytotoxicity (CDC), antibody-dependent cellular cytotoxicity (ADCC) or T cell function regulation); by directly interfering with the interaction of receptors and their ligands (receptor blockage or agonist activity); or by delivering a cytotoxic payload to the tumor cell (antibody-drug conjugates) (72-74).

The nature of the target antigen determines the efficacy and safety profile of therapeutic mAbs. The ideal tumor antigen should be accessible and abundantly and homogeneously expressed on cancer cells exclusively. In addition, antigen internalization (especially for cell surface expressed targets) is also an important feature to consider. If the intended mechanism of action is ADCC or CDC, then slow internalization of the antigen is desired to allow immune effector components to recognize the antigen-mAb complex. In contrast, if the desired mechanism of action is the delivery of a cytotoxic payload, then good antigen internalization is required to effectively deliver the toxin to the cell machinery (75).

In addition, there are a few characteristics to consider to successfully develop mAbs for the clinic, such as the analysis of antigen expression on normal and malignant tissues, the effect of

the mAb on immune and signaling pathways, antibody chimerization and humanization, and the *in vivo* therapeutic effect of the mAb alone or conjugated to a toxic agent (72,74,76-80).

1.1.4.2.2 Antibody-drug conjugates (ADC)

Antibody-drug conjugates (ADCs) are mAbs linked to anti-tumor toxic agents. Thus, ADCs can be considered as "biological vehicles" that transport supertoxic agents to tumor cells that, otherwise, would not be suitable for therapy due to their high toxicity.

The mechanism of action of ADCs is based on a series of extra- and intracellular steps: after intravenous administration, ADCs circulate in the bloodstream as inactive agents until they reach their target antigen on the surface of tumour cells. Once bound, the antigen-ADC complex is internalized via receptor-mediated endocytosis that culminates with the fusion of the prodrug-containing endosome with an activated lysosome. Here, the mAb-toxin covalent linker is degraded thanks to the acidic and proteolytic environment of the lysosome, resulting in the release of the toxic payload (81). The ADC payload can exert cytotoxicity by either inducing DNA damage (i.e. DNA double-strand breakers or intercalators), or microtubulin disruption (i.e. auristatins and maytansines). In addition, increased tumor cytotoxicity might be achieved with a phenomenon called bystander effect in which the freed payload, reactive oxygen species or cytotoxic metabolites are able to diffuse, penetrate and kill neighbouring tumor cells and vessels (82).

The clinical efficacy of ADCs is determined by the target antigen, the antibody component, the cytotoxic payload and the linker. As with mAbs, an ideal ADC target should have relatively high

levels of expression, be located in the extracellular compartment and not be secreted into circulation. In addition, ADCs targets are required to have good internalization since the toxin delivery is dependent on it. However, in contrast to unconjugated therapeutic mAbs, low levels of antigen expression in healthy cells is sufficient to induce ADC activity and thus, tumor-antigen specificity is essential for ADC safety. Additionally, since the ADCs mode of action is through internalization and release of a toxin payload, targets are not required to intervene in tumor cell growth or survival pathways (83). Lastly, an advantage of ADC is that, since ADCs can possess bystander killing-effect, they can circumvent the lack of homogeneous target expression that would otherwise be a concern for conventional mAb therapy (84-86).

ADCs and mAbs share similar considerations regarding the antibody component. In both cases, the antibody is required to have high specificity to the target to minimize toxicity. In addition, good antibodies (and ADCs) should have low immunogenicity to avoid elimination before reaching their target. One approach to reduce immunogenicity is to generate humanized antibodies, where the hypervariable loop regions of a fully human antibody (i.e. an immunoglobin peptide sequence with a human-native repertoire) are replaced with peptides from the specific non-human antibody of interest, resulting in an 85 to 90% human antibody (87). Lastly, high antibody affinity is also desired for the antibody component of an ADC since it can affect receptor-antibody mediated internalization (83).

Regarding the cytotoxic payload, there are a few criteria to be considered. ADCs can only carry a small number of toxic payload (commonly 4 to 8 drugs per antibody) and therefore, it is bound to be highly toxic to eradicate a large number of tumor cells (88). In addition, such toxic payload

must have minimal immunogenic potential. For this reason, small molecule anti-cancer drugs are the most common class since they show less immunogenicity in circulation than glycol/peptide cytotoxic agents (83).

Lastly, when choosing a linker, one should consider the conjugation site, drug-to-antibody ratio (DAR) and the linkage stability. Additionally, linkers can also be classified as cleavable, which are to be cleaved immediately after internalization (89,90), and non-cleavable, which are designed to remain stable until the antibody degrades in the lysosome (91). Though there are several linkers available for the generation of ADCs, about 50% of ADCs in clinical development are using the valine-citrulline peptidyl (Val-Cit) linker.

1.1.4.2.3 Limitations of antibody therapy

One big limitation on the usage of antibodies and their derivatives as therapeutics has to do with their pharmacokinetics and their ability to penetrate tumor tissue. Whereas antibodies are very long lasting in the blood, only about 20% of the administered dose ends up interacting with the tumor (92). Antibody uptake by the tumor depends on a delicate balance between the antibody pharmacokinetics and its efficient penetration and retention within the tumor tissue. Various antibody characteristics influence this balance, including molecular size and affinity. As mentioned before, antibodies are large (150 kDa) that have very long half-life in the serum. This is due to their large size exceeding the renal filtration threshold (70 kDa), and their ability to interact with various cell surface receptors via their Fc region, the most important being the neonatal Fc receptor (FcRn), a key regulator of IgG pharmacokinetics. FcRn is expressed on the surface of several cells such as vascular beds (including the blood-brain barrier), monocytes,

macrophages, intestinal epithelium, and glomerular filter (93). However, even though these factors that promote IgG longevity in circulation can be advantageous to increase IgG half-life in circulation, they can also represent a major setback to reach the antibody target, especially in solid tumors. The ability of an antibody to penetrate tissue is a crucial parameter, especially when treating solid tumors. Solid tumors are characterized by having poor vasculature and high interstitial fluid pressure. Consequently, therapeutic antibodies need to diffuse against this pressure gradient to penetrate the tumour tissue, and such diffusion is inversely correlated with molecular size (92).

Counterintuitively, another factor that can negatively impact tumor penetration is high affinity for the antigen of interest (94). The higher the affinity, the stronger the binding when antibodies first encounter their target. However, if high levels of the antigen are expressed in the periphery of the tumor, a high affinity antibody may accumulate in the tumor periphery until all antigen molecules are saturated. By contrast, medium affinity antibodies are released from this first antigen encountered at a rate that allows them to penetrate deeper into the tumor core, leading to a higher tumour uptake. This process is called the binding site barrier effect (95).

Though a few factors need to be carefully considered in the development of therapeutic antibodies and their derivatives, their introduction to the clinic has revolutionized the treatment of some types of cancers, thus highlighting the need to continue to investigate their complexity (81). The future promise of antibody therapeutics lies in the discovery of new targets and antibody structural optimization (75).

1.2 Podocalyxin in cancer

1.2.1 Basic overview of podocalyxin

Podocalyxin (Podxl), also known as TRA-1-60, TRA-1-81, gp135, gp200, PCLP1, MEP21 and GCTM2, is a member of the CD34-related cell surface sialomucin proteins, together with CD34 and endoglycan (96-98). Podxl is encoded by an 9-exon gene (*PODXL*) resulting in a 150-165 kDa single-pass transmembrane protein featuring an extracellular heavily glycosylated and sialylated proline-, serine- and threonine-rich mucin domain, a cysteine-bonded globular domain, and a juxtamembrane. The intracellular domain has a highly conserved cytoplasmic tail containing a juxtamembrane ezrin-binding site and a C-terminal PSD-95/DIg/ZO-1 (PDZ)-domain binding site terminating with an aspartate-threonine-histidine-lysine (DTHL) amino acid motif (**Figure 1.2**) (96,97,99).

Podxl has three known intracellular binding partners: the PDZ-domain proteins Na^+/H^+-exchanger regulatory factor (NHERF) 1 and 2, and ezrin (100-102). NHERF1/2 bind to Podxl through its DTHL C-terminal residues and act as scaffolding proteins linking Podxl to the actin cytoskeleton via ezrin (101) and, potentially, to other PDZ-binding partners such as the epidermal growth factor receptor (EGFR) (103). Ezrin is a member of the ezrin-radixin-moesin (ERM) family that, when activated, interacts with both transmembrane proteins and the actin cytoskeleton; it can bind to Podxl through NHERF, or via direct binding to the intracellular juxtamembrane region (12 amino acids) of Podxl (102). Importantly, ezrin is expressed in a variety of cancers where its presence is associated with poor outcome and enhanced metastasis, presumably by promoting cytoskeletal reorganization resulting in increased cell survival, motility, and invasion (104-106).

Despite being highly expressed during embryogenesis, Podxl expression in adult mice and humans is primarily restricted to podocytes (a specialized kidney epithelial cell), the vascular endothelia and a small subset of hematopoietic progenitors (99). Though it has been proposed that Podxl plays a role in trafficking of hematopoietic progenitor cells and the development of the lumen of tubular structures such as blood vessels, its only known essential role is as an anti-adhesive or “Teflon” in the development and maintenance of the kidney glomerular filtration apparatus (99,107).

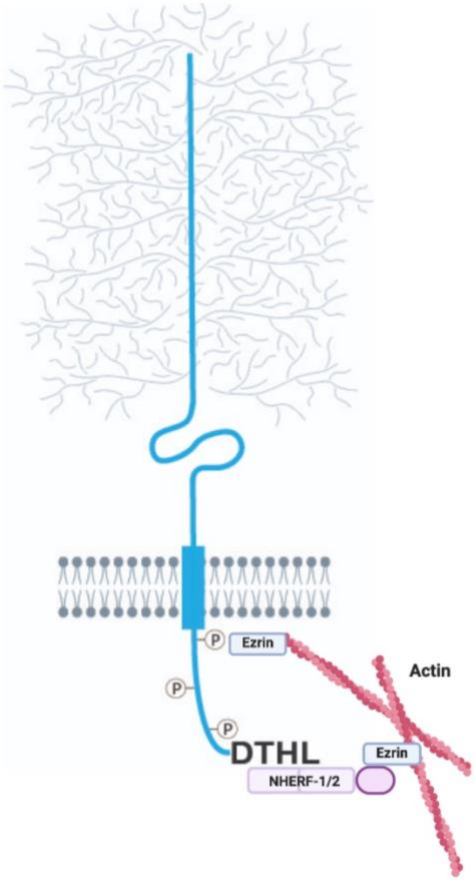

Figure 1.2 Structure of Podxl

Podxl extracellular domain contains a large O-glycosylated (branches) mucin domain followed by a cysteine globular domain and a juxtamembrane stalk. This is followed by a single pass transmembrane domain (blue rectangle), and a cytosolic domain with putative phosphorylation sites, a juxtamembrane ezrin binding site and a C-terminal DTHL sequence for interaction with NHERF1/2. Partially created with BioRender.

1.2.2 Podocalyxin as a prognostic marker in cancer

Podxl expression has been associated with increased tumor aggressiveness and poor outcome in a variety of cancers and thus, it has been proposed as a cancer prognostic marker and a predictor of patient outcome (108,109). Here we provide a brief overview of the prognostic value of Podxl in various human cancers.

Several studies have investigated the prognostic value of Podxl in over 10 types of cancer, most of them of epithelial origin, including breast (110,111), renal cell (112), colorectal (113-116), ovarian (117), urothelial (118), pancreatic (119-123), esophageal (124), gastric (125,126) and lung (127). Podxl is also a strong prognostic indicator in glioblastoma (128). In these studies, high Podxl expression is consistently associated with poor patient survival. Additionally, studies in pancreatic adenocarcinoma, ovarian, and colorectal carcinoma have investigated the relation between localization of Podxl expression and survival and demonstrated that cell-surface expressed Podxl correlates with poor patient survival (113,114,119,120,129) even in cancers where overall Podxl expression does not predict decreased survival (117).

Lastly, a few studies have suggested Podxl is a theranostic marker that can be used to help predict which colorectal cancer patients would benefit from adjuvant chemotherapy. In these studies, patients expressing high levels of Podxl on their tumors benefited from adjuvant chemotherapy, whereas survival of patients with low Podxl-expressing tumors was not significantly improved upon treatment, thus suggesting that assessment of Podxl expression in colorectal cancer could help guide treatment course (113,120).

Together, these studies show that Podxl expression is linked to advanced, poorly differentiated tumors with high incidences of metastasis, revealing Podxl as a promising prognostic biomarker for cancer (108,109). Since Podxl identifies tumors most likely to undergo progression, one could postulate an association between Podxl expression and enhanced tumorigenesis. Indeed, several studies have demonstrated that Podxl expression promotes cancer progression and metastasis (see section 1.2.3) and, thus, we hypothesize that Podxl is a potential candidate for targeted cancer therapeutics.

1.2.3 Insights into podocalyxin function in tumor progression

There are several steps in the metastatic cascade in which Podxl has been shown to promote progression. Here we briefly discuss the main processes where Podxl has been shown to be involved: promotion of tumor formation, cell dissemination and metastasis.

1.2.3.1 Podxl enhances tumor formation capacity

Podxl is a well-known marker of human pluripotent stem cells (hPSCs) and mouse embryonal stem cells (mESC) (130). Though highly expressed in these cell populations, as a ‘stem cell’ marker, Podxl expression is lost upon induction of cell differentiation (131,132). In the context of cancer, Podxl has been shown to be expressed in embryonal carcinoma (133), a malignant stem cell of testicular tumors, and on glioblastoma-derived stem-like cells (134). While Podxl expression is lost upon differentiation of glioblastoma (GBM) stem-like cells, it is present in GBM oncospheres where it is involved in cell proliferation and oncosphere formation (128). Additionally, Podxl-positive GBM cells had increased expression (compared to Podxl-negative cells) of stem cell markers SOX2, BMI1 and Musashi1.

Our previous work supports the idea that Podxl is expressed on stem-like breast cancer cells where it contributes to their tumorigenesis. We showed that decreased expression of Podxl on MCF7 and MDA-MB-231 breast cancer cells resulted in lower formation of tumorspheres (135). In this same study, using an MDA-MB-231 experimental lung colony forming assay, we showed that decreased Podxl expression resulted in lower metastatic nodules in the lung. While the size of the metastatic nodules was similar to those of the WT control, PODXL-deficient cells (Podxl shRNA knock-down cells) formed less metastatic nodules compared to the control, suggesting a lower frequency of stem-like, tumor-initiating cells (TICS) rather than impaired proliferation (136). Though further validation is required, these results suggest that Podxl is expressed in stem-like cancer cells where it enhances their tumor-forming capacity.

1.2.3.2 Podxl promotes cell dissemination and invasion

In general, tumor cells have decreased cell-cell and cell-extracellular matrix (ECM) interactions than normal cells because of changes in morphology and cytoskeletal abnormalities (137). Acquisition of motility and invasiveness properties is tightly linked to loss of adherence to neighboring cells and the ECM (138). Previous studies have shown that overexpression of Podxl on MCF7 cells causes β1-integrin re-localization and expansion of the apical membrane domain, which may weaken the basolateral adhesion and promote cell detachment (110,139). Consistently, MDA-MB-231 and MCF7 cells expressing high levels of Podxl display impaired adherence to ECM substrates (110,135). Together, these studies suggest that overexpression of Podxl promotes cancer progression by facilitating tumor cell detachment from the primary tumor mass.

Recent studies using hepatocellular carcinoma and pancreatic adenocarcinoma cells show that Podxl promotes cell invasion by facilitating remodeling of the actin cytoskeleton (122,140). Indeed, Cheng-Wei et al. showed that Podxl promoted invasion and metastasis of breast cancer cells by facilitating the formation of invadopodia via its intracellular, C-terminal DTHL motif (141). Similarly, we showed that expression of Podxl on MCF7 breast cancer cells induces lamellipodia and collective tumor invasion (142). We demonstrated that expression of Podxl promotes cohesive epithelial tumor buds to invade the stroma and regional lymph node in a xenograft model. Further, reduction of Podxl expression on 4T1 mouse breast cancer cells resulted in decreased *in vitro* collective invasion. Additionally, we demonstrated that Podxl stimulates *in vitro* collective 2-D cell migration and 3-D invasion of MCF7 cells via ezrin and actomyosin-dependent contractility (142). Together, these studies suggest that Podxl promotes tumor progression by enhancing cell invasiveness through promoting the remodeling of the actin cytoskeleton though, to date, the underlying molecular mechanisms remains unclear.

1.2.3.3 Podxl promotes cancer metastasis

Lastly, it has recently been shown that Podxl can promote cancer progression by facilitating metastasis. In Snyder et al., we showed that Podxl enhances primary tumor growth and metastasis of xenografted MDA-MB-231 cells. In the same study, Podxl was shown to enhance metastasis (but not primary tumor growth) on a syngeneic tumor model. Additionally, experiments using a competitive experimental lung metastasis model with MDA-MB-231 cells suggest that Podxl promotes metastasis through the establishment of a favourable niche in the metastatic organ that fosters tumor growth (136). In this model, Podxl does not alter initial cell seeding (up to 7 days), but rather enhances the establishment of metastatic nodules.

Others have shown that modification of Podxl to display O-linked sialofucosyl oligosaccharides promotes adhesion of colorectal and pancreatic cancer cells to E- and L-selectins (but not P-selectin) (143,144). These studies hypothesize that Podxl, when bearing the appropriate glycosylation, can promote cancer progression by enhancing adhesion of tumor cells to E-selectin on the vascular endothelia, thus facilitating tumor extravasation. Indeed, a recent study showed Podxl to be involved in MDA-MB-231 cell extravasation into the lung parenchyma via an ezrin-dependent mechanism (39). In this study, Podxl's cytosolic domain, and specifically the juxtamembrane ezrin binding site, was essential for extravasation of MDA-MB-231 cells into the lung parenchyma. This study proposes that tumor cell extravasation occurs within 24 hours of seeding the lungs. However, these data are contradictory with our previous results showing that Podxl is not required for up to 7 days of initial seeding (136). Moreover, our studies using systemic treatment with the human-specific Podxl monoclonal antibody (PODO83) in mice with an established MDA-MB-231 tumor burden suggests that Podxl's extracellular domain is critical for the establishment of lung metastasis (although this does not preclude a role for Podxl's ezrin binding function).

Together, these studies suggest a multifaceted role for Podxl in promoting tumor progression, whereby Podxl is capable of enhancing the intrinsic tumorigenesis capacity of cancer cells by increasing their tumor-forming ability; promoting cell detachment (from the primary tumor), motility and invasion within the stroma; facilitating adhesion to the vascular endothelium and extravasation; and promoting the establishment of a favorable metastatic niche. However, further studies are required to delineate the molecular mechanisms by which Podxl drives tumor progression and metastasis *in vivo*.

1.2.4 Overview of potential therapies targeting podocalyxin

Despite the potential of Podxl as a therapeutic target, at the time this project was started, only two studies had demonstrated that targeting Podxl could have a potential clinical application.

One example is the use of anti-Podxl antibodies to select against undifferentiated human pluripotent stem cells (hPSCs). Though undifferentiated hPSCs are an important research and clinical tool, they also carry the intrinsic risk of teratoma formation during cell therapy if non-differentiated cells are not carefully removed. Thus, identification and elimination of these cells is critical for future clinical cell therapies (145). Undifferentiated hPSC are characterized by the expression of cell-surface markers, which are lost upon differentiation. These include TRA-1-60, TRA-1-81, GP200 and mAb84, all of which constitute distinct markers expressed on the Podxl core protein. So far, two studies have shown the use of anti-Podxl antibodies to identify and eliminate undifferentiated hPSCs (130,145). Though insight into the mechanism of action was not provided, in both studies, the respective anti-Podxl antibodies caused cytotoxicity of undifferentiated hPSCs upon cell treatment, thus demonstrating that Podxl can successfully be targeted using an antibody-based agent.

At the start of this project, only one study performed in collaboration by us and others, demonstrated that targeting Podxl could delay breast cancer progression. In this study, we developed a novel anti-Podxl antibody, PODOC1 (thereafter named PODO83), and showed that systemic treatment with PODO83 reduced primary tumor growth of MDA-MB-231 cells subcutaneously injected into NSG mice (136). Further, PODO83 treatment in mice with an established tumor burden decreased the metastasis in the lungs. Thus, this study highlights

PODO83's epitope on Podxl as a driver of metastasis and demonstrates, for the first time, that Podxl expressed on cancer cells can successfully be targeted to decrease tumorigenesis, therefore validating Podxl as a potential therapeutic target.

However, pre-clinical assessment of PODO83 is required to determine if it is a suitable candidate for clinical development. Further investigation into PODO83's epitope is needed to determine the molecular mechanism by which is promoting cancer metastasis and, thus, to have a better understanding of PODO83's mechanism of action. Additionally, assessment of PODO83's epitope distribution within primary or metastatic tumors is required to determine the extent of potential application that a PODO83-based therapeutic could have. Lastly, though NSG mice showed no sign of toxicity when treated with PODO83, since Podxl is highly expressed in the kidney podocytes and vascular endothelium, further studies carefully looking into toxicity are required to assess any potential side-effects from Podxl-based targeted therapies.

1.3 Research aims

The literature presented here highlights the lack of understanding of the molecular mechanisms underlying tumor progression. It also demonstrates the need to identify new biomarkers that can be used for prediction of prognosis and treatment of cancers to improve patient outcomes. Podocalyxin is highly expressed in many cancers and our previous work demonstrated that it has a functional role in tumor progression, however the underlying mechanisms by which it exerts these effects remain unclear. Targeted immunotherapies against tumor-specific antigens have many advantages in the treatment of cancer and represent a relatively new therapeutic approach. Here, we present two novel antibodies targeting podocalyxin, PODO83 and PODO447 which we

examine in pre-clinical models and validate their use as diagnostic and therapeutic tools either alone or as antibody-drug conjugates.

The aims of this work are:

Aim 1: Understand the role of Podxl in tumor growth and metastasis using CRISPR/Cas9 technology and Podxl-deletion mutants. *Specifically, we wish to understand which domains of the Podxl protein are important for promoting tumor progression.*

Aim 2: Understand the mechanism of action of the function-blocking PODO83 antibody and its clinical potential. *Specifically, we wish to identify the binding epitope of PODO83 in the extracellular domain of Podxl, and to assess PODO83's antigen distribution across malignant and healthy tissues.*

Aim 3: To identify a tumor-specific anti-Podxl antibody and develop a Podxl-based cancer therapeutic. *We hypothesize that Podxl displays-tumor associated glycoepitopes that can be targeted with monoclonal antibodies.*

Chapter 2: Investigation of the functional role of podocalyxin in promoting tumor progression.

2.1 Synopsis

Podocalyxin (Podxl) is a CD34-related sialomucin involved in the regulation of cellular polarity, adhesion, and migration. Podxl is overexpressed in many epithelial cancers and its presence is linked with poor patient survival. In addition to identifying highly aggressive tumor types, Podxl plays a key role in the formation of primary tumors and metastasis. However, the underlying molecular mechanism by which Podxl promotes tumor progression is yet to be elucidated. Here we describe the generation and characterization of CRISPR/Cas9 *PODXL*-KO cells and investigate their use to study Podxl's role in tumor progression. We show that MDA-MB-231 cells are highly unstable after genetic manipulation and clonal selection and therefore may not constitute a good model for the study of molecular mechanisms. In addition, we demonstrate for the first time a role of Podxl in enhancing primary tumor growth in ovarian carcinoma.

2.2 Introduction

Though cancer mortality has greatly improved over the last three decades, it is still one of the leading causes of death worldwide (146,147). In Canadian women, breast and ovarian cancer account for almost 20% of all cancer deaths (148), hence there is an urgent need to elucidate the underlying mechanism of cancer progression in order to identify molecular targets that can be used to develop new treatments.

Podxl is a highly glycosylated sialomucin expressed by several cancers, with most of them being epithelial in nature. The presence of high levels of Podxl in these cancers correlates with poor patient survival (108,109). However, besides identifying a subset of aggressive cancers likely to undergo progression, little is known of the functional role of Podxl in tumorigenesis.

Recent studies (ours and others) clearly demonstrate that Podxl functionally promotes breast cancer progression and metastasis. Experiments using Podxl-overexpressing MCF7 human breast cancer cells demonstrated that high levels of Podxl expression result in altered morphogenesis and disrupted adherence to neighboring cells and the ECM (110,141). In addition, Graves et al. showed that Podxl overexpression *in vitro* and *in vivo* induces collective tumor budding and invasion of MCF7 and 4T1 murine breast cancer cells (142).

Moreover, through genetic knock down experiments we showed that Podxl enhances primary tumor growth and metastasis of xenografted MDA-MB-231 cells (136). In the same study, we showed that Podxl enhances metastasis (but not primary tumor growth) in a syngeneic mouse tumor model. In addition, experiments using a competitive experimental lung metastasis model with MDA-MB-231 tumor cells suggest that Podxl facilitates the finding of a favourable metastatic niche that fosters tumor growth (136). In these experiments, we found that Podxl did not alter initial cell seeding, but rather enhanced the establishment of metastatic nodules. This study was performed using MDA-MB-231 cells stably transfected with a drug-selectable knockdown construct that transcribed Podxl-silencing shRNA (*PODXL*-KD) to suppress Podxl expression. Since silencing of Podxl expression was not completely efficient in these cells, one caveat from this study is that *PODXL*-KD cells still retained a low level of Podxl expression which could mask or diminish the effect of Podxl in carcinogenesis. Moreover, Podxl expression

in these cells begins to return after 3 days in the absence of drug selection. Consequently, MDA-MB-231 *PODXL*-KD cells regain Podxl expression to WT levels after 14 days *in vivo*. Since MDA-MB-231 *in vivo* subcutaneous xenograft models take between 30 to 35 days to reach experimental endpoint, future studies using cells with a complete and sustained depletion of Podxl expression are required to assess Podxl true long-term role in tumor growth and metastasis.

Some efforts have been made in understanding the mechanisms by which Podxl promotes cancer progression. Using MCF7 cells, Nielsen et al. showed that Podxl's C-terminal DTHL residues are responsible for the recruitment of $Na^{(+)}/H^{(+)}$ exchange regulatory cofactor 1 (NHERF1) to the apical membrane, suggesting that Podxl's cytosolic domain may be involved in signal transduction via NHERF1. In the same study, Podxl's ectodomain was shown to be essential for microvillus formation, suggesting that the extracellular domain of Podxl is important for the disruption of cell adhesion and cell dissemination. Further, the therapeutic efficacy of a novel antibody we developed, PODO83, which targets the core peptide sequence in Podxl's extracellular domain (see Chapter 3), suggests that Podxl's extracellular domain plays a critical role in cancer metastasis (136).

To gain further insights into the molecular mechanisms by which Podxl promotes tumor growth and metastasis we used the CRISPR/Cas9 approach to irreversibly delete endogenous expression of Podxl and replace it with different Podxl-deletion mutants.

2.3 Materials and Methods

2.3.1 CRISPR/Cas9 plasmid design

To establish MDA-MB-231 and SKOV3 *PODXL*-KO cells we followed a two-cut approach using clustered regularly interspaced short palindromic repeat (CRISPR)/CRISPR-associated nuclease 9 (Cas 9) technology. Target sites flanking the first exon were selected (combined cut size of 753 bp). Target sequences were designed using the Zhang's lab online CRISPR design tool (http://crispr.mit.edu). Oligonucleotides used to generate the guide RNAs (gRNAs) to edit the human *PODXL* gene were: g-PODXLup-FW (5'- caccgCCGCCCTGGAGCGCGACGGG-3'), g-PODXLup-RV (5'-aaacCCCGTCGCGCTCCAGGGCGGc-3'), g-PODXLdw-FW (5'-caccgGTGGAGACGAATCTACGCCC-3'), g-PODXLdw-RV (5' aaacGGGCGTAGATTCGTCTCCACc 3'). Each target's pair of annealed oligonucleotides was cloned into pSpCas9(BB)-2A-GFP (PX458) gRNA expression vector (Addgene #48138; http://n2t.net/addgene:48138 ; RRID:Addgene_48138) following digestion with *Bbs*I (10 U/µl, ThermoFisher Scientific, #ER1011) as previously described (149). These constructs were denominated pX458-Cas9-gPODXLup and pX458-Cas9-gPODXLdw, respectively. Sequences of all constructs were confirmed by Sanger sequencing.

2.3.2 Cell culture

MDA-MB-231 and SKOV3 were obtained from the American Tissue Culture Collection (ATCC). Breast cancer MDA-MB-231 cells were grown in DMEM (Gibco, #11965-092) supplemented with 10% FBS and 10 U/ml penicillin and streptomycin (P/S) (Gibco, #15140-122). Human ovarian cancer SKOV3 cells were grown in DMM F-12 with 15 mM HEPES

(Sigma, #D6421) supplemented with 10% FBS, 0.2 mM L-glutamine (Gibco, #25030-081) and 10 U/ml P/S. All cell lines were maintained at 37°C, 5% CO_2 and high humidity.

2.3.3 Generation of the CRISPR/Cas9-mediated *PODXL*-KO cells

MDA-MB-231 and SKOV3 cells (5 x 10^5) were co-transfected with 2 μg of both pX458-Cas9-gPODXLup and pX458-Cas9-gPODXLdw using Lipofectamine™ 3000 Transfection Reagent (ThermoFisher Scientific, #L3000015). Two days after transfection, cells were sorted for GFP-expression. Three days post-sorting, cells were single-cell cloned in a 96-well plate. After 3-4 weeks, single colonies were divided in half; one half was used for propagation and colony maintenance while the other was used to assess the *PODXL* locus. A 983 bp fragment including the segment flanked by the gRNA target regions was PCR-amplified from genomic DNA using PODXL-CRISPR4-FW (5'-CTCCTCCCGAGTGGAGAGT-3') and PODXL-CRISPR4-RV (5'-CTCCGGATTTGCTCGTAGTG-3') primers. PCR products were verified using gel electrophoresis (**Appendix A.1**). Colonies with a 230 bp amplicon were selected and *PODXL* expression was assessed using immunoblotting and flow cytometry. Populations within each colony were sorted to enrich for cells that were positive (WT) and negative (*PODXL*-KO) for *PODXL* expression.

2.3.4 Flow cytometry

Cells were washed 1X with Ca^{2+}- and Mg^{2+}-free HBSS (Gibco, #14170-112), incubated for 1-2 min at 37°C in a 0.25% trypsin solution, quenched with complete growth media, then centrifuged for 4 min at 394*g*, washed 2X with FACS buffer (PBS, 2 mM EDTA, 5% FBS, 0.05% sodium azide) and transferred to a 96 well 'v' bottom plate. Cells were resuspended in 100 μl blocking

buffer (FACS buffer, 1 μg/ml of anti-CD16/CD32 (clone 2.4G), 2% rat serum) for 20 min at 4°C in the dark, then spun at 394*g* for 4 min and incubated in 100 μl primary antibody (Ab) solution for 30 min at 4°C in the dark. Goat anti-human Podxl (1 μg/ml, R&D Systems, #AF-1658) and rabbit PODO83 (136) (2 μg/ml) were used to detect Podxl. Goat (1 μg/ml, R&D Systems, #AB-108-C) or rabbit IgG (5 μg/ml, Vector Laboratories, #I-1000-5) were used as isotype controls. Next, cells were washed 3X with FACS buffer and resuspended in 100 μl of secondary Ab solution (Alexa Fluor 647 (AF-647) chicken-anti-goat (2 μg/ml, Invitrogen, #A-21469) or AF-647 donkey-anti-rabbit (2 μg/ml, Invitrogen, #A31573)) for 30 min at 4°C in the dark. Cells were washed 2X with FACS buffer and resuspended in FACS buffer containing propidium iodide (PI) (0.5 μg/ml, Life Technologies, #P3566). All flow cytometry data were acquired using a BD LSRII and analyzed using FlowJo™ software (BD Biosciences, Ashland).

2.3.5 Western blotting

Cells were grown to 90% confluence, washed 2X with cold PBS and incubated in cold TNE buffer for 5min. Next, cells were scraped using a cell lifter in TNE buffer and spun at 394*g* for 4 min. Cells were rinsed 2X with PBS, transferred to a 1.5 ml microfuge tube and spun at 13,000*g* for 2 min. Cells were then resuspended in 600 μl of RIPA lysis buffer (150mM NaCl, 50mM Tris pH 7.4, 5mM EDTA, 1.0% NP-40, 0.5% sodium deoxycholate, 0.1% sodium dodecyl sulphate (SDS) and protease inhibitor cocktail (Calbiochem, Darmstadt, Germany)). Cells in lysis buffer were left on ice for 10 min, then passed through an 18G needle syringe and left on ice for an additional 10 min, followed by centrifugation at 13,000 g for 20 minutes. The supernatant was transferred to a new microfuge tube, and total protein concentration was

determined using the BCA assay (Pierce, Rockford, IL) according to the manufacturer's instructions. Equal amounts of protein were separated by SDS-polyacrylamide gel electrophoresis (PAGE) and transferred onto polyvinylidene fluoride (PVDF) membranes (Biorad, Hercules, CA). Membranes were blocked for 1 hour in Odyssey® blocking buffer (LI-COR, #927-4000) at room temperature, then incubated with primary antibody overnight at 4°C. All primary antibodies were prepared in Odyssey® blocking buffer. Membranes were probed with goat-anti-human Podxl (1μg/ml; R&D Systems, #AF-1658) and mouse-anti-β actin as loading control (0.2μg/ml; Ablab UBC Antibody Facility, Vancouver, BC). Membranes were washed with wash buffer (PBS + 0.1% Tween 20; 3X, 5 min), and incubated with secondary antibody for 1 h at RT and protected from light (0.05 μg/ml, IRDye® 800CW Goat anti-Rabbit IgG secondary antibody (LI-COR, #926-32211) or IRDye® 680RD Donkey anti-Mouse IgG secondary antibody (LI-COR, #926-68072)). The membrane was then washed with wash buffer (3X, 5 min) protected and protein was visualized using a LI-COR Odyssey imaging system (LI-COR, Lincoln, NE).

2.3.6 Tumorsphere assay

MDA-MB-231 cells were harvested as follows: adherent cells were rinsed with 5ml of Ca^{2+}-, Mg^{2+}-free HBSS and lifted using a cell scraper. Cells were then spun at 394g for 4 min and resuspended in 5ml of complete Mammocult™ media (1/10 dilution of MammoCult™ proliferation supplement (#05620), 4 μg/ml heparin (#07980) and 0.48 μg/ml hydrocortisone (#07925) in MammoCult™ basal medium (#05620), StemCell Technologies). Viable cells were counted using trypan blue stain. MDA-MB-231 (5×10^3) cells were seeded in triplicate in 2 ml of complete MammoCult™ medium in ultra-low adherent six-well plates. Cells were incubated

for seven days without disruption under standard cell culture conditions (37°C in 5% CO_2). On day 7, tumorspheres were manually counted using a transparent counting grid. Only spheres with 12 or more cells were counted. Average tumorsphere forming efficiency (%) was calculated as (number of tumorspheres / number of cells seeded) x 100, and statistical analysis was performed using one-way ANOVA followed by Bonferroni's post-test in GraphPad Prism software. A *P* value less than 0.05 was considered statistically significant.

2.3.7 Secreted extracellular vesicle analysis

MDA-MB-231 (3×10^6) cells were plated in 10 cm tissue-culture-treated petri dishes and cultured in 10ml of media supplemented with exosome depleted FBS. After 24 h, culture media was reduced to 4 ml. 48 h from initial seeding, the 4ml of culture media were harvested and centrifuged at 3,000 *g* for 15 min to remove cells and debris. Debris-free supernatant was then transferred to a new tube and ExoQuick Exosome Isolation reagent was added at 5:1 media to ExoQuick ratio (System Biosciences, #EXOTC10A-1). The culture media/reagent mixture was mixed to a homogeneous solution and left to incubate overnight at 4 °C. Samples were then centrifuged at 1,500 *g* for 30 min at RT and supernatant was discarded. Pellets were resuspended in 200 μl of 0.02 μm-filtered PBS and extra cellular vesicles were analyzed using the NanoSight instrument. Statistical analysis was performed using one-way ANOVA followed by Bonferroni's post-test in GraphPad Prism software. A *P* value less than 0.05 was considered statistically significant.

2.3.8 Mice

Tumor model animal experiments were carried out using 6-12-week-old female NOD.Cg-*Prkdc*^{scid}*Il2rg*^{tm1Wjl}/SzJ (NSG) and NU/J (nude) mice obtained from Jackson's Laboratories (#005557 and #002019, respectively). Animals were bred in a clean, pathogen-free facility and all experiments were carried out under approved Canadian Council on Animal Care (CCAC) protocols.

2.3.9 Subcutaneous xenograft model of primary tumor development

MDA-MB-231 ($1x10^6$) or SKOV3 ($1x10^5$) cells were injected subcutaneously into the right flank of NSG or nude mice in a 1:1 solution of sterile Matrigel™ (BD Biosciences, #) and Hank's Balanced Salt Solution (HBSS) (Gibco, #). Tumor dimensions were measured twice a week with a manual caliper, and the tumor volumes (cm^3) were calculated by (($length \times width^2$)/2). Mice were sacrificed when tumors reached $1cm^3$ in size, and tumors were excised and fixed with 10% formalin for long term storage. Average tumor volume overtime was calculated and statistical analysis was performed using two-way ANOVA test in GraphPad Prism software. A *P* value less than 0.05 was considered statistically significant.

2.3.10 Re-expression of WT Podxl, on MDA-MB-231 *PODXL*-KO cells.

MDA-MB-231 (5×10^5) *PODXL*-KO cells were stably transfected with 2 μg of WT Podxl- or control-pTT22 using Lipofectamine™ 3000 Transfection Reagent (ThermoFisher Scientific, #L3000015), and maintained under puromycin selection (5 μg/ml, Gibco, #A1113802). Expression was analyzed using western blotting and flow cytometry, and cells were sorted to enrich for construct-expressing cells.

2.4 Results

2.4.1 *PODX*L-KO CRISPR/Cas9 design

Previous studies using *PODXL*-KD MDA-MB-231 cells showed Podxl to be involved in *in vivo* tumor growth and metastasis to the lung (39,136). However, the molecular mechanisms by which Podxl drives breast tumor progression and metastasis remain unclear. *PODXL*-KD MDA-MB-231 cells re-express WT-levels of Podxl expression after 14 days without drug selection (136), highlighting the need for a method to ***permanently*** inactivate (i.e., gene knock-out) Podxl expression in MDA-MB-231 cells to delineate the molecular mechanisms by which Podxl is promoting tumor progression. Here, we designed a strategy to ablate Podxl expression on MDA-MB-231 cells using clustered regularly interspaced short palindromic repeat (CRISPR)/CRISPR-associated nuclease 9 (Cas9) technology (149).

In order to ensure complete ablation of Podxl's expression, we chose to delete Podxl's first exon as well as its 5' UTR (**Fig 2.1**). To do that, we designed a two-cut approach with gRNAs guiding the Cas9 enzyme to perform a double-strand cut both upstream of the 5'UTR region and downstream of the first exon (combined cut size of 753 bp, **Fig 2.1**).

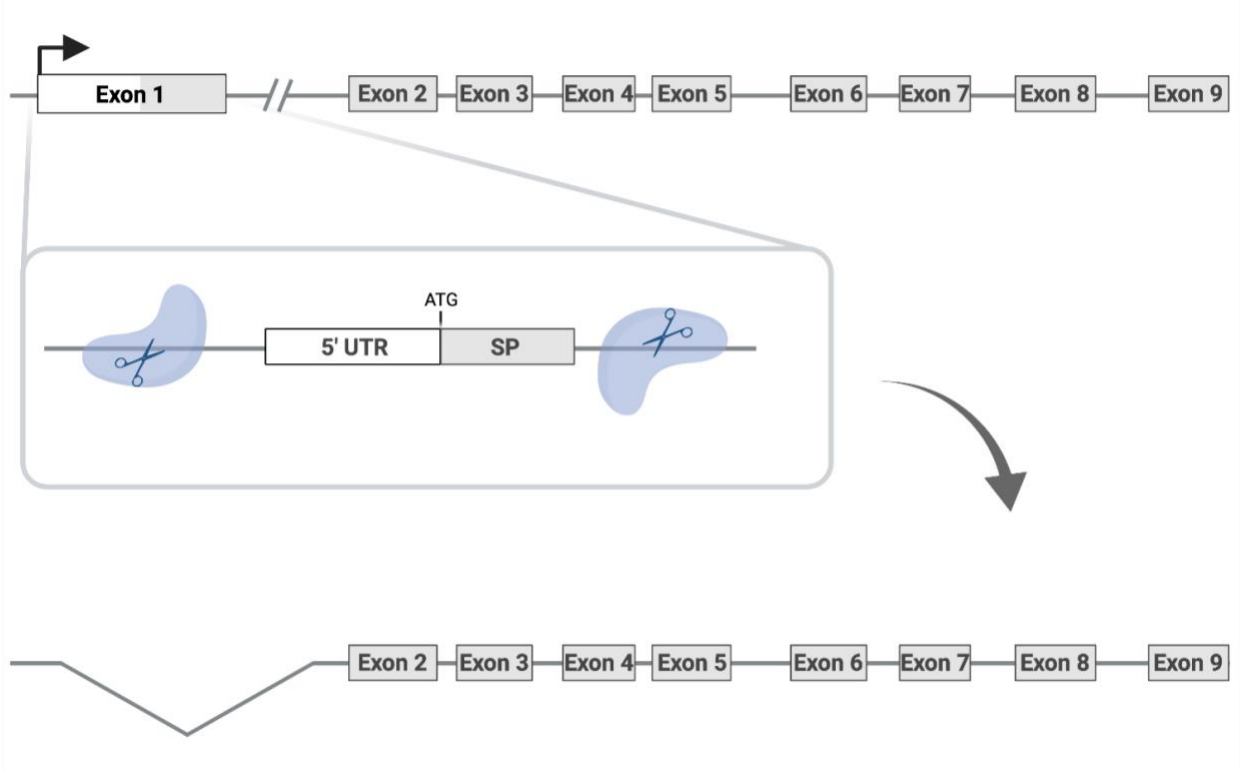

Figure 2.1 CRISPR/Cas9 strategy to ablate Podxl expression on MDA-MB-231 cells

Map showing the two-cut CRIPSR/Cas9 approach to ablate Podxl expression on MDA-MB-231 cells. Target sites were designed to flank *PODXL*'s 5'UTR and first exon, with a combined cut size of 750bp.

2.4.2 Isolation and validation of MDA-MB-231 *PODXL*-KO clones

To generate CRISPR/Cas9 *PODXL*-KO clones, MDA-MB-231 cells were transfected, sorted and single-cells were cloned in culture. Briefly, parental cells were transfected with plasmid constructs containing GFP, Cas9 and gRNAs sequences (see methods section 2.3.2). Successful cell transfection was confirmed via GFP expression using a fluorescent microscope and cells were sorted by flow cytometry to enrich for transfected (GFP-expressing) cells. Next, cells were serially diluted in a 96-well plate to achieve single-cell clones. Once single colonies were identified, successful deletion of Podxl's 5'UTR and first exon was assessed by genomic DNA polymerase chain reaction (PCR, **Appendix A.1**) and clones lacking the target fragment were selected for further validation.

Next, we performed flow cytometry to assess Podxl expression on selected colonies at the single cell level (**Appendix A.2**). Clones showing a Podxl-negative population (Colonies #1, #4, #19 and #23, **Appendix A.2**) were sorted to enrich for Podxl-expressing (WT) and Podxl-deficient (*PODXL*-KO) cells. After several rounds of sorting, two MDA-MB-231 *PODXL*-KO clones were selected based on their lack of Podxl expression by flow cytometry (**Fig 2.2 A**) and western blot (**Fig 2.2 B**)

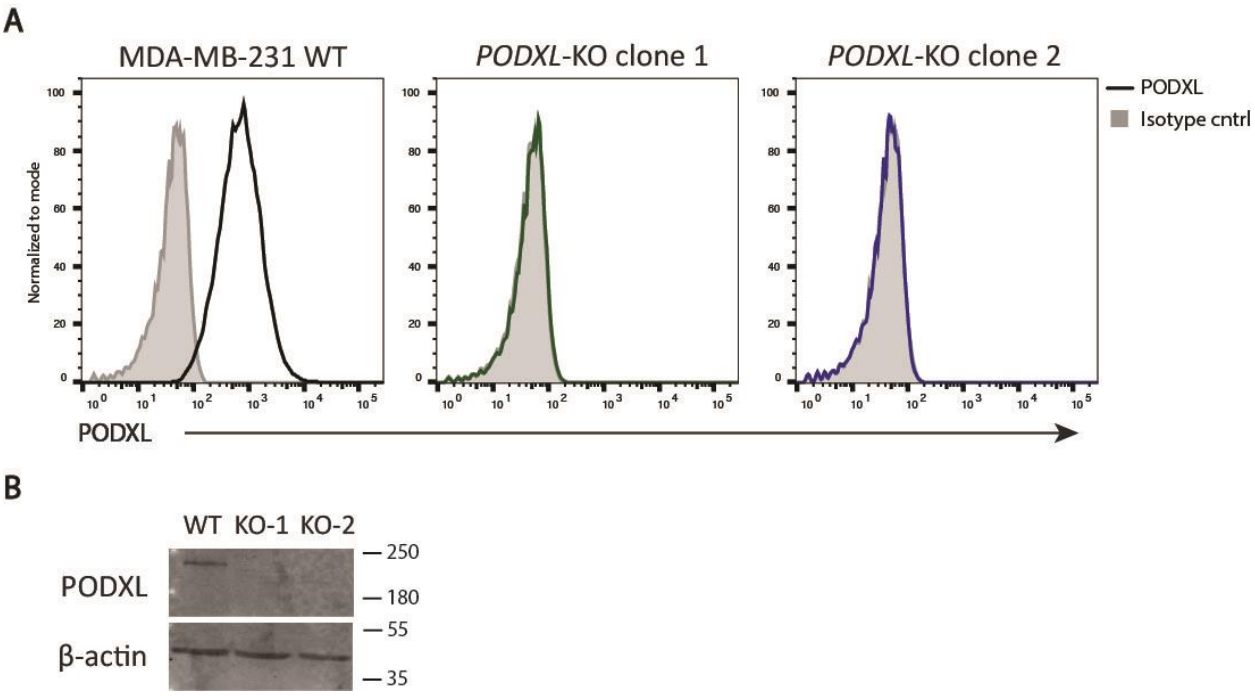

Figure 2.2 Validation of MDA-MB-231 PODXL-KO clones

Validation of selected MDA-MB-231 *PODXL*-KO clones. (**A**) Flow cytometric profiles showing Podxl cell surface expression on MDA-MB-231 WT and two *PODXL*-KO clones. (**B**) Western blot showing Podxl total protein expression on cell lysates from MDA-MB-231 WT and two *PODXL*-KO clones. Numerals indicate molecular weight marker positions (in kDa).

2.4.3 MDA-MB-231 *PODXL*-KO cells show decreased tumorgenicity *in vitro*

Previous studies have shown that, while Podxl does not alter cell proliferation, it increases tumorsphere-forming efficiency of breast cancer cells when cultured in anchorage-independent conditions (135,136,150) which, in the literature, has been taken as a crude measure of tumor "stem cell" or "tumor initiating cell (TIC)" activity (151,152). These studies were performed using Podxl-overexpressing MCF7 and MDA-MB-231 *PODXL*-KD cells. Since the newly generated MDA-MB-231 *PODXL*-KO clones completely lack expression of Podxl, we hypothesized that they would likewise lack an appreciable difference in *in vitro* proliferation but display impaired tumorsphere-forming capacity under similar culture conditions. As expected, *PODXL*-KO cells had similar proliferation rates as the vector control. Moreover, both *PODXL*-KO clones displayed significantly lower efficiency to form tumorspheres compared to WT cells ($P < 0.001$, **Fig 2.3 A**), thus confirming our previous results and suggesting that the newly generated *PODXL*-KO cells may have a decreased tumorigenic phenotype similar to the *PODXL*-KD cells.

Recent studies have shown that extracellular vesicles (EVs) secreted by cancer cells play an important role in cancer progression by promoting angiogenesis (153) and enhancing invasion (154). Indeed, Podxl was shown to be expressed on exosomes from highly metastatic breast cancer cells (155). Thus, we hypothesized that the MDA-MB-231 *PODXL*-KO cells would have decreased EV secretion. Briefly, EVs secreted by MDA-MB-231 WT and *PODXL*-KO cells were isolated from culture media and particle concentration was analyzed using the NanoSight instrument, which utilizes both light scattering and Brownian motion properties to determine particle size and concentration. As expected, both *PODXL*-KO clones displayed decreased EV

concentration compared to WT cells ($P < 0.001$, **Fig 2.3 B**). Since both tumorsphere formation and exosome secretion have been positively correlated with a highly-aggressive *in vivo* neoplastic phenotype, these data suggest that lack of Podxl expression could result in lower tumorgenicity of MDA-MB-231 cells.

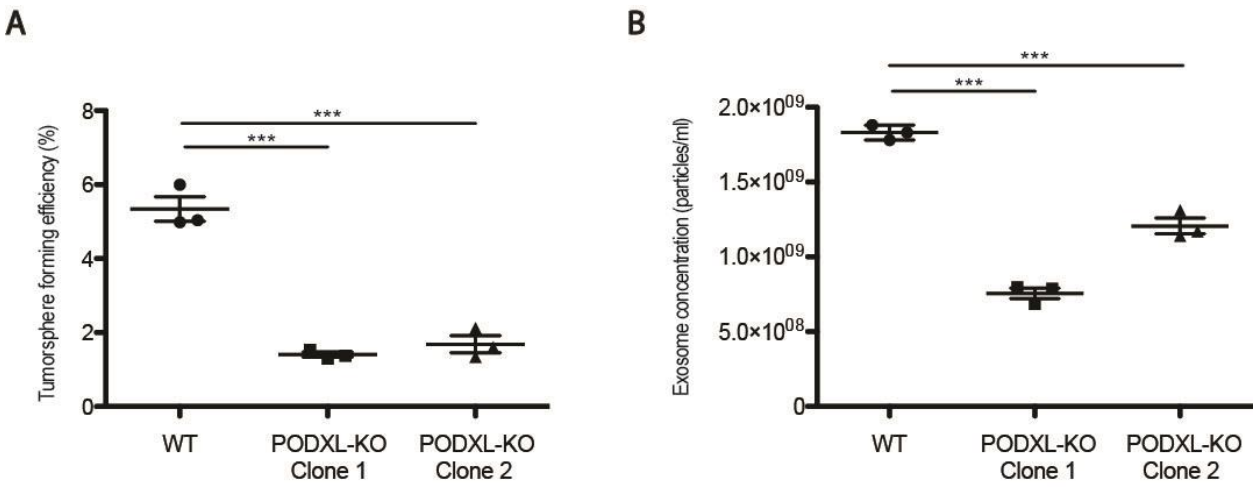

Figure 2.3 MDA-MB-231 PODXL-KO cells display lower tumorigenic phenotype *in vitro*.

In vitro validation of MDA-MB-231 *PODXL*-KO cells. (**A**) Tumorsphere-forming efficiency of MDA-MB-231 WT and both *PODXL*-KO clones ($P < 0.001$). (**B**) Extracellular vesicle concentration on the culture medium of MDA-MB-231 WT and *PODXL*-KO clones ($P < 0.001$). The data in A come from 1 experiment with three technical replicates per cell type. The data from B come from 1 experiment with three technical replicates per group. Statistical analysis was performed using one-way ANOVA test and a *P* value less than 0.05 was considered statistically significant. Error bars in all panels show SEM.

2.4.4 *PODXL* is required for MDA-MB-231 *in vivo* tumor growth

Previous studies using MDA-MB-231 *PODXL*-KD cells have shown Podxl to promote primary tumor growth and metastasis (135). Since the newly generated MDA-MB-231 *PODXL*-KO cells recapitulate the *in vitro* phenotype (attenuated tumorsphere-forming efficiency) previously observed with *PODXL*-KD cells, we hypothesized that the *PODXL*-KO cells would also display decreased neoplastic growth and metastasis in a xenograft model. We injected MDA-MB-231 WT and *PODXL*-KO cells into the right flank (subcutaneously) of NSG mice. WT tumors were palpable 16 days after injection, and tumor size reached experimental humane endpoint by day 34 (**Fig 2.4 A**). In contrast, neither *PODXL*-KO clone developed palpable tumors (> 0.1 cm^3) during the same timeframe (**Fig 2.4 A**). On day 34, animals were sacrificed, and tumors were resected. As shown in Figure 2.4 B, only mice injected with WT cells developed tumors, while animals injected with *PODXL*-KO cells showed no sign of tumor growth (**Fig 2.4 B**). Thus, these data suggest that deletion of Podxl expression in MDA-MB-231 cells results in a complete inhibition of primary tumor growth. This is a more robust phenotype than we previously observed with MDA-MB-231 cells transfected with an shRNA targeting Podxl, which retained some endogenous Podxl expression that returned to WT levels on tumor cells *in vivo* due to withdrawal of drug selection.

Due to the inability of both *PODXL*-KO tumor cell clones to grow *in vivo*, assessment of the role of Podxl in metastasis may require a different approach, such as an experimental model of metastasis were cells are injected intravenously, or a model where ectopic Podxl expression in tumor cells may be switched on and off conditionally.

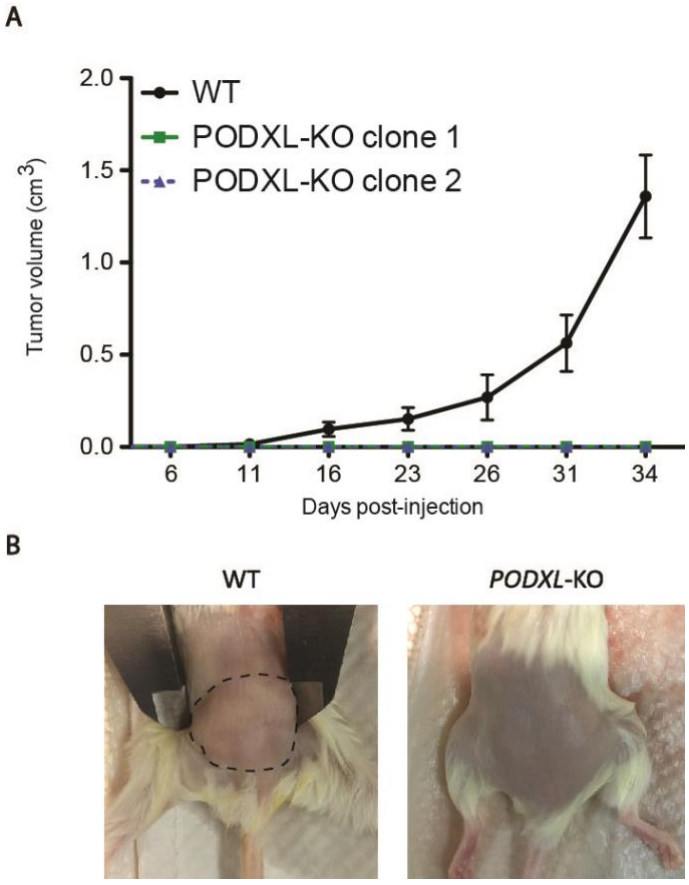

Figure 2.4 Podxl is critical for MDA-MB-231 primary tumor growth

A total of 1 x 10^6 MDA-MB-231 WT and *PODXL*-KO cells were subcutaneously injected into the right flank of NSG mice. (**A**) Tumor growth overtime of WT and *PODXL*-KO cells ($P < 0.0001$) (**B**) Representative pictures of WT and *PODXL*-KO tumors at time of resection. Dashed line delineates tumor edge. The data in this figure come from 1 experiment with 4 mice per group. Statistical analysis was performed using two-way ANOVA test and a *P* value less than 0.05 was considered statistically significant. Error bars represent SEM.

2.4.5 The phenotype of MDA-MB-231 *PODXL*-KO cells changed over time

Since our aim was to evaluate the molecular mechanism by which Podxl promotes tumor progression, we generated MDA-MB-231 *PODXL*-KO cells with the aim of re-expressing Podxl protein mutants to identify domains critical for tumor growth and metastasis. However, we noticed that the newly generated MDA-MB-231 *PODXL*-KO cells changed their behaviour (reverted) with progressive *in vitro* passaging of these new cell clones. This change was despite the cell line clones maintaining complete Podxl-deficient status (**Appendix B**).

As shown in figure 2.5 A, *PODXL*-KO cells remained less efficient at forming tumorspheres under non-adherent conditions. In contrast, analysis of EVs secreted by WT and *PODXL*-KO cells revealed an evolving phenotype, with variable number of particles secreted by the *PODXL*-KO clones (**Fig 2.5 B**). While clone 1 still showed a significant reduction of secreted EVs compared to WT cells ($P < 0.001$), clone 2 displayed levels of secreted particles similar to WT cells. Given that tumorsphere-forming ability and secretion of EVs is positively correlated with a more tumorigenic phenotype, we set to investigate the *in vivo* phenotype of these serially passaged and altered *PODXL*-KO clones.

We injected WT and *PODXL*-KO cells subcutaneously into the flank of NSG mice and monitored their growth overtime (**Fig 2.5 C**). Surprisingly, WT cells displayed slower tumor growth compared to what we observed previously, with tumor sizes less than 0.2 cm^3 by day 31 post-injection (vs. the 0.5 cm^3 size originally observed). *PODXL*-KO clone 1 still displayed impaired tumor growth when compared to WT cells ($P < 0.0001$), with only 1 palpable tumor (out of 3) at the time of excision. In contrast, *PODXL*-KO clone 2 showed significantly faster primary tumor growth than WT cells ($P < 0.0001$), reaching 0.8 cm^3 in tumor size by day 31 post-injection (**Fig 2.5 C**). No metastatic lung nodules were found for any of the experimental

groups. We have repeated this experiment twice since, with 3 to 4 mice per group each time, and obtained similar results. *PODXL*-KO clone 2 displays rapid tumor growth when compared to WT cells, and *PODXL*-KO clone 1 shows a variable phenotype ranging from the formation of small, palpable tumors (0.1 cm^3) to the lack of *in vivo* tumor growth. In addition, we have attempted to "bypass" the altered phenotype by going back to early passages of the original *PODXL*-KO stocks. Unfortunately, they too showed a variable behaviour, suggesting that alterations in behaviour occur during culture expansion after freezing and thawing of primary clones.

These results suggest that MDA-MB-231 cells, which are known to be aneuploid (156), have an unstable phenotype, and that further validation is required to determine whether these cells (both WT and *PODXL*-KO) can be used to investigate the role of Podxl in tumor progression.

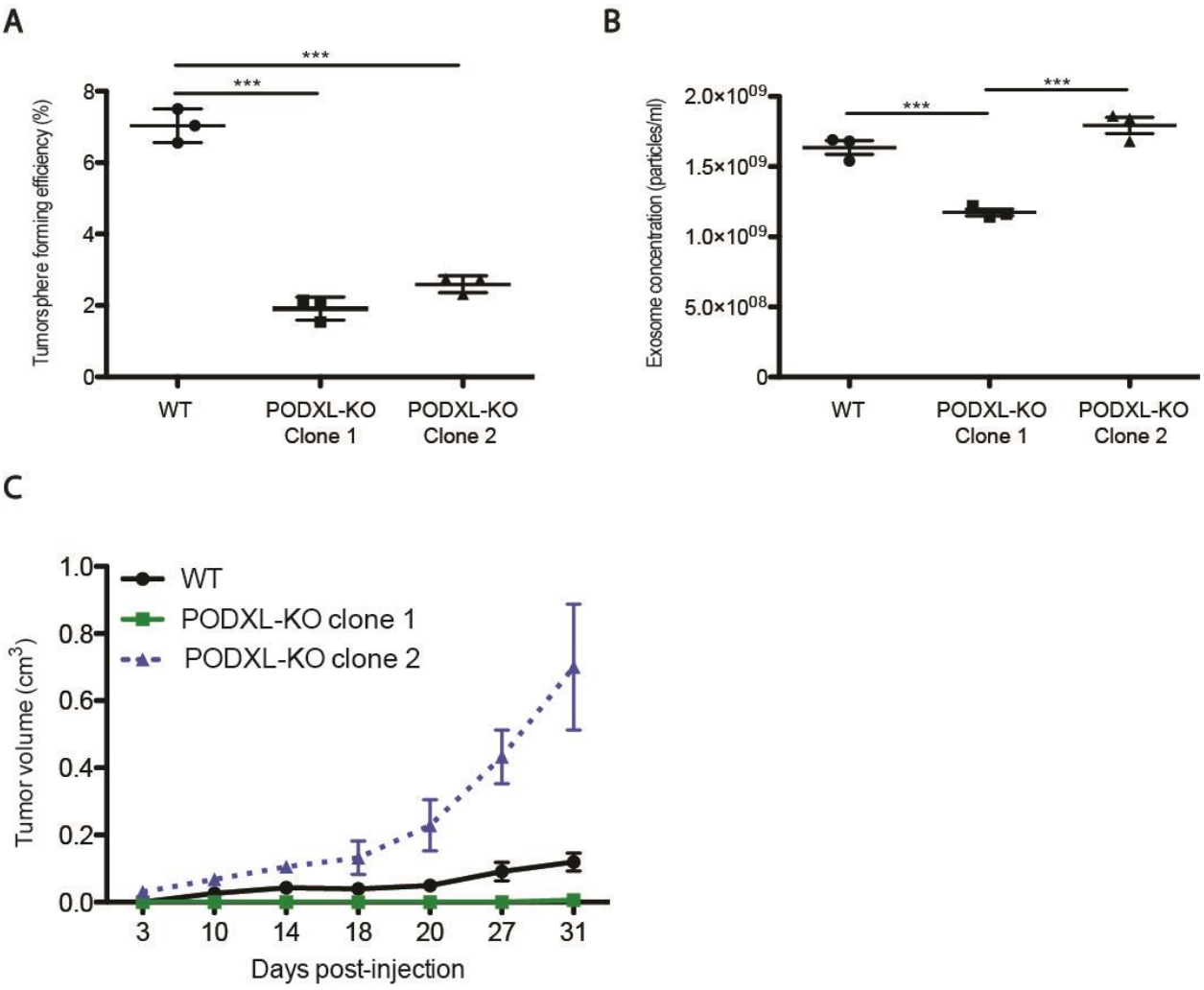

Figure 2.5 MDA-MB-231 WT and PODXL-KO cells changed their phenotype

Re-assessment of MDA-MB-231 WT and *PODXL*-KO *in vitro* and *in vivo* phenotype 18 months after generation. (**A**) Tumorsphere-forming efficiency of WT and *PODXL*-KO clones ($P < 0.001$) (**B**) Extracellular vesicle concentration on the culture medium of MDA-MB-231 WT and *PODXL*-KO clones ($P < 0.001$). (**C**) Tumor growth overtime of WT and *PODXL*-KO cells ($P < 0.0001$). The data in A come from 1 experiment with three technical replicates per cell type. The data from B come from 1 experiment with three technical replicates per group. The data from C come from 1 experiment with 3 mice per group. Statistical analysis was performed using one-

way ANOVA (A, B) and two-way ANOVA test (C). A *P* value less than 0.05 was considered statistically significant. Error bars in all panels show SEM.

2.4.6 Re-expression of hPODXL does not rescue the phenotype of MDA-MB-231 *PODXL*-KO cells

Since the newly generated MDA-MD-231 *PODXL*-KO cells appeared to have an unstable phenotype, to determine if they could be used to investigate Podxl's role in cancer progression, we attempted to rescue their phenotype by re-expressing the human Podxl protein.

Briefly, WT and *PODXL*-KO cells were stably transfected with either a control (pIRES) or a human Podxl expression plasmid. WT cells were sorted to enrich for Podxl-overexpressing cells (**Fig 2.6 A**). In addition, transfected *PODXL*-KO clones were sorted to enrich for cells expressing low and high levels of Podxl on their surface (**Fig 2.6 A**).

Next, since EV secretion appeared to correlate with their *in vivo* phenotype (**Fig 2.5 B, C**), we assessed the number of particles secreted by WT and *PODXL*-KO cells overexpressing hPodxl. WT cells overexpressing hPodxl had increased secretion of EVs when compared to the pIRES control ($P < 0.0001$). Consistently, EV secretion correlated with the level of hPodxl expression on *PODXL*-KO clone 1 cells ($P < 0.0001$). In contrast, on *PODXL*-KO clone 2 hPodxl expression did not correlate with particle secretion, with the highest concentration of EVs being secreted by cells expressing low levels of Podxl.

In an effort to confirm a rescue of the tumorigenic phenotype of hPodxl-overexpressing cells, we injected them subcutaneously into NSG mice and monitored their tumor growth. Surprisingly, over- or re-expression of hPodxl had no effect on the *in vivo* tumor growth of WT or the *PODXL*-KO clones ($P > 0.05$; **Fig 2.6 C**). This result confirms that rescue of the *PODXL*-KO phenotype could not be achieved and, therefore, we are unable to confidently determine if MDA-MB-231 *PODXL*-KO cells are suitable for further studies on the role of Podxl in promoting tumor progression. Together, these data suggest that MDA-MB-231 cells are not a good model

for the study of the role of Podxl in cancer progression, due to the instability of their phenotype, likely the result of their inherent genetic instability.

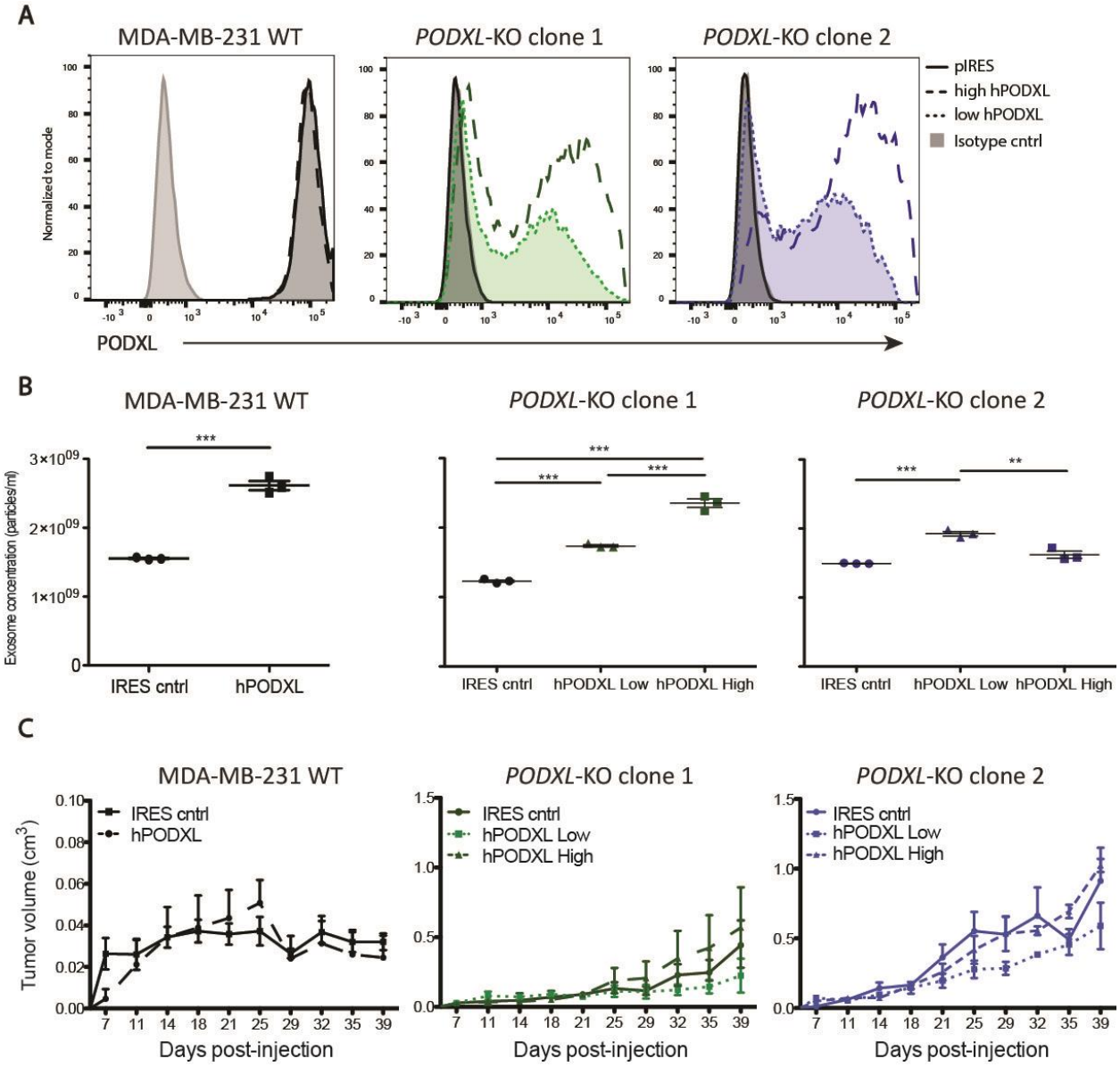

Figure 2.6 hPodxl re-expression does not rescue the phenotype of MDA-MB-231 PODXL-KO cells

(A) Flow cytometric profiles of sorted MDA-MB-231 WT and *PODXL*-KO cells stably transfected with hPodxl or control (pIRES) expression plasmid. WT cells were sorted to enrich for cells with endogenous (pIRES) or high hPodxl expression levels. *PODXL*-KO clone 1 and 2 were sorted to enrich for cells with no Podxl expression (pIRES), or cells expressing low and high levels of hPodxl. **(B)** EV secretion of WT and *PODXL*-KO clones expressing various levels

of hPodxl on their surface (*** = $P < 0.001$, ** = $P < 0.01$). (**C**) Tumor growth overtime of WT and *PODXL*-KO cells expressing low and high levels of hPodxl (n.s = $P > 0.05$). The data in A come from 1 experiment. The data from B come from 1 experiment with three technical replicates per group. Statistical analysis was performed using one-way ANOVA test. The data from C come from 1 experiment with 3-5 mice per group. Statistical analysis was performed using two-way ANOVA test. A *P* value less than 0.05 was considered statistically significant. Error bars in all panels show SEM.

2.4.7 SKOV3 *PODXL*-KO cells show delayed *in vivo* tumor growth

Given the phenotypic instability of the highly aggressive MDA-MB-231 cancer cells, we changed our approach to use a more genetically stable and less aggressive tumor model. Since Podxl has been correlated with poor prognosis and survival of high-grade serous ovarian carcinoma patients (117), we chose to continue our studies using SKOV3 cells, a human ovarian carcinoma cell line expressing high levels of Podxl. Based on previous studies showing Podxl promotes breast carcinoma progression, and a study by Cipollone *et al.* showing that Podxl correlates with poor prognosis in ovarian carcinoma, we hypothesized that Podxl may promote disease progression in ovarian tumor malignancy.

To test this hypothesis, we ablated Podxl expression on SKOV3 cells using CRISPR/Cas9 using the same approach previously described for the MDA-MB-231 *PODXL*-KO cells. Two SKOV3 *PODXL*-KO cells were generated, validated, and kindly donated by the Roskelley lab.

First, we assessed the tumorsphere-forming ability of SKOV3 WT and *PODXL*-KO cells. Interestingly, *PODXL*-KO clone 1 showed tumorsphere-forming efficiency similar to WT cells ($P > 0.05$, **Fig 2.7 A**). In contrast, SKOV3 *PODXL*-KO clone 2 had decreased ability to form tumorspheres ($P < 0.01$, **Fig 2.7 A**). These data show some phenotypic variability between the *PODXL*-KO clones, and suggests that *PODXL*-KO clone 2 might have a less tumorigenic phenotype compared to WT or *PODXL*-KO clone 1 cells.

Since tumorsphere-forming efficiency is a very crude predictor of *in vivo* tumorgenicity, we confirmed the SKOV3 *PODXL*-KO phenotype in a tumor growth xenograft model by

subcutaneously injecting SKOV3 WT and *PODXL*-KO cells into the right flank of NSG mice. As expected, WT cells displayed the fastest rate of tumor growth overtime. In contrast, both SKOV3 *PODXL*-KO clones showed delayed tumor growth when compared to WT cells ($P < 0.0001$, **Fig 2.7 B**). These data suggests that Podxl is also promoting tumor progression in ovarian carcinoma.

In addition, we confirmed the delayed primary tumor growth phenotype of SKOV3 *PODXL*-KO cells 17 months after the first experiment (data not shown), suggesting the SKOV3 cells have a more stable phenotype and, therefore, are suitable to continue our studies on the role of Podxl in promoting cancer progression.

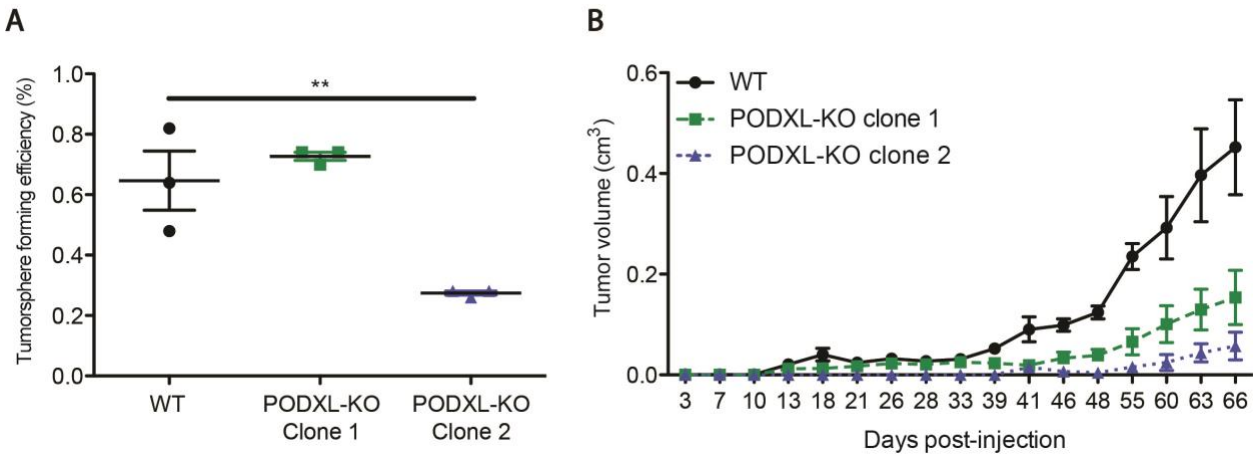

(A) Tumorsphere-forming efficiency of SKOV3 WT and *PODXL*-KO clones (** = $P < 0.01$)

Figure 2.7 Podxl expression promotes primary tumor growth on ovarian carcinoma

(**B**) Tumor growth overtime of SKOV3 WT and *PODXL*-KO cells ($P < 0.0001$). The data in A come from 1 experiment with three technical replicates per cell type. Statistical analysis was performed using one-way ANOVA test. The data from B come from 1 experiment with 4 mice per group. Statistical analysis was performed using two-way ANOVA test. A *P* value less than 0.05 was considered statistically significant. Error bars in all panels show SEM.

2.5 Discussion

It has previously been shown that Podxl expression in primary tumors is correlatively linked to poor patient survival in a wide variety of tumors including breast, ovarian, bladder, colorectal, embryonal, oral squamous, esophageal, gastric, pancreatic, prostate, thyroid and renal carcinoma, astrocytoma, glioblastoma and acute myeloid leukemia (112,114,117,123-125,128,143,144,157-166). Recently, Podxl has been shown to promote tumorigenesis of breast, pancreatic, gastric, liver and lung cancer, glioblastoma and astrocytoma (39,136,139-142,167-172). Though it has been proposed that Podxl enhances tumorigenesis by promoting epithelial-to-mesenchymal (EMT) transition and altering cytoskeletal dynamics to enhance cell migration, invasion and extravasation, the molecular mechanisms by which it does so remain largely undefined.

Here, we sought to investigate the molecular mechanisms by which Podxl promotes *in vivo* tumor growth and metastasis of MDA-MB-231 cells by generating CRISPR/Cas9 *PODXL*-KO cells. Initial characterization of the two MDA-MB-231 *PODXL*-KO clones suggested a critical role of Podxl in primary tumor growth. Though exacerbated compared to transient *PODXL*-KD by shRNA (MDA-MB-231 *PODXL*-KD cells) this phenotype was consistent with what we previously observed (136). Unfortunately, the CRISPR/Cas9 *PODXL*-KO cells rapidly evolved with passage *in vitro* and a variable tumorigenic phenotype independent of Podxl levels emerged. MDA-MB-231 cells are an aggressive breast cancer line characterized for being highly invasive and metastatic in mouse xenograft models. In addition, MDA-MB-231 cells possess a highly aberrant karyotype with numbers ranging from 52 to 68 chromosomes. Recent studies demonstrate that such cell lines frequently evolve in culture due to clonal dynamics and continuous genetic instability resulting in variability in cell line behavior (173-175). Further, a recent study using subclones derived from a clonal cell line showed a significant variability in

cell growth, protein expression and gene copy number between subclones, despite the stability of the parental clone (176). In order to generate *PODXL*-KO clones, cells were subjected to single-cell clonal selection, multiple passages and several rounds of cell-sorting. Thus, we postulate that these processes enhanced their already high chromosomal instability and caused them to drift, resulting in variable phenotypes that are independent from the initial genetic manipulation. Together, our results suggest that MDA-MB-231 cells are not a good model for the study of the role of Podxl in cancer progression.

Next, since Podxl is expressed in many high grade serous epithelial ovarian carcinomas where surface localization correlates with decreased disease-free survival (117), we sought to investigate whether Podxl promotes ovarian cancer progression. In order to test this, we ablated Podxl expression in human SKOV3 cells, a commonly used ovarian serous grade 2 cancer line that forms tumors in immunocompromised mice (177,178). For the first time, we showed that Podxl plays a critical role on SKOV3 cells primary tumor growth. Specifically, we observed that ablation of Podxl expression on SKOV3 cells severely impairs growth of subcutaneous tumors in a xenograft model using NSG mice. Moreover, the phenotypic growth impairment of SKOV3 *PODXL*-KO cells was maintained 17 months after initial characterization.

We are currently working on the re-expression of the WT Podxl protein in *PODXL*-KO cells to confirm that the phenotype observed is Podxl-dependent. Moreover, future studies may include the validation of the SKOV3 *PODXL*-KO cells phenotype using an shRNA Podxl-knockdown approach. Since this approach does not require direct DNA editing or single-cell clonal selection, if SKOV3 shRNA Podxl-knockdown cells were to exhibit a similar behavior as that of the

CRISPR/Cas9 KO cells, it would confirm that Podxl affects the tumor growth of these cells and support the use of the SKOV3 CRISPR *PODXL*-KO cells to further explore the functional role of this protein in tumor growth. In addition, another approach to confirm whether the phenotype observed is Podxl-dependent could be to generate additional SKOV3 CRISPR/Cas9 *PODXL*-KO cells using a "pooled" approach where *PODXL*-KO cells are isolated via cell-sorting from the pool of cells originally transfected with the CRISPR/Cas9 construct, thus avoiding the single-cell clonal selection step. Lastly, another approach could be to generate inducible *PODXL*-KO cells where Podxl deletion could be studied shortly after induction thus avoiding serial passaging and clonal selection steps. These aforementioned approaches could increase confidence in that the lower tumorigenic phenotype we observe in SKOV3 *PODXL*-KO cells is a result of the lack of Podxl expression. In addition, future avenues of exploration may include re-expression of the newly generated human Podxl protein domain mutants (**Appendix C**) to investigate which domain of Podxl is responsible for promoting SKOV3 tumor aggressiveness.

Chapter 3: Pre-clinical characterization of function-blocking anti-PODXL antibody PODO83

Section 3.4.3 is modified from a published manuscript: Snyder KA, Hughes MR, Hedberg B, Brandon J, **Canals Hernaez D**, Bergqvist P, Cruz F, Po K, Graves ML, Turvey ME, Nielsen JS, Wilkins JA, McColl SR, Babcook JS, Roskelley CD, McNagny KM. Podocalyxin enhances breast tumor growth and metastasis and is a target for monoclonal antibody therapy. *Breast Cancer Res.* 2015; doi: 10.1186/s13058-015-0562-7

3.1 Synopsis

Podxl is expressed in a wide variety of cancers where it correlates with poor patient survival. In addition, Podxl plays a key role in promoting tumor progression and metastasis, making it a promising target for cancer therapy. However, to date, no Podxl-based cancer therapy or diagnostic is currently available. Here we further examine PODO83, a novel anti-Podxl monoclonal antibody, as a therapeutic candidate for cancer treatment. We show that PODO83 decreases *in vitro* tumor cell invasion and that, in mice with an established tumor burden, systemic treatment with PODO83 blocks metastasis to the lungs. We demonstrate that PODO83's epitope lies within the extracellular stalk domain of Podxl and show that PODO83 recognizes the core Podxl protein in both tumour and healthy tissue. This work highlights the importance of PODO83's epitope in cancer metastasis and supports its further development as a research and prognostic clinical tool.

3.2 Introduction

Though cancer diagnosis and treatment have greatly improved in the last 30 years, it remains the second leading cause of death worldwide, accounting for about 1 in 6 deaths (146). Importantly,

most cancer-related deaths are the result of metastatic disease (disseminated tumor cells) (25), highlighting the need for biomarkers capable of identifying tumors at high risk of metastasizing, and the generation of targeted therapies against them.

Podocalyxin (Podxl, also known as TRA-1-60, TRA-1-81, gp135, gp200, PCLP1, MEP21 and GCTM2) is a CD34-related sialomucin expressed in normal adult tissue where is predominantly located in vascular endothelia(179,180), kidney podocytes(181), and a restricted subset of epithelial lumens(107). However, Podxl is also overexpressed in multiple types of cancer and its expression is correlated with poor prognosis (108,109).

Early studies of breast cancer found that Podxl overexpression is an indicator of poor prognosis (110). Since, the correlation of Podxl expression with high-risk tumors has been demonstrated in a multitude of other malignancies including high grade serous ovarian carcinoma (117), colorectal cancer (114), colon carcinoma (143), oral squamous cell carcinoma (158,182), esophageal and gastric adenocarcinoma (124), gastric cancer (125), pancreatic cancer (119,144,159), prostate cancer (160), thyroid carcinoma (161), renal cell carcinoma (112), astrocytoma (162,163), glioblastoma multiforme (128), acute myeloid leukemia (164,165) and embryonal carcinoma (157). In addition, Podxl overexpression is a predictor of both poor prognosis and poor treatment response for bladder (118,183), oral tongue squamous (184) and colorectal carcinoma (113). Moreover, we have previously demonstrated that Podxl plays a key role in promoting tumor progression and metastasis (See chapter 2, (136)). Together, these studies suggest that Podxl is a promising target for cancer therapy. Despite this, only a few efforts have been made to develop a targeted therapy.

Podxl is well-known to be expressed on human pluripotent stem cells (hPSCs). Specifically, TRA-1-60 and TRA-1-81, two distinct epitopes on Podxl, are commonly used to define hPSCs. Therapeutic applications using differentiated hPSCs carry the risk of teratoma formation by the inevitable (with current technology) presence of undifferentiated hPSCs. To date, two studies have proposed the use of anti-Podxl antibodies: mAb84 (145) and commercially available anti-Podxl 3D3 (130) to selectively eliminate undifferentiated hPSCs in cell transplantation applications using hPSC-derived cells.

In the context of cancer, two antibodies targeting Podxl have been recently described: chPcMab-47, a human-mouse chimeric anti-Podxl antibody shown to have *in vivo* anti-tumor activity against Podxl-expressing CHO cells and HCT-15 colorectal cancer cells (185). This anti-tumor effect was dependent on the injection of NK cells near the tumor site, suggesting that chPcMab-47's effect relies on antibody-dependent cellular cytotoxicity (ADCC).
Lastly, we recently described PODOC1 (thereafter named PODO83), a novel anti-Podxl antibody capable of inhibiting tumor growth and blocking metastasis to the lung *in vivo* (136).

In this pre-clinical study, we further characterized PODO83 to validate its use as a potential therapeutic. Using *in vitro* and *in vivo* assays we studied PODO83's mode of action on human cancer cell lines. We demonstrated that PODO83 does not affect the ability of cancer cells to form tumorspheres, but rather decreases *in vitro* tumor cell invasion. Consistent with our *in vitro* results, we observed that PODO83 treatment blocks metastasis to the lungs in mice with an established tumor burden. We also assessed PODO83's epitope distribution among four cancer types where Podxl has been associated with poor prognosis and highlighted breast and ovarian

cancer as possible therapeutic applications. Moreover, we identified PODO83's epitope to be in Podxl's extracellular stalk domain and showed that PODO83 is able to recognize the Podxl core protein expressed by healthy tissues.

3.3 Materials and Methods

3.3.1 Antibody generation

The antibody generation and initial characterization was performed at the Centre for Drug Research and Development. New Zealand White rabbits were immunized with Podxl-expressing human glioblastoma A-172 cells (#CRL-1620, ATCC). Rabbit monoclonal antibodies (mAbs) were isolated using SLAM technology (186). Briefly, individual B-cell clones whose supernatants reacted with Podxl-expressing MDA-MB-231 cells were selected. These were then screened via enzyme-linked immunosorbent assay (ELISA) for high reactivity against Podxl isolated from human breast cancer MDA-MB-231 and low reactivity to the human embryonic kidney 293 (HEK 293) cells. Next, selected clones were screened against Podxl expressing-MDA-MB-231 and its *PODXL*-KO counterpart to confirm Podxl specificity. Supernatants were also screened for reactivity with Chinese hamster ovary (CHO) cells expressing Podxl, and low reactivity to CHO cells expressing related family members CD34 (*CD34*) and endoglycan (*PODXL2*). Binding profiles for tumour versus normal cells were generated to enrich for those that preferentially bound to Podxl on tumour cells. Ab V_H and V_L regions were subsequently cloned into expression vectors containing the constant regions of the rabbit, human, or rabbit/human chimeric heavy and light chains, respectively, in order to generate high-affinity anti-Podxl rabbit and rabbit/human chimeric IgG_1 Abs.

3.3.2 Flow Cytometry

Adherent cells were washed 1X with Ca^{2+}- and Mg^{2+}-free HBSS (Gibco, #14170-112), then incubated for 1-2 min at 37°C in a 0.25% trypsin solution and quenched with complete growth media. Cells were then centrifuged for 4 min at 394*g*, washed 2X with FACS buffer (PBS, 2 mM

EDTA, 5% FBS, 0.05% sodium azide) and transferred to a 96 well 'v' bottom plate. Cells were resuspended in 100 µl blocking buffer (FACS buffer, 1 µg/ml of anti-CD16/CD32 (clone 2.4G), 2% rat serum) for 20 min at 4°C in the dark, then spun at 394*g* for 4 min and incubated in 100 µl primary antibody (Ab) solution for 30 min at 4°C in the dark. Rabbit-PODO83 (136) (2 µg/ml) and either rabbit or chimeric-PODO447 (5 µg/ml) were used to detect Podxl. Rabbit-IgG (5 µg/ml, Vector Laboratories, #I-1000-5) and mouse/human-chimeric palivizumab (5 µg/ml, National Research Council, NRC) were used as isotype controls. Next, cells were washed 3X with FACS buffer and resuspended in 100 µl of secondary Ab solution (Alexa Fluor 647 (AF647) donkey-anti-rabbit (2 µg/ml, Invitrogen, #A31573) or AF647 goat-anti-human (2 µg/ml, Jackson ImmunoResearch Laboratories, #109-605-098)) for 30 min at 4°C in the dark. Cells were washed 2X with FACS buffer and resuspended in FACS buffer containing propidium iodide (PI) (0.5 µg/ml, Life Technologies, #P3566). All flow cytometry data were acquired using a BD LSRII and analyzed using FlowJo™ software (BD Biosciences, Ashland).

3.3.3 Tumorsphere assay

MDA-MB-231 and MCF7 cells were harvested as follows: adherent cells were rinsed with 5ml of Ca^{2+}-, Mg^{2+}-free HBSS and lifted using a cell scraper. Cells were then spun at 394g for 4 min and resuspended in 5ml of complete Mammocult™ media (1/10 dilution of MammoCult™ proliferation supplement (#05620), 4 µg/ml heparin (#07980) and 0.48 µg/ml hydrocortisone (#07925) in MammoCult™ basal medium (#05620), StemCell Technologies). Viable cells were counted using trypan blue stain. MDA-MB-231 (5×10^3) and MCF7 (5×10^3) cells were seeded in triplicate in 2 ml of complete MammoCult™ medium in ultra-low adherent six-well plates.

Cells were incubated for seven days without disruption under standard cell culture conditions (37°C in 5% CO_2). On day 7, tumorspheres were manually counted using a transparent counting grid. Only spheres with 12 or more cells were counted. Tumorsphere forming efficiency (%) was calculated as (number of tumorspheres / number of cells seeded) x 100, and statistical analysis was performed using one-way ANOVA followed by Bonferroni's post-test in GraphPad Prism software. A *P* value less than 0.05 was considered statistically significant.

3.3.4 *In vitro* migration and invasion

On day 0, 96-well ImageLock plates (Essen Bioscience, #4379) were coated with 50 μl of BD Matrigel TM diluted to 100 μg/ml in MDA-MB-231 culture media. On day 1, sub-confluent MBA-MB-231 cells were harvested using 0.25% Trypsin and counted on a hemocytometer using trypan blue stain. Cells were resuspended in culture media at 1.8 x 10^5 cells/ml and 100 μl of cell suspension were plated in each well (i.e. 18K cells per well). Cells were then incubated for 4 h at 37°C, in 5% CO_2. Wounds were created simultaneously in all wells using the 96-well WoundMaker™ procedure detailed by the manufacturer (Essen Bioscience). Immediately after, cells were washed twice with cell culture media. After the final wash, 100 μl of culture media was added to the cells and the plate was placed in a pre-chilled CoolBox 96F (Essen Bioscience, #1500-0080-A00) to equilibrate for 5 min, and then the (cool) media was discarded, and 50 μl of either media (migration) or BD Matrigel™ (invasion) containing 9 μg/ml of the test antibodies (rabbit/Hu chimeric PODO83 and PODO173) were added to the cells. The plate was then placed on to a pre-warmed CoolSink 96F in a 37°C, 5% CO_2 incubator for 30 min. Next, additional 100 μl of culture media containing 9 μg/ml of the test antibodies was added to the cells and the plate

was placed in the Incucyte ZOOM. The Incucyte ZOOM software was set in "scratch wound" mode to scan one image per well every 3h, with the first scan beginning 10 min after the plate was placed in the instrument. Migration and invasion rate were calculated as relative wound density (%) and analyze using the Incucyte ZOOM scratch wound software, and statistical analysis was performed using two-way ANOVA in GraphPad Prism software. A *P* value less than 0.05 was considered statistically significant.

3.3.5 Mice

Tumor model animal experiments were carried out using 6-12-week-old female NOD.Cg-*Prkdc*^{scid}*Il2rg*^{tm1Wjl}/SzJ (NSG) mice obtained from Jackson's Laboratories. Animals were bred and maintained in a pathogen-free facility. All animal procedures were approved by the University of British Columbia Animal Care Committee.

3.3.6 Pre-clinical *in vivo* xenograft model to assess PODO83 efficacy

MDA.MB.231 ($1x10^6$) cells were injected subcutaneously into the right flank of NSG mice. Tumor dimensions were measured twice a week and the tumor volumes (cm^3) were calculated by (($length \times width^2$)/2). Once tumors reached $0.5cm^3$ in size, mice were treated with 4.5mg/kg of rabbit PODO83 or chimeric anti-OVA control antibody by intraperitoneal injection every 4 days. When tumors reached humane endpoint ($1cm^3$) mice were anesthetized with 2,2,2-tribromoethanol (avertin), followed by lung perfusion with ice cold PBS and excision of the lungs and tumors. Lungs were minced and digested in a collagenase/dispase (2mg/ml) in HBSS for 2h at 37C, then filtered through a 70μm strainer to obtain a single cell solution. Red cell lysis was then performed by resuspending cells in 5ml of ACK lysis buffer for 10 min at room

temperature, then quenched with 5ml of PBS, and rinsed twice with FACS buffer. Cells were then stained and analyzed by flow cytometry as described above. Average tumor volume overtime was calculated and statistical analysis was performed using two-way ANOVA test. Mean GFP-positive lung cells were calculated and statistical analysis was performed using a Student's *t*-test. All statistical analysis was performed in GraphPad Prism software. A *P* value less than 0.05 was considered statistically significant

3.3.7 Immunohistochemistry

EOC tissue microarrays (TMA) were obtained from the Genetic Pathology Evaluation Centre (GPEC) TMA Database (Vancouver, Canada), and stained with either rabbit-PODO83 (2 μg/ml) or rabbit-PODO447 (5 μg/ml). Tissue cross-reactivity TMAs were purchased from US Biomax Inc. (#MNO1021) and stained with either Rbt PODO83-BIOT (2 μg/ml) or Mo/Hu-chimeric pavilizumab-BIOT control (5 μg/ml) (187). Briefly, slides were deparaffinized and rehydrated in 100% xylene (3X, 5 min), 100% ethanol (2X, 3 min), 95% ethanol (1X, 3 min), 70% ethanol (1X, 3 min) and distilled water (1X, 3 min). Antigen retrieval was performed by heating slides in citrate buffer at 90°C for 30 min. For staining, slides were washed in PBS (3X, 5min), incubated for 30 min in blocking solution (PBS, 5% donkey serum, 1% BSA, 0.2% Triton X-100, 0.05% Tween 20), and incubated in primary Ab solution overnight at 4°C. Slides were then washed with TBST (3X, 15 min), incubated with secondary Ab (anti-rabbit-BIOT, 2 μg/ml, SouthernBiotech, #6440-06) in blocking solution for 30 min at room temperature (RT), and washed again with TBST (4X, 15 min). Endogenous peroxidase was blocked with 0.3% hydrogen peroxide in methanol for 30 min at RT prior to rinsing 3X with PBS. Signal was

amplified using Vectastain® Elite® ABC HRP Kit (Vector Laboratories, #PK-6100) according to manufacturer's instructions, and then washed with PBS (3X, 5min). Signal was visualized using a DAB peroxidase (HRP) Substrate Kit (Vector Laboratories, #SK-4100) following the manufacturer's recommendations. Each slide was incubated with DAB solution for 1-5 min until strong signal appeared, then the reaction was stopped by dilution with PBS. Slides were washed with PBS (2X, 5 min), distilled water (2X, 2 min), stained in hematoxylin (12 s, VWR, #10143-150) and rinsed with tap water. Staining was fixed in Bluing Solution (0.1% sodium bicarbonate) for 1 min and rinsed in distilled water (2X, 2 min) prior to dehydration in graded alcohols and xylene. Slides were mounted using Permount solution (Fisher Scientific, #SP15100) and subsequently analyzed for Podxl staining and localization.

3.3.8 Immunohistochemical scoring

EOC TMAs were blindly scored by four independent observers (DCH, KW, CDR), including a pathologist (MK), compared and combined. Initially, scoring was based on number of stained cells, intensity and staining pattern. Number of stained cells was represented by an overall percentage of stained cells in the tumour, and then translated into a scoring scale of 0 (no staining, <1%), +1 (intermediate, 1-50%) and +2 (high, >50%). Intensity was scored based on a scale of 0 (negative), 1 (weak), 2 (intermediate) and 3 (strong). We then combined +1 and +2 cases with weak or higher staining and grouped them as PODO83-positive. The dominant staining pattern of each case was scored as A (apical), AL (apicolateral), L (lateral), B (basal), BL (basolateral), and CY (cytoplasmic). We then combined A, AL, B and BL groups as M (membranous), and compared CY versus M staining. For the TCR TMAs, the frequency of stained cells was identified as negative (Neg), very rare (<1%), rare (1-5%), rare to occasional

(5-25%), occasional (>25-50%), occasional to frequent (>59-75%), and frequent (>75-100%). Blood vessel (endothelium) staining was included as part of the overall score for each individual tissue.

3.4 Results

3.4.1 PODO83 has no effect on tumorsphere-forming efficiency *in vitro*

To identify antibodies that could target Podxl expressed on cancer cells, we further examined the effect of PODO83 treatment on human cancer cells. We previously showed in a competitive *in vivo* experimental metastasis xenograft model that *PODXL*-KD MDA-MB-231 cells form fewer metastatic nodules in the lung compared to WT cells (136). In addition, systemic treatment of MDA-MB-231 tumor-bearing mice with PODO83 resulted in smaller primary lesions and decreased metastatic burden in the lungs (136). Because the PODO83 antibody, but not other Podxl finding antibodies, inhibits tumor growth and metastases, the results led us to hypothesize that PODO83 is inhibiting a functional epitope required for the tumorigenic capacity of breast cancer cells.

The tumorsphere formation assay is a useful tool to enrich for and assess the tumorigenic capacity of cancer stem/progenitor cells *in vitro*. It has been shown that Podxl plays a role in the ability of MCF7 and MDA-MB-231 cells to form tumorspheres *in vitro* where low Podxl expression resulted in attenuated tumorsphere-forming efficiency (**Fig 3.1 A,** (136)).

To test if PODO83 could mimic the effects of a *PODXL* KD we performed a tumorsphere assay with MDA-MB-231 and MCF7 Podxl-high cells treated with either PODO83, OVA, or PODO173, a control antibody that binds the Podxl protein but has no inhibitory effect. There were three treatment conditions: pre-treatment (cells were incubated with antibody prior to seeding); pre-treatment and initial supplementation at day 0 (antibody was added to the cells at the time of seeding); or pre-treatment, initial supplementation at day 0 and an additional spike of

antibody after 4 days of initial plating. Contrary to our initial hypothesis, treatment with PODO83 did not affect the ability of either MDA-MB-231 nor MCF7 Podxl-high cells to form tumorspheres *in vitro* (**Fig 3.1 B**).

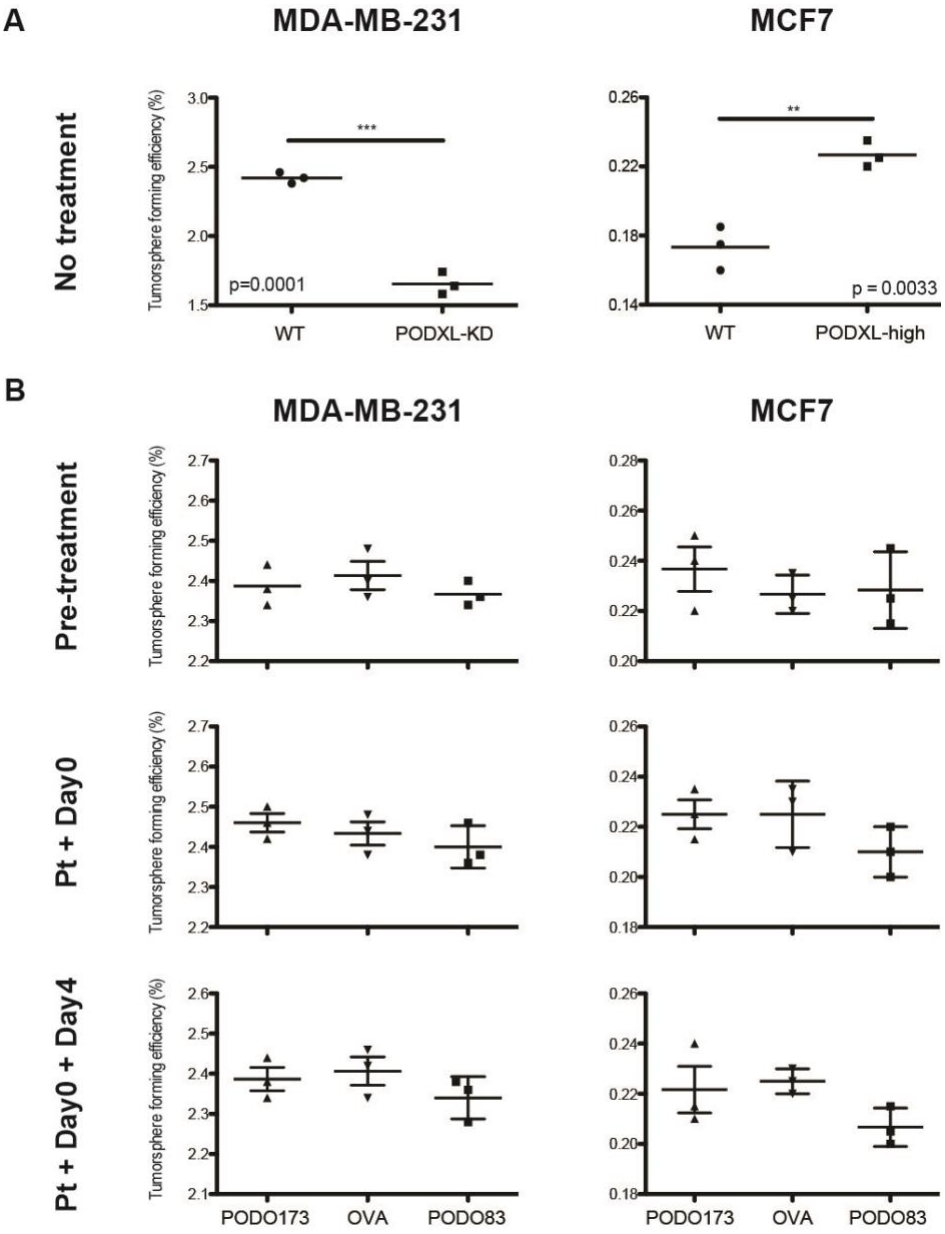

Figure 3.1 PODO83 treatment does not affect tumorsphere-forming ability of MDA-MB-231 or MCF7 cells

(A) Tumorsphere-forming efficiency of untreated MDA-MB-231 WT vs. *PODXL*-KD cells (left panel), and MCF7 WT vs *PODXL*-overexpressing cells (right panel) (B) Tumorsphere-forming efficiency of MDA-MB-231 WT and MCF7 *PODXL*-overexpressing (PODXL-High) cells treated with PODO83, PODO173 or anti-OVA control antibody. Treatment conditions were: pre-treatment (pt, upper panel), pre-treatment and supplementation at time of seeding (Pt + Day 0, middle panel), pre-treatment, supplementation at day 0 and additional antibody supplementation

4 days after plating (Pt + Day 0 + Day 4, lower panel). The data in this figure come from 1 experiment with three technical replicates per group. Statistical analysis was performed using one-way ANOVA test and a *P* value less than 0.05 was considered statistically significant. Error bars in all panels show SEM. ** P < 0.01, *** P < 0.001

3.4.2 PODO83 delays invasion of cancer cells *in vitro*

Given that we observed a dramatic effect of PODO83 on blocking the ability of breast cancer cells to metastasize to the lung (136), we investigated if PODO83 could be affecting the motility of cancer cells.

To address this, we first compared the motility of MDA-MB-231 WT and *PODXL*-KD cells in a migration wound-scratch assay (**Fig 3.2 A)**. Briefly, MDA-MB-231 monolayers were cultured in 96-ImageLock plates. Next, wounds were created simultaneously in all wells using the 96-well WoundMaker™ and rate of wound closure was determined using the Incucyte® imaging instrument and analysis software. As predicted, *PODXL*-KD cells took longer to migrate and close the wound compared to WT cells (**Fig 3.2 A**). We next compared how PODO83 or PODO173 control antibody treatments affected MDA-MB-231 motility and observed that neither treatment affected the ability of MDA-MB-231 cells to migrate *in vitro* (**Fig 3.2 B**).

We then assessed the role of Podxl on tumor invasion *in vitro*. To test this, a scratch-wound assay was performed as described previously, but with the addition of gel matrix overlaid on top of the scratch wound. We then assessed the ability of MDA-MB-231 WT and *PODXL*-KD cells to move through a Matrigel™-filled wound scratch assay. Consistently, *PODXL*-KD cells demonstrated a decreased ability to invade the Matrigel compared to WT cells (**Fig 3.2 C**). We next assessed the effect of antibody treatment on cell invasion. Cells treated with control PODO173 antibody behaved similarly to WT cells (**Fig 3.2 D**). In contrast, cells treated with PODO83 showed delayed invasion, mimicking the behavior of *PODXL*-KD cells (**Fig 3.2 D**).

These results suggest that PODO83 may affect the ability of tumour cells to invade reconstituted basement membrane.

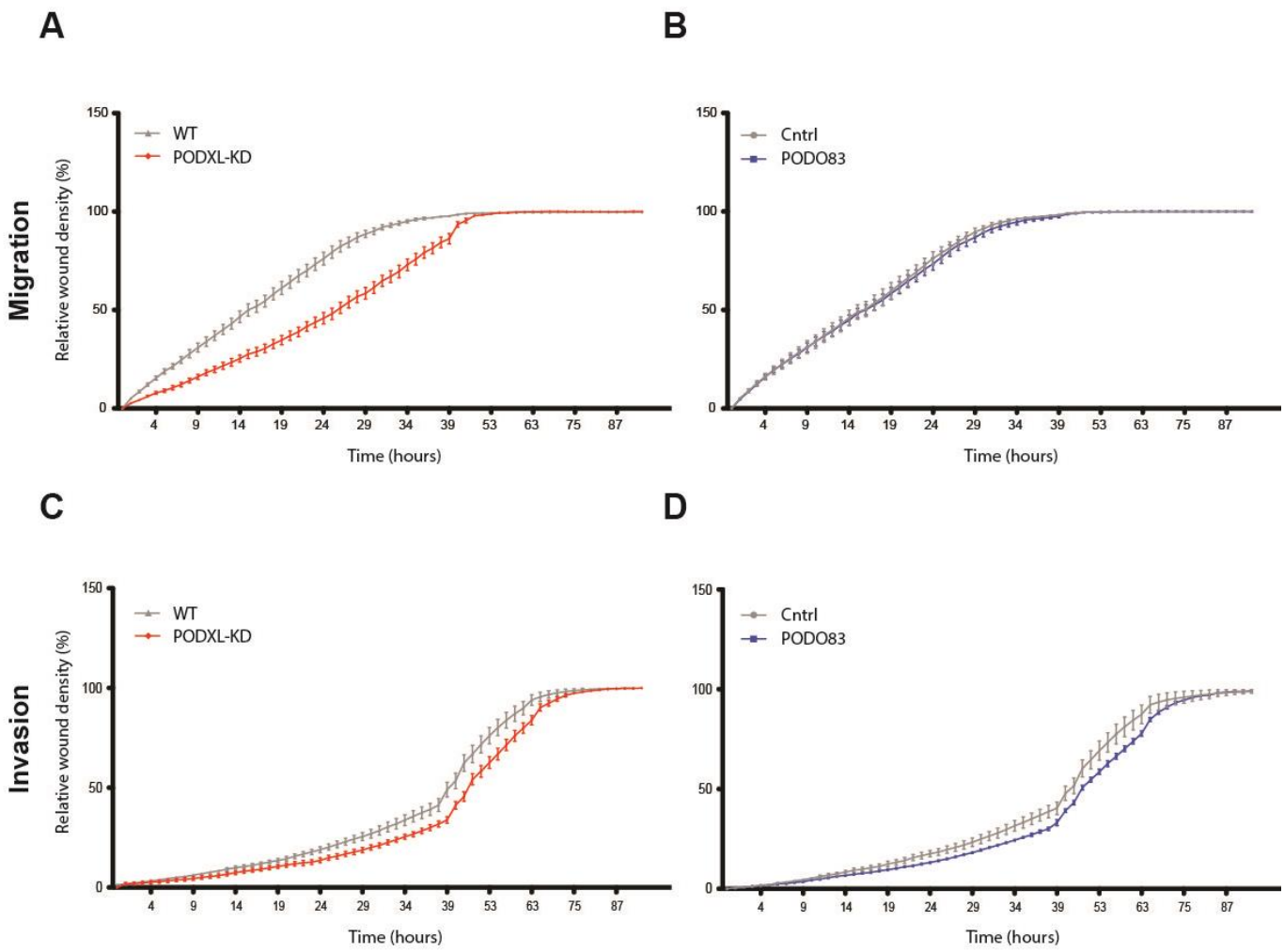

Figure 3.2 PODO83 delays invasion of cancer cells *in vitro*

(A, B) Representative graphs from an IncuCyte® *in vitro* wound-scratch migration assay of MDA-MB-231 WT and *PODXL*-KD cells (A; $P < 0.001$); or MDA-MB-231 parental cells treated with PODO83 or PODO173 control antibody (B; n.s). (C, D) Representative graphs from an *in vitro* IncuCyte® invasion wound-scratch assay with MDA-MB-231 WT and *PODXL*-KD cells (C; $P < 0.001$); or MDA-MB-231 parental cells treated with PODO83 or PODO173 control antibody (D; $P < 0.01$). The data in this figure is representative of 2 independent experiments with 8 technical replicates per group. Statistical analysis was performed using two-way ANOVA

and a *P* value less than 0.05 was considered statistically significant Error bars in all panels show SEM.

3.4.3 PODO83 delays primary tumor growth and decreases metastasis *in vivo*

We previously showed that PODO83 reduces primary tumor growth in an *in vivo* xenograft model (136). However, as clinical patients present with varied sizes of tumors at the time of diagnosis, we assessed the inhibitory effect of PODO83 in mice with an established tumor burden. To do so, we initiated antibody treatment only after the tumors reached $0.5cm^3$ (compared to $0.1cm^3$ in previous experiments). Although there was a trend towards a smaller tumor size and weight in these large tumors, this did not reach statistical significance (**Fig 3.3 A, B**). Strikingly, however, compared to controls, lungs harvested from mice treated with PODO83 exhibited a lower weight and much lower number of GFP-positive metastatic cells (**Fig 3.3 C-E**). These results indicate that while the effects of PODO83 on primary tumor growth may be dependent on the size of the tumor at the time of treatment initiation, the main effect of PODO83 may be to suppress metastasis to the lung.

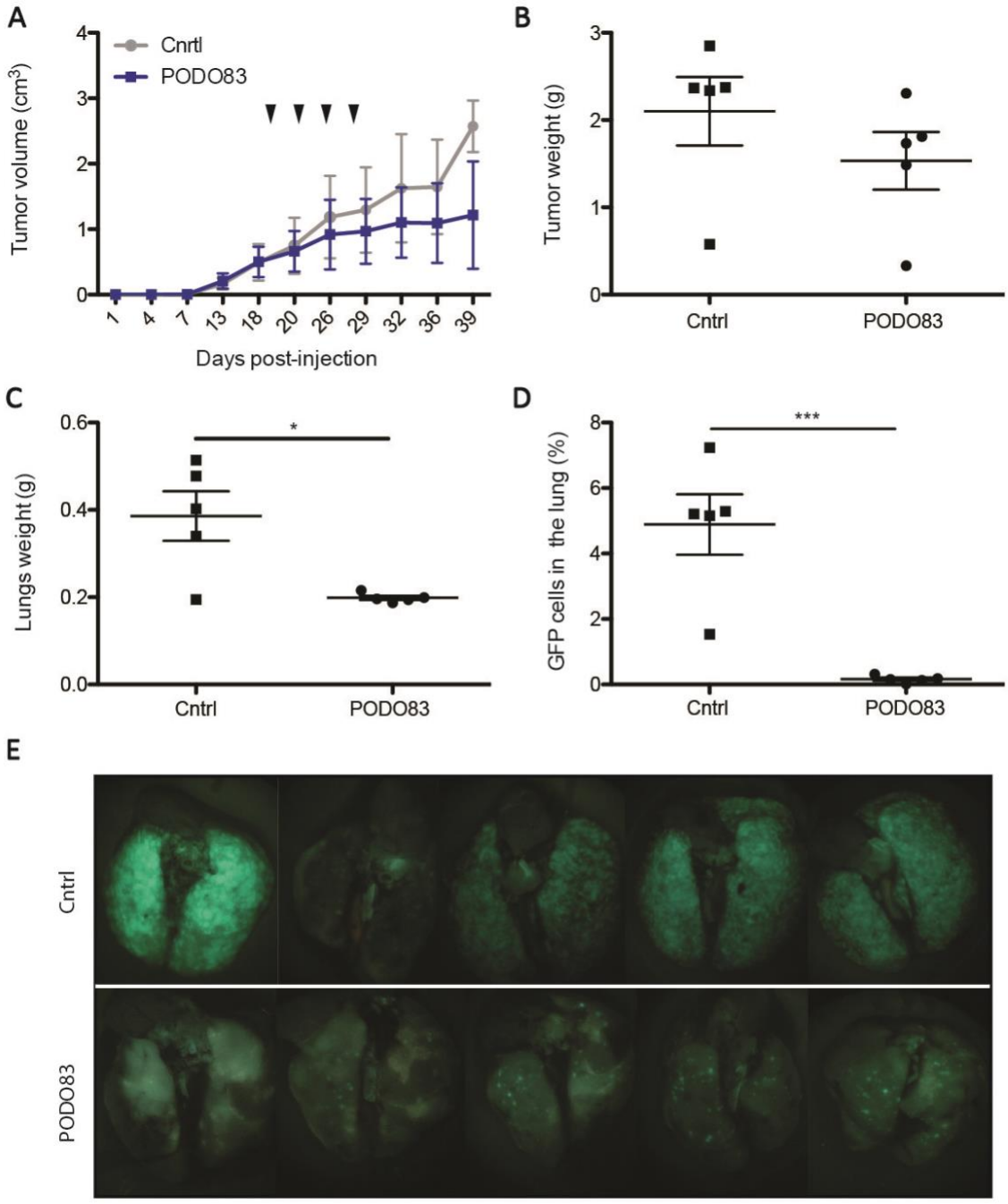

Figure 3.3 PODO83 blocks lung metastasis in mice with an established tumor burden

(A) Tumor growth curve in mice treated intraperitoneally (i.p) with 4.5 mg/kg of anti-OVA control (Cntrl) or PODO83 Ab. Arrowheads represent i.p injection of the antibody. (B) Tumor

weight (g) from mice treated with control or PODO83 Ab. (C) Lung weight (grams) from mice treated with control or PODO83 Ab. (D) Percentage of GFP-positive tumor cells in the lungs of mice treated with control or PODO83 Ab as determined by flow cytometric analysis. (E) Fluorescence microscopy images showing GFP-positive metastatic lung nodules from mice treated i.p with control (upper panel) or PODO83 (lower panel) Ab. The data from this figure come from 1 experiment with 5 mice per group. Statistical analysis was performed using two-way ANOVA (A) and Student t-test (B-D) , and a *P* value less than 0.05 was considered statistically significant. Error bars in all panels represent SEM. * $P < 0.05$, *** $P < 0.001$

3.4.4 PODO83 staining in human cancer

The Podxl core protein is known to be expressed at high levels in a variety of human tumors, where it has been associated with poor outcome. Some examples include breast, pancreatic, ovarian, bladder, embryonal, oral squamous, esophageal, gastric, prostate, thyroid, uterine, colorectal and renal carcinoma, as well as astrocytoma, glioblastoma and acute myeloid leukemia.

In order to assess the potential application of PODO83 as a function-blocking antibody in cancer, we evaluated staining of a series of tissue microarrays (TMAs) of bladder, pancreatic ductal adenocarcinoma, breast and ovarian cancers, all of which have previously been found to overexpress the Podxl core protein, and examined the expression of the PODO83 epitope. Each case on the TMAs was scored based on the percentage of cells stained, with a scoring scale of 0 (negative, <1%), +1 (intermediate, 1-50%) and +2 (high, >50%). Tumors scored as +1 and +2 were grouped as PODO83 positive.

3.4.4.1 PODO83 in urothelial carcinoma

Membranous expression of Podxl has been shown to be an independent prognostic factor of both disease specific survival (DSS) and overall survival (OS), as well as a predictive biomarker in urothelial bladder cancer (118,183). For that reason, we hypothesized bladder cancer could be a potential application for a PODO83-based therapy. To explore this, we assessed the distribution of PODO83 epitope in two urothelial bladder carcinoma TMAs. The first TMA was comprised of tumor tissue from 70 individual patients who underwent radical cystectomy. From this cohort, 36 out of 70 patients presented with non-invasive tumors while the remaining 34 patients

presented invasive tumors with metastasis in the lymph node (LN). For the invasive cases, we were able to access matched tissue from the submucosal (less invasive) and muscle invasive tumor area, and the LN metastatic tumor. We observed < 50% of both non-invasive and invasive primary tumors to be PODO83 positive (**Table 3-1**). Interestingly, within the invasive tumors, only 32% of the tissues from the muscle invasive area were positive for PODO83, compared to 44% of the submucosal area, however, almost 70% of matched LN metastatic tumor showed reactivity with PODO83. In all cases, consistent with previously reported localization of Podxl in bladder cancer, we observed predominantly cytoplasmic staining (118), suggesting that the epitope might not be accessible to circulating PODO83 *in vivo*.

We further examined a second urothelial bladder cancer TMA with a better representation of low- and high-grade bladder cases, and combined it with the first TMA for analysis. In disagreement with previous results (118), we did not observe any association between cell surface PODXL and high-grade tumours (**Table 3-1**). We did observe variability in our results which could in part be due to the low membranous staining we and others have observed. A larger sample size might be required to accurately determine the true number of cell surface PODO83 tumours and correlation with advanced T-stage, high-grade and overall survival.

Table 3-1 PODO83 expression and localization within urothelial cell carcinoma

Patient characteristics	Scorable Cases n	PODO83 positive		
		Total positive n (%)	Cell surface positive n (%)	Cytoplasmic positive n (%)
All scorable cases	225	118 (52.4)	16 (13.5)	97 (82.0)
Histological cell type (n)	137	66 (48.2)	4 (6.1)	61 (92.4)
Non-invasive tumour	36	17 (47.2)	2 (11.8)	15 (88.2)
Invasive tumour				
Submucosal area	34	15 (44.1)	0 (0.0)	15 (100.0)
Muscle invasive area	34	11(32.4)	0 (0.0)	11 (100.0)
Metastatic tumour	33	23 (69.7)	2 (8.7)	20 (86.9)
Grade (n)	88	52 (59.1)	12 (23.1)	36 (69.2)
Low	44	26 (59.1)	9 (34.6)	15 (57.7)
High	44	26 (59.1)	3 (11.5)	21 (80.8)

3.4.4.2 PODO83 in pancreatic adenocarcinoma

Podxl expression has previously been associated with a higher risk of death from pancreatic adenocarcinoma (PDAC) (119). For this reason, we next assessed PODO83 staining pattern in PDAC. Immunostaining of a TMA containing 77 PDAC cases we observed 74% (57/77) were PODO83 positive, compared to the 98% previously reported (119) (**Table 3-2**). We observed that 19.3% (11/57) of the PODO83-positive cases exhibited cell-surface staining, while the remaining 79% (45/57) cases showed diffuse cytoplasmic PODO83 staining. This was in contrast to previous studies which observed cell-surface staining in 44% of cases with a polyclonal anti-Podxl antibody (119). One explanation could be that the polyclonal antibody produces a stronger signal in paraffin-emended sections compared to PODO83, which might require higher antigen density to produce a similar staining. However, this seems unlikely since PODO83 has high affinity for the Podxl core protein (dissociation constant (K_d) = 46 pM or (10^{-12} M)). Since polyclonal antibodies are prone to cross-react with other proteins, a more likely explanation could be that the cell-surface staining observed with the polyclonal antibody is the result of higher background.

Table 3-2 PODO83 expression and localization within the pancreatic TMA cohort

Patient characteristics	Scorable Cases n	PODO83 positive		
		Total positive n (%)	Cell surface positive n (%)	Cytoplasmic positive n (%)
All scorable cases	96	72 (75.0)	15 (20.8)	55 (76.4)
Histological cell type (n)				
Ductal adenocarcinoma	77	57 (74.0)	11 (19.3)	45 (79.0)
Normal pancreas	19	15 (79.0)	4 (26.7)	10 (66.7)

3.4.4.3 PODO83 in breast cancer

High expression of Podxl in breast tumours has been previously correlated with poor outcome (110) and has been shown to play a role in disease progression (142,166). We previously showed that PODO83 could delay primary tumor growth of MDA-MB-231 breast cancer cells by targeting the extracellular domain of Podxl in a xenograft tumor model (136). Therefore, we assessed breast cancer as a potential application for a PODO83-based therapy by staining a breast carcinoma TMA (**Table 3-3**). In contrast to previously reported rates of Podxl expression in breast carcinomas (40%) (110), we observed 93% (300/325) of cases to be PODO83-positive. This discrepancy could be explained by the differences in antibody used to stain the breast TMA. In previous studies, a commercial anti-human Podxl mAb (clone 3D3) was used. The commercial antibody gives a much weaker staining when compared to PODO83, which has a high affinity for the Podxl core protein (dissociation constant (K_d) = 46 pM or (10^{-12} M)) [personal communication, Centre for Drug Research and Development]. Further, most of the staining observed was cytoplasmic in nature (64% of all PODO83-positive cases),however, 35% (88/252) ductal carcinomas presented cell-surface PODO83 staining. Given that breast cancer is the most common cancer among women and that ductal carcinoma accounts for 80% of all breast cancer diagnoses, PODO83 could be a candidate worth exploring for therapy or diagnoses of this tumour histotype.

Table 3-3 PODO83 expression and localization within the breast TMA cohort

Patient characteristics	Scorable Cases n	PODO83 positive		
		Total positive n (%)	Cell surface positive n (%)	Cytoplasmic positive n (%)
All scorable cases	325	300 (92.3)	92 (30.7)	193 (64.3)
Histological cell type (n)				
Ductal Carcinoma	275	252 (91.6)	88 (34.9)	159 (63.1)
Lobular Carcinoma	47	45 (95.7)	4 (8.9)	31 (68.9)
Medullary Carcinoma	3	3 (100.0)	0 (0.0)	3 (100.0)

3.4.4.4 PODO83 in ovarian carcinoma

Finally, we stained an ovarian carcinoma (EOC) TMA consisting of 219 cases with PODO83 (**Table 3-4**). As expected, most ovarian tumors (91.3%, 200/219) were PODO83 positive.

We previously showed that localization of Podxl core protein on the cell surface correlates with disease-free survival in high-grade serous ovarian carcinoma (HGSOC) (117). Therefore, we next examined the cellular localization of PODO83 staining in the PODO83-positive cases. Overall, many ovarian tumors displayed predominantly cytoplasmic staining (**Table 3-4**). However, 45.3% (67/148) of HGSOC, 35% (7/20) of clear cell and 45.8% (11/24) of endometroid samples exhibited PODO83 cell-surface staining. Unfortunately, we were unable to infer any prognostic conclusions of PODO83 staining in mucinous and low-grade serous tumor histotypes due to their low case representation on the TMA. Given that ovarian cancer has one of the highest mortality rates due to cancer in women, a PODO83-based therapy that recognizes Podxl on the cell surface of a variety of ovarian carcinomas could potentially benefit a large number of patients.

Table 3-4 PODO83 expression and localization within the Ovarian TMA cohort

Patient characteristics	Scorable Cases n	PODO83 positive		
		Total positive n (%)	Cell surface positive n (%)	Cytoplasmic positive n (%)
All scorable cases	219	200 (91.3)	89 (44.5)	111 (55.5)
Histological cell type (n)				
High-grade serous	158	148 (93.7)	67 (45.3)	81 (54.7)
Clear cell	25	20 (80.0)	7 (35.0)	13 (65)
Endometroid	27	24 (88.9)	11 (45.8)	13 (54.2)
Mucinous	5	4 (80.0)	1 (25.0)	3 (75.0)
Low-grade serous	4	4 (100.0)	4 (100.0)	0 (0.0)

3.4.5 PODO83 binds to the stalk domain of the PODXL protein

Given that PODO83 recognizes the Podxl core protein expressed on the surface of live cells by flow cytometry, we hypothesized that PODO83's epitope is situated in the extracellular domain of the protein. In order to test this, we assessed the ability of PODO83 to bind to SKOV3 *PODXL*-KO cells expressing the WT Podxl protein or a Podxl mutant lacking either the mucin domain (ΔMucin) or the entire extracellular domain (ΔEC) (**Fig 3.4**). PODO83 was able to bind to both the WT Podxl and ΔMucin protein, which contain the juxta-membrane and stalk domain. However, PODO83 was not able to bind to ΔEC, suggesting that PODO83's epitope lays on the protein stalk domain.

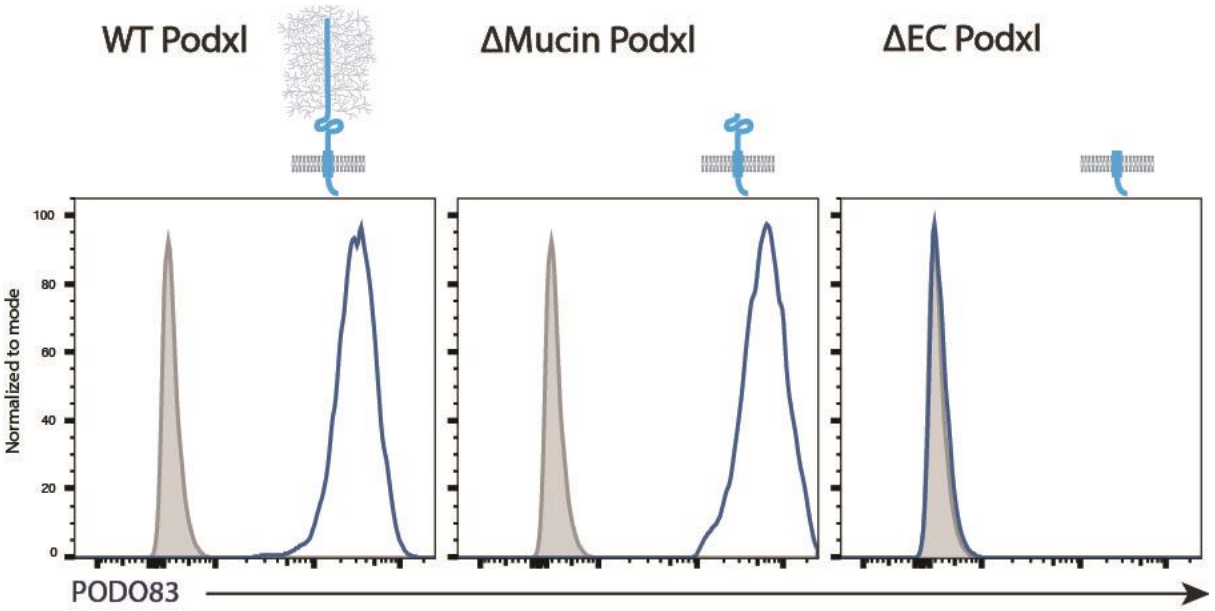

Figure 3.4 PODO83 binds to the stalk domain of the Podxl protein

Flow cytometric histograms showing PODO83 (blue lines) immunoreactivity to SKOV3 *PODXL-KO* cells re-expressing the wild-type Podxl (WT Podxl) protein, a Podxl-mutant lacking the mucin domain (ΔMucin Podxl), or a Podxl-mutant lacking the extracellular domain (ΔEC).

3.4.6 PODO83 recognizes PODXL expressed in healthy tissues

Based on our evidence that PODO83 recognizes and blocks a functional epitope on the stalk domain of the Podxl core protein, we hypothesized that PODO83 would recognize the core protein of Podxl, in both tumor and normal tissues.

Podxl is highly expressed in the kidney podocytes of the glomerulus as well as in the vascular endothelium. Therefore, we assessed the ability of PODO83 to recognize Podxl expressed in these structures in formalin-fixed paraffin embedded normal kidney tissue sections. As expected, we observed readily evident strong staining of the glomerulus and the surrounding vascular endothelium tissue (**Figure 3.5 A**).

To further assess PODO83's reactivity with Podxl across the different tissues, we stained an array of normal human tissues (**Figure 3.5 B, Table 3-5**). We observed PODO83 staining across most tissues examined, except for the parathyroid and the peripheral nerve in which neither cellular nor vascular staining was observed. (**Table 3-5**) While most of the staining was cytoplasmic in nature, we did observe PODO83 cell-surface staining on the podocytes of the kidney cortex, cerebral cortex, breast, fallopian tube, spleen and endometrium. Interestingly, in some tissues, cells that otherwise appeared to be PODO83 negative, we noted rare to occasional staining in the nuclear compartment. We observed strong vascular staining across all tissues examined, suggesting that therapeutic use of PODO83 might result in off-target vascular toxicity. However, when used systemically to treat mice in an *in vivo* xenograft model, we did not observe any visible signs of acute toxicity. This could reflect either a selective requirement of the PODO83 epitope on proliferating and migrating cells (endothelial cells are neither proliferating

nor migrating), functional compensation by another related family member (CD34 is also highly expressed by vascular endothelia) or a lack of PODO83 reactivity with mouse Podxl (addressed below).

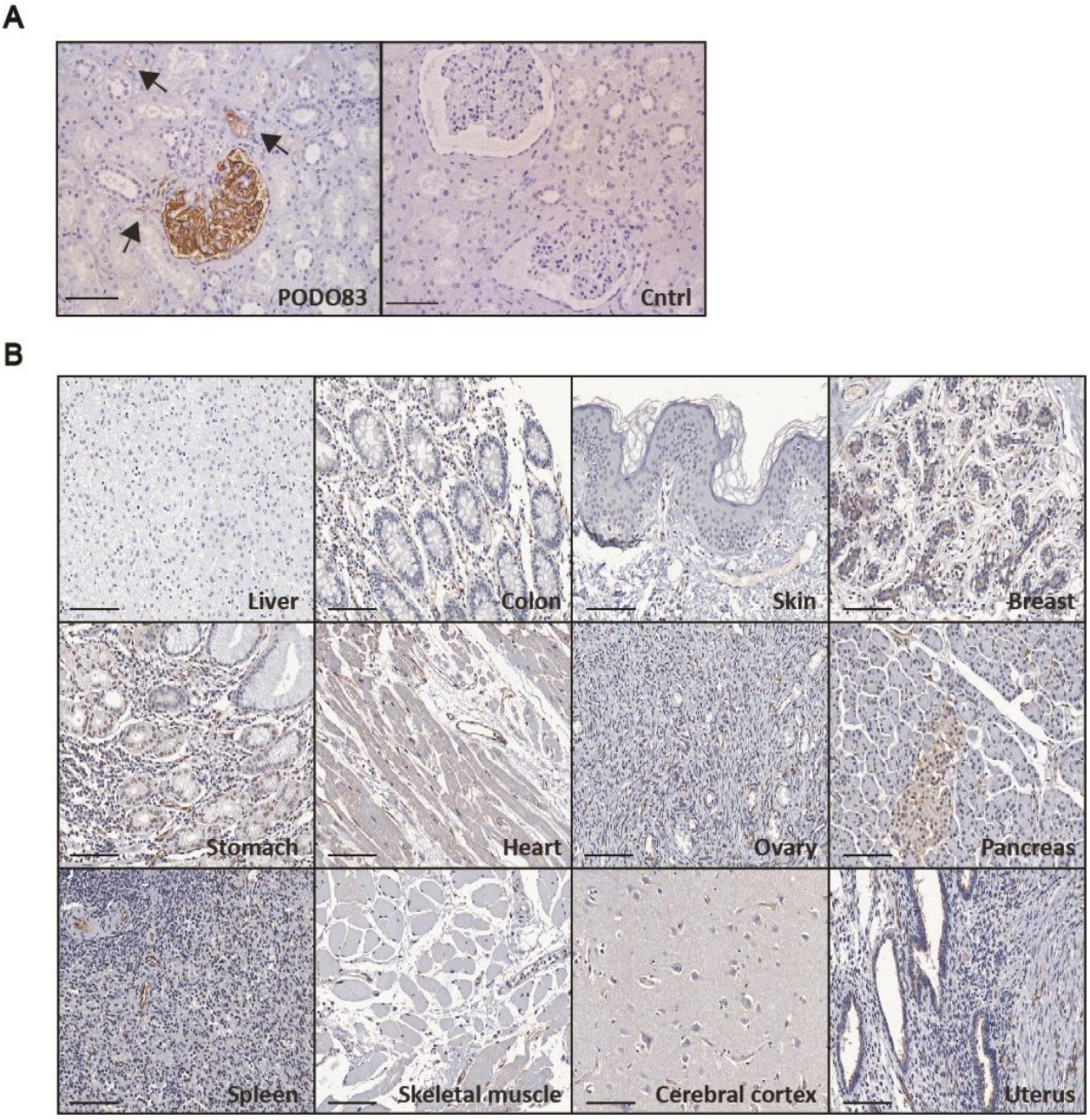

Figure 3.5 Representative images of healthy human tissue stained with PODO83

(A) Normal human kidney serial sections stained with either PODO83 or isotype-matched control. Note the strong PODO83 staining (brown color) present on the podocytes in the glomerulus and on vascular endothelia (arrows). **(B)** Examples of normal human tissue sections stained with PODO83. Scale bars = 100 μm.

Table 3-5 Summary of PODO83 cross-reactivity with normal human tissues

Tissue	PODO83		
	Frequency (intensity)	Localization	Vasculature (intensity)
Adrenal gland	Occasional	Nuclear	Occasional (1)
Bladder	Occasional	Cytoplasmic	Rare to occasional (2)
Bone	Neg		Rare (2)
Bone marrow			
Brain			
Cerebellum	Neg		Occasional (2)
Cerebral Cortex	Rare	Membranous	Frequent (2)
Breast	Occasional	Membranous	Rare to occasional (1)
Fallopian Tube	Frequent	Membranous	Occasional to Frequent (2)
GI – Track			
Esophagus	Neg		Rare to occasional (2)
Stomach	Occasional	Nuclear	Occasional (2)
Small Intestine	Rare to occasional	Cytoplasmic	Occasional to Frequent (2)
Colon	Rare to occasional	Nuclear	Occasional to frequent (2)
Rectum	Very rare	Cytoplasmic	Rare to occasional (2)
Head and neck	Occasional	Nuclear	Rare to occasional (2)
Salivary gland			
Heart	Neg		Frequent (2)
Kidney			
Cortex	Rare to occasional	Membranous (podocytes)	Occasional to frequent (2)
Medulla	Occasional	Cytoplasmic	Occasional to frequent (2)
Liver	Rare to occasional	Nuclear	Rare to occasional (2)
Lung	Rare to occasional	Nuclear	Occasional to frequent (2)
Ovary	Occasional to frequent	Nuclear	Occasional (2)
Pancreas	Very rare	Cytoplasmic	Occasional to frequent (2)
Parathyroid	Neg		Neg
Peripheral nerve	Neg		Neg
Pituitary gland	Neg		Occasional (1)
Placenta	Neg		Occasional (2)
Prostate	Rare to occasional	Nuclear	Occasional to frequent (2)
Skeletal muscle	Neg		Occasional (2)
Skin	Rare to occasional	Nuclear	Very rare (1)

Tissue	PODO83		
	Frequency (intensity)	Localization	Vasculature (intensity)
Spinal cord	Neg		Rare to occasional (2)
Spleen	Rare to occasional	Membranous	Occasional (2)
Testis	Neg		Occasional to frequent (2)
Thymus	Neg		Rare (2)
Thyroid	Neg		Occasional to frequent (2)
Tonsil	Rare to occasional	Nuclear	Occasional (2)
Ureter	Neg		Rare to occasional (1)
Uterus			
Cervix	Rare to occasional	Nuclear	Occasional to frequent (2)
Endometrium	Occasional to frequent	Membranous	Occasional to frequent (2)

The frequency of cells with staining was identified as follows: negative (Neg), very rare (<1% cells of a particular cell type), rare (1-5% of cells of a particular cell type), rare to occasional (5-25% of cells of a particular cell type), occasional (>25-50% of cells of a particular cell type), occasional to frequent (>59-75% of cells of a particular cell type), frequent (>75-100% of cells of a particular cell type). Blood vessel (endothelium) staining is detailed under each individual tissue. The intensity of the staining as indicated in brackets, was scored as: 1+ = weak, 2+ = moderate, 3+ = strong, 4+ = intense. Palivizumab was used as negative (Neg) isotype control.

3.4.7 PODO83 binds exclusively to the human PODXL protein

To determine if treatment with PODO83 might result in off-target toxic effects in humans that were not observed in our murine model, we examined the ability of the PODO83 to bind to murine and human Podxl. We stained 4T1 mouse breast cancer cells, which express high levels of murine Podxl, with PODO83. While the positive control, a commercial anti-mPodxl antibody, was able to recognize the Podxl protein on the surface of the 4T1 cells, we observed no staining of these cells with PODO83 (**Figure 3.6**). To confirm these results, we stained Chinese hamster ovarian (CHO) cells expressing different Podxl orthologs (human, murine, and macaque), and the Podxl-related protein CD34. Interestingly, PODO83 was only able to recognize the human Podxl core protein and failed to bind to its macaque or murine orthologs or to human CD34 (**Figure 3.6**). These results indicate that PODO83 is specific to the human Podxl protein, and that further toxicity studies will need to be performed using a different pre-clinical model, such as transgenic mice expressing the human Podxl protein, in order to determine whether there are acute toxic side effects of PODO83 treatment (in progress).

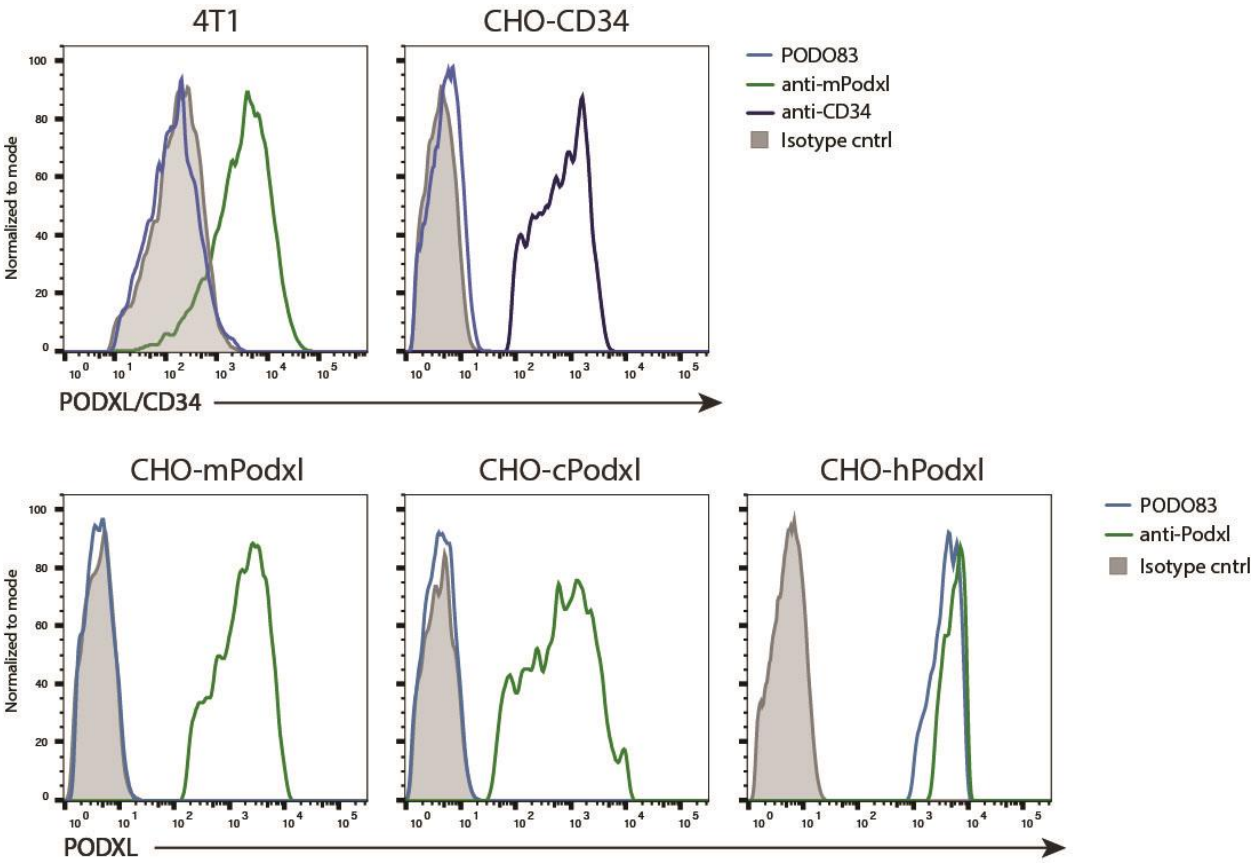

Figure 3.6 PODO83 exclusively recognizes human Podxl

Flow cytometric histograms showing a commercial anti-Podxl (green line) or PODO83 (light blue line) antibody immunoreactivity to 4T1 cells and CHO cells expressing human CD34 (CHO-CD34), and murine (CHO-mPodxl), macaque (CHO-cPodxl) and human (CHO-hPodxl) Podxl protein.

3.5 Discussion

Though Podxl has been associated with poor prognosis in a wide variety of cancers, including those with some of the highest mortality rates (pancreatic adenocarcinoma and high-grade serous ovarian cancer) (109), to date, no Podxl-based cancer therapeutics or diagnostics are currently available. Here we examined a variety of properties of PODO83, a novel anti-Podxl monoclonal antibody, as an important step in advancing it as a therapeutic candidate for cancer treatment.

We previously showed that PODO83 is a function-blocking antibody that delays primary tumor growth and blocks metastasis to the lung in an *in vivo* xenograft model (136). Here, we further explored PODO83's mechanism of action. Although we previously showed that ablating Podxl expression in MDA-MB-231 cells dramatically reduces their tumorsphere forming ability *in vitro*, we found that PODO83 had no effect. Thus, the tumorsphere forming function conferred by Podxl expression in MDA-MB-231 or MCF7 breast cancer cells appears to be independent of the epitope required for *in vivo* growth and metastases. Podxl expression greatly impacts the ability of MDA-MB-231 and MCF7 cells to form tumorspheres and, as such, we hypothesized that PODO83 would have a similarly large effect on tumorsphere forming efficiency (i.e. a functional blocking effect). However, we did not observe a change in tumorsphere-formation in the presence of PODO83 for either MDA-MB-231 or MCF7 cells. It is possible that PODO83 exerts a subtle, yet significant effect on tumorsphere formation that would only be discernable when multiple biological replicates are compared. Nevertheless, PODO83 treatment does not appear to have the same tumorsphere-blocking capacity as Podxl gene ablation.

In addition, while PODO83 treatment did not result in a statistically significant delay of the growth of primary tumors in mice with an established tumor burden ($\geq 0.5 cm^3$), it was able to

block metastasis to the lungs in these mice. Moreover, PODO83 treatment caused delayed invasion (but not migration) of cancer cells *in vitro*. PODO83 treatment mimicked the invasion (but not migration) behavior of MDA-MB-231 *PODXL*-KD cells. Moreover, PODO83 treatment also delayed invasion (but not migration) of SKOV3 cells *in vitro* (**Fig 5.1**). Since the effect size is small, further biological replicates would be required to confirm the significance of these results. However, taken together, these results suggest that PODO83 treatment primarily affects the ability of tumor cells to invade tissues, rather than their ability to grow or migrate. Since cell migration is a characteristic feature of invasive cells, it is possible that PODO83 is affecting the breakdown of the basal membrane (BM) or extracellular matrix (ECM), a step unique to the invasion process. Notably, we have previously shown that Podxl regulates adhesion and spreading of endothelial cells to the basal matrix, specifically to laminin and collagen proteins (180,188). Proteins of the ECM and BM can bind cell surface receptors to induce ECM/BM degradation through the activation and release of proteinases (189). Moreover, tumor cell attachment to exogenous laminin promotes ECM degradation via type IV collagenolytic activity (190). As such, one could speculate that the binding of PODO83 to Podxl is preventing proteinase activation through altering receptor-ligand interaction (i.e. Podxl-laminin) by directly blocking a functional epitope on Podxl and thus resulting in decreased cell invasion. Since metastatic disease is responsible for most cancer deaths, PODO83 poses as a potential therapeutic candidate to treat this unmet clinical need.

Given that PODO83 is a function-blocking antibody, we sought to identify its reactive epitope and shed some light on Podxl's functional role in promoting cancer progression. Here we find that PODO83 binds to the Podxl extracellular stalk domain and show that it recognizes the Podxl core protein expressed by several types of cancer. Intriguingly, though Podxl is a transmembrane

protein, we observe intracellular staining with PODO83. Since we are using DAB staining which is based on the formation of a brown precipitate when the DAB is oxidized at the location of the horseradish peroxidase (HRP)-Ab conjugate, we are unable to determine the specific cellular compartment localization of the PODO83 staining. Thus, one can postulate that the observed intracellular staining is the result of the accumulation of vesicles containing Podxl that are in transit to the cellular membrane or awaiting signaling to be shed. In addition, we observe occasional nuclear staining with PODO83. Since we can't determine subcellular staining localization using DAB, one explanation could be that the antibody is recognizing the Podxl protein in the endoplasmic reticulum (ER) which expands across the nucleus and can be mistaken for nuclear staining. Since other Abs, including commercially available anti-Podxl Abs, display occasional nuclear staining, another explanation could be that the observed nuclear staining is the result of a staining artefact due to Ab cross-reactivity with nuclear components.

In addition, we show that PODO83 recognizes healthy tissue, especially vascular endothelium and kidney glomeruli. This raises the potential for off-tumor side effects that need to be examined further. Unfortunately, as we showed that PODO83 binds specifically to the human Podxl core protein and does not recognize macaque or murine Podxl, or human CD34, assessment of the potential toxicity associated with PODO83 treatment still needs further evaluation. Towards that goal we recently generated an ES cell line where the mouse extracellular domain encoding exons have been replaced with the human encoding exons. These are currently being used to generate a "humanized" Podxl mouse which will prove ideal for identifying PODO83 associated toxicities.

Although more studies are required to determine PODO83's mechanism of action, in this Chapter we have provided novel insight into its functionality and highlighted its value as a research and clinical tool. PODO83 recognizes a functional epitope involved in cancer metastasis which highlights its value as a research tool to further investigate the role of Podxl in cancer progression. Additionally, PODO83 has a high affinity for the core Podxl protein and has a higher affinity and produces a much higher signal than commercial antibodies in paraffin-embedded tissues, making it a potential diagnostic tool and, pending toxicity studies, potential therapeutic application to prevent metastases. Lastly, to circumvent the potential vascular and renal toxicity associated with antibodies reactive to the core Podxl polypeptide, future studies may include the exploration of potential tumor-associated glycoforms of Podxl and the generation of antibodies to target them.

Chapter 4: Development and characterization of novel tumor-restricted anti-podocalyxin PODO447 and investigation of its use as a cancer therapeutic.

Sections 4.4.1-5 are modified from a published manuscript: **Canals Hernaez D**, Hughes MR, Dean P, Bergqvist P, Samudio I, Blixt O, Wiedemeyer K, Li Y, Bond C, Cruz E, Köbel M, Gilks CB, Roskelley C, McNagny KM. *J Immunother Cancer*. 2020; doi:10.1136/jitc-2020-001128

4.1 Synopsis

Cancer therapy has seen remarkable improvements in the past decade with the introduction of new targeted therapies. However, most of the success stories have been limited to "liquid" malignancies. The progress in development of new treatments for solid tumors has been slow due, in part, to the lack of good target antigens. Here we describe a novel tumor-restricted glycoantigen on Podxl and the development of an antibody against it (PODO447). We demonstrate that PODO447 recognises a glycoepitope present in tumor cells but not in healthy human tissue. Further, we analyze the presence of this novel tumor antigen in several human cancers, and identify ovarian high-grade serous carcinoma as a potential therapeutic application. This work identifies for the first time a tumor-restricted epitope on Podxl and validates PODO447 as a potential therapeutic antibody.

4.2 Introduction

According to the latest cancer statistics, in 2018 there were an estimated 18.1 million new cancer cases and 9.6 million cancer deaths (146). These numbers are only expected to grow, with 29.5 million incident cases and 16.4 million cancer deaths estimated worldwide by 2040 (191).

Although genetic and/or epigenetic changes are known to drive tumour development, dysregulation of protein expression and altered post-translational modifications are also known to occur. Specifically, changes in the patterns of protein glycosylation are well-known to occur in cancer (46) and, in some cases, are thought to drive tumour progression (53). This can be through well-known effects on protein stability and folding; or through modification of processes including protein trafficking, immune recognition, cell migration, ligand-receptor interaction, signal transduction, and cell adhesion (44,192-195). Indeed, glycans can confer a selective advantage on cells that facilitates tumour spread (196,197). Moreover, cancerous cells undergo reprograming and transcriptional changes that greatly impact their glycome and glycoproteome, leading to overexpression or *de novo* expression of specific glycoepitopes. Importantly, these cancer-specific alterations in protein glycosylation may also provide a unique opportunity for clinical intervention with reduced toxicity since these modifications are largely tumour-specific.

Podocalyxin (Podxl) is a member of a three-gene family of sialomucins that includes Podxl, CD34 and endoglycan. These proteins can be distinguished from other cell surface sialomucins based on a shared genomic organization (each encoded by a similar, 8-exon, genomic locus) and a shared protein domain structure: they each contain a large, highly-glycosylated mucin domain followed by a cysteine-bonded globular domain, stalk domain, transmembrane domain, and a short (approximately 70 amino acid) cytoplasmic tail with a consensus C-terminal binding site for PDZ-domain proteins (107,198,199). Although widely expressed during embryonic development (107,200), in normal adult tissue Podxl is primarily expressed on vascular endothelia (179,180), kidney podocytes (107) and a restricted subset of epithelial lumens (107). Nevertheless, Podxl is also aberrantly expressed by a wide variety of cancer types, and this expression is consistently an

indicator of poor prognosis (108,110,112,117,136,144,158,163,164,184,201). For example, in early retrospective studies of breast cancer, patients with tumours expressing high levels of Podxl exhibited a greatly reduced disease-specific survival, and multi-variant analysis showed Podxl to be a highly-significant independent predictor of poor outcome (110). Similarly, in EOC where Podxl is expressed by the majority of high-grade serous carcinomas, cell surface expression of Podxl correlated with a significant decrease in disease free survival (117). Interestingly, recent gene silencing experiments suggest that upregulation of Podxl is not merely a predictor of poor outcome but also an important player in disease progression by enhancing tumour invasion and metastasis (39,108,136,172). In summary, because of its cell surface localization and its direct role in tumour metastasis, Podxl is a promising target for cancer therapy.

As a first foray into exploiting this opportunity, we generated a series of anti-Podxl monoclonal antibodies (mAbs) to the extracellular domain of Podxl expressed on the surface of tumour cells (136). One mAb, PODO83, showed a potent ability to restrict primary tumour growth *in vivo* and to block metastatic progression when administered to tumour bearing mice (136) (and see Chapter 3). While PODO83 harbors potential as a therapeutic, its ability to recognize the stalk domain of the Podxl core protein poses a possible risk of toxicity due to its reactivity with normal kidney podocytes and vascular endothelia.

Intriguingly, however, Podxl is known to undergo tissue-specific glycosylation (201), a process that is frequently altered in cancer (49,53,202). Accordingly, to circumvent the potential toxicity associated with antibodies reactive to the core polypeptide, we carefully rescreened our panel of anti-Podxl antibodies for those that react selectively with a tumour-restricted glycoform of Podxl

but not with normal tissue. Here we report the identification of PODO447, a novel monoclonal antibody with exquisite specificity for a tumour specific glycoepitope on Podxl. As such, PODO447 offers a unique opportunity to selectively target tumour tissue while sparing normal tissue and highlights its promise as a therapeutic.

4.3 Materials and Methods

4.3.1 Antibody generation

Rabbit and rabbit/human chimeric PODO447 antibodies were developed as previously described in Chapter 3 (3.2.1 Antibody generation). The antibody generation and initial characterization was performed at the Centre for Drug Research and Development.

4.3.2 Cell culture

HEK293, HUVEC, SKOV3, SUM149, PANC-1, A-172, MIAPACA and MDA-MB-231 cells were obtained from the American Tissue Culture Collection (ATCC). HEK293, human pancreatic adenocarcinoma (PANC-1, MIAPACA), A-172, and MDA-MB-231 cells were grown in DMEM (Gibco, #11965-092) supplemented with 10% FBS and 10 U/ml penicillin and streptomycin (P/S) (Gibco, #15140-122). Human umbilical vein endothelial (HUVEC) cells were harvested from donor umbilical cords (Human Ethics no. H10-00643), grown in Endothelial Cell Growth Medium-2 Bulletkit™ (LONZA, #CC-3162), and used between passages 2 and 8. Human ovarian cancer SKOV3 cells were grown in DMEM F-12 with 15 mM HEPES (Sigma, #D6421) supplemented with 10% FBS, 0.2 mM L-glutamine (Gibco, #25030-081) and 10 U/ml P/S . Human breast cancer SUM149 cells were grown in DMEM F-12 with 15 mM HEPES supplemented with 5% FBS, 5 μg/ml insulin (Sigma, #234-291-2), 1 μg/ml hydrocortisone (StemCell Technologies, #07904) and 10 U/ml P/S. All cell lines were maintained at 37°C, 5% CO_2 and high humidity.

4.3.3 Flow Cytometry

Cells were washed 1X with Ca^{2+}- and Mg^{2+}-free HBSS (Gibco, #14170-112), incubated for 1-2 min at 37°C in a 0.25% trypsin solution, quenched with complete growth media, then centrifuged for 4 min at 394*g*, washed 2X with FACS buffer (PBS, 2 mM EDTA, 5% FBS, 0.05% sodium azide) and transferred to a 96 well 'v' bottom plate. Cells were resuspended in 100 µl blocking buffer (FACS buffer, 1 µg/ml of anti-CD16/CD32 (clone 2.4G), 2% rat serum) for 20 min at 4°C in the dark, then spun at 394*g* for 4 min and incubated in 100 µl primary antibody (Ab) solution for 30 min at 4°C in the dark. Rabbit-PODO83 (136) (2 µg/ml) and either rabbit or chimeric-PODO447 (5 µg/ml) were used to detect Podxl. Rabbit-IgG (5 µg/ml, Vector Laboratories, #I-1000-5) and mouse/human-chimeric pavilizumab (5 µg/ml, National Research Council, NRC) were used as isotype controls. Next, cells were washed 3X with FACS buffer and resuspended in 100 µl of secondary Ab solution (Alexa Fluor 647 (AF647) donkey-anti-rabbit (2 µg/ml, Invitrogen, #A31573) or AF647 goat-anti-human (2 µg/ml, Jackson ImmunoResearch Laboratories, #109-605-098)) for 30 min at 4°C in the dark. Cells were washed 2X with FACS buffer and resuspended in FACS buffer containing propidium iodide (PI) (0.5 µg/ml, Life Technologies, #P3566). All flow cytometry data were acquired using a BD LSRII and analyzed using FlowJo™ software (BD Biosciences, Ashland).

4.3.4 Glycan array

Fabrication of the printed glycan array slides and high-throughput analysis were performed as previously described (203). Printed glycochips were incubated in blocking buffer (50 mM ethanolamine buffer, pH 8.5) for 1 h at room temperature (RT). Slides were rinsed with PBS (3X,

30 s), deionized water (1X, 30 s), and incubated with 50 μg/ml of humanized PODO447 or human IgG1κ isotype control for 1 h with gentle rotation (200 rpm) in a sealed, humidified environment. Next, slides were washed with PBS-T (PBS, 0.05% Tween20, pH 7.4 (1X, 5 min)) and PBS (1X, 30 s), followed by a short centrifugation. Slides were incubated with goat anti-human IgG-Cy3 (Fc specific, 10 μg/mL, Sigma-Aldrich, #C2571) for 1 h at RT. Slides were washed with PBS (3X, 30 s), deionized water (1X, 30 s), and dried by centrifugation (30 s). Fluorescent signals from the bound Ab were detected using ScanArray microarray scanner (PerkinElmer). Scanned images were analyzed using ScanArray Express software. Spots were identified using automated spotfinding with manual adjustments for occasional irregularities. Spot relative fluorescent intensity was determined by subtracting the median pixel intensity of the local background from the average pixel intensity within the spot. Triplicate spots were averaged and the mean value of relative fluorescent (RFU) intensity was used.

4.3.5 Enzymatic treatment

SKOV3 cells (2.5×10^6) were washed 1X with PBS, incubated in enzyme-free dissociation buffer (ThermoFisher Scientific, #13151-014) for 15 min, centrifuged at 394*g* and washed 1X with assay buffer (Ca^{2+}/Mg^{2+}-free DMEM/F12 (Sigma, #D9785), 2mM $CaCl_2$, 0.1% BSA). Aliquots were resuspended into three treatment conditions: Control (500 μl; assay buffer), neuraminidase (500 μl; 5 U/ml of neuraminidase (New England BioLabs, #P0720S) in assay buffer), or endopeptidase treatment (500 μl; 0.24 mg/ml of endopeptidase (Cedarlane, #CLE100) in assay buffer). Cells were treated for 45 min at 37°C, and tubes were inverted at 10 min intervals. Cells were then centrifuged

at 394*g* for 5 min and washed 2X with assay buffer prior to staining with rabbit PODO83, PODO447 and isotype control, and flow cytometric analysis.

4.3.6 Immunohistochemistry

EOC tissue microarrays (TMA) were obtained from the Genetic Pathology Evaluation Centre (GPEC) TMA Database (Vancouver, Canada), and stained with rabbit-PODO447 (5 μg/ml). Tissue cross-reactivity TMAs were purchased from US Biomax Inc. (#MNO1021) and stained with either Rbt/Hu-chimeric PODO447-BIOT (5 μg/ml) or Mo/Hu-chimeric pavilizumab-BIOT control (5 μg/ml). Additionally, humanized PODO447 was sent to Charles Rivers Laboratories for independent testing of Ab tissue cross-reactivity. Briefly, slides were deparaffinized and rehydrated in 100% xylene (3X, 5 min), 100% ethanol (2X, 3 min), 95% ethanol (1X, 3 min), 70% ethanol (1X, 3 min) and distilled water (1X, 3 min). Antigen retrieval was performed by heating slides in citrate buffer at 90°C for 30 min. Slides were washed in PBS (3X, 5min), incubated for 30 min in blocking solution (PBS, 5% donkey serum, 1% BSA, 0.2% Triton X-100, 0.05% Tween 20), and incubated in primary Ab solution overnight at 4°C. Slides were then washed with TBST (3X, 15 min), incubated with secondary Ab (anti-rabbit-BIOT, 2 μg/ml, SouthernBiotech, #6440-06) in blocking solution for 30 min at RT, and washed again with TBST (4X, 15 min). Endogenous peroxidase was blocked with 0.3% hydrogen peroxide in methanol for 30 min at RT prior to rinsing 3X with PBS. Signal was amplified using Vectastain® Elite® ABC HRP Kit (Vector Laboratories, #PK-6100) according to manufacturer's instructions, and then washed with PBS (3X, 5min). Signal was visualized using a DAB peroxidase (HRP) Substrate Kit (Vector Laboratories, #SK-4100) following the manufacturer's recommendations. Each slide

was incubated with DAB solution for 1-5 min until strong signal appeared, then the reaction was stopped by dilution with PBS. Slides were washed with PBS (2X, 5 min), distilled water (2X, 2 min), stained in hematoxylin (12 s, VWR, #10143-150) and rinsed with tap water. Staining was fixed in Bluing Solution (0.1% sodium bicarbonate) for 1 min and rinsed in distilled water (2X, 2 min) prior to dehydration in graded alcohols and xylene. Slides were mounted using Permount solution (Fisher Scientific, #SP15100) and subsequently analyzed for Podxl staining and localization.

4.3.7 Immunohistochemical scoring

EOC TMAs (219 cases) were blindly scored by four independent observers (DCH, KW, CDR), including a pathologist (MK), compared and combined. Initially, scoring was based on number of stained cells, intensity and staining pattern. Number of stained cells was represented by an overall percentage of stained cells in the tumour, and then translated into a scoring scale of 0 (no staining, <1%), +1 (intermediate, 1-50%) and +2 (high, >50%). Intensity was scored based on a scale of 0 (negative), 1 (weak), 2 (intermediate) and 3 (strong). We then combined +1 and +2 cases with weak or higher staining and grouped them as PODO83 or PODO447-positive, respectively. The dominant staining pattern of each case was scored as A (apical), AL (apicolateral), L (lateral), B (basal), BL (basolateral), and CY (cytoplasmic). We then combined A, AL, B and BL groups as M (membranous), and compared CY versus M staining for each of the mAbs. The tissue cross-reactivity (TCR) studies were performed by two independent facilities, including the preclinical contract research organization (CRO) Charles River Laboratories were the analysis was carried out by an independent pathologist under good laboratory practices (GLP). For the TCR TMAs, the frequency of stained cells was identified as

negative (Neg), very rare (<1%), rare (1-5%), rare to occasional (5-25%), occasional (>25-50%), occasional to frequent (>59-75%), and frequent (>75-100%). Blood vessel (endothelium) staining was included as part of the overall score for each individual tissue.

4.4 Results

4.4.1 PODO447: Identification of a novel anti-Podxl tumor-specific antibody

Though PODO83 harbors great potential as a function-blocking antibody, its recognition of the Podxl core protein expressed in normal tissue could hamper its application as a cancer therapeutic due to potential toxicity. Therefore, our next objective was to identify an anti-Podxl antibody that could preferentially recognize Podxl expressed in tumor tissue. To do this, we re-screened our array of anti-Podxl Abs for those reactive with Podxl-expressing human tumour cell lines from diverse tissue origins including PC3 (prostate), A-172 (glioblastoma), SUM 149 (breast), PANC-1, CFPAC and BXPC3 (pancreatic), A-549 (lung), A-375 and WM115 (melanoma), SKOV3 (ovarian), MDA-MB-231 (breast) and MIAPaCa2 (pancreatic), and then counter-screened against normal human umbilical endothelial cells (HUVEC) to identify tumor-specific Abs. PODO83 bound strongly to all tumor cells as well as HUVEC cells, with the exception of BXPC3 cells where PODO83 displayed lower immunoreactivity. In contrast, while we observed binding of PODO447 to A-172, SUM 149, PANC-1, BXPC3, A-549 and, to a lesser extent, to PC3, CFPAC and WM115 tumor cells, no immunoreactivity was observed on A-375 skin cancer cells or normal HUVECs. Thus, PODO447 surfaced as the only antibody in our panel that showed high specificity only for Podxl expressed on tumour cell lines, compared to PODO83 that recognized Podxl both on tumor and normal cells (**Fig 4.1**).

To confirm Podxl specificity, we ablated Podxl expression in three PODO447/83-positive tumor lines (SKOV3, MIAPACA and MDA-MD-231) using CRISPR-mediated gene deletion. We observed complete loss of PODO447 and PODO83 binding on all CRISPR-*PODXL*-knockout

(*PODXL*-KO) cells compared to the parental (WT) lines (**Fig 4.2**), thus confirming that both PODO447 and PODO83's epitopes are specific to the Podxl protein.

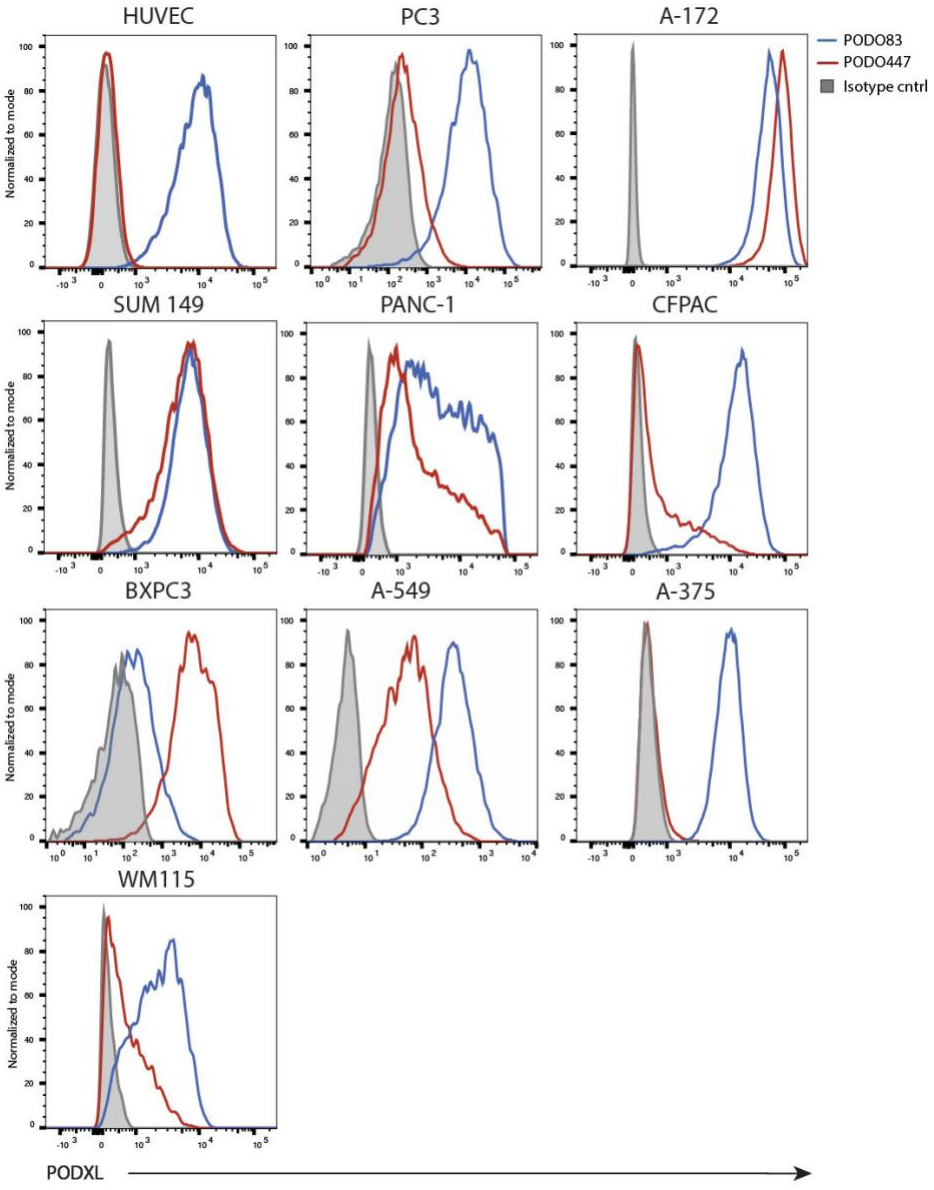

Figure 4.1 PODO447 and PODO83 binding profile on tumor and normal cell lines

Flow cytometric PODO83 (blue lines) and PODO447 (red lines) binding profiles of Podxl-positive normal (HUVEC) and tumour cells: prostate adenocarcinoma (PC3), glioblastoma (A-172), triple-negative breast cancer (SUM149), pancreatic adenocarcinoma (PANC-1, CFPAC, BXPC3), lung carcinoma (A-549), and melanoma (A-375, WM115).

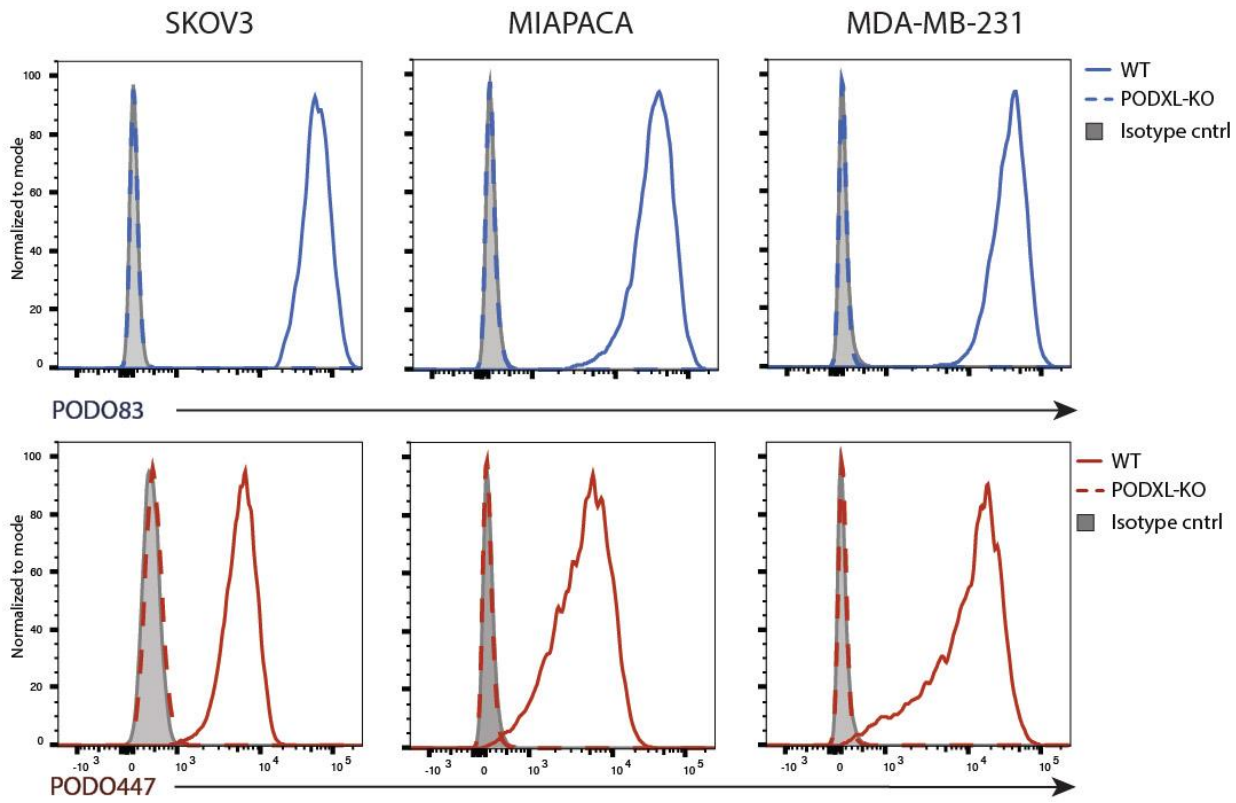

Figure 4.2 PODO447 and PODO83 specifically recognize the Podxl protein

Flow cytometric histograms showing PODO83 (blue lines) and PODO447 (red lines) immunoreactivity to Podxl-positive (WT, solid lines) or -deficient (*PODXL*-KO, dashed lines) ovarian (SKOV3), pancreatic (MIAPACA) and breast (MDA-MB-231) cancer cells.

4.4.2 The PODO447 epitope is not present on healthy human tissue

Our next objective was to further assess the specificity of PODO447 for tumor-expressed Podxl. To do so, we evaluated the reactivity of PODO447 to normal human kidney, where Podxl is highly expressed in podocytes of the glomerulus (107), and compared it to that of PODO83 immunoreactivity. As mentioned before, in formalin-fixed paraffin embedded tissue, PODO83 staining is readily evident in the glomerulus and the vascular endothelium, whereas PODO447 staining is not detectable (**Fig 4.3A**). Next, we further evaluated PODO447's cross-reactivity on an array of normal human histological sections. While PODO447 demonstrated intense staining of cryo-sectioned, control A-172 cells (**Table 4-1)**, we found it to be minimally reactive on normal tissue (**Figure 4.3B, Table 4-2**). We detected rare-to-occasional reactivity (<10%) on mucosal epithelial cells in breast, fallopian tube and endometrium. In addition, we observed occasional weak cytosolic positivity in cells of the salivary gland and adrenal gland, stomach, rectum, pancreas and kidney cortex. This intracellular reactivity was also evident in tissues stained with an isotype-matched negative control, arguing against specific reactivity. Importantly, we found minimal expression of the PODO447 epitope on normal endothelia of all tissue sites examined. The sole exception was occasional vessel-like structures restricted to the kidney medulla. We hypothesize that these structures are likely vasa-recta, a highly specialized type of vessels that collect water from the medulla interstitium. We are currently working on confirming this hypothesis and the potential toxic effect that PODO447 might have if it were to bind *in vivo*.

In addition, PODO447's minimal normal tissue cross-reactivity was independently confirmed by the Charles River Laboratories (CRL) at both low (2 μg/ml) and high (20 μg/ml) Ab concentrations

(**Appendix D)**. Concordantly, CRL found that PODO447 stained the cytoplasm of a very low number of podocytes, rare cells of the mucosal epithelia of the fallopian tube and small intestine, and rare cells of the skin sweat gland epithelia. Therefore, we conclude that PODO447 does not recognize the Podxl core protein (or other epitopes) expressed by most, if not all, normal tissue (**Figure 4.3, Table 4-2, Appendix D**).

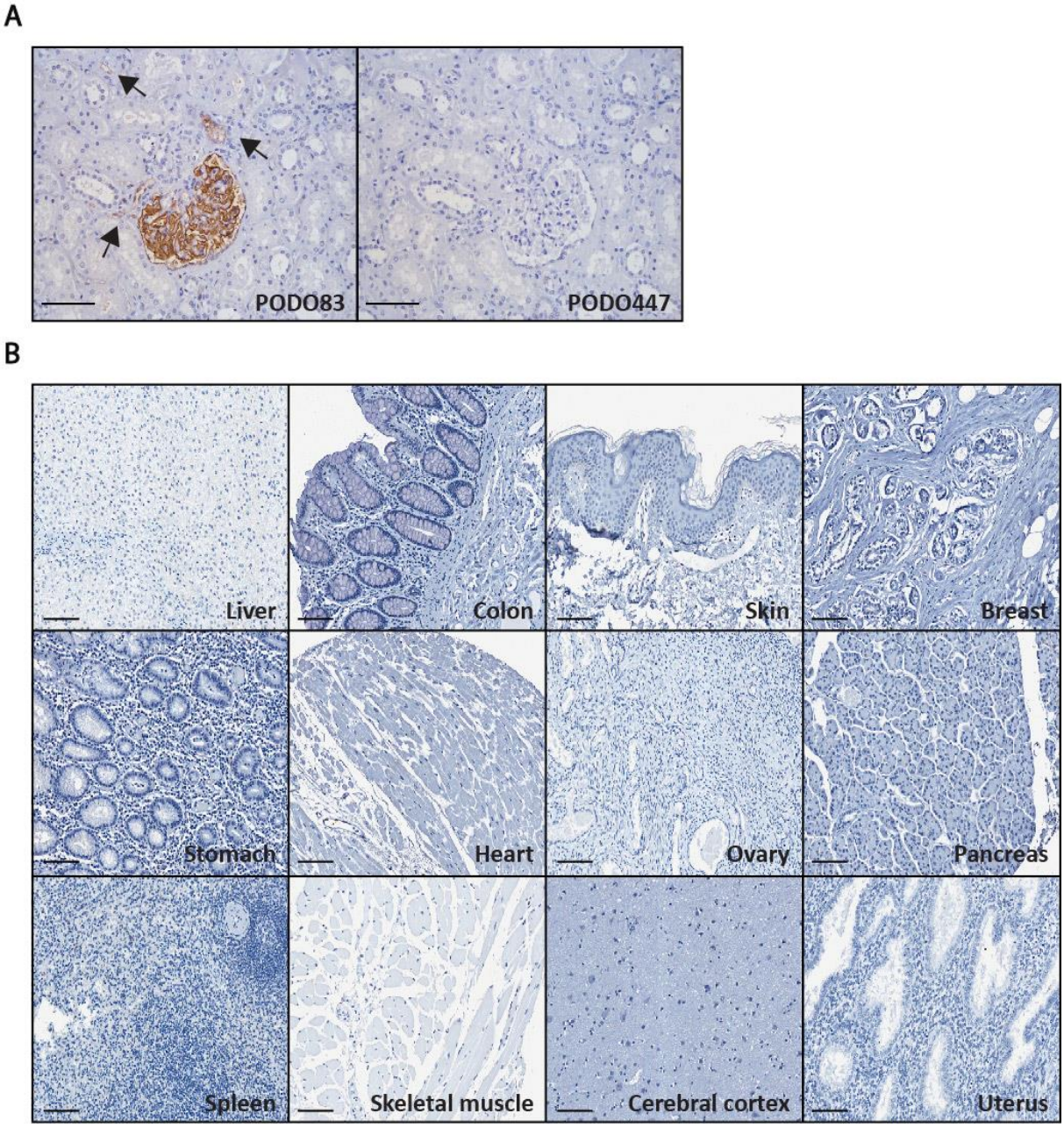

Figure 4.3 Representative images of healthy human tissue stained with PODO447

(A) Normal human kidney serial sections stained with either PODO83 or PODO447. Note the strong PODO83 staining (brown color) present on the podocytes in the glomerulus and on vascular endothelia (arrows). **(B)** Examples of normal human tissue sections stained with PODO447. Scale bars = 100 μm.

Table 4-1 Summary of PODO447 cross reactivity with control tissues

Tissue	PODO447		Neg Control	
	2μg/ml	20μg/ml	2μg/ml	20μg/ml
Cryosections of A-172 cells Positive control material	Frequent (3-4+)	Frequent (3-4+)	Neg	Neg
Cryosections of MDA-MB-231 *PODXL-KO* cells Negative control material	Neg	Neg	Neg	Neg
Cryosections of human fetal kidney Ancillary control material	Rare to occasional (1-3+)	Rare (1-3+)	Neg	Neg

The frequency of cells with staining was identified as follows: no staining (Neg), very rare (<1% cells of a particular cell type), rare (1-5% of cells of a particular cell type), rare to occasional (5-25% of cells of a particular cell type), occasional (>25 50% of cells of a particular cell type), occasional to frequent (>59-75% of cells of a particular cell type), frequent (>75-100% of cells of a particular cell type). Intensity of staining was scored as: 1+ = weak, 2+ = moderate, 3+ = strong, 4+ = intense, Neg = Negative. HuIgG1 was used as negative (Neg) control.

Table 4-2 Summary of PODO447 cross-reactivity with normal human tissues

Tissue	PODO447	Neg Control
Adrenal gland	Very rare (1)	Very rare (1)
Bladder	Neg	Neg
Bone	Neg	Neg
Bone marrow		
Brain		
Cerebellum	Neg	Neg
Cerebral Cortex	Neg	Neg
Breast	Rare to occasional (2)	Neg
Fallopian Tube	Rare to occasional (1)	Neg
GI – Track		
Esophagus	Neg	Neg
Stomach	Rare (2)	Rare (1)
Small Intestine	Neg	Neg
Colon	Neg	Neg
Rectum	Rare (1)	Rare (1)
Head and neck	Rare (2)	Rare (1)
Salivary gland		
Heart	Neg	Neg
Kidney		
Cortex	Occasional (1)	Occasional (1)
Medulla	Rare to occasional (2)	Neg
Liver	Neg	Neg
Lung	Neg	Neg
Ovary	Neg	Neg
Pancreas	Neg	Rare (1)
Parathyroid	Neg	Neg
Peripheral nerve	Neg	Neg
Pituitary gland	Neg	Neg
Placenta	Neg	Neg
Prostate	Neg	Neg
Skeletal muscle	Neg	Neg
Skin	Neg	Neg
Spinal cord	Neg	Neg
Spleen	Neg	Neg
Testis	Neg	Neg

Tissue	PODO447	Neg Control
Thymus	Neg	Neg
Thyroid	Neg	Neg
Tonsil	Neg	Neg
Ureter	Neg	Neg
Uterus		
Cervix	Neg	Neg
Endometrium	Very rare (2)	Neg

The frequency of cells with staining was identified as follows: negative (Neg), very rare (<1% cells of a particular cell type), rare (1-5% of cells of a particular cell type), rare to occasional (5-25% of cells of a particular cell type), occasional (>25-50% of cells of a particular cell type), occasional to frequent (>59-75% of cells of a particular cell type), frequent (>75-100% of cells of a particular cell type). Blood vessel (endothelium) staining is detailed under each individual tissue. The intensity of the staining as indicated in brackets, was scored as: 1+ = weak, 2+ = moderate, 3+ = strong, 4+ = intense. pavilizumab was used as negative (Neg) isotype control.

4.4.3 PODO447 immunoreactivity requires the mucin domain of Podxl

Given that both PODO83 and PODO447 bind to the extracellular domain of the protein, we hypothesized that PODO447 may bind to a region subject to post-translational modifications and likely within the mucin domain. To test this, we performed a series of enzyme degradation assays using PODO83- and PODO447-reactive SKOV3 ovarian carcinoma cells (**Figure 4.4A**). Treatment of SKOV3 cells with neuraminidase, which removes terminal sialic acids on glycoproteins, did not affect binding of either Ab. However, O-sialoglycoprotein endopeptidase, a proteolytic enzyme that specifically cleaves proteins bearing clusters of negatively charged sugars, attenuated PODO447, but not PODO83, immunoreactivity (**Figure 4.4A**). From this, we conclude that the PODO447 epitope lies within the mucin domain.

To further confirm this result, we reconstituted SKOV3 *PODXL*-KO cells with either the full length, wild-type (WT) protein or a mutant lacking the N-terminal mucin domain (ΔMucin), and evaluated the ability of these to restore the PODO83 and PODO447 epitope **(Figure 4.4B)**. Whereas both Abs bound to *PODXL*-KO cells expressing the WT protein, only PODO83 (but not PODO447) reacted with cells expressing the Podxl-ΔMucin protein. From these data, we conclude that the PODO83 epitope is present within the extracellular stalk domain of Podxl, whereas PODO447 binds selectively to an epitope within the glycosylated mucin domain

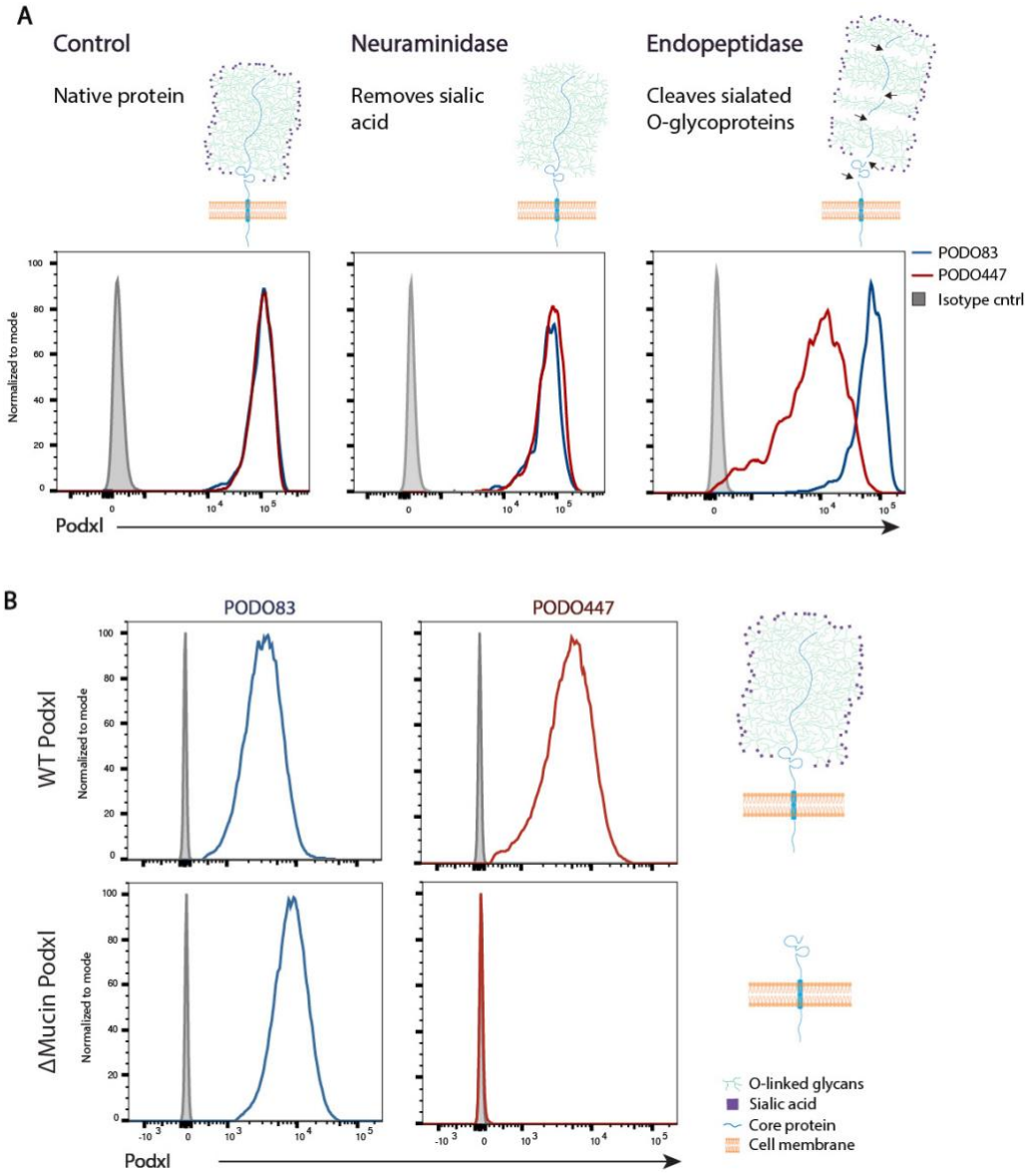

Figure 4.4 PODO447 recognizes a glycomotif on the mucin domain

(A) Flow cytometric histograms of SKOV3 WT cells treated with either assay buffer (control), neuraminidase (which removes the terminal sialic residues) or O-sialoglycoprotein endopeptidase (which cleaves the mucin domain). Cells were then stained with either PODO83 (blue) or PODO447 (red). **(B)** Flow cytometric histograms showing PODO83 (blue lines) and PODO447 (red lines) immunoreactivity to SKOV3 *PODXL-KO* cells re-expressing the wild-type Podxl (WT Podxl) protein or a Podxl-mutant lacking the mucin domain (ΔMucin Podxl).

4.4.4 PODO447 recognizes a tumour-restricted terminal GalNacβ1 glycoepitope

Since PODO447 showed selective binding to the mucin domain of Podxl on tumour cells we hypothesized that it may react with a modified glycoepitope generated exclusively by tumour cells. To gain further insights into its specificity, we probed a well-characterized glycan array (204) with PODO447 to map potential glycoepitopes (**Table 4-3, Appendix E**). This printed array includes 320 distinct glycan structures and serves as an ideal platform for identifying binding structures required for carbohydrate recognition (205). PODO447 exhibited the highest affinity to a rare, terminal N-acetylgalactosamine-beta1 (GalNAcβ1) motif on O-linked glycans (**Table 4-3, Appendix E**). This glycomotif has been previously found on cancer-associated glycoepitopes such as globotetraose (Gb4, P) (206) and LadiNAc (207). However, to the best of our knowledge, this is the first time the GalNAcβ1 motif has been observed on Podxl, and PODO447 represents the first mAb against it.

Table 4-3 PODO447 recognizes a rare glycomotif

Glycan Structure	Common name	Median RFU (10^3)
GalNAcβ1-3Galα1-4Galβ1-4Glcβ-sp3	Gb4, P	46.9
GalNAcβ-sp10	beta-GalNAc	37.8
(GalNAcβ-PEG2)3-β-DD	(ANb-PEG2)3	37.2
GalNAcβ-sp3	beta-GalNAc	26.4
GalNAcα1-OSer	TnSer	20
GalNAcβ1-4GlcNAcβ-sp2	LacdiNAc	11.9
GalNAcα1-3Galβ-sp3	A_{di}	5.7
Fucα1-2Galβ-sp3	H_{di}	3.4
GalNAcβ1-3GalNAcβ-sp3	para-Fs	2.2
Fucα1-2(3-O-Su)Galβ-sp3	3-O-Su-H_{di}	1.5

List of top 10 glycans and magnitude of their median binding to PODO447. RFU = relative fluorescent units (range 0-50 x 10^3). See results of full array in **Appendix E**.

4.4.5 Tn epitope is not involved in PODO447 recognition

PODO447 showed significant binding to the Tn antigen (GalNAcα1-OSer) on the glycan array (**Table 4-3**), which has previously been reported to be abundantly expressed on podocalyxin in the kidney (208). However, the Tn antigen is most likely not involved in PODO447's recognition of cancer cells, as we observe a low number of Tn-positive cells on cell lines expressing high levels of the PODO447 epitope (**Figure 4.5**).

To further determine the possible role of the Tn antigen in PODO447's epitope recognition, we performed a competitive binding assay using an anti-Tn antibody (clone 5F4) and PODO447. Briefly, we selected cells showing the highest level of Tn-antibody reactivity (MCF7 and A172) and pre-treated them with either anti-Tn antibody or an isotype control, followed by staining with PODO447 (**Figure 4.6A**). We observed identical PODO447 binding profiles between cells pre-treated with anti-Tn or isotype control, even at the lowest PODO447 concentrations (**Figure 4.6B**). Thus, the anti-Tn antibody fails to show the ability to block reactivity of PODO447 with its epitope. Differences in binding affinity and stability of the anti-Tn antibody (compared to PODO447) could account for its failure to block PODO447 binding. However, since the pre-treated cells (anti-Tn vs. control) show virtually identical PODO447 binding profiles and we observe low numbers of Tn-positive cells on high PODO447-expressing cell lines, together, these data suggest that the Tn antigen is not involved (or plays a minor role) in the recognition of PODO447 on cancer cells.

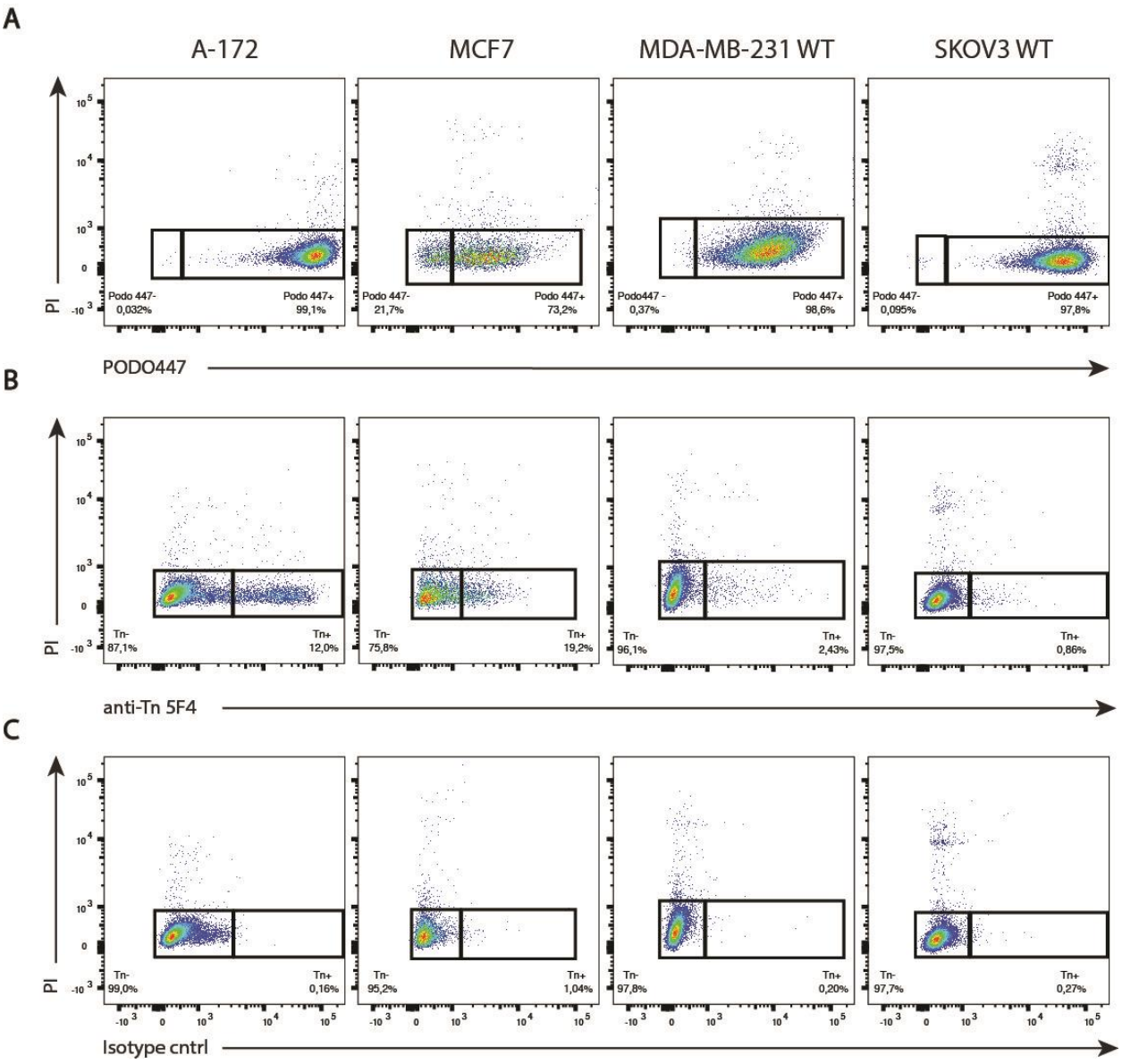

Figure 4.5 Tn expression on PODO447-positive tumor cells

Flow cytometry profiles of tumor cells stained with **(A)** PODO447, **(B)** anti-Tn (clone 5F4) or **(C)** IgM isotype control antibody. Propidium iodide (PI) shows non-viable cells.

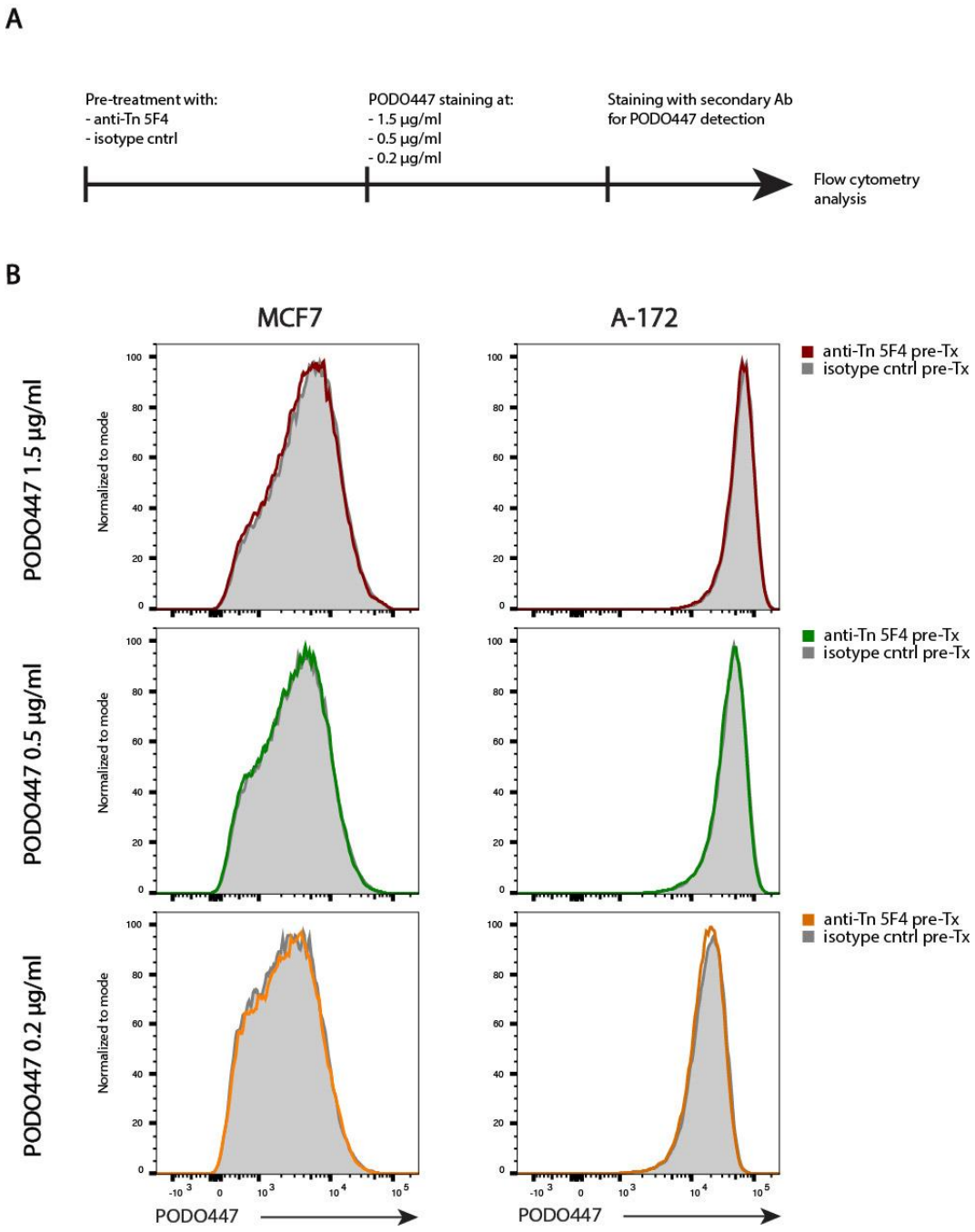

Figure 4.6 PODO447 vs anti-Tn competitive binding assay

(A) Experimental procedure diagram **(B)** PODO447 flow cytometric binding profiles of MCF7 and A-172 cells pre-treated (pre-Tx) with either anti-Tn (clone 5F4) or isotype control. Cells were stained with PODO447 at the indicated concentrations (1.5, 0.5 and 0.2 µg/ml).

4.4.6 PODO447 epitope across different carcinomas

The finding that PODO447 recognises a highly unusual tumor-specific residue present on Podxl and that it does not cross-react with normal human tissues encouraged us to further evaluate possible therapeutic indications. In order to do so, we stained several cancer TMAs with PODO447, including glioblastoma, urothelial cell, pancreatic, breast and ovarian carcinoma. In each case, PODO447 staining was initially scored based on the percentage of cells stained, with a scoring scale of 0 (negative, <1%), +1 (intermediate, 1-50%) and +2 (high, >50%). Tumors scored as +1 and +2 were grouped as PODO447 positive.

4.4.6.1 PODO447 in urothelial cell carcinoma

Expression of Podxl has been correlated with poor prognosis in urothelial bladder carcinoma, where Podxl identified tumors most likely to undergo progression. Here, we sought to investigate urothelial bladder cancer as a potential application for a PODO447-based therapy by assessing PODO447's binding profile within urothelial carcinoma (**Table 4-4**). We stained two different urothelial bladder cancer TMAs, one containing different histotypes (benign, malignant and metastatic tumors) and the second in which the cases were classified based on tumor grade (low- vs. high-grade). Out of all 226 cases, we observed 110 (49%) to be PODO447 positive. From this, 31 (28%) showed PODO447 staining in the cell surface while the remaining 79 (72%) were predominantly cytoplasmic. Given that our goal was to study the potential of bladder carcinoma as a potential therapeutic application, we focused on the cases that presented membranous staining.

Despite Podxl being correlated with lower overall (OS) and disease-specific survival (DSS) and being an independent predictor of tumor progression in urothelial bladder cancer (118), only a

small number (6-11%) of malignant and metastatic tumors showed PODO447 cell surface staining. However, 5 out of 14 (36%) benign tumors presented membranous staining. Interestingly, these results correlate with the second cohort classified by tumor grade, where 19 out of 35 (54%) of low-grade tumors had PODO447 cell surface staining, compared to 17% of high-grade tumors. These results suggest that PODO447 staining might not correlate with tumor progression, but rather with early stages of disease (**Table 4-4**).

Table 4-4 PODO447 expression and localization within a urothelial carcinoma TMA

Patient characteristics	Scorable Cases n	PODO447 positive		
		Total positive n (%)	Cell surface positive n (%)	Cytoplasmic positive n (%)
All scorable cases	226	110 (48.7)	31 (28.2)	79 (71.8)
Histological cell type (n)	138	51 (37.0)	8 (15.7)	43 (84.3)
Benign tumour	36	14 (38.9)	5 (35.7)	9 (64.3)
Malignant tumour				
Submucosal area	34	9 (26.5)	1 (11.1)	8 (88.9)
Muscle invasive area	34	16 (47.1)	1 (6.3)	15 (93.8)
Metastatic tumour	34	12 (35.5)	1 (8.3)	11 (91.7)
Grade (n)	88	59 (67.1)	23 (39.0)	36 (61.0)
Low	44	35 (79.6)	19 (54.3)	16 (45.7)
High	44	24 (54.5)	4 (16.7)	20 (83.3)

4.4.6.2 PODO447 in glioma

Podxl correlates with tumor grade and poor overall survival in patients with glioblastoma multiforme (128). As such, we assessed PODO447 binding to a glioma TMA (**Table 4-5**). As expected, PODO447 did not recognize any of the normal cerebrum tissue. However, PODO447 produces strong signal in all 22 (100%) glioblastoma cases while not binding to any astrocytoma tissue (**Table 4-5**). These results are consistent with previous studies showing higher expression of Podxl in glioblastoma tumors compared to diffuse or anaplastic astrocytomas (128). However, the staining of 21 out of 22 (96%) glioblastoma cases was of cytoplasmic nature, which might at first deter the impulse to pursue glioblastoma as a therapeutic indication for PODO447. Nevertheless, the strong Podxl staining in glioblastoma tumors by immunohistochemistry showed by previous studies was also predominantly cytoplasmic, yet researchers were able to find Podxl on the surface of freshly resected glioblastoma tumors by flow cytometry (128). Taken together these results suggest that, while predominantly cytoplasmic, PODO447 might correlate with glioma grade. Further analysis of fresh tumors might be required to determine the potential of glioblastoma as a therapeutic application for PODO447.

Table 4-5 PODO447 expression and localization within the glioma TMA cohort

Patient characteristics	Scorable Cases n	PODO447 positive		
		Total positive n (%)	Cell surface positive n (%)	Cytoplasmic positive n (%)
All scorable cases	80	22 (27.5)	1 (1.3)	21 (26.3)
Histological cell type (n)				
Glioblastoma		22 (100.0)	1 (1.5)	21 (95.5)
Astrocytoma		0 (0.0)	0 (0.0)	0 (0.0)
Normal Cerebrum		0 (0.0)	0 (0.0)	0 (0.0)

4.4.6.3 PODO447 in pancreatic ductal adenocarcinoma

Previous studies in have shown that Podxl can selectively identify pancreatic ductal adenocarcinomas (PDAC) from other adenocarcinomas of the gastrointestinal and biliary ducts (159). In addition, overexpression of Podxl is an independent predictor of poor prognosis and it is associated with unfavorable clinicopathological factors such as poor tumor differentiation or advanced stage (119,144). As such, we sought to investigate PDAC as an application for PODO447 by exploring this antibody's binding profile on a PDAC TMA. Out of 77 PDAC cases, 30 (39%) were PODO447-positive (**Table 4-6**). In previous studies, Podxl positivity within the TMA varied from 44 - 92%. One possible explanation might be the difference in antibodies. Previous studies have used different monoclonal and polyclonal antibodies against Podxl which, depending on their epitope, might show a variety of staining patterns. In fact, in Saukkonen et al. they show that a commercial anti-Podxl polyclonal antibody gives both membranous and cytoplasmic staining compared to their monoclonal antibody which only stains the cytoplasm. We have showed that PODO447 has a distinct glycoepitope on Podxl that is not always present when the core Podxl protein is expressed, therefore giving a unique staining pattern that is not always comparable to that of the core Podxl protein. In addition, from the 30 PDAC PODO447-positive cases, the majority (73%) presented cytoplasmic staining while only 8 (27%) showed membranous immunopositivity (**Table 4-6**). Interestingly, we observed PODO447 reactivity in 3 (16%) cases of normal pancreatic tissue, where 2 out of 3 cases were of cytoplasmic nature and 1 case had weak membranous staining. However, these are more likely the result of unspecific staining given that similar amounts were also present in the equivalent cases that were stained with the isotype control.

Table 4-6 PODO447 expression and localization within the pancreatic TMA cohort

Patient characteristics	Scorable Cases n	PODO44 positive		
		Total positive n (%)	Cell surface positive n (%)	Cytoplasmic positive n (%)
All scorable cases	96	33 (34.4)	9 (27.3)	24 (72.7)
Histological cell type (n)				
Ductal adenocarcinoma	77	30 (39.0)	8 (26.7)	22 (73.3)
Normal pancreas	19	3 (15.8)	1 (33.3)	2 (66.7)

4.4.6.4 PODO447 in breast carcinoma

High Podxl expression is associated with a higher risk of undergoing tumor progression and it constitutes, on its own, an independent predictor of poor outcome in breast carcinoma (110). Previously, Somasiri et al showed that about 40% of breast cancer tumors were positive for Podxl, from which about 6% of them had high levels of Podxl expression. Here, we assessed PODO447 binding to a similar breast carcinoma TMA (**Table 4-7**). Overall, we observed 83 (26%) out of 325 cases to be positive for PODO447, where the majority of the staining was localized in the cell surface. Even if in a low number of breast carcinomas, given that breast cancer is the most common cancer among women (147) and that most Podxl-positive breast carcinomas are negative for estrogen receptor (ER) (110), PODO447 might surface as an alternative therapeutic for those cases in which standard therapy has failed.

Table 4-7 PODO447 expression and localization within the breast TMA cohort

Patient characteristics	Scorable Cases n	PODO447 positive		
		Total positive n (%)	Cell surface positive n (%)	Cytoplasmic positive n (%)
All scorable cases	325	83 (25.5)	50 (60.2)	33 (39.6)
Histological cell type (n)				
Ductal Carcinoma	275	74 (26.9)	45 (60.8)	29 (39.2)
Lobular Carcinoma	47	9 (19.2)	5 (55.6)	4 (44.4)
Medullary Carcinoma	3	0 (0.0)	0 (0.0)	0 (0.0)

4.4.6.5 PODO447 is a potential therapeutic for ovarian carcinoma

Podxl is known to be expressed at high levels in ~90% of high grade serous ovarian carcinomas (HGSOC), where cell surface localization is a strong predictor of poor outcome(117). Given the high lethality of HGSOC tumors, we carried out a detailed evaluation of the PODO447 epitope expression by these malignancies in an effort to evaluate the potential for PODO447 as a new therapeutic. We immune-stained a tissue microarray (TMA) consisting of 219 scorable cases of epithelial ovarian carcinoma (EOC). Of 219 cases, 144 (65.8%) were PODO447 positive (**Table 4-8**). We did note however, that PODO447 reactivity across the major EOC histological subtypes was significantly different. While only 40% of the mucinous EOC tumors were PODO447 positive, the majority of endometrioid (74.1%), clear cell (68.0%), low grade serous (75.0%) and HGSOC (65.8%) subtype tumors were PODO447 positive.

As it has previously been shown that cell surface expression of Podxl (versus cytoplasmic expression) is associated with decreased disease-free survival in HGSOC (117), we also scored PODO447's predominant localization (cytoplasmic versus membranous) amongst the PODO447-positive cases on the TMA (**Table 4-8, Fig 4.7**). 115 (79.9%) of the 144 PODO447-positive cases exhibited membranous PODO447 staining (**Table 4-8, Fig 4.7B**). The remaining 29 cases exhibited diffuse, cytoplasmic staining (**Table 4-8, Fig 4.7C**). Unfortunately, due to the lower representation of mucinous and low-grade serous tumors in the TMA, we were unable to infer any meaningful conclusions about PODO447 localization in these EOC subtypes. However, 19 of 20 (95.0%) endometrioid tumors and 14 of 17 (82.4%) clear cell tumors exhibited cell-surface PODO447-positive staining. Importantly, we noted that 78 of 102 (76.5%) HGSOC PODO447 positive tumors had membranous staining. Given that HGSOC tumors have the worst

outcome of all the EOC subtypes (209,210), the reactivity of PODO447 with the majority of these tumors bodes well for this antibody's utility in addressing this unmet clinical need.

Table 4-8 PODO447 expression and localization within an ovarian carcinoma TMA cohort

Patient characteristics	Scorable Cases n	PODO447 positive		
		Total positive n (%)	Cell surface positive n (%)	Cytoplasmic positive n (%)
All scorable cases	219	144 (65.8)	115 (79.9)	29 (20.2)
Histological cell type (n)				
High-grade serous	158	102 (64.6)	78 (76.5)	24 (23.5)
Clear cell	25	17 (68.0)	14 (82.4)	3 (17.7)
Endometroid	27	20 (74.1)	19 (95).0	1 (5.0)
Mucinous	5	2 (40.0)	1 (50.0)	1 (50.0)
Low-grade serous	4	3 (75.0)	3 (100.0)	0 (0.0)
FIGO stage (n)				
I	37	29 (78.4)	23 (79.3)	6 (20.7)
II	31	20 (64.5)	18 (90.0)	2 (10.0)
III	130	83 (63.8)	66 (79.5)	17 (20.5)
IV	21	12 (57.1)	8 (66.7)	4 (33.3)

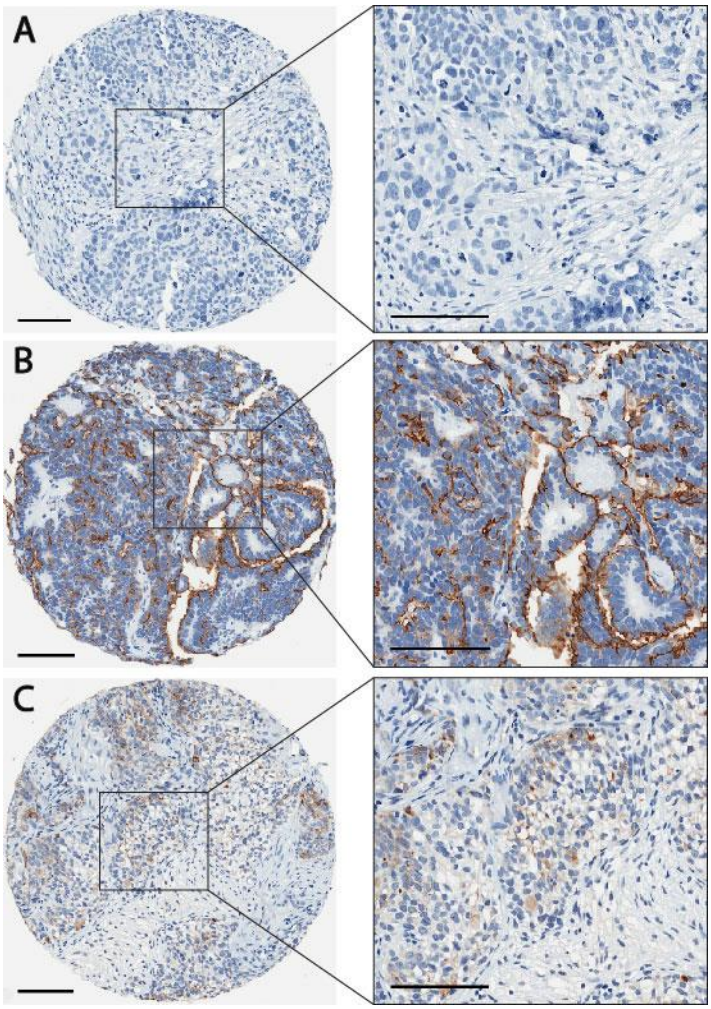

Figure 4.7 PODO447 differentially recognizes HGSOC in a tumour microarray

Representative HGSOC tumour sections stained with PODO447 (brown color) that were scored as (**A**) negative **(B)** positive (membranous staining) or **(C)** positive (cytoplasmic) (see inset for higher magnification). Scale bars = 100 μm.

4.5 Discussion

Podxl is a member of the CD34 family of sialomucins, a family of transmembrane proteins that has been shown to play a role in modifying cell adhesion and making cells more mobile and invasive (99,142). Interestingly, Podxl is frequently upregulated in a variety of cancers and invariably correlates with poor outcome (108,110,112,117,136,144,158,163,164,184,201). In those studies where its oncogenic function has been evaluated in detail, Podxl has been shown to play a critical role in metastatic progression; gene inactivation or dampening of its mRNA expression cripples the ability of tumour cells to metastasize in xenografted mice (39,108,110). Thus, as a membrane protein involved in tumour progression together with our previous study showing that mAbs targeting its extracellular domain can delay primary tumour growth and block metastasis in mice (136), Podxl stands out as a promising target for immunotherapy. Further development of a Podxl-targeted therapeutic Ab has been hampered, however, by concerns over potential toxicity since Podxl is also normally expressed at high levels by vascular endothelia and kidney podocytes. Accordingly, in this study we sought to screen for a novel mAb with high specificity for a tumour glycoform of Podxl, and lack of reactivity with any normal cells. PODO447 emerged as uniquely fulfilling these key criteria. This mAb recognizes an array of human tumour cell lines while exhibiting minimal activity with normal cell types or tissues, including those that express the Podxl core protein at high levels. Specifically, we observed no reactivity of PODO447 with kidney podocytes and, with the sole notable exception of vessel-like structures in kidney medulla that appear to be vasa recta (under investigation), we observed minimal binding of PODO447 to any other peripheral vessels. Although we observed rare and weak PODO447 reactivity with the mucosal epithelia of the breast, fallopian tube and intestinal tract, as well as the parenchyma of the adrenal, salivary and sweat glands, the level and frequency

of this reactivity was low and could, in fact, represent spurious cross-reactivity since, in most cases, a similar staining pattern was also observed in the staining control. Moreover, the rare staining of these normal epithelial cells was observed to be largely cytoplasmic making it unlikely that this compartment would be accessible to circulating PODO447 *in vivo.* Importantly, these results have been independently confirmed by a preclinical contract research organization which speaks to the reproducibility and reliability of our findings.

Epithelial ovarian cancer (EOC) is one of the leading causes of cancer mortality in women (147). Frequently diagnosed only at advanced stages and with a 5-year survival of approximately 47% (211), EOC is a "silent killer" that offers few treatment options. Although new diagnostic and treatment options have led to a significant improvement in survival rates for many cancers over the last 50 years, the 5-year survival for EOC has hardly changed since 1980 (212,213), highlighting the urgent need for new treatment strategies. Here we highlight the use of PODO447-based agents as a promising therapeutic avenue for EOC. The Podxl core protein is known to be expressed at robust levels by the majority of high-grade serous carcinomas (117), the most prevalent histotype of EOC (214) for which the prognosis is poor and antigen-specific therapeutic options are extremely limited (209,210). We found that a high percentage of such HGSOC tumours express the PODO447 glycoepitope, thus offering a large population who could benefit from treatment.

Although we have explored the reactivity of PODO447 in ovarian carcinomas in detail, further studies on other forms of cancer could widen the scope of its potential therapeutic use. For example, here we show that PODO447 seems to exclusively recognize glioblastoma (GBM) over

astrocytoma or normal cerebrum samples. Intriguingly, PODO447 staining of GBM was predominantly cytoplasmic. While Podxl is a transmembrane protein, since we also observe Podxl cytoplasmic staining with PODO83 (section 3.4.4.), one can speculate that it is the result of intracellular accumulation of vesicles containing Podxl that are awaiting signaling to be shed or in transit to the cellular membrane. Although we hypothesize that the patients most likely to benefit are those expressing the PODO447 epitope on the surface of tumor cells, it is possible that GBM patients could benefit from PODO447. Binder et al. previously reported Podxl on the surface of GBM tumors by flow cytometry, despite observing that the majority of Podxl staining by immunohistochemistry of paraffin-embedded glioma sections was of cytoplasmic nature. Thus, these results suggest that immunohistochemistry alone might not be sufficient and additional analysis of fresh tumors might be required to determine the potential of glioblastoma as a therapeutic application for PODO447. Given that glioblastoma (high-grade astrocytoma) is the most common and deadliest type of malignant primary brain tumors in adults, it could be a promising avenue worth pursuing for targeted therapeutic intervention using this Ab.

In this study, we have described for the first time a novel Podxl-targeting mAb that binds to a unique tumour-restricted glycoepitope with high specificity. PODO447 primarily recognizes a rare, terminal GalNAcβ1 motif on a glycan array, that is located within Podxl's mucin domain. Unlike other anti-Podxl Abs, PODO447 does not recognize Podxl expressed on healthy human tissue. Therefore, due to its potentially favorable safety profile, this study supports further development of PODO447 as a therapeutic agent. Coupling of PODO447 with various cytotoxic compounds to selectively target neoplastic cells could offer a novel therapeutic approach with

minimal toxicity to normal tissues, an issue that plagues most traditional chemotherapy treatments.

Chapter 5: Investigation of PODO447 use as a cancer therapeutic.

5.1 Synopsis

Antibody-drug conjugates are a class of targeted therapies that hold great promise as a new generation of cancer therapeutics. However, to date only a few have been approved for clinical use. The challenge lies in the identification of true tumor-specific antigens and the development of effective antibodies against them. Here, we explore the potential application of PODO447 in cancer immunotherapy. We show that "naked" PODO447 (mAb alone, without a conjugated payload) does not exert toxic or inhibitory properties on cancer cells, however, when conjugated to a toxic payload, we show that PODO447 has potent cytotoxic activity on cancer cells both *in vitro* and *in vivo*. This work highlights the therapeutic potential of a PODO447 antibody-drug conjugate and supports its further clinical development.

5.2 Introduction

The emergence of antibody-drug conjugates (ADC) has shifted the cancer treatment landscape from conventional chemotherapy to more targeted approaches. Chemotherapy is the administration of unconjugated cytotoxic drugs that destroy rapidly dividing cells. In contrast, ADCs selectively target tumor cells by linking a potent cytotoxic payload to a monoclonal antibody (mAb), allowing for lower systemic toxicity and improved benefit-risk ratio. Briefly, ADCs act as molecular vehicles that selectively target toxins to malignant tissue thereby removing tumors while preserving healthy tissue. Despite the theoretical simplicity of the ADC concept, they are complex biochemical compounds and their clinical efficacy depends on the

binding and pharmacokinetic properties of the mAb component, the cytotoxic potency of the cell-killing agent, and the stability of the chemical linker that holds them together.

Despite the large number of ADCs in clinical pipelines, to date, only a handful of them have received regulatory approval by the U.S. Food and Drug Administration (FDA) agency for oncological indications. These include gemtuzumab ozogamizcin (acute myeloid leukemia), brentuximab vedotin (Hodgkins Lymphoma, acute lymphoid-cell leukemia), ado-trastuzumab emtansine (HER2+ advanced breast cancer), inotuzumab ozogamicin (acute lymphoid leukemia), polatuzumab vedotin (diffuse large B-cell lymphoma), enfortumab vedotin (advanced urothelial cancer), fam-trastuzumab deruxtecan (metastatic Her2+ breast cancer) and sacituzumab govitecan (advanced triple-negative breast cancer) (81).

Here we examine PODO447's potential as a cancer therapeutic both as an unconjugated mAb and as an antibody-drug conjugate coupled to monomethyl auristatin E (MMAE) as the toxic payload. Treatment with unconjugated PODO447 has no toxic or inhibitory properties on cancer cells *in vitro* or *in vivo*, despite observing good tumor specific targeting of the antibody and good internalization of PODO447 in a variety of cancer cells, including ovarian, glioblastoma and pancreatic cancer. More promising, PODO447 ADC shows potent cytotoxicity of cancer cells *in vitro* which is limited to Podxl-expressing cells. Further, this toxicity translates into mice xenograft tumor models, where PODO447 ADC exerts cytotoxic activity in a dose-dependent manner. This work supports further development of PODO447 as a cancer therapeutic.

5.3 Materials and Methods

5.3.1 Cell culture

THP-1, Jurkat, HUVEC, SKOV3, MCF7, A-172, MIAPACA and MDA-MB-231 cells were obtained from the American Tissue Culture Collection (ATCC). HUVEC cells were kindly obtained from the laboratory of Dr. Pascal. OV3331, OV2805, TOV3133D patient-derived high-grade serous ovarian cancer cells were generously provided by the laboratory of Dr. Mes-Masson. OSN76 medulloblastoma cells were obtained from the laboratory of Dr. Sorenson. Human pancreatic adenocarcinoma (MIAPACA), glioblastoma (A-172), and breast cancer (MDA-MB-231, MCF7) cells were grown in DMEM (Gibco, #11965-092) supplemented with 10% FBS and 10 U/ml penicillin and streptomycin (P/S) (Gibco, #15140-122). Human acute monocytic (THP-1), acute T-cell (Jurkat) leukemia and medulloblastoma (OSN76) cells were cultured in RPMI-1640 (Gibco, #11875093) supplemented with 10% FBS. Human umbilical vein endothelial (HUVEC) cells were harvested from donor umbilical cords (Human Ethics no. H10-00643), grown in Endothelial Cell Growth Medium-2 Bulletkit™ (LONZA, #CC-3162), and used between passages 2 and 8. Human ovarian cancer SKOV3 cells were grown in DMM F-12 with 15 mM HEPES (Sigma, #D6421) supplemented with 10% FBS, 0.2 mM L-glutamine (Gibco, #25030-081) and 10 U/ml P/S . OV3331, OV2805, TOV3133D were cultured in complete OSE medium (215). All cell lines were maintained at 37°C, 5% CO_2 and high humidity.

5.3.2 Tumorsphere assay

SKOV3 and MCF7 cells were harvested as follows: adherent cells were rinsed with 5ml of Ca^{2+}-, Mg^{2+}-free HBSS and lifted using a cell scraper. Cells were then spun at 394g for 4 min and

resuspended in 5ml of complete Mammocult™ media (1/10 dilution of MammoCult™ proliferation supplement (#05620), 4 μg/ml heparin (#07980) and 0.48 μg/ml hydrocortisone (#07925) in MammoCult™ basal medium (#05620), StemCell Technologies). Viable cells were counted using trypan blue stain. SKOV3 (5×10^3) and MCF7 (5×10^3) cells were seeded in triplicate in 2 ml of complete MammoCult™ medium in ultra-low adherent six-well plates. Cells were incubated for seven days without disruption under standard cell culture conditions (37°C in 5% CO_2). On day 7, tumorspheres were manually counted using a transparent counting grid. Only spheres with 12 or more cells were counted. Average tumorsphere forming efficiency (%) was calculated as (number of tumorspheres / number of cells seeded) x 100, and statistical analysis was performed using one-way ANOVA followed by Bonferroni's post-test in GraphPad Prism software. A *P* value less than 0.05 was considered statistically significant.

5.3.3 *In vitro* migration and invasion

On Day 0, 96-well ImageLock plates (Essen Bioscience, #4379) were coated with 50 μl of BD Matrigel TM diluted to 100 μg/ml in MDA-MB-231 culture media. On day 1, sub-confluent SKOV3 cells were harvested using 0.25% Trypsin and counted on a hemocytometer using trypan blue stain. Cells were resuspended in culture media at 1.8×10^5 cells/ml and 100 μl of cell suspension were plated in each well (i.e. 18K cells per well). Cells were then incubated for 4 h at 37°C, in 5% CO_2. Next, wounds were created simultaneously in all wells using the 96-well WoundMaker™ procedure detailed by the manufacturer (Essen Bioscience). Immediately after, cells were washed twice with cell culture media. After the final wash, 100 μl of culture media was added to the cells and the plate was placed in a pre-chilled CoolBox 96F (Essen Bioscience,

#1500-0080-A00) to equilibrate for 5 min, and then the (cool) media was discarded, and 50 μl of either media (migration) or BD Matrigel™ (invasion) containing 9 μg/ml of the test antibodies (chimeric anti-OVA, rabbit/Hu chimeric PODO83 and rabbit/Hu chimeric PODO447) were added to the cells. The plate was then placed on to a pre-warmed CoolSink 96F in a 37°C, 5% CO_2 incubator for 30 min. Next, additional 100 μl of culture media containing 9 μg/ml of the test antibodies was added to the cells in the invasion assay, and the plate was placed in the Incucyte ZOOM. The Incucyte® ZOOM software was set in "scratch wound" mode to scan one image per well every 3h, with the first scan beginning 10 min after the plate was placed in the instrument. Migration and invasion rate were calculated as relative wound density (%) using the Incucyte ZOOM scratch wound software, and statistical analysis was performed using two-way ANOVA in GraphPad Prism software. A *P* value less than 0.05 was considered statistically significant.

5.3.4 Generation of antibody-drug conjugates

The antibody-drug-conjugate generation and initial characterization was performed at the National Research Council (NRC) of Canada. MMAE linked to a synthetic dipeptide linker (MC-vc-PAB-MMAE) was used for conjugation with rabbit/human-chimeric PODO447. Mouse/human-chimeric palivizumab was also conjugated with MMAE (MC-vc-PAB-MMAE) and served as the control (187). All conjugates were verified by high-performance liquid chromatography (HPLC) for the drug to antibody ratio (DAR) target of 4.0.

5.3.5 *In vitro* antibody and ADC cytotoxicity

On day 0, cells were plated on 96-well plates in 100µl culture medium and allowed to adhere overnight. SKOV3, MIAPACA, A172, THP-1, HUVEC and Jurkat, were seeded at 2.5 x 10^3 cells per well; OV3331, OV2805, TOV3133D and OSN76 were seeded at 5 x 10^3 cells per well. On day 1, a 5X stock solution of each mAb/ADC concentration to be tested was prepared in a stepwise 1:3 serial dilution series in cell culture medium, and 25µl of each dilution was added to cells in triplicate. Treated cells were cultured at 37°C, 5% CO_2 and high humidity for 144 h. On day 6, the thiazolyl blue tetrazolium bromide (MTT) assay was used to determine relative cytotoxicity. Briefly, 100µl of MTT (1mg/ml, AC158990010) was added to the cells and left to incubate for 3 h at 37°C. Next, MTT media was removed and 50µl of DMSO was added to the cells and allowed to incubate for 15 min at RT, protected from light and with mild shaking. Absorbance was then read at 570nm. The percent viability was calculated as follows: (1-(absorbance of treated samples/average absorbance of control samples)) x 100. Average relative cytotoxicity was calculated and statistical analysis was performed using two-way ANOVA in GraphPad Prism software. A *P* value less than 0.05 was considered statistically significant.

5.3.6 *In vitro* antibody internalization

On Day 0, sub-confluent cells were harvested using 0.25% Trypsin and counted on a hemocytometer using trypan blue stain. Cells were resuspended in culture media and plated in 50 µl per well at the following concentrations: MIAPACA (8 x 10^3 cells/well), A172 (8 x 10^3 cells/well), SKOV3 (1 x 10^4 cells/well) and MDA-MB-231 (8 x 10^3 cells/well). Cells were then incubated for overnight at 37°C, in 5% CO_2. On day 1, coupling of the antibodies was performed

by incubation of biotinylated PODO447 or palivizumab control mAb (187) with pHRodo (ThermoFisher, #P35362) at 1:1 Molar ratio for 30 min at 4°C. Next, 50 µl of cold pHRodo-mAb mix was added to the cells and the plate was placed in the Incucyte®. The Incucyte® ZOOM software was set in "standard" mode with the phase and red channels selected and set to scan every 10 min for 24 hours. The rate of antibody internalization was determined based on the increase in fluorescent area, reported here as total internalization area (μm^2/well). Average internalization was calculated and statistical analysis was performed using two-way ANOVA in GraphPad Prism software. A *P* value less than 0.05 was considered statistically significant.

5.3.7 Mice

Tumor model animal experiments were carried out using 6-12-week-old female NOD.Cg-*Prkdc*^{scid}*Il2rg*^{tm1Wjl}/SzJ (NSG) and NU/J (nude) mice obtained from Jackson's Laboratories (#005557 and #002019, respectively). Animals were bred in a clean, pathogen-free facility and all experiments were carried out under approved University of British Columbia Animal Care Council protocols.

5.3.8 Pre-clinical *in vivo* xenograft model to assess PODO447-ADC efficacy

SKOV3 ($1x10^6$) or MIAPACA ($1x10^6$) cells were injected subcutaneously into the right flank of NSG or nude mice. Tumor dimensions were measured twice a week and the tumor volumes (cm^3) were calculated by ((length x $width^2$)/2). Once tumors reached either $0.1cm^3$ or $0.15cm^3$ in size, mice were treated with either PODO447- or palivizumab-Vedotin at different concentrations ranging from 9.8 – 2 mg/kg. ADC treatments were administered intravenously every 4 days. When tumors reached humane endpoint ($1cm^3$), mice were sacrificed, and tumors

were excised and fixed with 10% formalin for long term storage. Average tumor volume overtime was calculated and statistical analysis was performed using two-way ANOVA test in GraphPad Prism software. Survival Kaplan-Meier curves were calculated and statistical analysis was performed using a Log-rank (Mantel-Cox) test in GraphPad Prism software. A *P* value less than 0.05 was considered statistically significant.

5.4 Results

5.4.1 Unconjugated PODO447 does not affect tumorigenesis of cancer cells *in vitro*

The discovery that PODO447 recognizes a novel tumor antigen on Podxl encouraged us to investigate the potential use of PODO447 as a cancer therapeutic. Tumorsphere formation assays have been shown to be effective *in vitro* platforms for screening of anti-cancer drugs (151). Since we previously demonstrated that Podxl plays a role in *in vitro* tumorsphere formation (136), we investigated whether binding of non-conjugated ("naked") PODO447 is sufficient to reduce the tumorigenic capacity of cancer cells *in vitro*. Since MCF7 Podxl overexpressing cells and, especially, SKOV3 cells both express the PODO447 epitope in their surface and form well-defined tumorspheres, we performed a tumorsphere assay using these cells treated with either PODO447, PODO83 or palivizumab control antibody. Cells were pre-incubated with antibody and cultures were further treated with the antibody at the time of plating. In all treatment conditions with both SKOV3 (**Fig 5.1 A**) and MCF7 (**Fig 5.1 B**) cells, we observed no significant difference between PODO447 or control on tumorsphere-forming efficiency.

As shown in Chapter 3 (section 3.3.2), PODO83 does not alter migration of cancer cells *in vitro*, but does decrease their *in vitro* invasion abilities. Therefore, we tested whether PODO447 is able to reduce *in vitro* migration or invasion of SKOV3 cells, an ovarian cell line that expresses high levels of the PODO447 epitope on its surface. Unconjugated PODO447 did not alter neither the migration (**Fig 5.1 C)** nor the invasion (**Fig 5.1 D)** of SKOV3 cells, while PODO83 significantly decreased invasion of these cells *in vitro* ($P < 0.001$). These data suggest that PODO447 does not affect the ability of cancer cells to undergo tumor progression.

To confirm these results, we tested whether unconjugated PODO447 could decrease tumor growth *in vivo*. We pre-incubated SKOV3 cells with either PODO83, PODO447 or anti-OVA control antibody and transplanted them subcutaneously in NSG mice (**Fig 5.1E**). Though not statistically significant ($P = 0.088$), SKOV3 cells pre-treated with PODO83 demonstrated a trend toward delayed tumor growth, consistent with our previous results showing that PODO83 can delay primary tumor growth and metastasis *in vivo* (136). In contrast, cells pre-treated with either anti-OVA or unconjugated PODO447 were unaffected by the antibody treatment and showed no decrease or delay in tumor growth ($P = 0.52$). Though further studies examining systemic treatment with unconjugated PODO447 are required, these results suggest that PODO447 alone does not alter the tumorgenicity of cancer cells *in vitro* or *in vivo*.

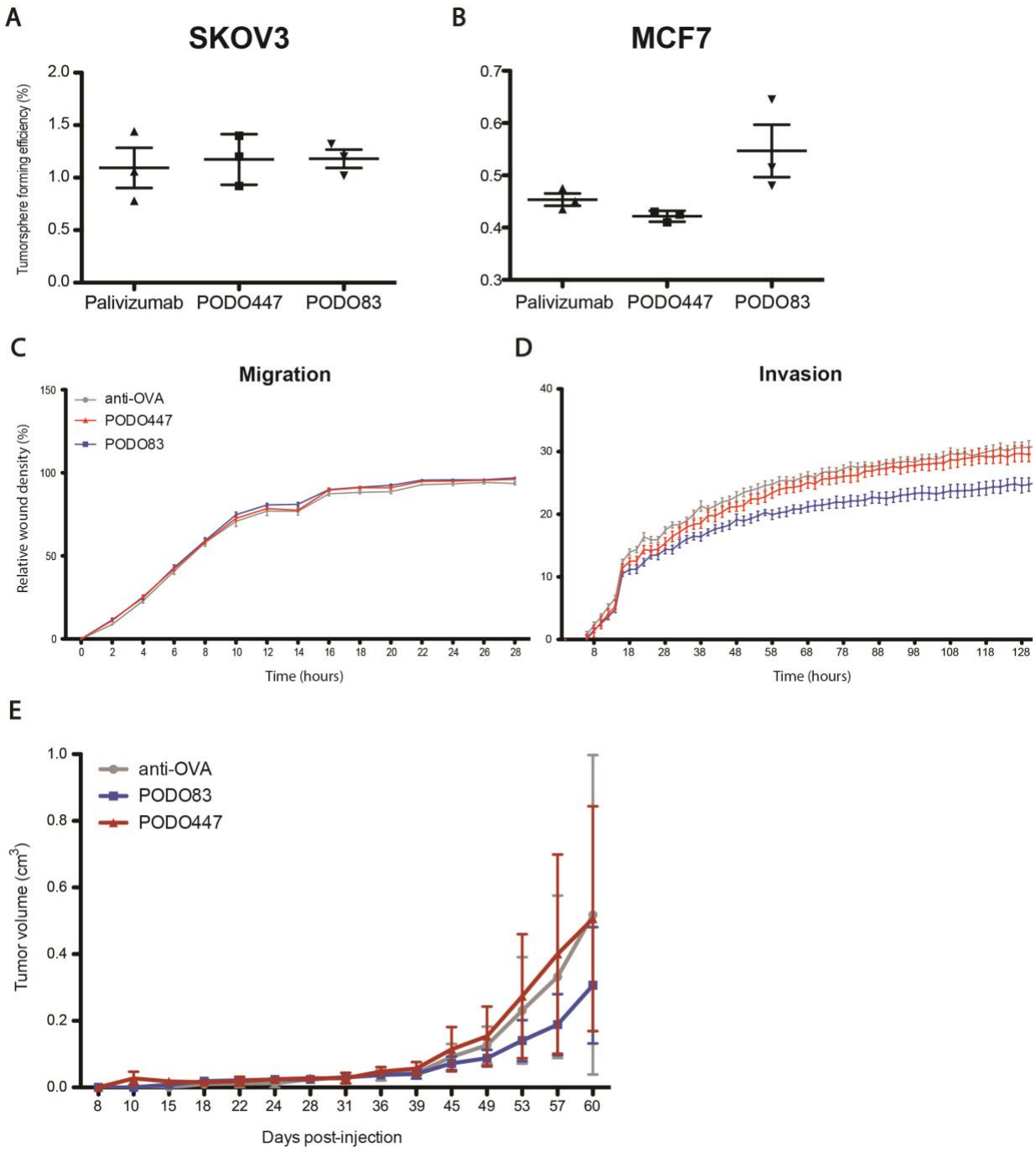

Figure 5.1 PODO447 does not alter cancer cell tumorigenesis

(A) Tumorsphere-forming efficiency after treatment with PODO447, PODO83 or palivizumab control antibody in SKOV3 (**A**, n.s.) and Podxl-high MCF7 (**B**, n.s.). **(C-D)** Effect of PODO447,

PODO83 and anti-OVA control antibody on migration (**C**, n.s) and invasion (**D**, $P < 0.001$) of SKOV3 cells *in vitro*. **(E)** *In vivo* tumor growth of SKOV3 cells pre-treated with PODO447, PODO83 and anti-OVA control antibody and injected s.c. into NSG mice. The data in A and B come from 1 experiment with 3 technical replicates per group and cell line. Statistical analysis was performed using one-way ANOVA test. The data in C and D come from 2 independent experiments with 8 replicates per group. Statistical analysis was performed using two-way ANOVA test. The data in E come from 1 experiment with 4 mice per group. Statistical analysis was performed using two-way ANOVA test. A *P* value less than 0.05 was considered statistically significant. Error bars in all panels show SEM. n.s = non-significant

5.4.2 PODO447 alone does not cause cytotoxicity

Although PODO447 alone did not seem to influence cancer cell tumorgenicity *in vitro* or *in vivo*, it has previously been reported that two other anti-Podxl antibodies can have cytotoxic effects on undifferentiated human embryonic stem cells in a dose-dependent manner (130,145). Thus, in collaboration with the CDRD, we investigated whether PODO447 alone could cause similar cytotoxicity on cancer cells. Initially, the CDRD performed a long-term (144h) *in vitro* drug exposure assay using unconjugated PODO447 on an array of cancer cells, including pancreatic (MIAPACA), glioblastoma (A172), acute monocytic (THP-1) and T cell (Jurkat) leukemia, and normal endothelial cells (HUVEC) (**Figure 5.2 A-E**). No cytotoxicity with unconjugated PODO447 was observed in these cells *in vitro*. While the cell viability profiles of PODO447-treated MIAPACA, A-172, THP-1, and Jurkat cells were similar to those of untreated cells, HUVEC cells responded differently when treated with PODO447. It is possible that HUVEC cells are more sensitive to the presence of an antibody in the media, thus further biological replicates using an appropriate control would be required to confirm the significance of these results. To circumvent this issue, and since ovarian cancer surface as a potential application for PODO447 (section 4.4.6.5), we next repeated the experiment on ovarian cancer OV3331 and SKOV3 cells using an appropriate control. As expected, we observed no cytotoxicity with "naked" PODO447 on these cells *in vitro* (**Figure 5.2 F-G**), and therefore moved on to test the efficacy of PODO447 as a toxin-coupled antibody.

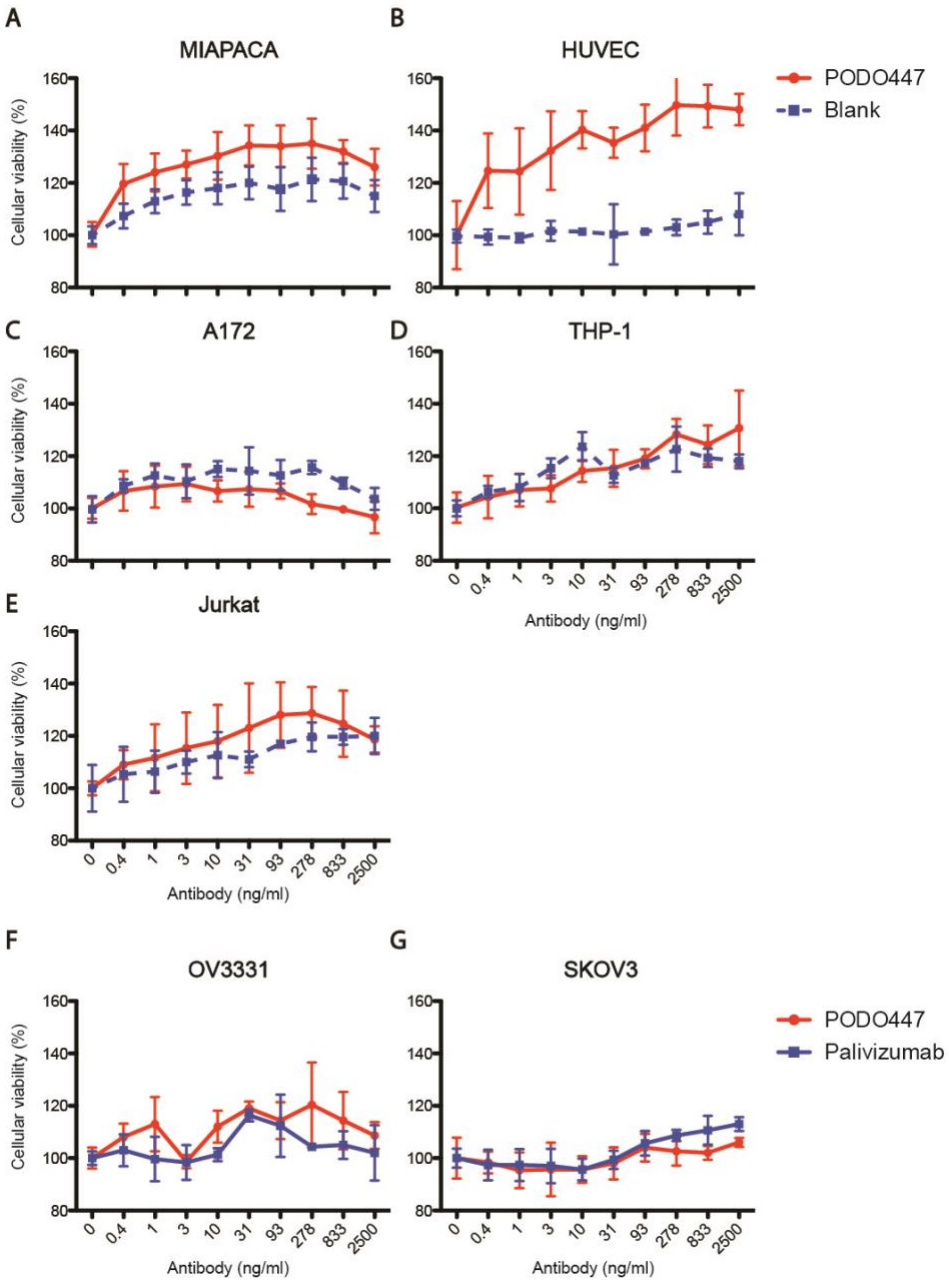

Figure 5.2 Non-conjugated PODO447 does not affect cellular viability

In vitro cytotoxic assay with PODO447, palivizumab control antibody or no antibody (blank) treatment of (**A**) pancreatic ductal adenocarcinoma (MIAPACA), (**B**) normal human umbilical vein endothelial cells (HUVEC), (**C**) glioblastoma (A172), (**D**) acute monocytic leukemia (THP-1) and (**E**) acute T cell leukemia (Jurkat), and (**F, G**) ovarian carcinoma cells (OV3331,

SKOV3). Results for each study are representative of 1-2 experiment with 3 technical replicates per group. Statistical analysis was performed using two-way ANOVA test and a *P* value less than 0.05 was considered statistically significant. All error bars in this figure represent SEM.

5.4.3 PODO447-based antibody drug conjugate (ADC)

Since, as a naked antibody, PODO447 did not alter cancer tumorigenesis or affect cellular viability of cancer cells, we sought to investigate the potential use of PODO447 as the targeting arm of an antibody-drug conjugate (ADC) immunotherapeutic. We selected monomethyl auristatin E (MMAE) as our toxin payload, a well-known tubulin polymerization inhibitor that has been widely used as a cancer therapy due to its potent and broad antitumor activity. We conjugated rabbit/human-chimeric PODO447 and a control mouse/human-chimeric palivizumab mAb to MMAE using a valine-citrulline (val-cit) proteolytically cleavable linker, resulting in Vedotin (Val-Cit-PABC-MMAE) ADCs (**Fig 5.3**). This particular linker-payload combination was selected as it is used in three of the eight approved ADCs (81).

Since an ADC's mechanism of action is dependent on cellular intake, we next tested the efficiency of internalization of PODO447 bound to surface Podxl in cancer cell lines. We conjugated PODO447 to pHRodo, a pH sensitive dye that becomes fluorescent in the acidic intracellular environment, and we monitored antibody internalization by high PODO447-expressing cancer cells. We observed a 1- to 3-fold increase in PODO447 intake (compared to palivizumab control) in SKOV3 (**Fig 5.4 A**, $P < 0.001$), MIAPACA (**Fig 5.4 B,** $P < 0.001$) and A172 (**Fig 5.4 C,** $P < 0.001$) cancer cells, as shown by the increase in red fluorescence signal. In contrast, we observed no significant internalization of PODO447 by MDA-MB-231 cells (**Fig 5.4 D,** $P > 0.05$).

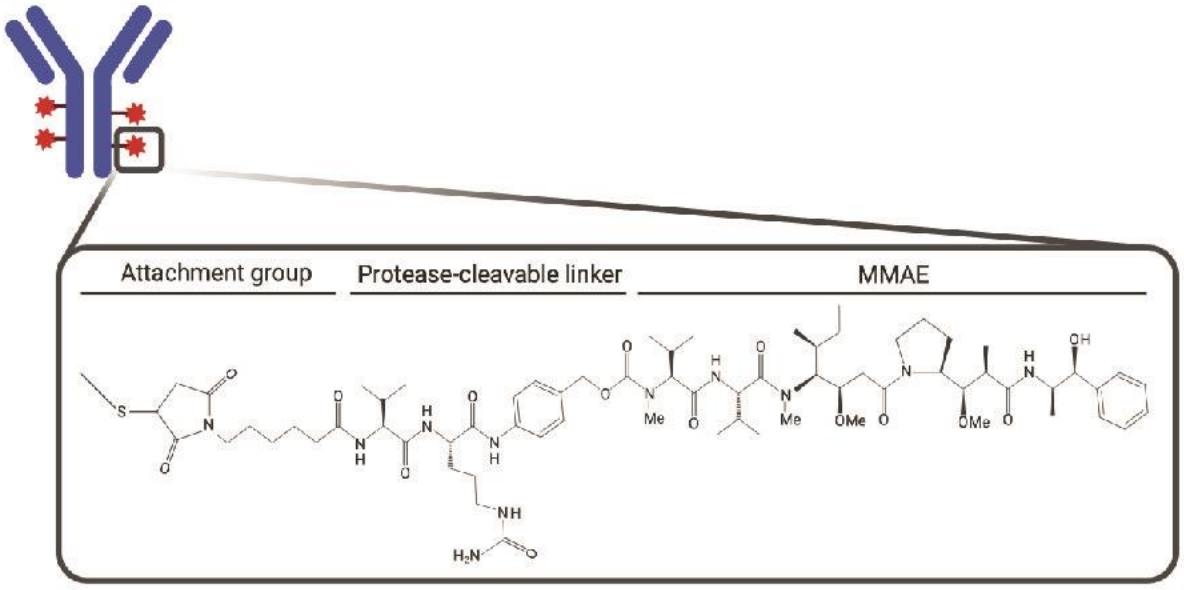

Figure 5.3 PODO447 antibody-drug conjugate structure

Representative image of mAb-Vedotin conjugate structure (created with Biorender.com)

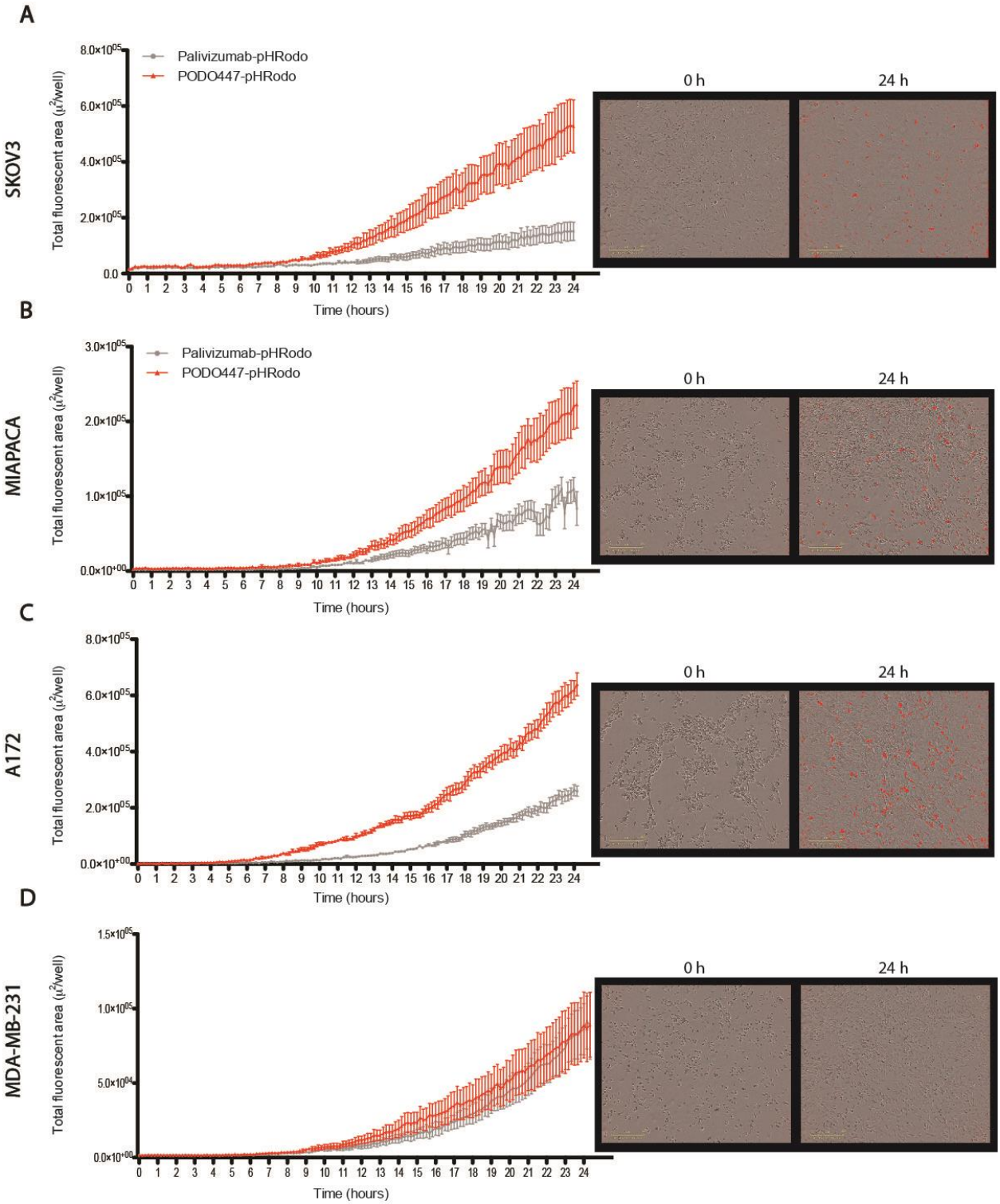

Figure 5.4 PODO447 internalization on cancer cells

Incucyte® assay using PODO447 and palivizumab control antibody conjugated to a pH-sensitive dye (pHRodo) to determine *in vitro* internalization on (A) SKOV3 ($P < 0.001$), (B) MIAPACA

($P < 0.001$), (C) A172 ($P < 0.001$) and (C) MDA-MB-231 ($P > 0.05$) cells. Left graphs show internalization overtime as determined by the increase of total fluorescent area per well. Pictures on the right are representative images of PODO447 internalization at 0- and 24-hour timepoints. The data in this figure come from 1 experiment with 5 technical replicates per group and cell line. Statistical analysis was performed using two-way ANOVA test and a *P* value less than 0.05 was considered statistically significant. Error bars in all panels show SEM.

5.4.4 PODO447-ADC has potent cytotoxic activity *in vitro*

Internalization of antigen-bound PODO447 in various cancerous cell lines suggested that the PODO447-ADC would be able to effectively deliver the cytotoxic payload. We therefore, in collaboration with the CDRD, investigated the cytotoxic effect of PODO447-Vedotin conjugates. To do this, we performed a long-term (144 h), dose-dependent drug exposure assay on an array of cancerous cells where Podxl has been shown to be highly expressed, with an emphasis on the cancer types we observed to exhibit the greatest PODO447 positivity: ovarian, breast and glioblastoma (see section 4.3.6).

CDRD initially assessed PODO447-Vedotin cytotoxicity on an acute monocytic leukemia (THP-1) and an acute T cell leukemia (Jurkat) cell line. While the cytotoxic effect of PODO447-ADC on Jurkat cells was modest and only observed at the highest dose (2500 ng/ml), THP-1 cells appeared to be more susceptible to PODO447-Vedotin treatment (IC_{50} of 31 ng/ml) (**Fig 5.5 A-B**). We next assessed PODO447-ADC cytotoxicity in medulloblastoma (OSN76) and glioblastoma (A172) cancer cells. We saw a significant but modest (~40%) toxic effect on OSN76 medulloblastoma cells at 2500 ng/ml (**Fig 5.5 C**). In contrast, we observed potent cytotoxicity of PODO447-Vedotin in A172 glioblastoma cells with an IC_{50} of 278 ng/ml and 90% cytotoxicity at the highest dose of ADC tested (2500 ng/ml) (**Fig 5.5 D**).

Lastly, we assessed PODO447-Vedotin cytotoxicity in three patient-derived high-grade serous ovarian cancer cell lines derived from solid tumor (TOV3133D) or ascites (OV3331, OV2805) that were kindly donated by the Mes-Masson lab (215,216). While we did not observe significant cytotoxicity of PODO447-Vedotin on OV2805 cells (**Fig 5.5 E**), we observed a potent cytotoxic effect in both OV3331 and TOV3133D cells with IC_{50} values ranging from 278 to 833 ng/ml and

60-90% cytotoxicity at 2500 ng/ml of ADC (**Fig 5.5 B-C**). In contrast, no significant toxicity was observed on cells treated with control palivizumab-Vedotin conjugates, suggesting that PODO447-Vedotin's toxic effect in these cells was specifically associated with their binding to the PODO447 reactive epitope.

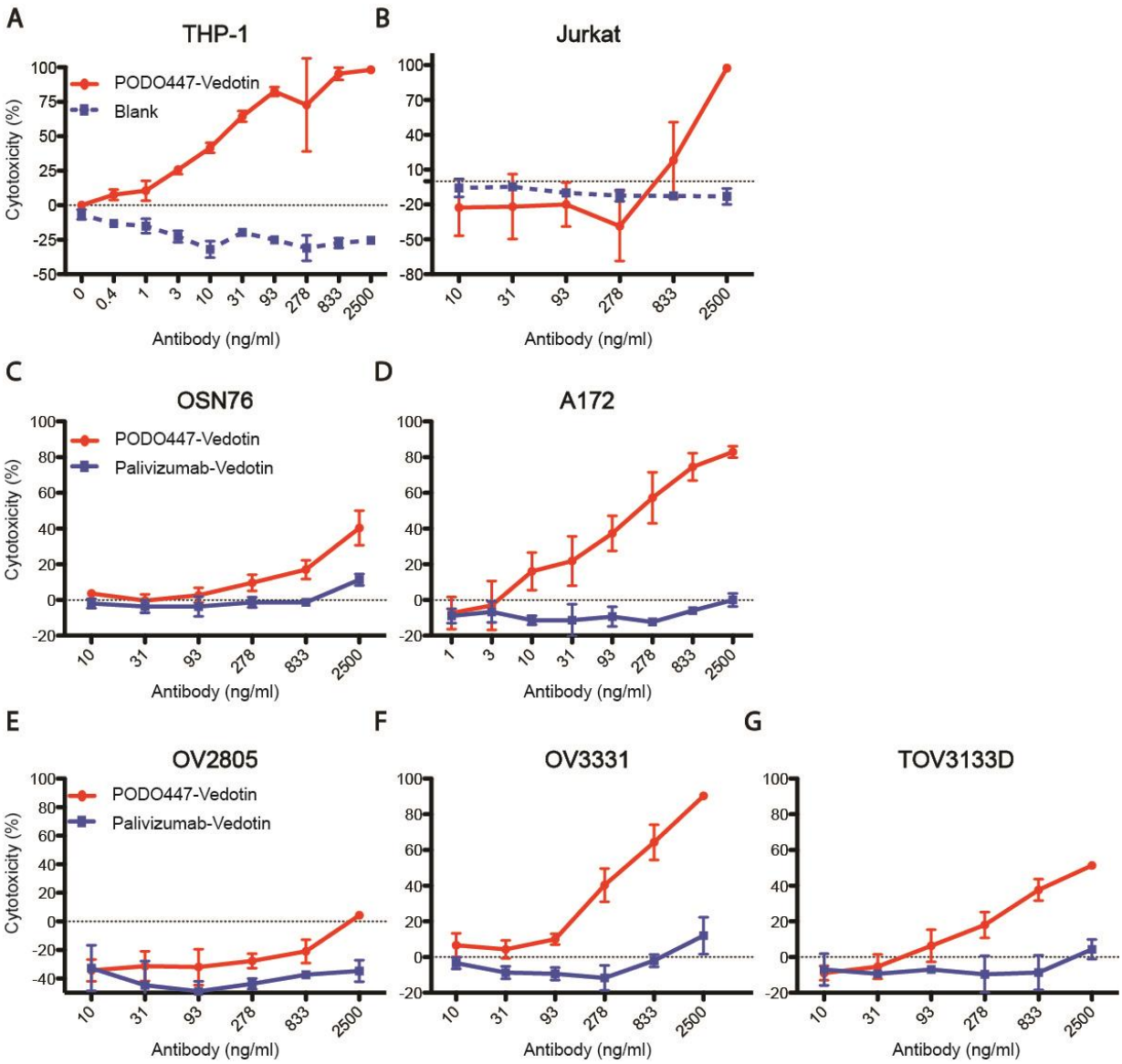

Figure 5.5 *In vitro* cytotoxicity and selectivity of PODO447-Vedotin

(**A**) Acute monocytic (THP-1) and (**B**) T cell (Jurkat) leukemia, (**C**) medulloblastoma (OSN76), (**D**) glioblastoma (A172), and (**E-G**) Ovarian high-grade serous cells were exposed to a graded titration of PODO447-, palivizumab-Vedotin or PBS (blank). Cells were assessed for cytotoxicity by 3-(4,5-dimethylthiazol-2-yl)-2,5-diphenyltetrazolium bromide (MTT) after 114 hours of continuous exposure. Horizontal line at 0% cytotoxicity is representative of untreated parental growth rate. Results for each study are representative of 1-3 independent experiments

with three technical replicates. Statistical analysis was performed using two-way ANOVA test. A *P* value less than 0.05 was considered statistically significant.Error bars indicate SEM.

To confirm the specificity of PODO447-Vedotin's cytotoxicity, we performed an *in vitro* killing assay on WT and *PODXL*-KO ovarian (SKOV3), pancreatic (MIAPACA) and breast (MDA-MB-231) cancer cells (**Fig 5.6**). We observed reduced cell viability in PODO447-Vedotin-treated SKOV3 (3-fold reduction) and MIAPACA cells (8-fold reduction) compared to control treated cells (**Fig 5.6 A, B**). In both cell types, this cytotoxic effect was due to specific drug delivery as we did not observe a reduction in cell viability of control-Vedotin treated cells, nor in *PODXL*-KO cells treated with PODO447-Vedotin (**Fig 5.6 A, B**). In contrast, MDA-MB-231 cells did not appear to be susceptible to PODO447-Vedotin treatment (**Fig 5.6 C**), most likely due to their poor PODO447 internalization (**Figure 5.4 B**). These results strongly indicate that PODO447 can effectively deliver a toxic payload to tumour cells expressing an appropriately tumor-glycosylated form of Podxl and that are able to successfully internalize the PODO447-Podxl protein complex.

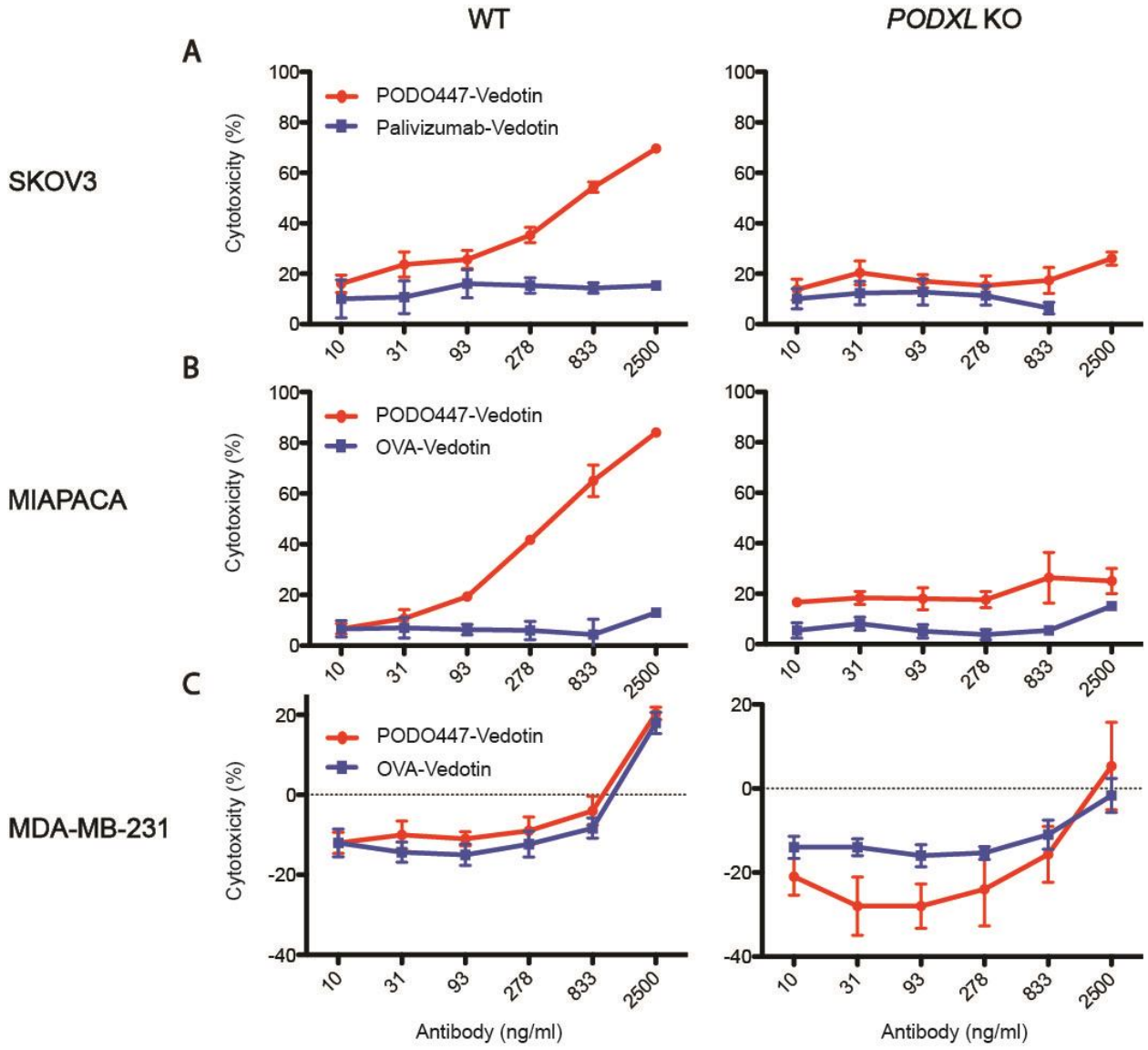

Figure 5.6 *In vitro* toxicity specificity of PODO447-Vedotin

(**A**) SKOV3 (ovarian), (**B**) MIAPACA (pancreatic) and (**C**) MDA-MB-231 (breast) WT and *PODXL*-KO cells treated with serial dilutions of PODO447-, palivizumab- or OVA-Vedotin. Cells were assessed for cytotoxicity using MTT after 114 hours of continuous exposure. Horizontal line at 0% cytotoxicity is representative of untreated parental growth rate. Results for each study are representative of 2-4 independent experiments with three technical replicates.

Statistical analysis was performed using two-way ANOVA test. A *P* value less than 0.05 was considered statistically significant.Error bars indicate SEM.

5.4.5 PODO447-ADC has *in vivo* cytotoxic activity in carcinoma xenograft models

Since PODO447-Vedotin showed significant *in vitro* cytotoxicity on cells expressing the PODO447 epitope, we hypothesized that PODO447-Vedotin treatment of high PODO447-expressing xenografted tumors would result in increased survival of treated mice. We selected three cancer lines (A172, SKOV3 and MIAPACA) that express high levels of the PODO447 epitope (**Fig 4.1 & 4.2**) and are highly susceptible to PODO447-Vedotin treatment *in vitro* (**Fig 5.5 & 5.6**) as test tumor models for this pilot study. While we attempted to xenograft A172 cells by injecting them both subcutaneously and intravenously into NSG mice, neither model produced tumors in these mice (data not shown), and we were therefore unable to evaluate PODO447-Vedotin efficacy on A172 cells *in vivo*.

Next, we injected SKOV3 cells subcutaneously into NSG mice and initiated PODO447- or palivizumab-Vedotin treatment when the tumors reached 0.1 cm^3 in size. Tumor size was then monitored and survival was determined as days from the start of treatment to experimental endpoint (tumor size ≥ 1cm^3). Mice received intravenous injections of PODO447- or palivizumab-Vedotin every 4 days, for a total of 4 treatments. Antibody dosages were selected based on previous studies of a Lewis Y-Vedotin conjugate tested on ovarian and lung carcinoma cells. In this previous study, the authors found the conjugate had an *in vitro* IC_{50} of 10ng/ml and *in vivo* therapeutic efficacy at 3mg/kg/injection on human tumor xenografts (217). Given the limited availability of PODO447-Vedotin conjugates and the fact that the *in vitro* IC_{50} on SKOV3 cells is approximately 30 times higher (300ng/ml) than the aforementioned Lewis Y-Vedotin study, we selected a 9.5mg/kg/injection dose for this proof-of-concept experiment. We observed regression of the tumors in both PODO447 and control ADC treated groups, most

likely because of non-specific killing due to a high ADC dose (**Fig 5.7A**). Interestingly, tumors in control-treated mice recovered more quickly from ADC-treatment, resulting in modest but significantly increased survival of the PODO447-Vedotin treated mice ($P < 0.01$, **Fig 5.7B**). These data suggest that despite the non-specific toxicity, PODO447-ADC may still be targeting a subpopulation of cells driving tumor growth.

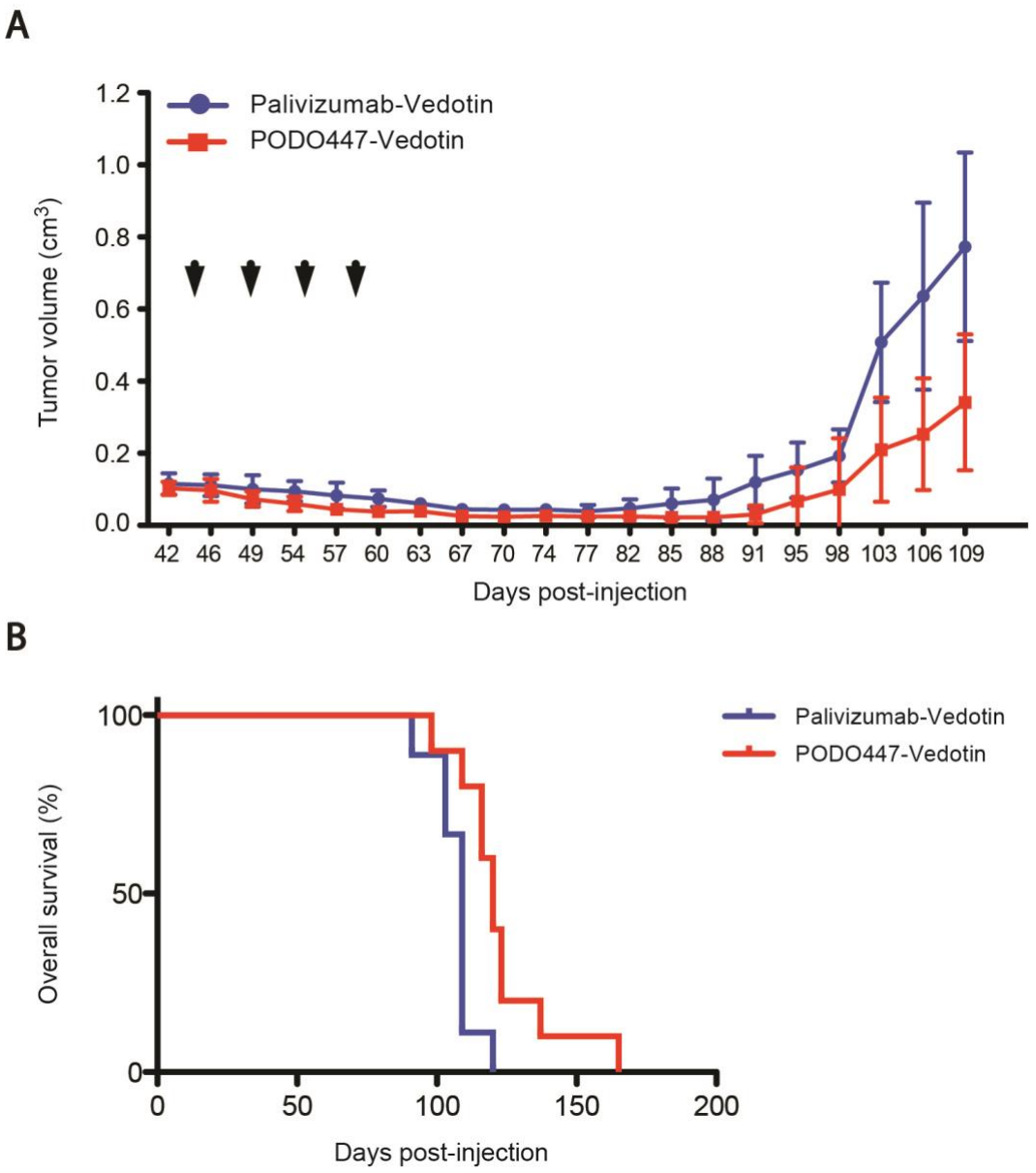

Figure 5.7 PODO447-Vedotin *in vivo* therapeutic effect on ovarian cancer xenograft

Therapeutic effect of PODO447-Vedotin treatment in SKOV3 tumors injected subcutaneously into the right flank of NSG mice (**A**) Tumor growth overtime of SKOV3 cells treated with PODO447 or control ADC (9.5 mg/kg/injection, administered i.v.). Antibody-ADC treatment administrations are indicated by the arrowheads ($P < 0.001$) (**B**) Overall survival of mice treated with the conjugates ($P < 0.01$). The data in this figure come from 1 experiment with 10 mice per

group. Statistical analysis was performed using two-way ANOVA test (A) and Log-rank test (B). A *P* value less than 0.05 was considered statistically significant.Error bars represent SEM.

Finally, we evaluated the therapeutic effect of PODO447-Vedotin on a pancreatic xenograft model using MIAPACA cells injected subcutaneously into the flank of NSG mice. To avoid the non-specific toxicity we observed with the 9.5mg/kg/injection dose, we lowered the dose to 4 and 2 mg/kg/injection (**Fig 5.8A** and **B**, respectively). At the 4 mg/kg/injection dose (4 treatments total), even though we observed a small growth delay of tumors in mice treated with control ADC, PODO447-Vedotin treatment led to long-term regression of established tumors ($P < 0.001$) and resulted in significantly increased ($P < 0.001$) survival of treated mice (**Fig 5.8A**). In contrast to the high-dose, the low-dose (2 mg/kg/injection) administration of the control ADC showed no discernable toxicity but the PODO447-Vedotin conjugate, at this dose, was less efficacious and required 10 treatments at 2 mg/kg/inj (compared to 4 treatments at the 4 mg/kg/injection dose) to impact tumor growth. These data suggest that optimal efficacy requires a balance between low doses that have less off target toxicity but poorer on target killing, and higher doses that show greater unspecific toxicity but more robust on target killing and long-term tumor regression. Regardless, both regimens lead to increased survival when compared to the control treated animals ($P < 0.001$, **Fig 5.8**).

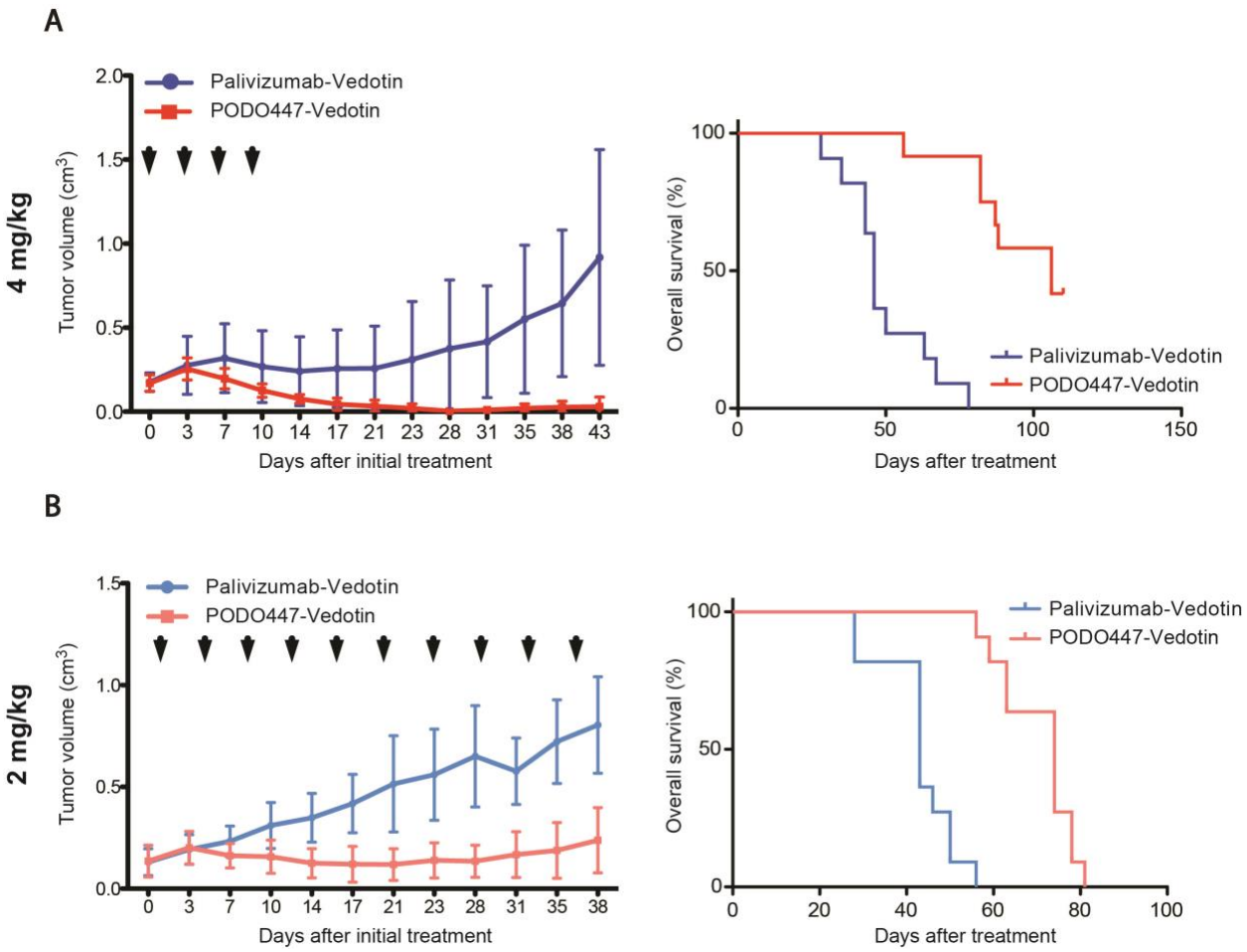

Figure 5.8 *In vivo* PODO447-Vedotin therapeutic effect on a pancreatic NSG xenograft

Assessment of PODO447-Vedotin *in vivo* therapeutic effect on MIAPACA pancreatic cancer cells injected subcutaneously into the flank of NSG mice. Mice were treated with PODO447- or palivizumab-Vedotin control conjugates by i.v. injections at either 4 mg/kg/injection (**A**) or 2 mg/kg/injection (**B**) according to the treatment schedule indicated by the arrowheads. Left panel shows tumor growth over time **(A, B** $P < 0.001$). Right panel shows overall survival of ADC treated mice (**A**, **B** $P < 0.0001$). The data in this figure come from 2 independent experiments with 5 to 6 mice per group, samples from replicate groups were combined for data analysis. Statistical analysis of the tumor growth over time was performed using two-way ANOVA test.

Statistical analyses of survival was performed using a Log-rank test . A *P* value less than 0.05 was considered statistically significant.Error bars in all panels show SEM.

Previous studies have found that, intriguingly, the efficacy of therapeutic antibodies and antibody-drug conjugates, and the level of off-target cytotoxicity varies widely depending on the degree of immunodeficiency of the mouse strain used in pre-clinical trials; nude mice being T cell deficient, RAG mice being T and B cell deficient and NSG or NRG mice being T, B and NK cell deficient (218). This likely reflects the fact that B cell deficient mice fail to produce endogenous immunoglobulin and therefore have an abundance of Fc receptor positive cells that have not been pre-saturated with serum immunoglobulin. Accordingly, we confirmed the *in vivo* effect of PODO447-Vedotin on MIAPACA cells injected subcutaneously into nude mice, a less immunocompromised strain than NSG. In general, we observed a strong therapeutic effect consistent with our previous results in NSG mice. At 4mg/kg/injection, we observed complete tumor regression in all mice treated with PODO447-Vedotin ($P < 0.01$), resulting in long term regression (no tumor relapse present at 100 days after treatment start date) of 4 out of 7 mice (**Fig 5.9A**). Interestingly, in contrast to what we observed in NSG mice, control ADC administered at 4mg/kg/injection had no significant effect on tumor burden compared to PODO447-ADC, suggesting that nude mice can tolerate a higher dose of ADC without unspecific tumor toxicity. Here, again, PODO447-Vedotin treatment significantly increased overall survival (**Fig 5.9A**, $P < 0.05$).

We, again, also tested PODO447 ADC at 2 mg/kg/injection. While we observed a clear trend toward tumor regression in mice treated with PODO447 ADC compared to controls, this did not reach statistical significance due to the fact that half of the control-treated mice reaching their humane endpoint early (see arrow highlighting the drop on tumor growth curve of palivizumab ADC-treated mice at 18 days after initial treatment, **Fig 5.9B**). Nevertheless, we could show that treatment of PODO447-Vedotin at 2 mg/kg/injection significantly increased the overall survival

($P < 0.01$) and resulted in the complete remission of 1 out of 4 treated mice as determined at 95 days after initial treatment (**Fig 5.9B**).

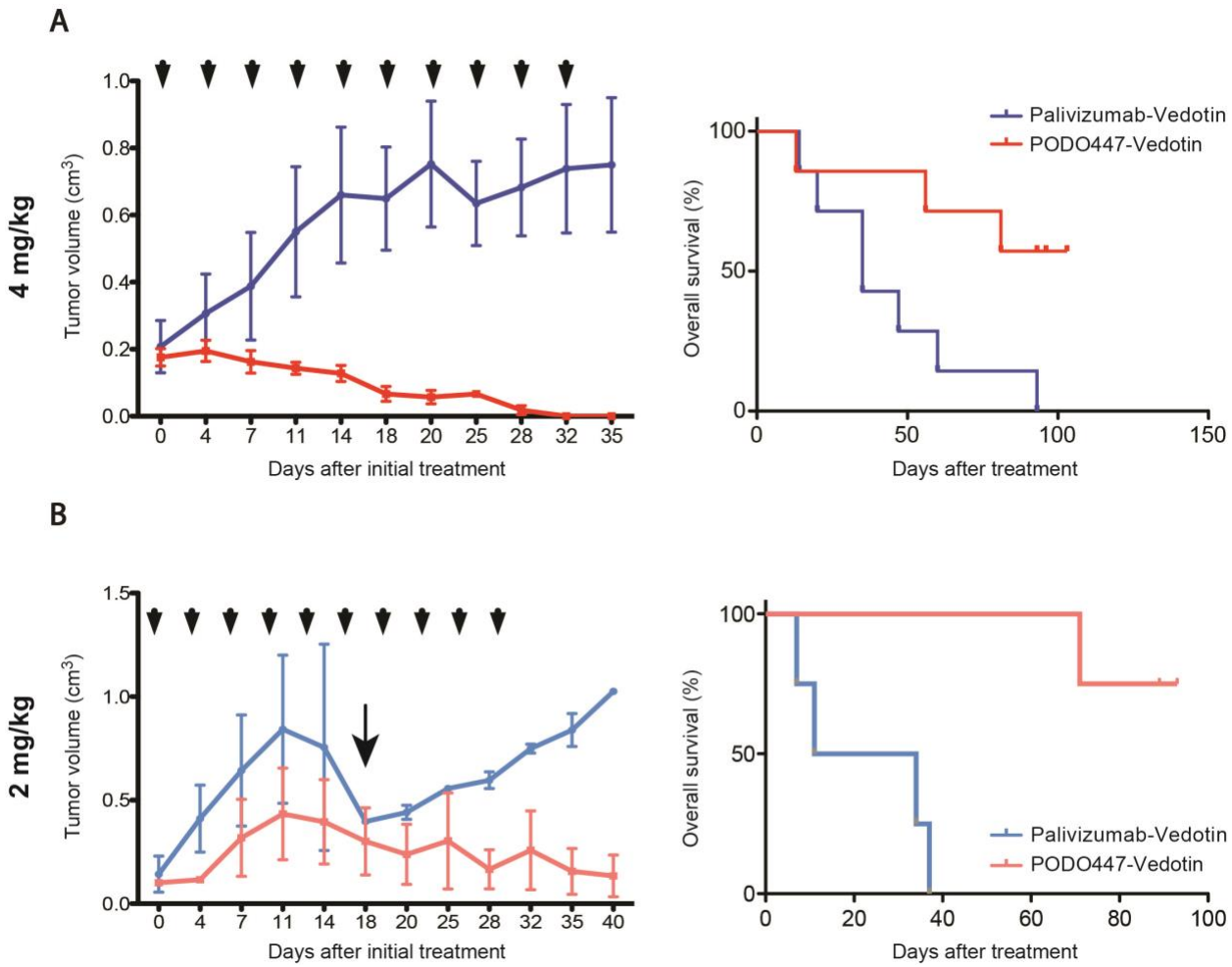

Figure 5.9 PODO447-Vedotin *in vivo* therapeutic effect in nude mice

PODO447 ADC *in vivo* therapeutic effect on nude mice injected subcutaneously with MIAPACA cells. (**A**) Mice were treated with conjugates at 4mg/kg/injection following the treatment schedule indicated by the arrowheads. Left panel shows PODO447 or palivizumab control ADC-treated tumor growth over time ($P < 0.01$). Right panel shows overall survival of conjugate-treated mice ($P < 0.05$). (**B**) Mice were treated with 2mg/kg/injection of ADC as indicated by the arrowheads. Left panel shows tumor growth over time (note that statistical significance could not be achieved due to 2 mice of the control group achieving early humane

endpoint at day 18 (arrow)). Right panel shows overall survival of treated mice ($P < 0.01$). Survival is not tumor size specific. Data in (**A**) come from 2 independent studies with 3-4 mice per group. Replicate groups were combined for data analysis. Data from (**B**) come from 1 experiment with 4 mice per group. Statistical analysis of the tumor growth over time was performed using two-way ANOVA test. Statistical analyses of survival was performed using a Log-rank test . A *P* value less than 0.05 was considered statistically significant.Error bars in all panels shows SEM.

5.5 Discussion

Cancer therapy has seen remarkable clinical successes in the last decade thanks to the development of new targeted therapies. However, efforts to target solid tumors remain an unmet clinical need and are still hampered by the lack of well validated tumor-specific targets. Podxl has surfaced as a promising new therapeutic target for cancer since its expression is associated with poor survival in a wide variety of cancers and it has been shown in several scenarios to play an active role promoting tumour progression. Unfortunately, efforts to develop Podxl-based therapies have been hampered due the expression of Podxl on a number of normal tissues, mainly the kidney podocytes and vascular endothelium. Thus, the discovery that PODO447 recognizes a tumour-specific antigen on Podxl encouraged us to investigate this new avenue as a potential cancer therapeutic.

We previously showed that unconjugated PODO83 mAb could delay *in vitro* cancer invasion, i*n vivo* primary tumor growth and block lung metastasis in mice with an established tumor burden (Chapter 3, (136)). Here, we similarly examined the therapeutic potential of PODO447 as an unconjugated mAb. We showed that, like PODO83, PODO447 mAb does not affect the tumorsphere forming ability of ovarian SKOV3 or breast cancer MCF7 cells *in vitro*. Unlike PODO83 however, we showed that PODO447 does not affect *in vitro* invasion of SKOV3 cells. Moreover, we showed that as an unconjugated mAb, PODO447 is not cytotoxic to cancer cells *in vitro*, and has no toxic or inhibitory effect on SKOV3 ovarian cancer cells *in vivo*. Together, these results suggest that unconjugated PODO447 alone does not alter the tumorgenicity of cancer cells *in vitro* or *in vivo* and therefore cannot be used alone as a therapeutic. It is noteworthy that of 18 novel antibodies against Podxl tested (8 published (136) and 9

unpublished) all failed to show any efficacy in blocking tumor growth *in vivo* with the exception of PODO83. There could be several explanations for this discrepancy including differences in affinity of these antibodies to Podxl (i.e. PODO83 could have exceptionally high affinity) or selective binding to a critical functional epitope on this large molecule. In this regard, among these antibodies, only PODO83 is known to selectively bind a juxtamembrane epitope which lacks cross-blocking activity with all other mAbs. We know that Podxl binds to and directs the subcellular localization of a family of multi-ligand intracellular scaffold proteins (NHERF1 and 2) (101) and therefore the selective binding to this epitope could interfere with co-association with other known NHERF ligands (219).

With regards to PODO447, because of its exquisite tumor cell specificity and the fact that as an unconjugated monotherapy it has no effect on cancer cells, we investigated whether PODO447 could instead be used as the targeting arm of a Vedotin antibody-drug conjugate (ADC) immunotherapy. Here we show significant internalization of PODO447 in most cancer cells expressing high levels of the PODO447 epitope. Further, we show that PODO447-Vedotin conjugates cause potent *in vitro* cytotoxicity in several cancer cell lines, including glioblastoma, pancreatic cancer and patient-derived high-grade serous tumour cells. Additionally, we show that this *in vitro* PODO447 ADC cytotoxicity is specific to tumour cells expressing the PODO447 epitope on Podxl, and did not observe a reduction in cell viability on *PODXL*-KO cancer cells or control-ADC treated cells. An exception to this were the MDA-MB-231 cells which express the PODO447 epitope on their surface, yet they do not internalize PODO447 nor display reduction of cell viability upon treatment with PODO447-ADC. One possible explanation could be the differential expression of Podxl's intracellular ligands. There are three known intracellular

ligands of Podxl (NHERF1/2 and ezrin) that function as scaffolding proteins to the actin cytoskeleton and, as such, might play a role in antibody-receptor complex internalization. Thus, one could speculate that differential expression of Podxl's intracellular binding partners across different tumor cells might account for the difference in PODO447 internalization efficiency and subsequent PODO447-ADC cytotoxic efficacy. Lastly, we show a significantly increased survival of ovarian and pancreatic tumour-bearing mice treated with different doses of PODO447-Vedotin. Together, all of these data bode well for PODO447 effectiveness as an anti-tumor therapeutic.

Interestingly, we observed strain-specifics differences in the therapeutic effect of PODO447-Vedotin. Compared to NSG mice, nude mice were able to tolerate higher doses without compromising treatment specificity. As noted, one explanation could be the difference in antibody biodistribution in highly immunodeficient mice. Previous studies showed that the performance and efficacy of antibody-based therapeutics is impacted in NSG mice possibly due to sequestration of antibody-based agents within the spleen, leading to increased plasma clearance (220). This could impact the bioavailability of PODO447-Vedotin and limit its efficacy in NSG versus nude mice. Further, in contrast with NSG mice, nude mice have active natural killer (NK) cells which might supplement PODO447-Vedotin's *in vivo* cytotoxicity via antibody-dependent cytotoxicity (ADCC). Together, these results suggest the use of a less immunodeficient mouse model, such as nude mice, may be more beneficial for future evaluation of antibody-based *in vivo* therapeutic studies.

Although there is a need to further investigate PODO447-Vedotin's pharmacokinetics and pharmacodynamics, we show for the first time, the *in vitro* and *in vivo* therapeutic effect of PODO447 as an ADC. As with any therapy, a nagging concern is the ability of cells to become resistant through down-regulation of the target antigen. However, we have previously shown that Podxl plays a direct functional role in endowing metastatic cells with rare tumour initiating capacity, suggesting that its expression is essential for tumor survival. With that in mind it is possible that, even if the bulk of solid tumors lose expression of Podxl, the key cells that will undergo tumor progression will still require Podxl in order to metastasize ((39,136,142,172)). It is noteworthy that tumor metastasis has been extremely difficult to target therapeutically, largely due to the inability to mimic this type of biological function in a way that lends itself to high-throughput *in vitro* screens. Thus, the discovery of Podxl as a molecule key to this process offers a rare opportunity to explore methods for its inhibition. Furthermore, with regards to PODO447, one could also speculate that targeting a fraction of tumour cells that express this epitope may selectively eliminate the subset of cells with the highest metastatic capacity, making it a more targeted therapy for this elusive subset of cells than standard chemotherapy (currently under investigation).

Another potential concern for PODO447 is the emergence of cells that have lost the glycotransferases required to generate the PODO447 epitope. Yet here too, the ability to become resistant will depend on the functional significance of this glycosylation on the PODO447 epitope. The GalNAcβ1 glycan motif that comprises part of this epitope is extremely unusual in normal eukaryotic settings. However, similar glycan structures such as the LacdiNAc-type (GalNAcβ1-4GlcNAc) motifs and the P antigen (Gb4) have previously been identified in ovarian

cancer tissue (206,207). Thus, these epitopes may have an important functional role in tumour cell spread. If this were indeed the case, one could envision that targeting a rare PODO447 subpopulation of tumour cells would have an outsized role in managing the cancers by targeting cells most likely to metastasize.

Lastly, the PODO447 epitope could be a promising new target for chimeric antigen receptor T cell (CAR-T) based therapies. Despite the success of CAR-T therapy in hard-to-treat B cell malignancies (B cell leukemia and some B cell lymphomas), to date, this approach has not yet been exploited widely for solid tumours, in part, due to the lack of appropriate tumour-specific epitopes. Thus PODO447, as a highly tumour-specific mAb, may offer an unprecedented opportunity to extend the promise of a CAR-T therapy approach to ovarian cancers and other solid tumours.

Chapter 6: Discussion

6.1 Contributions to the field and future directions

Despite rapid medical advances, cancer remains one of the leading causes of death worldwide with metastatic disease accounting for 90% of all cancer deaths (25,147). For decades, chemotherapy has been the standard of care in cancer treatment, however, the introduction of targeted immunotherapies has vastly improved patient outcome in certain malignancies including breast carcinomas and leukemia (71). The success of these targeted therapies relies heavily on the identification of unique tumor-antigens that permit delivery of potent therapeutic agents to cancerous cells while sparing healthy tissues. Thus, further research into the molecular mechanisms that facilitate cancer progression might reveal novel targets and help translate the success of targeted therapies to other cancer types that currently have poor treatment options. The work described here provides further understanding into the role of Podxl in cancer progression and its potential as a therapeutic target. Further, we identify a novel tumor-restricted glycoepitope and characterize a binding antibody that can be used to target cancer cells *in vivo*. The significance of these findings is highlighted below.

6.1.1 Podxl is important for ovarian tumor growth

Podxl is highly expressed in many cancers and is associated with decreased patient survival (108,109). However, aside from identifying a subset of aggressive cancers likely to undergo tumor progression, little is known about the role of Podxl in cancer tumorigeneses. In chapter 2, I attempt to further characterize the molecular mechanism by which Podxl promotes tumor growth and metastasis. By generating CRISPR/Cas9 MDA-MB-231 *PODXL*-KO cells, I confirmed that

Podxl plays a role in *in vivo* tumor growth. Unfortunately, I noted that the phenotype of the MDA-MB-231 *PODXL*-KO cells rapidly evolves ("drifts") with passage *in vitro,* resulting in a variable tumorigenic phenotype independent of Podxl expression, which made exploring the functional domains of Podxl through complementation extremely challenging. Because MDA-MB-231 cells are aneuploid and exhibit genomic instability (156), we postulate that the processes they were subjected to (single-clonal selection, multiple passages and several rounds of cell-sorting) accentuated their already high chromosomal instability permitting them to drift during cloning and expansion, thus rendering them unsuitable to study the role of Podxl in cancer progression. I attempted to circumvent this problem by using a different, potentially more stable, ovarian cancer cell line. Thus, we next generated CRISPR/Cas9 SKOV3 *PODXL*-KO cells and showed, for the first time, that Podxl expression is also important for the tumor growth of these ovarian cancer cells.

Limitations and future directions

There are, however, critical limitations to this study. In contrast to shRNA-dependent gene knockdown, to generate *PODXL*-KO clones, cells require single-cell clonal selection, multiple passages and several rounds of cell sorting. Recent studies have shown that subclones derived from a clonal cell line exhibit significant variability in their phenotype despite the more consistent behaviour of the parental clone (176). Thus, the observed SKOV3 *PODXL*-KO phenotype could be the result of genetic instability (and clonal selection) rather than Podxl-dependency.

Future studies should confirm that the impaired tumor growth phenotype observed in SKOV3 cells is indeed Podxl dependent. To this, one approach could be to generate shRNA Podxl-knockdown SKOV3 cells. Since this approach does not require direct DNA modification or single-cell clonal selection, if the SKOV3 shRNA knock-down cells also displayed impaired growth *in vivo*, it would confirm that indeed Podxl affects tumor growth of these cells and support the use of SKOV3 CRISPR *PODXL*-KO cells to further explore the key functional domains of this protein.

A second approach could be the generation of additional CRISPR/Cas9 *PODXL*-KO cells using a "pooled" approach. Using this method, cells would be bulk sorted and not subjected to single-cell clonal selection thus reducing the selective pressure and potential drifting. Additionally, gene rescue experiments should also be optimized and performed to confirm the phenotype's dependency on Podxl's expression.

Further, additional *PODXL*-KO cells could be generated using an inducible deletion strategy. Here, one could use a tamoxifen (TAM)-inducible CreERT2/loxP system to temporally delete the Podxl gene. Briefly, SKOV3 cells carrying a loxP-flanked Podxl gene (first exon) would be grown in mice until palpable tumors arise. Next, some mice would be treated with TAM, resulting in the deletion of PODXL in their tumors, and tumor behavior would be monitored. Since the cells injected would have originated from the same clone, differences in tumor behavior could be attributed to the presence or absence of Podxl.

Lastly, pending confirmation of the Podxl dependence of the phenotype, future studies should include the exploration of the molecular mechanisms by which Podxl promotes tumor growth of SKOV3 cells. One approach could be the re-expression of the newly generated Podxl-deletion mutants (Appendix C) in SKOV3 *PODXL*-KO cells to investigate the domain(s) responsible for promoting SKOV3 tumor aggressiveness. Additionally, an inducible approach could also be used to mutate Podxl and generate cells temporally expressing different Podxl-deletion mutants to explore Podxl's key functional domain(s) for tumor growth.

6.1.2 PODO83 targets the juxtamembrane extracellular domain of Podxl to block metastasis to the lung

Most cancer-related deaths are the result of metastatic disease highlighting the need for further research identifying new tumor biomarkers capable of detecting tumors at high risk of metastasizing (221). This would allow the generation of targeted therapies and improve patient survival. Podxl is highly expressed in a wide number of cancers and it is associated with poor patient outcome (108,109,201). Thus, it has emerged as a potential prognostic marker and therapeutic target. However, to date, no Podxl-based diagnostic or therapeutic is currently available.

In Chapter 3, I used *in vitro* and i*n vivo* pre-clinical models to further characterize PODO83's activity and validate its use as a potential therapeutic. I examined the mechanisms of action for PODO83 and demonstrated that, while treatment with PODO83 does not affect the tumorsphere formation *in vitro*, it does delay tumor cell invasion in *in vitro* (Matrigel assays). This suggests that PODO83 treatment primarily affects the ability of tumor cells to invade tissues, rather than

their ability to grow. Importantly, I confirmed the metastasis-blocking function of PODO83 *in vivo*, and demonstrated that PODO83 treatment blocks pulmonary metastases in mice with an established tumor burden. It is noteworthy that of all 18 novel antibodies we initially generated against Podxl, only PODO83 showed efficacy in blocking tumor growth and metastasis *in vivo* (136). There could be several explanations for this, including differences in antibody affinities (i.e. PODO83 having an exceptionally high affinity for Podxl) or the selective binding to a critical functional epitope. In this regard, of the anti-Podxl mAbs we have tested, only PODO83 shows selective binding to Podxl's juxtamembrane domain (discussed further below), thus suggesting a critical functional role for PODO83's reactive epitope. Since Podxl binds and directs the subcellular localization of the NHERF1/2 scaffolding proteins (139), it is possible that the functional epitope recognized by PODO83 is involved in the co-association of other known NHERF ligands and that the antibody disrupts signaling transduction in a way that promotes tumorigenesis. In this regard, NHERF1/2 are well-known to bind a large array of signaling molecules including tyrosine kinases (EGFR, PDGFR), transcription factors (β-catenin) and G-protein coupled receptors and transporters (CTFR, β-2-adrenergic receptor, NHE3, TRPV5, etc.) any one of which could further influence metastatic behavior (99,101). Since PODO83 treatment primarily affects the ability of cancer cells to invade (but not to migrate) *in vitro*, another possibility is that the PODO83 epitope is involved in the interaction of Podxl with an extracellular ligand (i.e. laminin, selectins, galectins, etc.) to promote ECM/BM degradation through the activation and release of proteinases, thus promoting cancer cell invasion.

I also assessed the expression of PODO83 in urothelial, pancreatic, breast and ovarian carcinomas. I found that PODO83 reacts with 75% (72/96) of pancreatic tumors, 92% (300/325)

of breast tumors and 91% (200/219) of ovarian carcinomas, suggesting that these cancers, which typically have poor prognosis, represent an unmet need that could be filled by a PODO83-based diagnostic or therapeutic.

Although I determined PODO83's reactive epitope to be on the well-conserved juxtamembrane stalk domain of the human Podxl core protein, I also found that PODO83 is exquisitely species specific and does not bind to macaque and murine Podxl or human CD34. I also find that it recognizes both malignant and healthy human tissue arguing against binding a tumor-specific post-translational modification. It is noteworthy that all *in vivo* studies to date have been performed in xenografted mice where the tissues that express endogenous murine Podxl will fail to be bound by PODO83. Thus, because of the potential for PODO83 to bind Podxl in healthy human tissues including the endothelium and kidney podocytes, assessment of the potential normal cell toxicity associated with PODO83 treatment still needs further evaluation. To this end, during the course of this thesis, I helped design a novel mouse model that could facilitate such studies. We recently generated a mouse where the murine Podxl encoding exons 5 to 7 have been replaced with the orthologous human exons. This should result in the expression of the PODO83 human reactive epitope on the murine Podxl protein in the appropriate mouse tissues, thus permitting vital pre-clinical safety testing in this "humanized" mouse model (currently in progress).

In summary, to our knowledge, we have characterized the first function-blocking antibody against Podxl, contributing to both the understanding of Podxl's role in promoting metastasis and the validation of potential Podxl-based cancer therapeutics and diagnostic tools.

Limitations and future directions

Chapter 3 identifies pancreatic, breast and ovarian carcinomas as potential applications for a PODO83-based therapeutic or diagnostic tool. However, as aforementioned, one limitation of this study is the potential vascular and renal cell toxicity associated with PODO83 treatment which could not be assessed due to the inability of PODO83 to bind murine or macaque Podxl. Thus, future work should make use of the newly generated mouse expressing the PODO83 reactive epitope on the murine Podxl protein across Podxl-expressing mouse tissues to evaluate potential off-tumor toxicity *in vivo.*

Future studies should also continue to investigate the diagnostic potential of PODO83. Since Podxl has been observed in cancer-derived extracellular vesicles as well as in the serum of pancreatic cancer patients (121,155), future work may include the investigation of Podxl detection in the serum of cancer patients using PODO83.

Lastly, previous studies have shown that cell-surface Podxl expression in pancreatic and ovarian carcinomas is associated with poor patient survival (117,119). As such, since the PODO83 staining observed was predominantly cytoplasmic, future studies should investigate whether PODO83 could be used as a prognostic antibody for these cancers. To do this, one approach could be to assess PODO83 immunoreactivity across larger cohorts of pancreatic and ovarian carcinoma TMAs that include patient outcome data to determine whether PODO83 staining is associated with worse patient survival.

6.1.3 PODO447 recognizes a tumor-restricted glycoepitope on Podxl

Development of targeted therapies for solid tumors has remained slow, in part, for reasons highlighted above: the lack of well-characterized tumor target antigens exhibiting a high degree of tumor specificity (75). Though others in previous publications, and I in this thesis, have identified Podxl as a promising target for cancer immunotherapy, development of a Podxl-based therapeutic has been hampered over concerns of potential toxicity since Podxl is normally also expressed at high levels by vascular endothelia and kidney podocytes. In Chapter 4, I attempted to circumvent this problem by describing a novel tumor-restricted glycoantigen on Podxl and the development of an antibody against it (PODO447).

In collaboration with Ola Blixt at the University of Copenhagen, I showed that PODO447 recognizes a terminal GalNAcβ1 motif located within the mucin domain of Podxl. Importantly, I demonstrated that PODO447 recognizes an array of human tumour lines while exhibiting minimal reactivity to normal cell types or tissues, including those that express the Podxl core protein at high levels. This represents the first report of a tumor-restricted epitope on the Podxl protein and presents PODO447 as the first antibody that can be used to target it.

Lastly, I also show that a high percentage of HGSOC tumors express the PODO447 glycoepitope. Since HGSOC is the most prevalent histotype of EOC for which the prognosis is poor and antigen-specific therapeutic options are extremely limited (222), a PODO447-based immunotherapy could present a promising avenue of treatment for these malignancies and likely many others.

Limitations and future directions

While PODO447 harbors great potential as a cancer therapeutic, the findings in Chapter 4 raise new questions that should be addressed in future studies.

One of particular interest is the significance of the PODO447 epitope in cancer progression. Since Podxl promotes cancer metastasis (39,136,142), one could speculate that PODO447's glycoepitope is associated with a subset of tumor cells likely to undergo tumor progression. Glycans can confer a selective advantage on cancer cells that facilitate tumor spread (195) and, since Podxl is known to undergo tissue-specific glycosylation (201), one could postulate that tumor-expressed Podxl undergoes specific glycosylation depending on the stage of tumor progression. For instance, Podxl expressed by high-endothelial venules (HEV) has been shown to promote lymphocyte adhesion when displaying sialyl Lewis X (SLeX) (99) thus, one could think that specific glycosylation of Podxl on tumor cells (perhaps the acquisition of the PODO447 glycoepitope or the loss of SLeX) could favor tumor spread by preventing immune recognition of cancer cells. Moreover, since glycosylation at the metastatic site is likely to be different to that of the primary tumor or circulating cells, it is possible that PODO447 glycoepitope is displayed on Podxl expressed on metastatic cells as a result of incomplete glycan synthesis (i.e. PODO447 glycoepitope is a truncated glycan structure) or neo-synthesis due to the induction of metastasis-associated genes involved in glycosylation, exciting areas for future exploration. Thus, future studies should investigate the role of the PODO447 epitope in cancer metastasis. To this, one approach could be to compare the *in vivo* metastatic potential of Podxl-expressing patient-derived cells or cell lines (i.e. CFPAC-1) displaying (or not) the PODO447 epitope on their surface. Additionally, future work may investigate the potential association of

PODO447 with development of metastatic disease by evaluating the immunoreactivity of PODO447 on TMAs containing primary and matched metastatic tumor tissue.

Lastly, one limitation of this study is the potential toxicity associated with PODO447 binding to vessel-like structures in the kidney medulla, Thus, future studies should focus on determining what such structures are, whether the staining observed in these structures is specific or spurious, and to investigate the potential toxic effect that PODO447 might have if it were to bind *in vivo*. Additionally, since pro-inflammatory cytokines or hypoxia have been shown to modulate cell surface glycosylation (223), future studies should also investigate whether the PODO447 epitope is expressed in inflamed, non-malignant tissues and, if so, the potential toxicity associated with it.

6.1.4 PODO447-ADC treatment effectively targets and kills tumor cells *in vivo*

Though antibody-drug conjugates hold great promise as a new generation of targeted therapies, only a few are currently approved for clinical use (81). One of the major hurdles in their development has been the identification of truly tumor-specific antigens and the successful generation of the appropriate antibodies against them (83).

In Chapter 5, I explored the potential application of PODO447 in cancer immunotherapy. Unconjugated PODO447 alone did not alter the behavior of cancer cells *in vitro* or *in vivo*, suggesting that while it effectively targets tumor-specific glycoepitopes on Podxl, it does not have a direct functional effect. I therefore utilized PODO447 as the targeting arm of a Vedotin antibody-drug conjugate, and demonstrated *in vitro* that PODO447-ADC exerts potent

cytotoxicity against several cancer cell lines that express the appropriate tumor-glycosylated form of Podxl.

I further confirm these effects *in vivo*, showing that PODO447-Vedotin can specifically target ovarian and pancreatic cancer cells and significantly increase the survival of xenografted tumor-bearing mice. A by-product of these studies is the observation that nude mice appear to show a lower degree of non-specific ADC-toxicity. This likely reflects the fact that these mice have a replete compartment of antibody-secreting B cells which provide antibody to saturate endogenous Fc receptors. Thus, this highlights the need for careful selection of pre-clinical animal models to assess the therapeutic potential of ADCs which could be impacted by the presence of immune effector cells.

Together, the study presented in Chapter 5 confirms Podxl as a promising therapeutic target and demonstrates that there is a unique tumor-specific glycomotif. This motif can be targeted with an antibody-drug conjugate to reduce tumor burden and increase survival in pre-clinical models, paving the way for future pre-clinical studies and, potentially, the transition of PODO447-ADC into the clinic.

Limitations and future research

Despite our promising results, it is worth considering the potential future roadblocks to adoption of this antibody as an immunotherapy. Since PODO447 recognizes a glycoantigen, there is the possibility that tumor-recognition could be lost if extended treatment causes the cancerous cells to mutate and lose the glycotransferases required to generate the PODO447 epitope, or gain

expression of enzymes that mask it. Thus, further research is required to determine the functional significance of this specific glycoepitope and its relationship to tumor cell behaviour (see section 6.1.3).

In Chapter 5 we show that PODO447-ADC has limited effect on MDA-MB-231 cells despite expressing the PODO447 epitope, most likely as a result of poor PODO447 internalization. Thus, future studies should investigate the molecular mechanisms by which Podxl is internalized when bound to an Ab. Since Podxl has three known intracellular binding partners (NHERF1/2 and ezrin) that act as scaffolding proteins to the actin cytoskeleton (107), one approach could be to use Podxl mutants to identify intracellular ligands involved in the internalization of Podxl-Ab complexes. This work could further the understanding of protein-Ab complex internalization, a key step for the success of ADCs, and possibly help identify PODO447-positive tumors that are likely to be non-responsive to PODO447-ADC treatment.

Another potential issue to consider is the lack of homogeneous PODO447 epitope expression in tumors. Though this might be circumvented by bystander effects, future work should evaluate PODO447-ADC efficacy in xenografted tumors with heterogeneous expression of the PODO447 epitope. Additionally, further studies are also needed to determine if the PODO447-ADC therapeutic activity can be enhanced via immune-mediated effector functions such as Antibody-Dependent Cellular toxicity (ADCC), Antibody-Dependent Cellular Phagocytosis (ADCP) or Complement-Dependent Cytotoxicity (CDC).

Lastly, to further PODO447 closer to the clinic, future studies should examine the biodistribution, pharmacokinetics, pharmacodynamics and linker stability of PODO447-ADC *in vivo*. Additionally, since tumors differ in their response to drugs, future work should evaluate PODO447-ADC efficacy using different linker and toxic payload combinations.

6.2 Final conclusions

In conclusion, this thesis confirms that Podxl plays an important role in tumor progression and highlights its potential as a tumor marker for the development of cancer diagnostics and therapeutics. Our pre-clinical validation of PODO83 established the location of the PODO83 reactive epitope on the Podxl core protein, and examined its distribution across malignant and healthy human tissues, thus contributing to the understanding of Podxl in cancer biology and providing a potential diagnostic tool. Although it is still in progress, I also highlight a path forward (development of a humanized PODXL mouse) for testing potential toxicity associated with PODO83 binding of Podxl on normal tissues. Finally, and most significantly, I also identified and characterized a novel tumor-specific epitope on Podxl that is recognized by the PODO447 antibody. I provide preclinical evidence supporting the use of a PODO447-based antibody-drug conjugate to target cancer cells *in vivo* validating, for the first time, Podxl as a therapeutic target in cancer. We hope that this work furthers scientific understanding of the mechanisms underlying cancer metastasis, and contributes to the development of new therapeutic strategies by providing two promising targets and a characterization of antibodies against them.

Bibliography

1. Gabriel, J. *The Biology of Cancer*. (John Wiley & Sons Ltd, 2007).
2. Catenacci, D. V. *et al.* Durable complete response of metastatic gastric cancer with anti-Met therapy followed by resistance at recurrence. *Cancer Discov* **1,** 573–579 (2011).
3. Hanahan, D. & Weinberg, R. A. Hallmarks of Cancer: The Next Generation. *Cell* **144,** 646–674 (2011).
4. Cheng, N., Chytil, A., Shyr, Y., Joly, A. & Moses, H. L. Transforming growth factor-beta signaling-deficient fibroblasts enhance hepatocyte growth factor signaling in mammary carcinoma cells to promote scattering and invasion. *Mol Cancer Res* **6,** 1521–1533 (2008).
5. Bhowmick, N. A., Neilson, E. G. & Moses, H. L. Stromal fibroblasts in cancer initiation and progression. *Nature* **432,** 332–337 (2004).
6. Wertz, I. E. & Dixit, V. M. Regulation of death receptor signaling by the ubiquitin system. *Cell Death Differ* **17,** 14–24 (2010).
7. Amit, I. *et al.* A module of negative feedback regulators defines growth factor signaling. *Nat. Genet.* **39,** 503–512 (2007).
8. Mosesson, Y., Mills, G. B. & Yarden, Y. Derailed endocytosis: an emerging feature of cancer. *Nat Rev Cancer* **8,** 835–850 (2008).
9. Burkhart, D. L. & Sage, J. Cellular mechanisms of tumour suppression by the retinoblastoma gene. *Nat Rev Cancer* **8,** 671–682 (2008).
10. Deshpande, A., Sicinski, P. & Hinds, P. W. Cyclins and cdks in development and cancer: a perspective. *Oncogene* **24,** 2909–2915 (2005).
11. Sherr, C. J. & McCormick, F. The RB and p53 pathways in cancer. *Cancer Cell* **2,** 103–112 (2002).
12. Adams, J. & Cory, S. The Bcl-2 apoptotic switch in cancer development and therapy. *Oncogene* **26,** 1324–1337 (2007).
13. Lowe, S. W., Cepero, E. & Evan, G. Intrinsic tumour suppression. *Nature* **432,** 307–315 (2004).
14. Junttila, M. R. & Evan, G. I. p53 - a Jack of all trades but master of none. *Nat Rev Cancer* **9,** 821–829 (2009).
15. Fidler, I. J. The pathogenesis of cancer metastasis: the 'seed and soil' hypothesis revisited. *Nat Rev Cancer* **3,** 453–458 (2003).
16. Jones, R. G. & Thompson, C. B. Tumor suppressors and cell metabolism: a recipe for cancer growth. *Genes Dev.* **23,** 537–548 (2009).
17. DeBerardinis, R. J., Lum, J. J., Hatzivassiliou, G. & Thompson, C. B. The biology of cancer: metabolic reprogramming fuels cell growth and proliferation. *Cell Metab* **7,** 11–20 (2008).
18. Hsu, P. P. & Sabatini, D. M. Cancer Cell Metabolism: Warburg and Beyond. *Cell* **134,** 703–707 (2008).
19. Ostrand-Rosenberg, S. & Sinha, P. Myeloid-derived suppressor cells: linking inflammation and cancer. *J Immunol* **182,** 4499–4506 (2009).
20. *International Classification of Diseases for Oncology*. (World Health Organization, 2013).

21. Terwilliger, T. & Abdul-Hay, M. Acute lymphoblastic leukemia: a comprehensive review and 2017 update. *Blood Cancer J* **7,** e577–e577 (2017).
22. De Kouchkovsky, I. & Abdul-Hay, M. 'Acute myeloid leukemia: a comprehensive review and 2016 update'. *Blood Cancer J* **6,** e441–e441 (2016).
23. Connors, J. M. *et al.* Hodgkin lymphoma. *Nat Rev Dis Primers* **6,** 1–25 (2020).
24. Rajkumar, S. V. Multiple myeloma: 2020 update on diagnosis, risk-stratification and management. *Am. J. Hematol.* **95,** 548–567 (2020).
25. Dillekås, H., Rogers, M. S. & Straume, O. Are 90% of deaths from cancer caused by metastases? *Cancer Medicine* **8,** 5574–5576 (2019).
26. Folkman, J. How is blood vessel growth regulated in normal and neoplastic tissue? G.H.A. Clowes memorial Award lecture. *Cancer Res.* **46,** 467–473 (1986).
27. Talmadge, J. E. & Fidler, I. J. AACR Centennial Series: The Biology of Cancer Metastasis: Historical Perspective. *Cancer Res.* **70,** 5649–5669 (2010).
28. Farber, E. The multistep nature of cancer development. *Cancer Res.* **44,** 4217–4223 (1984).
29. Foulds, L. Multiple etiologic factors in neoplastic development. *Cancer Res.* **25,** 1339–1347 (1965).
30. Klein, C. A. Parallel progression of primary tumours and metastases. *Nat Rev Cancer* **9,** 302–312 (2009).
31. Pavelic, S. K., Sedic, M., Bosnjak, H., Spaventi, S. & Pavelic, K. Metastasis: new perspectives on an old problem. *Mol Cancer* **10,** 22 (2011).
32. Sethi, N. & Kang, Y. Unravelling the complexity of metastasis - molecular understanding and targeted therapies. *Nat Rev Cancer* **11,** 735–748 (2011).
33. Talmadge, J. E. Clonal selection of metastasis within the life history of a tumor. *Cancer Res.* **67,** 11471–11475 (2007).
34. Fidler, I. J. & Kripke, M. L. The challenge of targeting metastasis. *Cancer Metastasis Rev* **34,** 635–641 (2015).
35. Weigelt, B., Peterse, J. L. & van 't Veer, L. J. Breast cancer metastasis: markers and models. *Nat Rev Cancer* **5,** 591–602 (2005).
36. Kalluri, R. & Weinberg, R. A. The basics of epithelial-mesenchymal transition. *J. Clin. Invest.* **119,** 1420–1428 (2009).
37. Thiery, J. P., Acloque, H., Huang, R. Y. J. & Nieto, M. A. Epithelial-Mesenchymal Transitions in Development and Disease. *Cell* **139,** 871–890 (2009).
38. Boyer, B. & Thiery, J. P. Epithelium-mesenchyme interconversion as example of epithelial plasticity. *APMIS* **101,** 257–268 (1993).
39. Fröse, J. *et al.* Epithelial-Mesenchymal Transition Induces Podocalyxin to Promote Extravasation via Ezrin Signaling. *Cell Rep* **24,** 962–972 (2018).
40. De Cock, J. M. *et al.* Inflammation Triggers Zeb1-Dependent Escape from Tumor Latency. *Cancer Res.* **76,** 6778–6784 (2016).
41. Shibue, T., Brooks, M. W. & Weinberg, R. A. An integrin-linked machinery of cytoskeletal regulation that enables experimental tumor initiation and metastatic colonization. *Cancer Cell* **24,** 481–498 (2013).
42. Rhim, A. D. *et al.* EMT and Dissemination Precede Pancreatic Tumor Formation. *Cell* **148,** 349–361 (2012).

43. Lambert, A. W., Pattabiraman, D. R. & Weinberg, R. A. EMERGING BIOLOGICAL PRINCIPLES OF METASTASIS. *Cell* **168,** 670–691 (2017).
44. Ohtsubo, K. & Marth, J. D. Glycosylation in cellular mechanisms of health and disease. *Cell* **126,** 855–867 (2006).
45. Reis, C. A., Osorio, H., Silva, L., Gomes, C. & David, L. Alterations in glycosylation as biomarkers for cancer detection. *J. Clin. Pathol.* **63,** 322–329 (2010).
46. Fuster, M. M. & Esko, J. D. The sweet and sour of cancer: glycans as novel therapeutic targets. *Nat Rev Cancer* **5,** 526–542 (2005).
47. Moremen, K. W., Tiemeyer, M. & Nairn, A. V. Vertebrate protein glycosylation: diversity, synthesis and function. *Nat Rev Mol Cell Biol* **13,** 448–462 (2012).
48. Brockhausen, I., Yang, J., Lehotay, M., Ogata, S. & Itzkowitz, S. Pathways of mucin O-glycosylation in normal and malignant rat colonic epithelial cells reveal a mechanism for cancer-associated Sialyl-Tn antigen expression. *Biological chemistry* **382,** 3136–232 (2001).
49. Pinho, S. S. & Reis, C. A. Glycosylation in cancer: mechanisms and clinical implications. *Nat Rev Cancer* **15,** 540–556 (2015).
50. Hakomori, S. & Kannagi, R. Glycosphingolipids as tumor-associated and differentiation markers. *Journal of the National Cancer Institute* **71,** 231–251 (1983).
51. Julien, S. *et al.* ST6GalNAc I expression in MDA-MB-231 breast cancer cells greatly modifies their O-glycosylation pattern and enhances their tumourigenicity. *Glycobiology* **16,** 54–64 (2006).
52. Kannagi, R., Yin, J., Miyazaki, K. & Izawa, M. Current relevance of incomplete synthesis and neo-synthesis for cancer-associated alteration of carbohydrate determinants—Hakomori's concepts revisited. *Biochimica et Biophysica Acta (BBA) - General Subjects* **1780,** 525–531 (2008).
53. Peixoto, A., Relvas-Santos, M., Azevedo, R., Santos, L. L. & Ferreira, J. A. Protein Glycosylation and Tumor Microenvironment Alterations Driving Cancer Hallmarks. *Frontiers in Oncology* **9,** 8256 (2019).
54. Dennis, J. W., Nabi, I. R. & Demetriou, M. Metabolism, cell surface organization, and disease. *Cell* **139,** 1229–1241 (2009).
55. Bassagañas, S. *et al.* Pancreatic Cancer Cell Glycosylation Regulates Cell Adhesion and Invasion through the Modulation of α2β1 Integrin and E-Cadherin Function. *PLoS ONE* **9,** e98595 (2014).
56. Zhao, Y. *et al.* Branched N-glycans regulate the biological functions of integrins and cadherins. *FEBS J* **275,** 1939–1948 (2008).
57. Pinho, S. S. *et al.* E-cadherin and adherens-junctions stability in gastric carcinoma: functional implications of glycosyltransferases involving N-glycan branching biosynthesis, N-acetylglucosaminyltransferases III and V. *Biochim Biophys Acta* **1830,** 2690–2700 (2013).
58. Pinho, S. S. *et al.* The role of N-acetylglucosaminyltransferase III and V in the post-transcriptional modifications of E-cadherin. *Human Molecular Genetics* **18,** 2599–2608 (2009).
59. Takeuchi, H. & Haltiwanger, R. S. Significance of glycosylation in Notch signaling. *Biochem and Biophys Res Commun* **453,** 235–242 (2014).

60. Boscher, C., Dennis, J. W. & Nabi, I. R. Glycosylation, galectins and cellular signaling. *Current Opinion in Cell Biology* **23,** 383–392 (2011).
61. de-Freitas-Junior, J. C. M. *et al.* Insulin/IGF-I Signaling Pathways Enhances Tumor Cell Invasion through Bisecting GlcNAc N-glycans Modulation. An Interplay with E-Cadherin. *PLoS ONE* **8,** e81579 (2013).
62. Gomes, C. *et al.* Expression of ST3GAL4 Leads to SLex Expression and Induces c-Met Activation and an Invasive Phenotype in Gastric Carcinoma Cells. *PLoS ONE* **8,** e66737 (2013).
63. Locker, G. Y. *et al.* ASCO 2006 update of recommendations for the use of tumor markers in gastrointestinal cancer. *J Clin Oncol* **24,** 5313–5327 (2006).
64. Gilgunn, S., Conroy, P. J., Saldova, R., Rudd, P. M. & O'Kennedy, R. J. Aberrant PSA glycosylation—a sweet predictor of prostate cancer. *Nat Rev Urol* **10,** 99–107 (2013).
65. Ebeling, F. G. *et al.* Serum CEA and CA 15-3 as prognostic factors in primary breast cancer. *British Journal of Cancer* **86,** 1217–1222 (2002).
66. Zurawski, V. R., Orjaseter, H., Andersen, A. & Jellum, E. Elevated serum CA 125 levels prior to diagnosis of ovarian neoplasia: relevance for early detection of ovarian cancer. *Int J Cancer* **42,** 677–680 (1988).
67. Cancer Treatment | SEER Training. *training.seer.cancer.gov* at <https://training.seer.cancer.gov/treatment/>
68. Introduction to Surgery | SEER Training. *training.seer.cancer.gov* at <https://training.seer.cancer.gov/treatment/surgery/>
69. Introduction to Radiation Therapy | SEER Training. *training.seer.cancer.gov* at <https://training.seer.cancer.gov/treatment/radiation/>
70. Introduction to Chemotherapy | SEER Training. *training.seer.cancer.gov* at <https://training.seer.cancer.gov/treatment/chemotherapy/>
71. Gerber, D. E. Targeted Therapies: A New Generation of Cancer Treatments. *AFP* **77,** 311–319 (2008).
72. Scott, A. M. *et al.* A phase I clinical trial with monoclonal antibody ch806 targeting transitional state and mutant epidermal growth factor receptors. *PNAS* **104,** 4071–4076 (2007).
73. Hughes, B. Antibody–drug conjugates for cancer: poised to deliver? *Nat Rev Drug Discov* **9,** 665–667 (2010).
74. Weiner, L. M., Surana, R. & Wang, S. Monoclonal antibodies: versatile platforms for cancer immunotherapy. *Nat Rev Immunol* **10,** 317–327 (2010).
75. Scott, A. M., Wolchok, J. D. & Old, L. J. Antibody therapy of cancer. *Nat Rev Cancer* **12,** 278–287 (2012).
76. Deckert, P. Current Constructs and Targets in Clinical Development for Antibody-Based Cancer Therapy. *Curr Drug Targets* **10,** 158–175 (2009).
77. Ravetch, J. In vivo veritas: the surprising roles of Fc receptors in immunity. *Nat Immunol* **11,** 183–185 (2010).
78. Cheson, B. D. & Leonard, J. P. Monoclonal antibody therapy for B-cell non-Hodgkin's lymphoma. *N Engl J Med* **359,** 613–626 (2008).
79. Wu, A. M. & Senter, P. D. Arming antibodies: prospects and challenges for immunoconjugates. *Nat. Biotechnol.* **23,** 1137–1146 (2005).

80. Herbertson, R. A. *et al.* Phase I Biodistribution and Pharmacokinetic Study of Lewis Y-Targeting Immunoconjugate CMD-193 in Patients with Advanced Epithelial Cancers. *Clin Cancer Res* **15,** 6709–6715 (2009).
81. Theocharopoulos, C., Lialios, P.-P., Gogas, H. & Ziogas, D. C. An overview of antibody-drug conjugates in oncological practice. *Ther Adv Med Oncol* **12,** 175883592096299 (2020).
82. Li, F. *et al.* Intracellular Released Payload Influences Potency and Bystander-Killing Effects of Antibody-Drug Conjugates in Preclinical Models. *Cancer Res.* **76,** 2710–2719 (2016).
83. Nejadmoghaddam, M.-R. *et al.* Antibody-Drug Conjugates: Possibilities and Challenges. *Avicenna Journal of Medical Biotechnology* **11,** 3–23 (2019).
84. Kovtun, Y. V. *et al.* Antibody-drug conjugates designed to eradicate tumors with homogeneous and heterogeneous expression of the target antigen. *Cancer Res.* **66,** 3214–3221 (2006).
85. Diamantis, N. & Banerji, U. Antibody-drug conjugates—an emerging class of cancer treatment. *British Journal of Cancer* **114,** 362–367 (2016).
86. Golfier, S. *et al.* Anetumab ravtansine: a novel mesothelin-targeting antibody-drug conjugate cures tumors with heterogeneous target expression favored by bystander effect. *Mol Cancer Ther* **13,** 1537–1548 (2014).
87. Chames, P., Van Regenmortel, M., Weiss, E. & Baty, D. Therapeutic antibodies: successes, limitations and hopes for the future. *British Journal of Pharmacology* **157,** 220–233 (2009).
88. Azvolinsky, A. Conjugating Antibodies to Cytotoxic Agents: Getting the Best of Both Worlds? *Journal of the National Cancer Institute* **105,** 1765–1766 (2013).
89. Widdison, W. C. & Chari, R. V. J. in *Antibody-Drug Conjugates and Immunotoxins* **8,** 93–115 (Springer, New York, NY, 2013).
90. Vankemmelbeke, M. & Durrant, L. Third-generation antibody drug conjugates for cancer therapy--a balancing act. *Ther Deliv* **7,** 141–144 (2016).
91. Ritter, A. Antibody-Drug Conjugates: Looking Ahead to an Emerging Class of Biotherapeutic. *Pharmaceutical Technology* **36,** (2012).
92. Beckman, R. A., Weiner, L. M. & Davis, H. M. Antibody constructs in cancer therapy. *Cancer* **109,** 170–179 (2007).
93. Roopenian, D. C. & Akilesh, S. FcRn: the neonatal Fc receptor comes of age. *Nat Rev Immunol* **7,** 715–725 (2007).
94. Adams, G. P. *et al.* High affinity restricts the localization and tumor penetration of single-chain fv antibody molecules. *Cancer Res.* **61,** 4750–4755 (2001).
95. Fujimori, K., Covell, D. G., Fletcher, J. E. & Weinstein, J. N. A modeling analysis of monoclonal antibody percolation through tumors: a binding-site barrier. *Journal of nuclear medicine : official publication, Society of Nuclear Medicine* **31,** 1191–1198 (1990).
96. Kershaw, D. B. *et al.* Molecular cloning, expression, and characterization of podocalyxin-like protein 1 from rabbit as a transmembrane protein of glomerular podocytes and vascular endothelium. *J. Biol. Chem.* **270,** 29439–29446 (1995).

97. McNagny, K. M. *et al.* Thrombomucin, a Novel Cell Surface Protein that Defines Thrombocytes and Multipotent Hematopoietic Progenitors. *J Cell Biol* **138,** 1395–1407 (1997).
98. McNagny, K. M., Lim, F., Grieser, S. & Graf, T. Cell surface proteins of chicken hematopoietic progenitors, thrombocytes and eosinophils detected by novel monoclonal antibodies. *Leukemia* **6,** 975–984 (1992).
99. Nielsen, J. S. & McNagny, K. M. Novel functions of the CD34 family. *J. Cell. Sci.* **121,** 3683–3692 (2008).
100. Takeda, T., Go, W. Y., Orlando, R. A. & Farquhar, M. G. Expression of podocalyxin inhibits cell-cell adhesion and modifies junctional properties in Madin-Darby canine kidney cells. *Mol. Biol. Cell* **11,** 3219–3232 (2000).
101. Tan, P. C. *et al.* Na+/H+ exchanger regulatory factor-1 is a hematopoietic ligand for a subset of the CD34 family of stem cell surface proteins. *STEM CELLS* **24,** 1150–1161 (2006).
102. Schmieder, S., Nagai, M., Orlando, R. A., Takeda, T. & Farquhar, M. G. Podocalyxin activates RhoA and induces actin reorganization through NHERF1 and Ezrin in MDCK cells. *J. Am. Soc. Nephrol.* **15,** 2289–2298 (2004).
103. Lazar, C. S., Cresson, C. M., Lauffenburger, D. A. & Gill, G. N. The Na+/H+ Exchanger Regulatory Factor Stabilizes Epidermal Growth Factor Receptors at the Cell Surface. *Mol. Biol. Cell* **15,** 5470–5480 (2004).
104. Elliott, B. E., Meens, J. A., SenGupta, S. K., Louvard, D. & Arpin, M. The membrane cytoskeletal crosslinker ezrin is required for metastasis of breast carcinoma cells. *Breast Cancer Res.* **7,** 989 (2005).
105. Khanna, C. *et al.* The membrane-cytoskeleton linker ezrin is necessary for osteosarcoma metastasis. *Nat. Med.* **10,** 182–186 (2004).
106. Meng, Y. *et al.* Ezrin promotes invasion and metastasis of pancreatic cancer cells. *J Transl Med* **8,** 61 (2010).
107. Nielsen, J. S. & McNagny, K. M. The role of podocalyxin in health and disease. *J. Am. Soc. Nephrol.* **20,** 1669–1676 (2009).
108. Wang, J. *et al.* Prognostic role of podocalyxin-like protein expression in various cancers: A systematic review and meta-analysis. *Oncotarget* **8,** 52457–52464 (2016).
109. He, S., Du, W., Li, M., Yan, M. & Zheng, F. PODXL might be a new prognostic biomarker in various cancers: a meta-analysis and sequential verification with TCGA datasets. *BMC Cancer* **20,** 5068 (2020).
110. Somasiri, A. *et al.* Overexpression of the anti-adhesin podocalyxin is an independent predictor of breast cancer progression. *Cancer Res.* **64,** 5068–5073 (2004).
111. Forse, C. L. *et al.* Elevated expression of podocalyxin is associated with lymphatic invasion, basal-like phenotype, and clinical outcome in axillary lymph node-negative breast cancer. *Breast Cancer Res. Treat.* **137,** 709–719 (2013).
112. Hsu, Y.-H. *et al.* Podocalyxin EBP50 ezrin molecular complex enhances the metastatic potential of renal cell carcinoma through recruiting Rac1 guanine nucleotide exchange factor ARHGEF7. *The American Journal of Pathology* **176,** 3050–3061 (2010).
113. Larsson, A. *et al.* Overexpression of podocalyxin-like protein is an independent factor of poor prognosis in colorectal cancer. *British Journal of Cancer* **105,** 666–672 (2011).

114. Kaprio, T. *et al.* A comparative study of two PODXL antibodies in 840 colorectal cancer patients. *BMC Cancer* **14,** 1–8 (2014).
115. Yuan, D. *et al.* Identification of LEA, a podocalyxin-like glycoprotein, as a predictor for the progression of colorectal cancer. *Cancer Medicine* **7,** 5155–5166 (2018).
116. Larsson, A. *et al.* Validation of podocalyxin-like protein as a biomarker of poor prognosis in colorectal cancer. *BMC Cancer* **12,** 277 (2012).
117. Cipollone, J. A. *et al.* The anti-adhesive mucin podocalyxin may help initiate the transperitoneal metastasis of high grade serous ovarian carcinoma. *Clin. Exp. Metastasis* **29,** 239–252 (2012).
118. Boman, K. *et al.* Membranous expression of podocalyxin-like protein is an independent factor of poor prognosis in urothelial bladder cancer. *British Journal of Cancer* **108,** 2321–2328 (2013).
119. Saukkonen, K. *et al.* Podocalyxin Is a Marker of Poor Prognosis in Pancreatic Ductal Adenocarcinoma. *PLoS ONE* **10,** e0129012 (2015).
120. Heby, M., Elebro, J., Nodin, B., Jirström, K. & Eberhard, J. Prognostic and predictive significance of podocalyxin-like protein expression in pancreatic and periampullary adenocarcinoma. *BMC Clin Pathol* **15,** 10 (2015).
121. Taniuchi, K., Tsuboi, M., Sakaguchi, M. & Saibara, T. Measurement of serum PODXL concentration for detection of pancreatic cancer. *OTT* **Volume 11,** 1433–1445 (2018).
122. Taniuchi, K. *et al.* Podocalyxin-like protein, linked to poor prognosis of pancreatic cancers, promotes cell invasion by binding to gelsolin. *Cancer Sci* **107,** 1430–1442 (2016).
123. Chijiiwa, Y. *et al.* Overexpression of microRNA-5100 decreases the aggressive phenotype of pancreatic cancer cells by targeting PODXL. *International Journal of Oncology* **48,** 1688–1700 (2016).
124. Borg, D. *et al.* Expression of podocalyxin-like protein is an independent prognostic biomarker in resected esophageal and gastric adenocarcinoma. *BMC Clin Pathol* **16,** 1406 (2016).
125. Laitinen, A. *et al.* Podocalyxin as a Prognostic Marker in Gastric Cancer. *PLoS ONE* **10,** e0145079 (2015).
126. Zhang, J. *et al.* PODXL, negatively regulated by KLF4, promotes the EMT and metastasis and serves as a novel prognostic indicator of gastric cancer. *Gastric cancer* **22,** 48–59 (2019).
127. Kusumoto, H. *et al.* Podocalyxin influences malignant potential by controlling epithelial-mesenchymal transition in lung adenocarcinoma. *Cancer Sci* **108,** 528–535 (2017).
128. Binder, Z. A. *et al.* Podocalyxin-Like Protein Is Expressed in Glioblastoma Multiforme Stem-Like Cells and Is Associated with Poor Outcome. *PLoS ONE* **8,** e75945 (2013).
129. Larsson, A. H. *et al.* Significant association and synergistic adverse prognostic effect of podocalyxin-like protein and epidermal growth factor receptor expression in colorectal cancer. *J Transl Med* **14,** 1965 (2016).
130. Kang, L. *et al.* The Universal 3D3 Antibody of Human PODXL Is Pluripotent Cytotoxic, and Identifies a Residual Population After Extended Differentiation of Pluripotent Stem Cells. *Stem Cells and Development* **25,** 556–568 (2016).

131. Cai, J. *et al.* Assessing Self-Renewal and Differentiation in Human Embryonic Stem Cell Lines. *STEM CELLS* **24,** 516–530 (2006).
132. Brandenberger, R. *et al.* Transcriptome characterization elucidates signaling networks that control human ES cell growth and differentiation. *Nat. Biotechnol.* **22,** 707–716 (2004).
133. Schopperle, W. M., Kershaw, D. B. & DeWolf, W. C. Human embryonal carcinoma tumor antigen, Gp200/GCTM-2, is podocalyxin. *Biochem and Biophys Res Commun* **300,** 285–290 (2003).
134. He, J. *et al.* Identification of Cell Surface Glycoprotein Markers for Glioblastoma-Derived Stem-Like Cells Using a Lectin Microarray and LC−MS/MS Approach. *J. Proteome Res.* **9,** 2565–2572 (2010).
135. Snyder, K. A. The role of podocalyxin in breast cancer progression and metastasis. (2015). doi:10.14288/1.0072153
136. Snyder, K. A. *et al.* Podocalyxin enhances breast tumor growth and metastasis and is a target for monoclonal antibody therapy. *Breast Cancer Res.* **17,** (2015).
137. Mei Chung Moh, S. S. The roles of cell adhesion molecules in tumor suppression and cell migration: A new paradox. *Cell Adhesion & Migration* **3,** 334–336 (2014).
138. Vleminckx, K., Vakaet, L., Jr, Mareel, M., Fiers, W. & Van Roy, F. Genetic manipulation of E-cadherin expression by epithelial tumor cells reveals an invasion suppressor role. *Cell* **66,** 107–119 (1991).
139. Nielsen, J. S. *et al.* The CD34-Related Molecule Podocalyxin Is a Potent Inducer of Microvillus Formation. *PLoS ONE* **2,** e237 (2007).
140. Flores-Téllez, T. N. J., Lopez, T. V., Vásquez Garzón, V. R. & Villa-Treviño, S. Co-Expression of Ezrin-CLIC5-Podocalyxin Is Associated with Migration and Invasiveness in Hepatocellular Carcinoma. *PLoS ONE* **10,** e0131605 (2015).
141. Lin, C.-W. *et al.* Podocalyxin-like 1 promotes invadopodia formation and metastasis through activation of Rac1/Cdc42/cortactin signaling in breast cancer cells. - PubMed - NCBI. *Carcinogenesis* **35,** 2425–2435 (2014).
142. Graves, M. L. *et al.* The cell surface mucin podocalyxin regulates collective breast tumor budding. *Breast Cancer Res.* **18,** 11 (2016).
143. Thomas, S. N., Schnaar, R. L. & Konstantopoulos, K. Podocalyxin-like protein is an E-/L-selectin ligand on colon carcinoma cells: comparative biochemical properties of selectin ligands in host and tumor cells. *AJP: Cell Physiology* **296,** C505–C513 (2009).
144. Dallas, M. R. *et al.* Sialofucosylated podocalyxin is a functional E- and L-selectin ligand expressed by metastatic pancreatic cancer cells. - PubMed - NCBI. *AJP: Cell Physiology* **303,** C616–C624 (2012).
145. Choo, A. B. *et al.* Selection against undifferentiated human embryonic stem cells by a cytotoxic antibody recognizing podocalyxin-like protein-1. *Stem cells* **26,** 1454–1463 (2008).
146. Ferlay, J. *et al.* Estimating the global cancer incidence and mortality in 2018: GLOBOCAN sources and methods. *Int J Cancer* **144,** 1941–1953 (2019).
147. Bray, F. *et al.* Global cancer statistics 2018: GLOBOCAN estimates of incidence and mortality worldwide for 36 cancers in 185 countries. *CA: A Cancer Journal for Clinicians* **68,** 394–424 (2018).

148. Committee, C. C. S. A. Canadian Cancer Statistics 2019. doi:https://doi.org/10.25318/1310039401-eng
149. Ran, F. A. *et al.* Genome engineering using the CRISPR-Cas9 system. *Nature Protocols* **8,** 2281–2308 (2013).
150. Graves, M. L. Modeling mammary epithelial cell polarization and the role of podocalyxin in breast tumor progression. (2008).
151. Lee, C.-H., Yu, C.-C., Wang, B.-Y. & Chang, W.-W. Tumorsphere as an effective in vitroplatform for screening anti-cancer stem cell drugs. *Oncotarget* **7,** 1215–1226 (2015).
152. Bahmad, H. F. *et al.* Sphere-Formation Assay: Three-Dimensional in vitro Culturing of Prostate Cancer Stem/Progenitor Sphere-Forming Cells. *Frontiers in Oncology* **8,** 20140376 (2018).
153. Skog, J. *et al.* Glioblastoma microvesicles transport RNA and protein that promote tumor growth and provide diagnostic biomarkers. *Nat. Cell Biol.* **10,** 1470–1476 (2008).
154. McCready, J., Sims, J. D., Chan, D. & Jay, D. G. Secretion of extracellular hsp90α via exosomes increases cancer cell motility: a role for plasminogen activation. *BMC Cancer* **10,** 663 (2010).
155. Hoshino, A. *et al.* Tumour exosome integrins determine organotropic metastasis. *Nature* (2015). doi:10.1038/nature15756
156. Satya-Prakash, K. L., Pathak, S., Hsu, T. C., Olivé, M. & Cailleau, R. Cytogenetic analysis on eight human breast tumor cell lines: High frequencies of 1q, 11q and HeLa-like marker chromosomes. *Cancer Genetics and Cytogenetics* **3,** 61–73 (1981).
157. Schopperle, W. M. & DeWolf, W. C. The TRA-1-60 and TRA-1-81 human pluripotent stem cell markers are expressed on podocalyxin in embryonal carcinoma. - PubMed - NCBI. *STEM CELLS* **25,** 723–730 (2006).
158. Itai, S., Yamada, S., Kaneko, M. K., Harada, H. & Kato, Y. Immunohistochemical Analysis Using Antipodocalyxin Monoclonal Antibody PcMab-47 Demonstrates Podocalyxin Expression in Oral Squamous Cell Carcinomas. *Monoclonal Antibodies in Immunodiagnosis and Immunotherapy* **36,** 220–223 (2017).
159. Ney, J. T. *et al.* Podocalyxin-like protein 1 expression is useful to differentiate pancreatic ductal adenocarcinomas from adenocarcinomas of the biliary and gastrointestinal tracts. *Human Pathology* **38,** 359–364 (2007).
160. Casey, G. *et al.* Podocalyxin variants and risk of prostate cancer and tumor aggressiveness. - PubMed - NCBI. *Human Molecular Genetics* **15,** 735–741 (2006).
161. Yasuoka, H. *et al.* Podocalyxin expression in undifferentiated thyroid carcinomas. *J. Clin. Pathol.* **61,** 1228–1229 (2008).
162. Hayatsu, N. *et al.* Podocalyxin expression in malignant astrocytic tumors. *Biochem and Biophys Res Commun* **374,** 394–398 (2008).
163. Wu, H. *et al.* Podocalyxin regulates astrocytoma cell invasion and survival against temozolomide. *Experimental and Therapeutic Medicine* **5,** 1025–1029 (2013).
164. Favreau, A. J., Cross, E. L. & Sathyanarayana, P. miR-199b-5p directly targets PODXL and DDR1 and decreased levels of miR-199b-5p correlate with elevated expressions of PODXL and DDR1 in acute myeloid leukemia. *Am. J. Hematol.* **87,** 442–446 (2012).

165. Kelley, T. W., Huntsman, D., McNagny, K. M., Roskelley, C. D. & Hsix, E. D. Podocalyxin A Marker of Blasts in Acute Leukemia. *Am J Clin Pathol* **124,** 134–142 (2005).
166. Sizemore, S., Cicek, M., Sizemore, N., Ng, K. P. & Casey, G. Podocalyxin increases the aggressive phenotype of breast and prostate cancer cells in vitro through its interaction with ezrin. *Cancer Res.* **67,** 6183–6191 (2007).
167. Jiang, J., Liu, Y., Fang, W. & Liu, F. Sperm-associated antigen 9 promotes astrocytoma cell invasion throu... - PubMed - NCBI. *Mol Med Rep* **10,** 417–422 (2014).
168. Liu, B., Liu, Y. & Jiang, Y. Podocalyxin promotes glioblastoma multiforme cell invasion and proliferation by inhibiting angiotensin-(1-7)/Mas signaling. *Oncol. Rep.* **33,** 2583–2591 (2015).
169. Liu, Y. & Jiang, Y.-G. Podocalyxin Promotes Glioblastoma Multiforme Cell Invasion and Proliferation via β-Catenin Signaling. *PLoS ONE* **9,** e111343 (2014).
170. Zhi, Q. *et al.* Podocalyxin-like protein promotes gastric cancer progression through interacting with RUN and FYVE domain containing 1 protein. - PubMed - NCBI. *Cancer Sci* **27,** 11–134 (2018).
171. Xu, Y., Pan, Z.-G., Shu, L. & Li, Q.-J. Podocalyxin-like, targeted by miR-138, promotes colorectal cancer cell proliferation, migration, invasion and EMT. *Eur Rev Med Pharmacol Sci* **22,** 8664–8674 (2018).
172. Wong, B. S. *et al.* A Direct Podocalyxin–Dynamin-2 Interaction Regulates Cytoskeletal Dynamics to Promote Migration and Metastasis in Pancreatic Cancer Cells. *Cancer Res.* **79,** 2878–2891 (2019).
173. Ben-David, U. *et al.* Genetic and transcriptional evolution alters cancer cell line drug response. *Nature* **560,** 325–330 (2018).
174. O'Driscoll, L. *et al.* Phenotypic and global gene expression profile changes between low passage and high passage MIN-6 cells. *J Endocrinol* **191,** 665–676 (2006).
175. Lorsch, J. R., Collins, F. S. & Lippincott-Schwartz, J. Fixing problems with cell lines: Technologies and policies can improve authentication. *Science* **346,** 1452–1453 (2014).
176. Tharmalingam, T. *et al.* Characterization of phenotypic and genotypic diversity in subclones derived from a clonal cell line. *Biotechnology Progress* **34,** 613–623 (2018).
177. Hernandez, L. *et al.* Characterization of ovarian cancer cell lines as in vivo models for preclinical studies. *Gynecologic oncology* **142,** 332–340 (2016).
178. Beaufort, C. M. *et al.* Ovarian Cancer Cell Line Panel (OCCP): Clinical Importance of In Vitro Morphological Subtypes. *PLoS ONE* **9,** e103988 (2014).
179. Horrillo, A., Porras, G., Ayuso, M. S. & González-Manchón, C. Loss of endothelial barrier integrity in mice with conditional ablation of podocalyxin (Podxl) in endothelial cells. *Eur. J. Cell Biol.* **95,** 265–276 (2016).
180. Cait, J. *et al.* Podocalyxin is required for maintaining blood–brain barrier function during acute inflammation. *PNAS* **116,** 4518–4527 (2019).
181. Kerjaschki, D. Identification and characterization of podocalyxin--the major sialoprotein of the renal glomerular epithelial cell. *J Cell Biol* **98,** 1591–1596 (1984).
182. Lin, C.-W., Sun, M.-S. & Wu, H.-C. Podocalyxin-like 1 is associated with tumor aggressiveness and metastatic gene expression in human oral squamous cell carcinoma. *International Journal of Oncology* **45,** 710–718 (2014).

183. Boman, K. *et al.* Podocalyxin-like and RNA-binding motif protein 3 are prognostic biomarkers in urothelial bladder cancer: a validatory study. *Biomark Res* **5,** 234 (2017).
184. Zhou, Y. *et al.* Bmi1 Essentially Mediates Podocalyxin-Enhanced Cisplatin Chemoresistance in Oral Tongue Squamous Cell Carcinoma. *PLoS ONE* **10,** e0123208 (2015).
185. Kaneko, M. K. *et al.* Antipodocalyxin Antibody chPcMab-47 Exerts Antitumor Activity in Mouse Xenograft Models of Colorectal Adenocarcinomas. *Monoclonal Antibodies in Immunodiagnosis and Immunotherapy* **36,** 157–162 (2017).
186. Babcook, J. S., Leslie, K. B., Olsen, O. A., Salmon, R. A. & Schrader, J. W. A novel strategy for generating monoclonal antibodies from single, isolated lymphocytes producing antibodies of defined specificities. *PNAS* **93,** 7843–7848 (1996).
187. Resch, B. Product review on the monoclonal antibody palivizumab for prevention of respiratory syncytial virus infection. *Human vaccines & immunotherapeutics* **13,** 2138–2149 (2017).
188. Debruin, E. J. *et al.* Podocalyxin Regulates Murine Lung Vascular Permeability by Altering Endothelial Cell Adhesion. *PLoS ONE* **9,** e108881 (2014).
189. Staff, A. C. An introduction to cell migration and invasion. *Scand J Clin Lab Invest* **61,** 257–268 (2001).
190. Yudoh, K., Matsui, H., Kanamori, M., Ohmori, K. & Tsuji, H. Tumor cell attachment to laminin promotes degradation of the extracellular matrix and cell migration in high-metastatic clone cells of RCT sarcoma in vitro. *Jpn. J. Cancer Res.* **86,** 685–690 (1995).
191. Ferlay, J. *et al.* Global Cancer Observatory: Cancer tomorrow. *httpsgco.iarc.frtomorrow* (2018). at <http://gco.iarc.fr/tomorrow>
192. Shental-Bechor, D. & Levy, Y. Effect of glycosylation on protein folding: a close look at thermodynamic stabilization. *PNAS* **105,** 8256–8261 (2008).
193. Vagin, O., Kraut, J. A. & Sachs, G. Role of N-glycosylation in trafficking of apical membrane proteins in epithelia. *American Journal of Physiology-Renal Physiology* **296,** F459–F469 (2009).
194. Stowell, S. R., Ju, T. & Cummings, R. D. Protein Glycosylation in Cancer. *Annu. Rev. Pathol. Mech. Dis.* **10,** 473–510 (2015).
195. Ono, M. & Hakomori, S. Glycosylation defining cancer cell motility and invasiveness. *Glycoconj J* **20,** 71–78 (2004).
196. Lima, L. *et al.* Sialyl-Tn identifies muscle-invasive bladder cancer basal and luminal subtypes facing decreased survival, being expressed by circulating tumor cells and metastases. *Urologic Oncology: Seminars and Original Investigations* **35,** 675.e1–675.e8 (2017).
197. Schultz, M. J., Swindall, A. F. & Bellis, S. L. Regulation of the metastatic cell phenotype by sialylated glycans. *Cancer Metastasis Rev* **31,** 501–518 (2012).
198. Sassetti, C., Van Zante, A. & Rosen, S. D. Identification of endoglycan, a member of the CD34/podocalyxin family of sialomucins. *J. Biol. Chem.* **275,** 9001–9010 (2000).
199. Doyonnas, R. *et al.* Anuria, Omphalocele, and Perinatal Lethality in Mice Lacking the Cd34-Related Protein Podocalyxin. *Journal of Experimental Medicine* **194,** 13–28 (2001).
200. Doyonnas, R. *et al.* Podocalyxin is a CD34-related marker of murine hematopoietic stem cells and embryonic erythroid cells. *Blood* **105,** 4170–4178 (2005).

201. McNagny, K. M., Roskelley, C. D., DeBruin, E. J. & Cipollone, J. *Podocalyxin in the diagnosis and treatment of cancer*. (2012).
202. Pearce, O. M. T. & Laubli, H. Sialic acids in cancer biology and immunity. *Glycobiology* **26,** 111–128 (2016).
203. Huflejt, M. E. *et al.* Anti-carbohydrate antibodies of normal sera: Findings, surprises and challenges. *Molecular Immunology* **46,** 3037–3049 (2009).
204. Bovin, N. *et al.* Repertoire of human natural anti-glycan immunoglobulins. Do we have auto-antibodies? *Biochimica et Biophysica Acta (BBA) - General Subjects* **1820,** 1373–1382 (2012).
205. Blixt, O. *et al.* Printed covalent glycan array for ligand profiling of diverse glycan binding proteins. *PNAS* **101,** 17033–17038 (2004).
206. Jacob, F. *et al.* The glycosphingolipid P₁ is an ovarian cancer-associated carbohydrate antigen involved in migration. *British Journal of Cancer* **111,** 1634–1645 (2014).
207. Anugraham, M. *et al.* Tissue glycomics distinguish tumour sites in women with advanced serous adenocarcinoma. *Molecular Oncology* **11,** 1595–1615 (2017).
208. Stotter, B. R. *et al.* Cosmc-dependent mucin-type O-linked glycosylation is essential for podocyte function. *American Journal of Physiology-Renal Physiology* **318,** F518–F530 (2020).
209. Gadducci, A. *et al.* Current strategies for the targeted treatment of high-grade serous epithelial ovarian cancer and relevance of BRCA mutational status. *J Ovarian Res* **12,** 1–8 (2019).
210. Lisio, M.-A., Fu, L., Goyeneche, A., Gao, Z.-H. & Telleria, C. High-Grade Serous Ovarian Cancer: Basic Sciences, Clinical and Therapeutic Standpoints. *IJMS* **20,** 952 (2019).
211. Lheureux, S., Braunstein, M. & Oza, A. M. Epithelial ovarian cancer: Evolution of management in the era of precision medicine. *CA: A Cancer Journal for Clinicians* **69,** 280–304 (2019).
212. Vaughan, S. *et al.* Rethinking ovarian cancer: recommendations for improving outcomes. *Nat Rev Cancer* **11,** 719–725 (2011).
213. Torre, L. A. *et al.* Ovarian cancer statistics, 2018. *CA: A Cancer Journal for Clinicians* **68,** 284–296 (2018).
214. Kurman, R. J. & Shih, I. M. Molecular pathogenesis and extraovarian origin of epithelial ovarian cancer—Shifting the paradigm. *Human Pathology* **42,** 918–931 (2011).
215. Sauriol, A. *et al.* Modeling the Diversity of Epithelial Ovarian Cancer through Ten Novel Well Characterized Cell Lines Covering Multiple Subtypes of the Disease. *Cancers* **12,** 2222 (2020).
216. Létourneau, I. J. *et al.* Derivation and characterization of matched cell lines from primary and recurrent serous ovarian cancer. *BMC Cancer* **12,** 379 (2012).
217. Doronina, S. O. *et al.* Development of potent monoclonal antibody auristatin conjugates for cancer therapy. *Nat. Biotechnol.* **21,** 778–784 (2003).
218. Li, F. *et al.* Mouse Strains Influence Clearance and Efficacy of Antibody and Antibody–Drug Conjugate Via Fc–FcγR Interaction. *Mol Cancer Ther* **18,** 780–787 (2019).

219. Vaquero, J., Ho-Bouldoires, T. N., Clapéron, A. & Fouassier, L. Role of the PDZ-scaffold protein NHERF1/EBP50 in cancer biology: from signaling regulation to clinical relevance. *Oncogene* **36,** 3067–3079 (2017).
220. Sharma, S. K. *et al.* Fc-Mediated Anomalous Biodistribution of Therapeutic Antibodies in Immunodeficient Mouse Models. *Cancer Res.* **78,** 1820–1832 (2018).
221. Steeg, P. S. Targeting metastasis. *Nat Rev Cancer* **16,** 201–218 (2016).
222. Lisio, M.-A., Fu, L., Goyeneche, A., Gao, Z.-H. & Telleria, C. High-Grade Serous Ovarian Cancer: Basic Sciences, Clinical and Therapeutic Standpoints. *IJMS* **20,** 952 (2019).
223. Dewald, J. H., Colomb, F., Bobowski-Gerard, M., Groux-Degroote, S. & Delannoy, P. Role of Cytokine-Induced Glycosylation Changes in Regulating Cell Interactions and Cell Signaling in Inflammatory Diseases and Cancer. *Cells* **5,** 43 (2016).
224. Gibson, D. G. *et al.* Enzymatic assembly of DNA molecules up to several hundred kilobases. *Nat. Methods* **6,** 343–345 (2009).

Appendices

Appendix A Generation of MDA-MB-231 *PODXL*-KO clones

A.1 *PODXL*-KO colony verification by gel electrophoresis

Successful deletion of Podxl's 5'UTR and first exon was assessed by genomic DNA polymerase chain reaction (PCR) to identify clones lacking the target fragment.

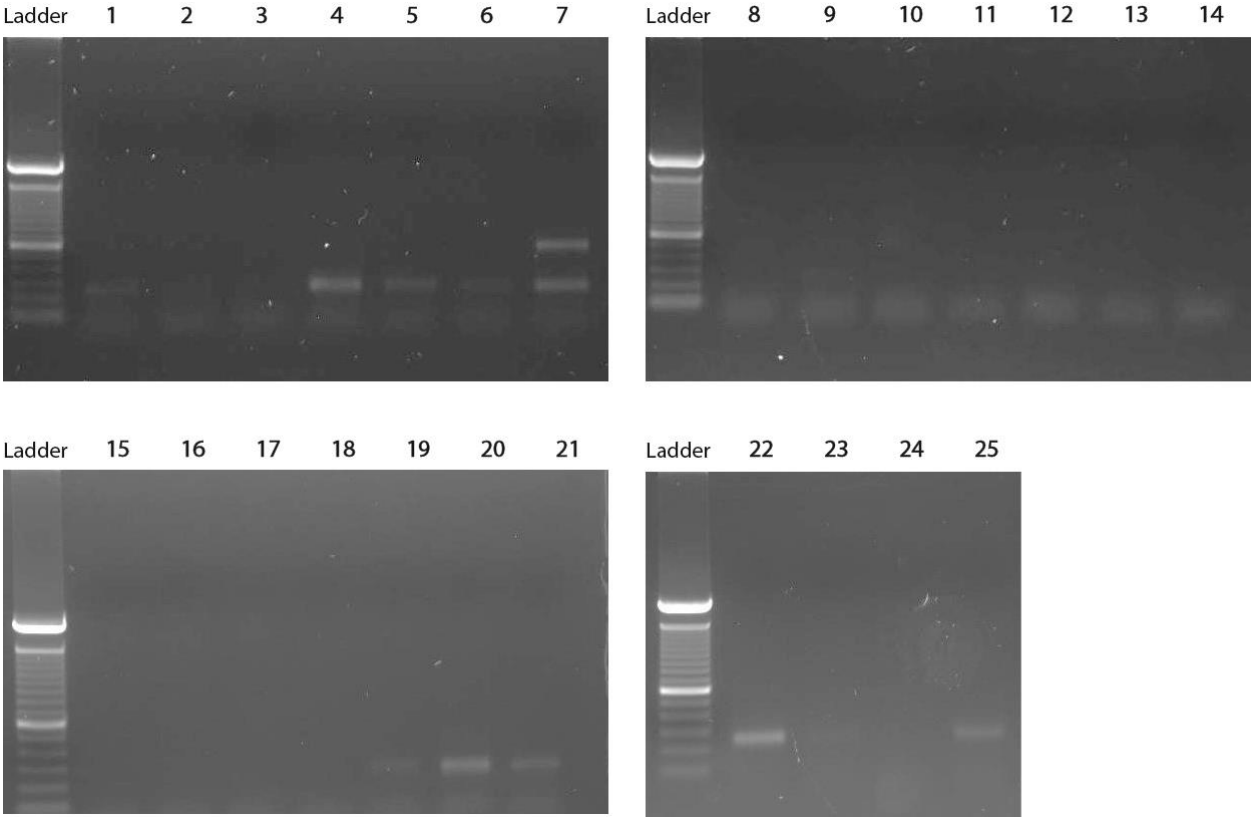

A.2 Podxl expression on selected MDA-MB-231 colonies by flow cytometry

Flow cytometric profiles showing Podxl expression on MDA-MB-231 colonies lacking the genomic Podxl target fragment by PCR.

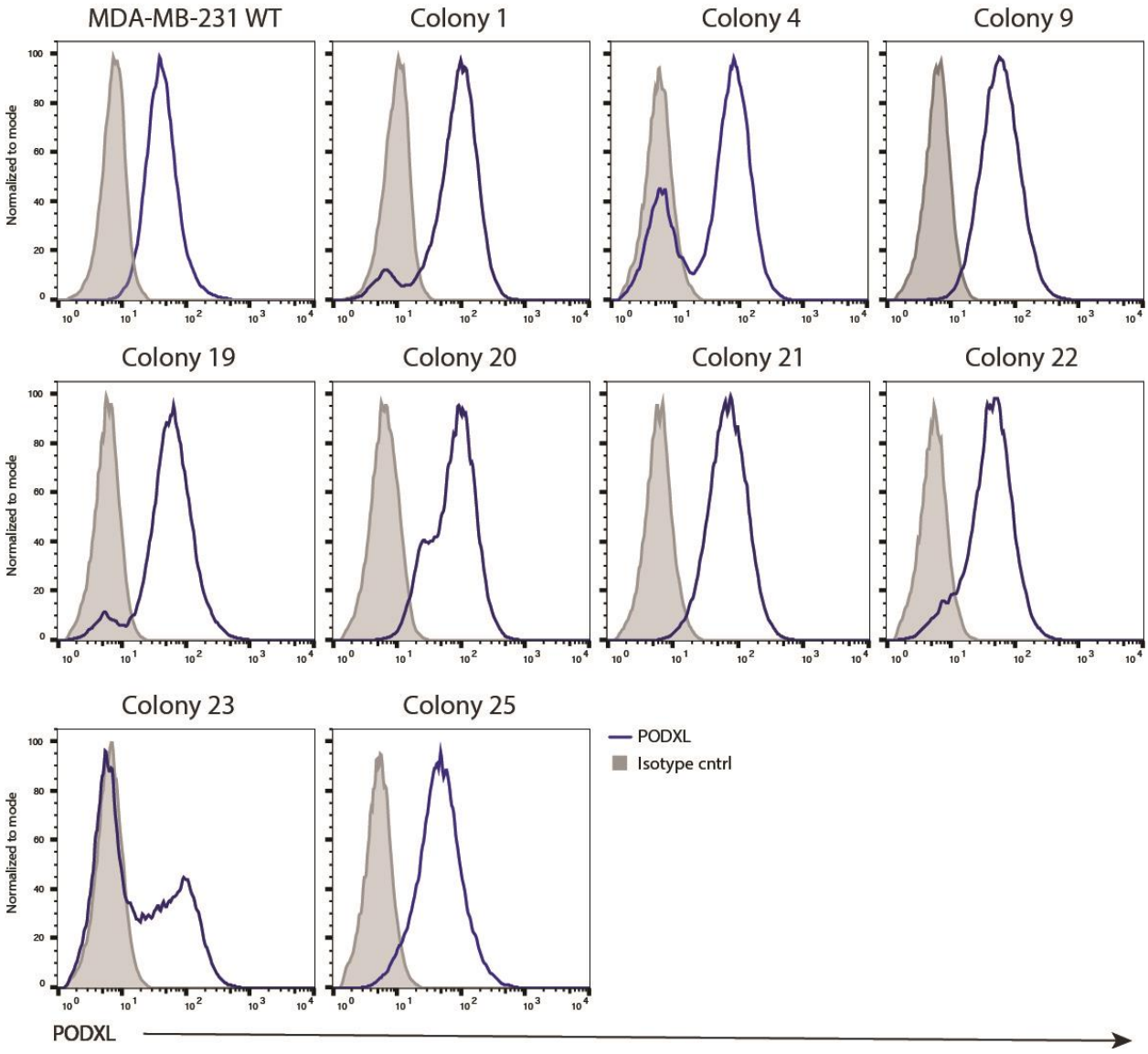

Appendix B Podxl expression on MDA-MB-231 *PODXL*-KO clones 17 months after generation

Flow cytometric profiles showing Podxl expression on MDA-MB-231 *PODXL*-KO clones displaying altered phenotype after 17 months post-generation.

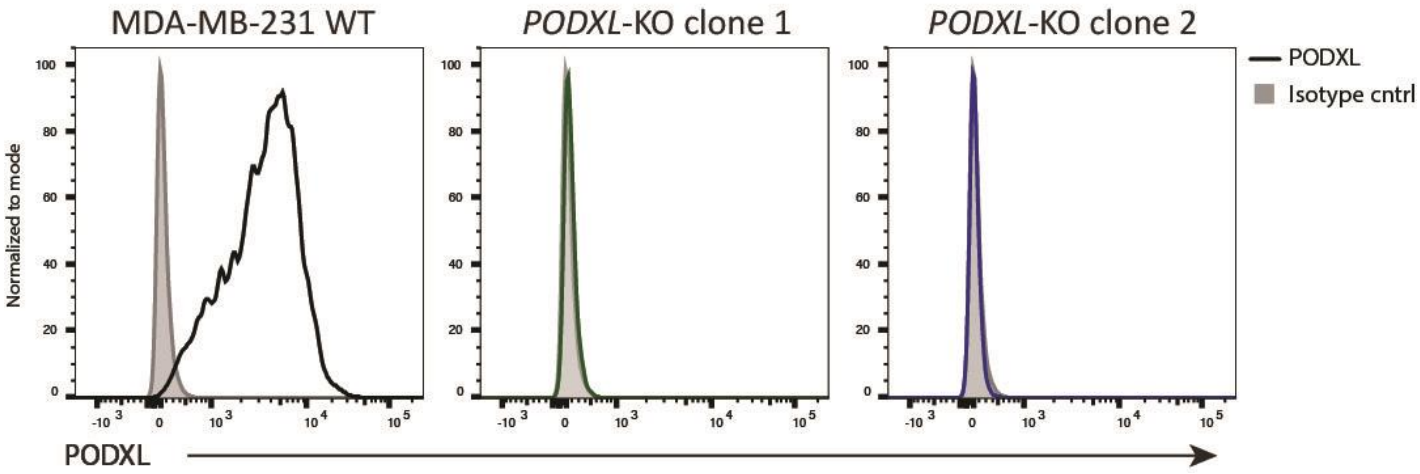

Appendix C Generation of hPODXL protein mutants

While it has been previously shown that Podxl plays a role in promoting tumor growth and metastasis, the underlying molecular mechanism by which it does so remains largely unclear. Expression of different murine Podxl mutants on MCF7 highlighted the importance of Podxl's extracellular domain on the formation of microvilli (139). Recently, Fröse et al., showed that the intracellular domain of Podxl, and specifically ezrin binding motifs, are responsible for the extravasation of MDA-MB-231 cells into the lung parenchyma (39). In addition, we showed that targeting of cell-surface expressed Podxl with the PODO83 antibody blocks metastasis of MDA-MB-231 cells (136). Since PODO83 binds to the extracellular stalk portion of Podxl (See Chapter 3), we hypothesize that this domain is important for promoting cancer metastasis. Given that the role of Podxl in promoting ovarian cancer progression in yet to be determined, we sought to investigate which domain of Podxl is responsible for promoting SKOV3 tumor aggressiveness.

We generated several human Podxl protein domain mutants (**Appendix Fig C.1**). Briefly, a FLAG-tag motif and the murine CD34 signal peptide were included in all constructs. The PODXL-ΔDTHL mutant lacks the last four carboxy-terminal DTHL residues, eliminating direct NHERF1/2 binding to Podxl and disrupting intracellular signaling and interactions of Podxl with the cortical cytoskeleton. PODXL-ΔTail is missing Podxl's entire cytosolic tail, including the juxtamembrane ezrin-binding site, and therefore lacks the ability to bind to the actin cytoskeleton. PODXL-ΔMucin mutant lacks the N- and O-glycosilation sites but includes the globular domain (four cysteines postulated to form disulfide bridges) and the "stalk" domain, hence retaining PODO83's epitope which might be involved in cancer metastasis. Finally,

PODXL-ΔEC is missing the extracellular domain in its entirety, thus lacking the ability to interact with any potential extracellular binding partners (**Appendix Fig C.1**).

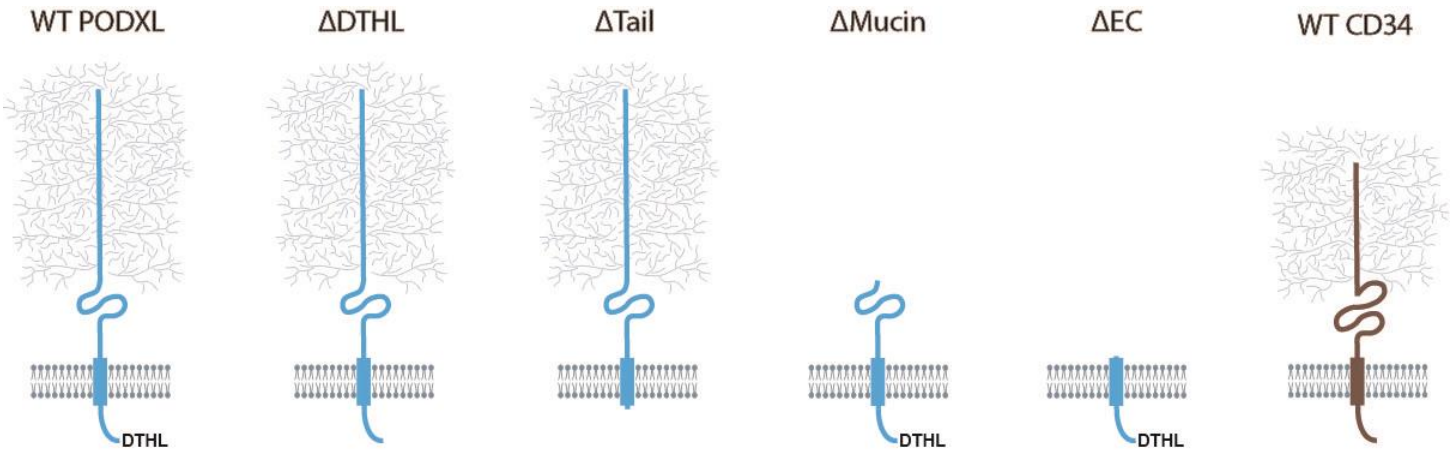

Appendix Fig C.1 Representation of Podxl mutants

Schematic of full-length (WT) CD34, Podxl and Podxl deletion mutants.

C.1 Materials and methods: Generation of full-length Podxl, CD34 and Podxl-deletion mutant expression constructs

Human full length (WT) Podxl, CD34 and Podxl-deletion mutant sequences were synthesized as gBlock® gene fragments purchased from Integrated DNA Technologies, and assembled and cloned into the pTT22 expression vector (National Research Council of Canada) using Gibson assembly (224). Sequences were designed to include mouse CD43 signal peptide (SP) and a FLAG-tag motif (sequences in **Appendix Table C.1**). Podxl-ΔDTHL was generated by substituting the C-terminal DTHL residues with an early stop codon. Podxl-ΔTail was generated by substituting Podxl's cytosolic domain by an early stop codon. Podxl-ΔMucin mutant was generated by substituting Podxl's mucin domain for CD43's SP and FLAG-tag motif. Podxl-ΔEC mutant was generated by substituting Podxl entire extracellular domain with CD43's SP and the FLAG-tag motif. Plasmids containing the constructs were confirmed by Sanger sequencing.

Appendix Table C.1 Full-length and Podxl-deletion mutant sequences

Construct name	Sequence (5’ – 3’)
Full-length Podxl (WT)	GCCACCATGGCCTTGCACCTTCTCCTCCTCTTTGGGGCATGCTGGGTCCAGGTGGCGAGCCCAGATTACAAGGACGACGATGACAAGGGCGGCG GATCCAGATCTGCGGCCGCCCCGTCGCCGTCGCCCTCCCAGAATGCAACCCAGACTACTACGGACTCATCTAACAAAACAGCACCGACTCCAGCA TCCAGTGTCACCATCATGGCTACAGATACAGCCCAGCAGAGCACAGTCCCCACTTCCAAGGCCAACGAAATCTTGGCCTCGGTCAAGGCGACCAC CCTTGGTGTATCCAGTGACTCACCGGGGACTACAACCCTGGCTCAGCAAGTCTCAGGCCCAGTCAACACTACCGTGGCTAGAGGAGGCGGCTCA GGCAACCCTACTACCACCATCGAGAGCCCCAAGAGCACAAAAAGTGCAGACACCACTACAGTTGCAACCTCCACAGCCACAGCTAAACCTAACAC CACAAGCAGCCAGAATGGAGCAGAAGATACAACAAACTCTGGGGGGAAAAGCAGCCACAGTGTGACCACAGACCTCACATCCACTAAGGCAGA ACATCTGACGACCCCTCACCCTACAAGTCCACTTAGCCCCCGACAACCCACTTCGACGCATCCTGTGGCCACCCCAACAAGCTCGGGACATGACCA TCTTATGAAAATTTCAAGCAGTTCAAGCACTGTGGCTATCCCTGGCTACACCTTCACAAGCCCGGGGATGACCACCACCCTACCGTCATCGGTTAT CTCGCAAAGAACTCAACAGACCTCCAGTCAGATGCCAGCCAGCTCTACGGCCCCTTCCTCCCAGGAGACAGTGCAGCCCACGAGCCCGGCAACGG CATTGAGAACACCTACCCTGCCAGAGACCATGAGCTCCAGCCCCACAGCAGCATCAACTACCCACCGATACCCCAAAACACCTTCTCCCACTGTGG CTCATGAGAGTAACTGGGCAAAGTGTGAGGATCTTGAGACACAGACACAGAGTGAGAAGCAGCTCGTCCTGAACCTCACAGGAAACACCCTCTG TGCAGGGGGCGCTTCGGATGAGAAATTGATCTCACTGATATGCCGAGCAGTCAAAGCCACCTTCAACCCGGCCCAAGATAAGTGCGGCATACGG CTGGCATCTGTTCCAGGAAGTCAGACCGTGGTCGTCAAAGAAATCACTATTCACACTAAGCTCCCTGCCAAGGATGTGTACGAGCGGCTGAAGGA CAAATGGGATGAACTAAAGGAGGCAGGGGTCAGTGACATGAAGCTAGGGGACCAGGGGCCACCGGAGGAGGCCGAGGACCGCTTCAGCATGC CCCTCATCATCACCATCGTCTGCATGGCATCATTCCTGCTCCTCGTGGCGGCCCTCTATGGCTGCTGCCACCAGCGCCTCTCCCAGAGGAAGGACC AGCAGCGGCTAACAGAGGAGCTGCAGACAGTGGAGAATGGTTACCATGACAACCCAACACTGGAAGTGATGGAGACCTCTTCTGAGATGCAGG AGAAGAAGGTGGTCAGCCTCAACGGGGAGCTGGGGGACAGCTGGATCGTCCCTCTGGACAACCTGACCAAGGACGACCTGGATGAGGAGGAA GACACACACCTCTAG
Podxl-ΔDTHL	GCCACCATGGCCTTGCACCTTCTCCTCCTCTTTGGGGCATGCTGGGTCCAGGTGGCGAGCCCAGATTACAAGGACGACGATGACAAGGGCGGCG GATCCAGATCTGCGGCCGCCCCGTCGCCGTCGCCCTCCCAGAATGCAACCCAGACTACTACGGACTCATCTAACAAAACAGCACCGACTCCAGCA TCCAGTGTCACCATCATGGCTACAGATACAGCCCAGCAGAGCACAGTCCCCACTTCCAAGGCCAACGAAATCTTGGCCTCGGTCAAGGCGACCAC CCTTGGTGTATCCAGTGACTCACCGGGGACTACAACCCTGGCTCAGCAAGTCTCAGGCCCAGTCAACACTACCGTGGCTAGAGGAGGCGGCTCA GGCAACCCTACTACCACCATCGAGAGCCCCAAGAGCACAAAAAGTGCAGACACCACTACAGTTGCAACCTCCACAGCCACAGCTAAACCTAACAC CACAAGCAGCCAGAATGGAGCAGAAGATACAACAAACTCTGGGGGGAAAAGCAGCCACAGTGTGACCACAGACCTCACATCCACTAAGGCAGA ACATCTGACGACCCCTCACCCTACAAGTCCACTTAGCCCCCGACAACCCACTTCGACGCATCCTGTGGCCACCCCAACAAGCTCGGGACATGACCA TCTTATGAAAATTTCAAGCAGTTCAAGCACTGTGGCTATCCCTGGCTACACCTTCACAAGCCCGGGGATGACCACCACCCTACCGTCATCGGTTAT CTCGCAAAGAACTCAACAGACCTCCAGTCAGATGCCAGCCAGCTCTACGGCCCCTTCCTCCCAGGAGACAGTGCAGCCCACGAGCCCGGCAACGG CATTGAGAACACCTACCCTGCCAGAGACCATGAGCTCCAGCCCCACAGCAGCATCAACTACCCACCGATACCCCAAAACACCTTCTCCCACTGTGG

	CTCATGAGAGTAACTGGGCAAAGTGTGAGGATCTTGAGACACAGACACAGAGTGAGAAGCAGCTCGTCCTGAACCTCACAGGAAACACCCTCTG TGCAGGGGGCGCTTCGGATGAGAAATTGATCTCACTGATATGCCGAGCAGTCAAAGCCACCTTCAACCCGGCCCAAGATAAGTGCGGCATACGG CTGGCATCTGTTCCAGGAAGTCAGACCGTGGTCGTCAAAGAAATCACTATTCACACTAAGCTCCCTGCCAAGGATGTGTACGAGCGGCTGAAGGA CAAATGGGATGAACTAAAGGAGGCAGGGGTCAGTGACATGAAGCTAGGGGACCAGGGGCCACCGGAGGAGGCCGAGGACCGCTTCAGCATGC CCCTCATCATCACCATCGTCTGCATGGCATCATTCCTGCTCCTCGTGGCGGCCCTCTATGGCTGCTGCCACCAGCGCCTCTCCCAGAGGAAGGACC AGCAGCGGCTAACAGAGGAGCTGCAGACAGTGGAGAATGGTTACCATGACAACCCAACACTGGAAGTGATGGAGACCTCTTCTGAGATGCAGG AGAAGAAGGTGGTCAGCCTCAACGGGGAGCTGGGGGACAGCTGGATCGTCCCTCTGGACAACCTGACCAAGGACGACCTGGATGAGGAGGAA TAG
Podxl-ΔTail	GCCACCATGGCCTTGCACCTTCTCCTCCTCTTTGGGGCATGCTGGGTCCAGGTGGCGAGCCCAGATTACAAGGACGACGATGACAAGGGCGGCG GATCCAGATCTGCGGCCGCCCCGTCGCCGTCGCCCTCCCAGAATGCAACCCAGACTACTACGGACTCATCTAACAAAACAGCACCGACTCCAGCA TCCAGTGTCACCATCATGGCTACAGATACAGCCCAGCAGAGCACAGTCCCCACTTCCAAGGCCAACGAAATCTTGGCCTCGGTCAAGGCGACCAC CCTTGGTGTATCCAGTGACTCACCGGGGACTACAACCCTGGCTCAGCAAGTCTCAGGCCCAGTCAACACTACCGTGGCTAGAGGAGGCGGCTCA GGCAACCCTACTACCACCATCGAGAGCCCCAAGAGCACAAAAAGTGCAGACACCACTACAGTTGCAACCTCCACAGCCACAGCTAAACCTAACAC CACAAGCAGCCAGAATGGAGCAGAAGATACAACAAACTCTGGGGGGAAAAGCAGCCACAGTGTGACCACAGACCTCACATCCACTAAGGCAGA ACATCTGACGACCCCTCACCCTACAAGTCCACTTAGCCCCCGACAACCCACTTCGACGCATCCTGTGGCCACCCCAACAAGCTCGGGACATGACCA TCTTATGAAAATTTCAAGCAGTTCAAGCACTGTGGCTATCCCTGGCTACACCTTCACAAGCCCGGGGATGACCACCACCCTACCGTCATCGGTTAT CTCGCAAAGAACTCAACAGACCTCCAGTCAGATGCCAGCCAGCTCTACGGCCCCTTCCTCCCAGGAGACAGTGCAGCCCACGAGCCCGGCAACGG CATTGAGAACACCTACCCTGCCAGAGACCATGAGCTCCAGCCCCACAGCAGCATCAACTACCCACCGATACCCCAAAACACCTTCTCCCACTGTGG CTCATGAGAGTAACTGGGCAAAGTGTGAGGATCTTGAGACACAGACACAGAGTGAGAAGCAGCTCGTCCTGAACCTCACAGGAAACACCCTCTG TGCAGGGGGCGCTTCGGATGAGAAATTGATCTCACTGATATGCCGAGCAGTCAAAGCCACCTTCAACCCGGCCCAAGATAAGTGCGGCATACGG CTGGCATCTGTTCCAGGAAGTCAGACCGTGGTCGTCAAAGAAATCACTATTCACACTAAGCTCCCTGCCAAGGATGTGTACGAGCGGCTGAAGGA CAAATGGGATGAACTAAAGGAGGCAGGGGTCAGTGACATGAAGCTAGGGGACCAGGGGCCACCGGAGGAGGCCGAGGACCGCTTCAGCATGC CCCTCATCATCACCATCGTCTGCATGGCATCATTCCTGCTCCTCGTGGCGGCCCTCTATGGCTGCTGCCACCAGCGCCTCTAG
Podxl-ΔMucin	GCCACCATGGCCTTGCACCTTCTCCTCCTCTTTGGGGCATGCTGGGTCCAGGTGGCGAGCCCAGATTACAAGGACGACGATGACAAGGGCGGCG GATCCAGATCTGCGGCCGCCCATGAGAGTAACTGGGCAAAGTGTGAGGATCTTGAGACACAGACACAGAGTGAGAAGCAGCTCGTCCTGAACCT CACAGGAAACACCCTCTGTGCAGGGGGCGCTTCGGATGAGAAATTGATCTCACTGATATGCCGAGCAGTCAAAGCCACCTTCAACCCGGCCCAA GATAAGTGCGGCATACGGCTGGCATCTGTTCCAGGAAGTCAGACCGTGGTCGTCAAAGAAATCACTATTCACACTAAGCTCCCTGCCAAGGATGT GTACGAGCGGCTGAAGGACAAATGGGATGAACTAAAGGAGGCAGGGGTCAGTGACATGAAGCTAGGGGACCAGGGGCCACCGGAGGAGGCC GAGGACCGCTTCAGCATGCCCCTCATCATCACCATCGTCTGCATGGCATCATTCCTGCTCCTCGTGGCGGCCCTCTATGGCTGCTGCCACCAGCGC CTCTCCCAGAGGAAGGACCAGCAGCGGCTAACAGAGGAGCTGCAGACAGTGGAGAATGGTTACCATGACAACCCAACACTGGAAGTGATGGAG

	ACCTCTTCTGAGATGCAGGAGAAGAAGGTGGTCAGCCTCAACGGGGAGCTGGGGGACAGCTGGATCGTCCCTCTGGACAACCTGACCAAGGAC GACCTGGATGAGGAGGAAGACACACACCTCTAG

Podxl-ΔEC	GCCACCATGGCCTTGCACCTTCTCCTCCTCTTTGGGGCATGCTGGGTCCAGGTGGCGAGCCCAGATTACAAGGACGACGATGACAAGGGCGGCG GATCCAGATCTGCGGCCGCCCCACCGGAGGAGGCCGAGGACCGCTTCAGCATGCCCCTCATCATCACCATCGTCTGCATGGCATCATTCCTGCTCC TCGTGGCGGCCCTCTATGGCTGCTGCCACCAGCGCCTCTCCCAGAGGAAGGACCAGCAGCGGCTAACAGAGGAGCTGCAGACAGTGGAGAATG GTTACCATGACAACCCAACACTGGAAGTGATGGAGACCTCTTCTGAGATGCAGGAGAAGAAGGTGGTCAGCCTCAACGGGGAGCTGGGGGACA GCTGGATCGTCCCTCTGGACAACCTGACCAAGGACGACCTGGATGAGGAGGAAGACACACACCTCTAG
Full-length CD34 (WT)	GCCACCATGGCCTTGCACCTTCTCCTCCTCTTTGGGGCATGCTGGGTCCAGGTGGCGAGCCCAGATTACAAGGACGACGATGACAAGGGCGGCG GATCCAGATCTGCGGCCGCCAACGGTACTGCTACCCCAGAGTTACCTACCCAGGGAACATTTTCAAATGTTTCTACAAATGTATCCTACCAAGAAA CTACAACACCTAGTACCCTTGGAAGTACCAGCCTGCACCCTGTGTCTCAACATGGCAATGAGGCCACAACAAACATCACAGAAACGACAGTCAAA TTCACATCTACCTCTGTGATAACCTCAGTTTATGGAAACACAAACTCTTCTGTCCAGTCACAGACCTCTGTAATCAGCACAGTGTTCACCACCCCAG CCAACGTTTCAACTCCAGAGACAACCTTGAAGCCTAGCCTGTCACCTGGAAATGTTTCAGACCTTTCAACCACTAGCACTAGCCTTGCAACATCTCC CACTAAACCCTATACATCATCTTCTCCTATCCTAAGTGACATCAAGGCAGAAATCAAATGTTCAGGCATCAGAGAAGTGAAATTGACTCAGGGCAT CTGCCTGGAGCAAAATAAGACCTCCAGCTGTGCGGAGTTTAAGAAGGACAGGGGAGAGGGCCTGGCCCGAGTGCTGTGTGGGGAGGAGCAGG CTGATGCTGATGCTGGGGCCCAGGTATGCTCCCTGCTCCTTGCCCAGTCTGAGGTGAGGCCTCAGTGTCTACTGCTGGTCTTGGCCAACAGAACA GAAATTTCCAGCAAACTCCAACTTATGAAAAAGCACCAATCTGACCTGAAAAAGCTGGGGATCCTAGATTTCACTGAGCAAGATGTTGCAAGCCA CCAGAGCTATTCCCAAAAGACCCTGATTGCACTGGTCACCTCGGGAGCCCTGCTGGCTGTCTTGGGCATCACTGGCTATTTCCTGATGAATCGCCG CAGCTGGAGCCCCACAGGAGAAAGGCTGGGCGAAGACCCTTATTACACGGAAAACGGTGGAGGCCAGGGCTATAGCTCAGGACCTGGGACCTC CCCTGAGGCTCAGGGAAAGGCCAGTGTGAACCGAGGGGCTCAGGAAAACGGGACCGGCCAGGCCACCTCCAGAAACGGCCATTCAGCAAGACA ACACGTGGTGGCTGATACCGAATTGTGA

Appendix D Charles River Laboratory summary report of PODO447 cross-reactivity with normal human tissues.

Tissue	PODO447	Neg Control	Pos Control
Brain			
Cerebellum	Neg	Neg	Pos
Cerebral Cortex	Neg	Neg	Pos
Breast	Neg	Neg	Pos
Colon	Neg	Neg	Pos
Fallopian Tube	Rare	Neg	Pos
Epithelium, mucosa	(1-2+)		
GI – Track			
Esophagus	Neg	Neg	Pos
Small Intestine	Rare	Neg	Pos
Epithelium, mucosa	(1-2+)		
Stomach	Neg	Neg	Pos
Heart	Neg	Neg	Pos
Kidney	Very rare	Neg	Pos
Podocytes	(2-3+)		
Liver	Neg	Neg	Pos
Ovary	Neg	Neg	Pos
Skin	Very rare	Neg	Pos
Epithelium, sweat gland	(1+)		

PODO447 staining was assessed as Neg = Negative, Pos = Positive. The frequency of cells with PODO447 positive staining was identified as follows: very rare (<1% cells of a particular cell type), rare (1-5% of cells of a particular cell type), rare to occasional (5-25% of cells of a particular cell type), occasional (>25-50% of cells of a particular cell type), occasional to frequent (>59-75% of cells of a particular cell type), frequent (>75-100% of cells of a particular cell type). Blood vessel (endothelium) staining is detailed under each individual tissue. Frequency modifiers were included to provide the approximate percentage staining of expected numbers of that cell type or tissue element at that location. The intensity of the staining was scored as: 1+ = weak, 2+ = moderate, 3+ = strong, 4+ = intense. HuIgG1 was used as negative (Neg) control, and anti-β_2-microglobulin as tissue staining (Pos) control.

Appendix E Complete list of glycans binding to PODO447

Median RFU	STD	Glycan Structure	Common Name	Short Name
46864.3	11346.6	GalNAcβ1-3Galα1-4Galβ1-4Glcβ-sp3	Gb4, P	Gb4
37815	10288	GalNAcβ-sp10	β-GalNAc	bAN-PEG2
37155	6796.1	$(GalNAc\beta\text{-}PEG_2)_3$-β-DD	(ANb-PEG2)3	
26355	3341	GalNAcβ-sp3	β-GalNAc	bAN
19964	6979	GalNAcα1-OSer	TnSer	TnSer
10932	3718	GalNAcβ1-4GlcNAcβ-sp2	LacdiNAc	LacdiNAc-C2
5723	1949	GalNAcα1-3Galβ-sp3	A_{di}	Adi
3390	1440	Fucα1-2Galβ-sp3	H_{di}	Hdi
2173	670	GalNAcβ1-3GalNAcβ-sp3	para-Fs	para-Fs
1646	708	Fucα1-2(3-O-Su)Galβ-sp3	3-O-Su-H_{di}	Hdi3Su
1355.3	633.30	Neu5Gcα2-6GalNAcα-sp3	Neu5Gc-T_n	Neu5GcTn
1329	31.1	Fucα1-2Galβ1-4GlcNAcβ-sp3	H (type 2)	Htype2
1260	481	GalNAcβ1-4GlcNAcβ-sp3	LacdiNAc	LacdiNAc
1215	465.1	6-O-Su-Galβ1-3(6-O-Su)GlcNAcβ-sp2	6,6'-di-O-Su-Le^c	LeC6,6'Su2
1062	373	GlcNAcβ1-3GalNAcα-sp3	core 3	core3
1022	423	Gala1-3Galβ-sp3	B_{di}	Bdi
790	280	GalNAcβ1-4(6-O-Su)GlcNAcβ-sp2	6-O-Su-LacdiNAc	LacdiNAc6Su
713	224.5	Galα1-3Galβ1-4GlcNAcβ-sp3	Galili (tri)	Galili3
687.7	215.5	GlcNAcβ1-6(Galβ1-3)GalNAcα-sp3	core 2	core2
602.7	272.9	4,6-O-Su_2-Galβ1-4GlcNAcβ-sp3	4',6'-di-O-Su-LN	LN4'6'Su2

Median RFU	STD	Glycan Structure	Common Name	Short Name
493	197	ManNAcβ-sp4	β-ManNAc	bMN
450	160.6	6-O-Su-GalNAcβ1-4GlcNAcβ-sp3	6'-O-Su-LacdiNAc	LacdiNAc6'Su
367	112	6-O-Su-Galβ1-4Glcβ-sp2	6'-O-Su-Lac	Lac6'Su
364	115.8	Gala1-3(Fucα1-2)Galβ-sp5	Btri-C8	Btri-C8
360	114	GlcNAcβ1-6GalNAcα-sp3	core 6	core6
324.3	93.0		α1-3, α1-6-mannotriose-BSA	
285	101.2	3,6-O-Su_2-Galβ1-4(6-O-Su)GlcNAcβ-sp2	3',6,6'-tri-O-Su-LN	LN3'66'Su3
274.3	98.8	GalNAcβ1-4Galβ1-4Glcβ-sp3	$GA_{2,}$ $GgOse_3$	GA2
227.3	71.1	Galβ1-3(Fucα1-4)GlcNAcβ-sp3	Le^a	LeA
220	33	4-O-Su-Galβ1-4GlcNAcβ-sp2	4'-O-Su-LN	LN4'Su-C2
208.3	23.1		Sia-Lex-BSA(NPG1403)	
170.3	27.2	3'-Sialyllactose-ADP-HSA, Isosep60/67	3'-Sialyllactose-HSA	
149	50	6'-O-Su-Galβ1-4GlcNAcβ-sp3	6'-O-Su-LN	LN6'Su
142.7	10.7	Lacto-N-fucopentaose III-ADP-HSA (LNF III-HSA)	Lex-HSA	
116.7	9.9		SO3-Lea-15atom-HSA	
113	21.5	Neu5Acα2-8Neu5Acα2-8Neu5Acα2-3(GalNAcβ1-4)Galβ1-4Glcβ-sp2	GT2	GT2
110	6.4	A-Hexasaccharide-APD-HSA	A-hexa-HSA	
109.7	8.1	GlcNAcβ1-3Galβ1-3GlcNAcβ-sp3	$GlcNAc3'Le^c$	$GlcNAc3'Le^c$
108.7	13.7	Lacto-N-neotetraose-ADP-HSA (lactosamin)	LNnT-HSA	
104.3	6.5	Lacto-N-tetraose-ADP-HSA, Isosep60/97	LNT-HSA	
103.3	17.5	GlcNAcα1-3Galβ1-4GlcNAcβ-sp3	GNa3'LN	GNa3'LN

Median RFU	STD	Glycan Structure	Common Name	Short Name
103	5.1	Sialyl-Lea-APD-HSA (19-9 antigen, Sialyl-Lea)	Sia-Lea-HSA	
92.3	8.4	4,6-O-Su_2-GalNAcβ1-4-(3-O-Ac)GlcNAcβ-sp3	4',6'-di-O-Su-LacdiNAc	3Ac-LacdiNAc4',6'Su2
78.3	21.4	3-O-Su-GalNAcβ1-4GlcNAcβ-sp3	3'-O-Su-LacdiNAc	LacdiNAc3'Su